Valorisation des sédiments de dragage dans l'industrie cimentaire

Duc Chinh Chu

IMT Nord Europe
École Mines-Télécom
IMT-Université de Lille

Université de Lille

École doctorale SPI 072 : Sciences pour l'Ingénieur

Thèse de Doctorat

Pour obtenir le grade de

Docteur de de l'Université de Lille

délivré par l'IMT Nord Europe

Spécialité : Génie Civil

Présentée et soutenue par : **CHU DUC CHINH**

Valorisation des sédiments de dragage dans l'industrie cimentaire

Soutenue le 17 décembre 2021

Membres du jury :

Ali-Nordine LEKLOU	*Pr, Université de Nantes*	*Président du jury*
Salima AGGOUN	*Pr, Université de Cergy Pontoise*	*Rapporteur*
Rose Marie DHEILLY	*Pr, Université de Picardie*	*Examinateur*
Fabrice BERNARD	*HDR, INSA de Rennes*	*Examinateur*
Ammar YAHIA	*Pr, Université de Sherbrooke*	*Examinateur*
Mahfoud BENZERZOUR	*Pr, IMT Nord Europe*	*Directeur de thèse*
Nor-Edine ABRIAK	*Pr, IMT Nord Europe*	*Co-Directeur de thèse*
Mouhamadou AMAR	*Dr, IMT Nord Europe*	*Examinateur, Encadrant*
Joelle KLEIB	*Dr, IMT Nord Europe*	*Encadrant, Invitée*
Jaouad NADAH	*Dr, EQIOM*	*Invité*

Institut Mines Telecom Nord Europe
CERI Matériaux et Procédés
Laboratoire Génie Civil et géo Environnement (LGCgE)

Résumé

En France, environ 56 Mm^3 de sédiments sont annuellement dragués mais sont considérés comme des déchets au vu de la réglementation. Cette quantité de sédiment pose aux gestionnaires la responsabilité de trouver des solutions adaptées afin d'éviter tout effet néfaste sur l'environnement. En outre, l'industrie cimentière Française, avec une production d'environ 16.7 Mt de ciment en 2019 consomme une très grande quantité des matières premières extraites des gisements telles que le calcaire, les argiles, etc. L'extraction de ces matières premières cause par ailleurs de sérieux enjeux environnementaux. Par conséquent, l'utilisation de sédiments en tant que matière première dans la fabrication de ciments et de liants pourrait être une solution à plusieurs avantages. Cette approche permettra ainsi une réutilisation de quantités importantes de sédiments disponibles en tant que matière première secondaire pour l'industrie cimentière et les liants pour la construction. Deux procédés de valorisation ont été étudiés pour atteindre les objectifs de ce travail de recherche : le premier concerne la valorisation du sédiment dans le cru cimentaire, l'évaluation les effets de l'incorporation du sédiment sur la formation des phases minérales du clinker et la réactivité du ciment à base sédiment. La seconde approche consiste quant à elle à l'utilisation du sédiment traité par la calcination Flash en tant qu'addition minérale dans les liants. Les différents essais réalisés permettent de mettre en évidence les effets du sédiment calciné sur l'hydratation du ciment et la contribution au développement des résistances mécaniques, ainsi que sur la microstructure. Le comportement des matériaux formulés a ainsi été étudié et validé à l'échelle expérimentale et numérique. Les résultats obtenus démontrent un fort potentiel d'utilisation des sédiments dans ce type d'applications.

Mots clés : Sédiment, Ciment, Hydratation, Calcination Flash, Pouzzolanique, CEMHYD3D.

Abstract

In France, approximately 56 Mm^3 of sediments are dredged annually but are considered as waste in view of the regulations. This amount of sediment places the onus on managers to find suitable solutions to avoid any negative effects on the environment. In addition, the French cement industry, with a production of around 16.7 Mt of cement in 2019, consumes a very large amount of raw materials extracted from deposits such as limestone, clays, etc. The extraction of these raw materials also causes serious environmental issues. Therefore, the use of sediment as a raw material in the manufacture of cements and binders could be a solution with several advantages. This approach will thus allow the reuse of large quantities of sediments available as secondary raw material for the cement industry and as binders for construction. Two valuation processes were studied to achieve the objectives of this research work: the first concerns the valuation of the sediment in the cementitious raw material, the evaluation of the effects of the incorporation of the sediment on the formation of the mineral phases of the clinker and the reactivity of sediment-based cement. The second approach consists of using the sediment treated by flash calcination as a mineral addition in the binders. The various tests carried out make it possible to demonstrate the effects of the calcined sediment on the hydration of the cement and the contribution to the development of mechanical resistance, as well as on the microstructure. The behavior of the formulated materials was thus studied and validated on an experimental and numerical scale. The results obtained demonstrate a strong potential for the use of sediments in this type of application.

Key words: Sediment, Cement, Hydration, Flash calcination, Pozzolanic, CEMHYD3D.

Remerciements

Les travaux de cette thèse ont été réalisés au sein du département Génie Civil et Environnemental de l'IMT Nord-Europe (Ex IMT Lille Douai).

Tout d'abord, je tiens à remercier le Professeur **Mahfoud Benzerzour**, directeur de cette thèse, et avec qui j'ai eu la chance de travailler également à partir de mon stage de Master. Je le remercie pour son aide, sa confiance, ses conseils scientifiques et ses encouragements dans les moments difficiles. Je tiens à remercier Professeur **Nor-Edine Abriak**, chef du Département Génie Civil et Environnemental de l'IMT Nord-Europe, et également co-directeur de la thèse. Je le remercie pour son aide et sa confiance durant ces trois années de thèse. Travailler avec vous à été une expérience très enrichissante.

Un grand merci également à mes encadrants : Dr **Mouhamadou Amar**, enseignant-chercheur à l'IMT Nord-Europe et Dr **Joelle Kleib**, maître-assistant de l'IMT Nord-Europe. Je voudrais leur adresser toute ma reconnaissance pour leurs réflexions scientifiques et leurs aides qui ont contribué à l'avancement de ce travail. Je ne suis pas sûr que ces quelques mots suffisent à vous exprimer ma gratitude.

Je remercie vivement Monsieur **Ali-Nordine LEKLOU**, Professeur de l'université de Nantes et Madame **Salima AGGOUN**, Professeure de l'université de Cergy Pontoise pour avoir rapporté ce travail. C'est pour moi un grand honneur.

Je tiens à remercier Madame **Rose Marie DHEILLY** Professeure de l'universite de Picardie**,** Monsieur **Fabrice Bernard**, Assistant professeur de l'INSA Rennes, Monsieur **Ammar YAHIA,** Professure de l'université de Sherbrooke et Monsieur **Mouhamadou Amar**, Enseignant-chercheur de l'IMT Nord-Europe pour avoir accepté d'examiner ce travail.

Je remercie également les techniciens : Damien Betrancourt, Johanna Caboche, Guillaume Potier, Dominique Dubois, Michael D'Helft pour leur gentillesse, leur aide et la patience dont ils ont fait preuve. En particulier, je voudrais adresser ma gratitude à Damien Betrancourt, Johanna Caboche, Guillaume Potier : Merci d'avoir passé des heures avec moi pour résoudre des problèmes.

Je n'oublie pas adresser le remerciement à mes amis de l'IMT Nord-Europe (thésard et post-doc) : Mathilde Betremieux, Mathilde Berthomier, Mohamed ElKarim Bouarroudj, Mel Constant, Jana Daher, Zeinab Mkahal, Bader Bouzar, Hamza El Moueden, Maria Taleb, Hongwei Wang, Salim Kourtaa, Ahmed Zaoui. Je n'oublierai jamais Mathilde Betremieux qui à été ma première amie lorsque je suis arrivé en France en 2015.

Je voudrais vivement adresser ma gratitude et mon infinie reconnaissance à l'ensemble de ma famille, qui à toujours été à mes côtés et qui m'a supoprté dans les moments difficiles. D'abord, je remerie mon grand père, qui à une place particulière dans la vie, et qui m'a encouragé à faire une thèse depuis mon enfance. Aussi, je remercie mes parents, qui ont tant fait pour moi, qui m'on donné tout ce qu'ils ont pu afin que je puisse réaliser des études. Je vous remercie pour votre soutien sans condition.

Je voudrais également adresser quelques mots à mes petits frères : Duc Anh et Duc Mai, mais aussi à la famille de ma petite sœur, pour m'avoir redonné espoirs. Particulièrement dans les moments les plus difficiles de ma vie. Je n'oublie bien évidemment pas « mon grand frère » Doan Tran qui m'a donné beaucoup de conseils et de soutiens.

Je voudrais dire « un grand merci, une reconnaissance infinie » à la famille de ma femme qui nous a donné, sans condition, beaucoup de soutiens. En particulier, je remercie nos oncles : Monsieur DO Dinh Chieu, Madame Kim Loan et Huyen My.

Enfin, je voudrais adresser un dernier mot pour exprimer ma gratitude et ma reconnaissance à la personne la plus importante dans ma vie. Elle m'a accompagné et à partagé avec moi des moments de bonheurs mais aussi des moments douloureux. Merci à ma femme **Huyen Trang**.
Enfin, comme une promesse, cette thèse est un cadeau particulier pour une personne qui restera à jamais dans mon cœur : **Noel** « Love U 3000 ». ♥

Table des matières

Liste des tableaux

Chapitre 1

Chapitre 2

Article 1

Article 2

Chapitre 3

Article 3

Article 4

Chapitre 4

Article 5

Chapitre 5

Article 6

Liste des figures

Chapitre 1

Chapitre 2

Article 1

Article 2

Chapitre 3

Article 3

Article 4

Chapitre 4

Article 5

Chapitre 5

Article 6

Introduction générale

Le monde est plus que jamais face à des défis économiques, sociaux et environnementaux conséquents. Ces défis opposent à l'être humain un nouveau paradigme : devoir améliorer ses modes de consommation et repenser son rapport avec son environnement. La révolution industrielle qui se voulait corréler la croissance à l'exploitation des ressources doit désormais intégrer dans son schéma la réutilisation des déchets et sous-produits. C'est donc par cette voix que la transition écologique et solidaire sera garantie et assurera aux générations futures un avenir serein. D'ailleurs c'est ce vers quoi aspirent les COP et le programme Européen Green Deal par exemple.

Les sédiments de dragage sont des matières extraites des fonds marins et fluviaux. Leur extraction permet de garantir la bonne circulation par les voies d'eau, la limitation des risques de crues et d'inondation, etc. Ces volumes extraits posent toutefois une problématique majeure en termes de gestion. Une fois extrait les sédiments sont considérés par la réglementation en vigueur comme des déchets. Ils doivent donc satisfaire à des conditions spécifiques avant de pouvoir être réutilisés notamment dans les filières de la construction. Cette thèse permet donc de lever certains verrous scientifiques et techniques quant 'à l'utilisation de ces derniers dans les matrices cimentaires.

Le dragage des sédiments, puis leur valorisation est donc un processus nécessaire, important et qui prend tout son sens dans le contexte de développement durable et de transition écologique actuel. D'autre part, le secteur de la construction est l'un des secteurs ayant le plus fort impact environnemental. L'industrie cimentaire, quelque peu victime de son succès produit environ 7% des émissions de CO_2 dans le monde et est fortement énergivore. En substituer alors tout ou partie dans la formulation de matrices cimentaires par des sous-produits tels que les sédiments pourraient représenter un avantage économique et écologique considérable. C'est d'ailleurs dans ce sens que la réglementation et la normalisation actuelle bougent avec l'arrivée tout récente en 2021 des normes CEM II/C et CEM VI permettant la composition de ciment ternaire notamment à base de terres et argiles calcinées. C'est d'ailleurs dans cette logique et cette démarche qu'a pris naissance le projet SEDICIM dans lequel cette thèse s'inscrit.
SEDICIM est un projet partenarial entre l'IMT Nord Europe et le cimentier EQIOM. L'objectif de ce projet est de substituer les sédiments dans le cru de cimenterie (aujourd'hui constitué de matériaux provenant de carrières) et/ou les valoriser en tant que additions minérales pour la fabrication de liants cimentiers, de liants hydrauliques routiers ou de bétons. L'ensemble des sédiments utilisés dans le cadre du projet SEDICIM sont caractérisés afin de connaître exhaustivement leurs caractéristiques physiques, chimiques et minéralogiques. Ainsi, à Dannes en région Hauts de France, un laboratoire de suivi environnemental de 100 m² a été conçu et dimensionné spécifiquement pour le projet. Un ciment contenant du sédiment dans son cru est préparé à échelle industrielle (plusieurs dizaines de tonnes). Les liants préparés sont utilisés pour la réalisation de plusieurs produits : dallage, bloc béton et route. Un suivi de l'impact environnemental est aussi effectué par l'industriel.

Le projet SEDICIM est un projet FEDER qui rentre dans le cadre de la démarche nationale SEDIMATERIAUX[(1)] et de la chaire industrielle et de recherche ECOSED 4.0.

[1] Démarche Sédimatériaux : démarche nationale d'accompagnement des projets de valorisation des sédiments pilotée par la région des Hauts de France

Des études précédentes ont montré la faisabilité de la valorisation des sédiments dans la fabrication de ciments mais la plupart sont restées au stade laboratoire sans prendre en compte des critères industriels. En outre, la réactivité pouzzolanique du sédiment traité par calcination traditionnelle a été établie antérieurement, mais cette méthode de calcination « traditionnelle » consomme une quantité importante d'énergie. Ceci empêche l'application de cette méthode pour traiter une grande quantité de sédiment notamment à cause de ce coût de traitement. C'est dans ce contexte que la méthode de calcination flash a été étudiée dans le cadre de cette thèse. Fort de ces constats, cette thèse a pour objectif d'étudier et de mettre en place des solutions innovantes de valorisation des sédiments de dragage dans les matrices cimentaires. Pour ce faire, deux axes de recherches sont développés. Le premier concerne la valorisation des sédiments dans le cru en prenant en compte les critères industriels et le second concerne le développement et l'adaptation de la méthode de calcination flash pour la réalisation de liants et d'additions minérales à base de sédiments. Ces deux volets ont pour soubassement une étape initiale de sélection de 07 sédiments de la région des Hauts de France tenant compte de plusieurs critères : importance du gisement, qualité des sédiments, propriétés intrinsèques, etc.

Les travaux de caractérisation des matériaux sont effectués en parallèle par les deux partenaires (EQIOM et IMT). Cela permet in fine de sélectionner les matériaux les plus pertinents et les plus optimaux pour chaque axe de recherche. Ces derniers sont ensuite caractérisés exhaustivement : caractérisation minéralogique, physique, chimique, environnementale.
Les travaux de la thèse contribueront aussi à concevoir, développer et mettre en place une installation semi-industrielle du four de calcination flash permettant le traitement des sédiments. Aussi, l'installation calcination flash a permis de traiter un tonnage suffisant au projet pour réaliser les ouvrages pilotes.

Au-delà des objectifs scientifiques de la thèse, la finalité de ce travail contribuera au développement de nouvelles filières industrielles de valorisation des sédiments de dragage permettant de créer des boucles d'économie circulaire et de créer, à terme, un produit cimentaire à base de sédiment commercialisable et Eco responsable dans le secteur BTP.
Apport scientifique
Les travaux effectués dans cette thèse permettront de résoudre certains verrous scientifiques, techniques et technologiques liés à l'utilisation des sédiments de dragage. En effet, la composition et les propriétés intrinsèques des sédiments, ne les prêtent pas à toute sorte de réutilisation et d'applications. Il peut souvent être nécessaire d'en améliorer les propriétés par traitement adapté.

Les travaux de cette thèse sur l'utilisation de sédiments dans les crus cimentaires permettent de développer de nouveaux liants cimentaires à moindre impact environnemental. Pour cela il faut aussi que ces sédiments aient des caractéristiques notamment chimiques permettant de reconstituer les modules cimentaires (module silicique, alumino-ferrique et facteur de saturation en chaux). Aussi, les travaux menés permettent de monter que des sédiments judicieusement choisis permettent de produire les phases cimentaires adéquatement avec des taux d'incorporation pouvant aller entre 2 et 32 %. La pertinence d'un développement industriel est aussi établie grâce aux essais et production à échelle industrielle réalisés (plusieurs dizaines de tonnes de ciment à base de sédiments produits).

Pour ce qui est du volet flash, le développement de l'unité semi-industrielle permet d'établir des résultats intéressants quant 'à l'optimisation du traitement des sédiments. Ce mode de traitement basé sur une consommation sobre d'énergie, permet de produire des sédiments élaborés et améliorées notamment du point de vue de leur réactivité chimique. Les résultats sur l'optimisation des conditions de traitement constituent un socle intéressant pouvant être

ultérieurement adapté à d'autres matériaux. Cette réactivité est étudiée sous différentes formes notamment par des essais Frattini, Calorimétrie, etc. et montre de réelles potentialités notamment la possibilité de substituer le ciment dans des matrices cimentaires, par ces sédiments flash calcinés à hauteur d'au moins 20%.
Enfin les travaux ont conduit à réaliser des ouvrages pilotes sur la base de ces matériaux. Ces derniers serviront de démonstrateurs et resterons en suivi sur une longue période (1 an) ce qui pourrait sans doute nous apporter des informations importantes à corréler avec nos résultats et notre démarche scientifique.

Les travaux de recherches ainsi réalisés sont présentés dans ce manuscrit est organisé en 2 parties composées de 5 chapitres :

Chapitre 1 : ***État des connaissances***. Dans ce chapitre, nous présentons une revue de littérature relative aux matériaux cimentaires et liants. Les mécanismes de formation des phases principales des clinkers, la composition, la structure de ces phases y ont été détaillées. En outre, l'hydratation du ciment et les hydrates formées au cours du temps sont aussi discutées. Dans ce chapitre nous présentons également, une littérature relative aux sédiments en termes d'origine, de composition, de propriétés intrinsèques, de valorisation, etc. Ainsi que les récentes recherches sur le principe de calcination flash.

Chapitre 2 : ***Valorisation des sédiments dans le cru : Fabrication de ciment portland, étude des performances, analyse et modélisation de l'Hydratation***. Ce chapitre est consacré à l'étude de l'influence de l'incorporation du sédiment sur le cru cimentaire, et donc la production des phases minérales du clinker. Les propriétés du polymorphe et l'influence des sédiments sur les performances mécaniques de la pâte de ciment hydratée est suivie. En outre, différentes méthodes de détermination du degré de l'hydratation ont été évaluées afin de trouver la méthode la plus adaptée. Dans ce chapitre, la cinétique de l'hydratation est modélisée par l'outil CEMHYD3D.

Chapitre 3 : ***Valorisation du sédiment dans le cru – Application dans un projet industriel « SEDICIM »***. Ce chapitre présente les résultats de la valorisation du sédiment dans des crus cimentaires. Des ciments CEM I et CEM III ont été synthétisés au laboratoire à partir des matières premières utilisées chez l'industriel partenaire et intégrant des sédiments à divers taux de substitution. La prise en compte des contraintes industrielles nous a permis de dresser un cahier des charges pour la fabrication du ciment chez l'industriel partenaire. Les méthodes et résultats sont décrits dans ce chapitre sous forme de deux articles.

Chapitre 4 *:* ***Optimisation de la température de calcination flash des sédiments***. Ce chapitre est consacré à l'évaluation de l'effet de calcination Flash sur le sédiment. Les analyses réalisées en pré et post traitement thermique permettent de déterminer une température optimale pour le processus de calcination. Ces analysent comprenant l'évaluation de l'activité chimique des matériaux, l'évaluation de l'impact du traitement sur les propriétés physiques notamment par observation MEB, analyses granulométriques, etc. Mais aussi le suivi des performances mécaniques des mortiers à base des matériaux traités.

Chapitre 5 : ***Hydratation du liant à base de sédiment Flash et impact du taux de substitution sur les performances mécaniques***. Ce chapitre présente l'étude de l'hydratation des liants à base de

sédiments flash calcinés avec différents taux de substitution. La composition chimique et minéralogique des hydrates formés au cours du temps a été étudiée. Ceci permet d'expliquer certains effets bénéfiques du sédiment flash calciné sur le développement de la micro structure et des résistances mécaniques obtenues.

CHAPITRE I : Etat des connaissances

I. Les sédiments et leurs problématiques de gestion et de valorisation

La valorisation des sédiments requiert de résoudre de multiples problématiques notamment liées à leurs compositions ainsi que les problématiques de gestion et de valorisation des sédiments.

I.1. Origine et composition des sédiments

I.1.1. Définition des sédiments

Le terme de sédiment a plusieurs définitions. Selon YANNICK [2], le sédiment est un dépôt de matériaux détritiques minéraux et organiques. BOUTIN [3] a donné la définition des sédiments comme correspondant à des particules fines minérales avec quelques petits éléments des roches auxquels sont mélangés des débris d'origine végétale ou animale. En outre, selon BEAUCHAMP [4], le sédiment peut être défini comme un état des matériaux fines issus de l'usure des continents. Ces actions d'usure sont d'origine des phénomènes physiques (fragmentation) ou chimique (lessivage). Sous l'effet du vent et des courants de l'eau, ces particules sont transportées et déposées.

I.1.2. Origine des sédiments

Les sédiments peuvent avoir des caractéristiques diverses qui dépendent de leur origine et nature. Selon SCHNEIDER [5], les sédiments peuvent être distingués par l'origine endogène et exogène. L'origine endogène est interne au milieu, en générale, est débris végétaux et animaux. Par contre, l'origine exogène est le produit d'un apport externe (des matières d'origine naturelle : érosion des sols, décomposition des matières animales ou végétales ou anthropique : apport de matière en suspension, de matières organiques, de nutriments, de micropolluants en raison des rejets agricoles, industriels et domestiques) au milieu immédiatement voisin.
En outre, BEAUCHAMP [4] a proposé la définition selon l'origine physique ou chimique :

- Les roches sédimentaires détritiques proviennent de la destruction de roches ou d'organismes : cailloutis, sables, grès.
- Les roches sédimentaires chimiquement issues des précipitations des corps dissous dans l'eau : sel gemme (roche saline à base de K_2CO_3), tufs calcaires, silex.
- Les roches sédimentaires biochimiques proviennent de l'activité synthétique des organismes : charbons, tuf calcaire continental (roche calcaire continental).

I.1.3. Granulométrie des sédiments

La granulométrie et la composition physico-chimique sont les paramètres essentiels pour la caractérisation des sédiments. Selon, SCHNEIDER [5], un sédiment se caractérise essentiellement par :

- Sa granulométrie.
- Sa composition minérale.
- Sa teneur en eau, en matières organiques et des éléments divers (métaux lourds, polluants et micropolluants).

La granulométrie des sédiments se compose essentiellement d'une partie minérale grossière (fraction sableuse) et d'une partie fine (fraction de la vase) [6].

- La fraction grossière des sédiments dont le diamètre supérieur à 63 µm se compose essentiellement de sables et de matières inorganiques silicatés. Les sédiments sableux ont une faible cohésion, une petite surface de contact entre les différentes particules du sédiment et peu d'affinité aux contaminants [7].

- La fraction fine des sédiments dont le diamètre inférieur 63µm, est constituée essentiellement de l'argile ayant un diamètre compris entre 0.2 µm et 2 µm, de silt ayant un diamètre compris entre 2µm et 63µm. Cette fraction fine contient généralement des argiles et des matières organiques [8].

La granulométrie du sédiment a un rôle majeur dans la capacité de fixation des contaminants ce qui permet d'avoir les solutions de traitement adaptées avec les différents sédiments. En effet, Gosselin et al [9] ont réalisé leur étude sur les sédiments de Hambourg et Montréal, leurs résultats ont montré que la contamination des particules grossières est quasiment nulle pendant que la fraction fine cumulait plus de 70% de contamination.

I.1.4. Composition des sédiments

Les études précédentes [10, 11] montre que les sédiments sont une matrice très hétérogène qui se compose essentiellement de l'eau, des matériaux détritiques inorganiques, et des matières organiques (Figure 1-25).

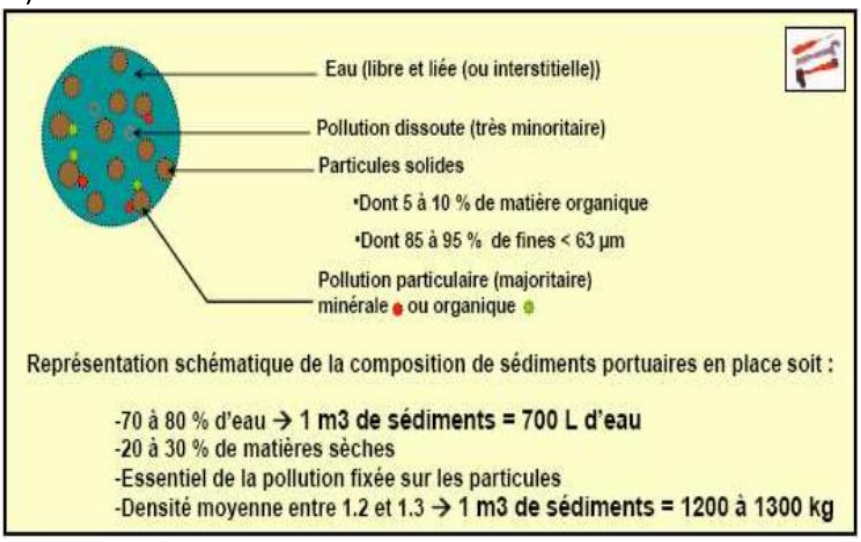

Figure 1- 1 : Composition simplifiée d'un sédiment [11].

- **Eau interstitielle des sédiments :**

L'eau interstitielle est une fraction importante (généralement de 70 à 80% de volume) dans les sédiments. Elle occupe l'espace entre les particules des sédiments.

- **Matériaux inorganiques :**

Ils sont constitués des minéraux provenant principalement de l'érosion terrestre et des débris coquilliers. Les carbonates, les silicates et les argiles sont les composants inorganiques majeurs. Ils ont aussi la taille très variable allant de la fraction colloïdale à la fraction sableuse. Les silicates sont des groupements chimiques anioniques très stables dont la structure est basée sur des tétraèdres de $[SiO_4]^{4-}$. Les argiles sont des silicates d'aluminium hydraté ayant une structure en feuillet une capacité de gonflement très importante [12, 13].

Les carbonates qui se trouvent dans le sédiment sont pour la plupart des calcites ($CaCO_3$) et potentiellement de la magnésite ($MgCO_3$), de la dolomite ($CaCO_3.MgCO_3$), du carbonate de sodium ($Na_2CO_3.10H_2O$) et de la sidérite (Fe_2CO_3) [14]. En outre, les particules inorganiques sont généralement enrobées par l'hydroxyde de fer, de manganèse et de substances organiques qui leur donne une grande capacité d'adsorption vis-à-vis des contaminants minéraux et organiques [2].

Le tableau 1-1 présente les principaux minéraux dans les sédiments.

Tableau 1- 1 : Principaux minéraux dans les sédiments [15]

Groupe de minéraux	Minéraux	Formule chimique
SILICATES	Quartz	SiO_2
	Mica	$K(Mg,Fe,Al)_3AlSi_3O_{10}(OH)_2$
	Feldspath	$(Na, Ca, K)AlSi_3O_8$
	Amphibole	$(Ca, Mg, Fe, Al)_3Si_4O_{11}(OH)$
	Pyroxène	$(Ca, Mg, Fe)_2Si_2O_6$
ARGILES	Illite	$KMgAl_2Si_3O_{10}(OH)_2$
	Smectite (montmorillonite)	$XMgAlSiO_{10}(OH)_2$
	Chlorite	$Mg_5Al_2Si_3O_{10}(OH)_8$
	Kaolinite	$Al_3Si_2O_5(OH)_4$
CARBONATES	Calcites	$CaCO_3$
	Dolomite	$CaMgCO_3$
	Sidérite	$FeCO_3$
(HYDR)OXYDE DE FER	Goethite	FeOOH
	Magnétite	Fe_3O_4
PHOSPHATES	Apatite	$Ca_5(PO_4)_3(OH,F)$
	Vivianite	$Fe_3(PO_4)_2.8H_2O$
SULFURE	Pyrite	FeS_2

- **Matières organiques :**

La fraction organique associe des composants organiques simples et complexes, isolés ou associés entre eux dans des ensembles vivants ou non vivants [14]. En outre, selon Mustin [16], les matières organiques se composent des 4 classes suivantes :

- La matière vivante (biomasse active)
- La matière organique fraiche (débris végétaux, cadavre, excrément…)
- Les composés en cours d'évolution dits transitoires.
- Les composés organiques stabilisés, appelés communément humus.

D'après Schneider [5], la proportion de matières organiques dans la matière sèche des sédiments est très variable, 90% dans le cas de la tourbe, et 2% pour les sables rivières. En général, la proportion des matières organiques dans les sédiments des cours d'eaux vives est de l'ordre de 2 à 10%.

La présence des matières organiques présente le risque de modification des caractéristiques géotechniques du sol à cause de l'interaction entre eux et les fractions minérales [17]. En effet, certains éléments minéraux (éléments traces métalliques) et la fraction organique (HAP, TBT…) sont considérés comme des contaminants.

I.2. Les contaminants inorganiques et organométalliques

Selon Le Hecho [18], les contaminants inorganiques dans les sédiments sont :

- Les métaux
- Certains sels (sulfates, phosphates, nitrates, chlorures et ammonium)
- Les cyanures

Les métaux lourds dans les sédiments peuvent avoir comme origine l'érosion des roches, des sols où ils sont naturellement présents, mais principalement des activités humaines. Certains éléments entre eux sont essentiels pour les organismes vivants à l'état de trace par exemple : Ti,

V, Cr, Mn, Fe, Co, Ni, Cu, Zn, As, Mo, Sn et Sb) mais ils deviennent toxiques à forte dose [19] . Par contre, les éléments comme Pd, Ag, Cd, Au, Hg et Pd, sont toxiques pour les organismes vivants même à une faible dose [19].

I.3. Les contaminants organiques

Les polluants organiques dans les sédiments sont essentiellement suivants [20] :

- Les hydrocarbures aromatiques polycycliques (HAP), issus de la biosynthèse et de la pyrolyse de la matière organique. Ces hydrocarrbures proviennent essentiellement des carburants fossiles.
- Les polychlorobiphényles (PCB), utilisés avant la fin des années 90 comme additifs dans les peintures, les encres, les apprêts pour les revêtements muraux.
- Le tributylétain (TBT), matières actives des anciennes peintures antisalissures pour la protection des navires.

L'adsorption des composés organiques dépend des facteurs suivants :

- Le carbone organique : avec la présence du carbone organique, l'adsorption des contaminants organiques dont les molécules organiques ne sont pas dissociées, est possible.
- La température : plus la température est élevée, plus l'adsorption estplus faible.
- L'acidité : le pH du milieu affecte légèrement les composés organiques non associés.
- La salinité : une légère augmentation de l'adsorption est observée avec l'augmentation de concentration en sels.
- La texture : le pourcentage des matières organiques influence la variation de l'adsorption en fonction de la granulométrie.
- La contamination par l'huile : l'adsorption des contaminants hydrophobes peut se faire préférentiellement dans la fraction huileuse.

Les molécules organiques ont des cibles et des effets plus ou moins spécifiques et très variables. Elles peuvent être génotoxiques (HAP), neurotoxiques (pesticides chlorés, organophosphorés et carbamates), inhibitrices de la croissance ou de la reproduction (TBT, médicaments). Selon Bonnet [15], en générale, les formes non ionisées sont plus toxiques que les formes ionisées car elles peuvent pénétrer plus facilement à travers les membranes cellulaires par transport passif au travers de la bicouche lipidique.

I.4. Interaction entre les sédiments et les contaminants

D'après Calmano et al [21] ; Chapman et al [22], les trois compartiments des sédiments (eau interstitielle, compartiment minéral et organique) ont les affinités variables pour les contaminants. En effet, les études précédentes sur l'interaction entre les polluants et les matériaux ont montré que les contaminants ont la tendance de se fixer sur la fraction fine.

La répartition des contaminants dans les sédiments est contrôlée par les processus physico-chimique et biologique [2] (Figure 1-2). Les polluants peuvent exister dans l'eau interstitielle sous la forme dissoute ou complexée des éléments inorganiques ou des molécules.

Pour les polluants associés au compartiment solide, ils peuvent être transférés dans la phase aqueuse sous l'effet de processus physique (diffusion) ou chimique (désorption). En effet, selon

Luoma et al [19] les organismes vivants peuvent modifier les caractéristiques physico-chimiques du milieu (bioturbation, biodégradation) et accumuler des polluants à partir des phases aqueuses et particulaires par adsorption ainsi que transférer les contaminants dans la chaîne alimentaire.
La répartition des contaminants de la forme dissoute à la forme colloïdale ou particulaire dépend des conditions hydrodynamiques, des paramètres physico-chimiques du milieu (pH, salinité, potentiel rédox) des constituants (particules inorganiques ou organiques, sulfures, oxydes de fer et de manganèse) et de l'activité biologique (activité bactérienne, bioturbation, dégradation…) [10], [15, 23].
En conclusion, les polluants et particules fines minérales etles molécules organiques ont un lien strict, ce qui entraine des difficultés dans la valorisation des sédiments car il faut avoir des solutions pour éliminer les polluants tout en évitant les risques environnementaux.

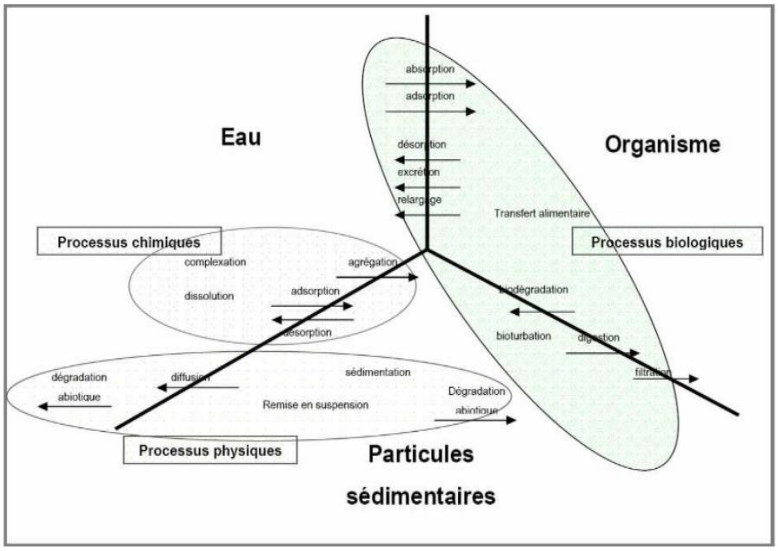

Figure 1- 2 : Les principaux processus contrôlant le cycle des contaminants dans le milieu aquatique [23]

I.5. Problématique des sédiments de dragage

La gestion des sédiments de dragage est de plus en plus importante dans la méthodologie de gestion des ports. Ceci doit permettre d'aider les ports à évacuer ces matériaux en prenant en compte des critères économiques et environnementaux qui sont fixés par les gestionnaires et les décideurs (État, Région…).

I.5.1. Contexte législatif

L'immersion des sédiments en mer peut provoquer des impacts environnementaux locaux ou régionaux. Par conséquence, depuis trente ans, les activités d'immersion vis-à-vis de la protection du milieu marin doivent respecter plusieurs accordsnotamment :

- La convention de Londres (prévention de la pollution des mers résultant de l'immersion des déchets, 1972).
- La convention d'Helsinki (convention de protection de l'environnement marin de la mer Baltique, 1974).
- La convention de Barcelone (convention de Barcelone pour la protection de la mer Méditerranée contre la pollution et pour le développement durable, 1976)

Malgré plusieurs conventions internationales sur les gestions des sédiments et la directive relative aux déchets dangereux, ces textes ne fixent pas des seuils qui permettent de déterminer le degré de pollution des sédiments ainsi d'avoir le choix plus adapté dans la valorisation [Bel-Hadj-Ali 2013]. Certains pays et régions ont donnés les seuils de référence comme : France : GEODE, 1996 ; Royaume – Uni : HKWB, 2000, Canada : CCME, 1999 ; Etats – Unis : US EPA et ACOE, 1998) pour la réglementation des activités de déposition des sédiments.

I.5.2. Présentation de référentiel français GEODE

En France, le Groupe d'Étude et d'Observation de Dragage et l'Environnement (GEODE) a été créé en 1990 par la Direction des Ports et de la navigation maritime. Il a proposé le référentiel français de dragage qui a été présenté dans l'arrêté du 14 juin 2000.

- L'arrêté du 14 juin 2000 relatif aux niveaux référence à prendre en compte lors d'une analyse de sédiment marins ou estuariens présents en milieu naturel ou portuaire est publié officiellement le 10 aout 2000. Ce texte fixe les seuils de contamination à partir desquels l'incidence des opérations sur le milieu doit être appréciée. Les valeurs présentées dans le tableau sont les valeurs retenues dans ce texte et peuvent être susceptibles d'être modifiées ou complétées en fonction de l'évolution de connaissances. L'arrêté du 14 juin 2000 a défini les deux valeurs référentielles des seuils de contamination (N1, N2) pour les teneurs en composés chimiques (actuellement métaux et PCB).
- Le niveau 1 (N1) : Si les valeurs de la teneur des contaminants sont au-dessous des valeurs du niveau N1, les opérations de dragage et d'immersion seraient autorisées sans autres études : l'impact potentiel est jugé neutre ou négligeable, les valeurs observées se relèvent comparables aux « bruits de fond » environnementaux.
- Le niveau 2 (N2) : Si les valeurs de la teneur des contaminants sont au-dessus des valeurs du niveau N2, les opérations de dragage et d'immersion en mer sont susceptibles d'être interdites car cette interdiction est une solution de gestion la moins dommageable pour l'environnement : une investigation complémentaire est généralement nécessaire car des indices notables laissent présager un impact potentiel négatif de l'opération.
- Si les valeurs de la teneur des contaminants sont entre les valeurs N1 et N2, une investigation complémentaire est généralement nécessaire en fonction du projet considéré et du degré du dépassement du seuil N1.

Les arrêtés du 9 août 2006, du 23 décembre 2009 et du 23 février 2013 ont complété le précédent (en fonction de l'évolution des connaissances scientifiques et techniques), et établi des nouveaux tableaux de référence qui définissent des valeurs des seuils pour les contaminants des éléments traces, des composés de traces et des hydrocarbures aromatiques polycycliques (tableaux 1-2, 1-3 et 1-4).

Tableau 1- 2 : Les seuils relatifs aux éléments traces métalliques (en $mg.kg^{-1}$ de sédiment sec analysé sur la fraction inférieure à 2mm).

Éléments traces	Niveau N1	Niveau N2
	(mg/kg)	

Arsenic	As	25	50
Cadmium	Cd	1,2	2,4
Chrome	Cr	90	180
Cuivre	Cu	45	90
Nickel	Ni	37	74
Plomb	Pb	100	200
Zinc	Zn	276	552
Mercure	Hg	0,4	0,8

Tableau 1- 3 : Les seuils relatifs aux composés traces (en mg/kg de sédiment sec analysé sur la fraction inférieure à 2mm).

PCB	Niveau N1	Niveau N2
	(mg/kg)	
PCB congénère 28	0,025	0,05
PCB congénère 52	0,025	0,05
PCB congénère 101	0,05	0,1
PCB congénère 118	0,025	0,05
PCB congénère 138	0,05	0,1
PCB congénère 153	0,05	0,1
PCB congénère 180	0,025	0,05
PCB totaux	0,5	1
TBT	0,1	0,4

Tableau 1- 4 : Les seuils relatifs aux hydrocarbures aromatiques polycycliques (HAP) (en µg/kg de sédiment sec analysé sur la fraction inférieure à 2mm).

HAP	Niveau N1	Niveau N2
	(µg/kg)	
Naphtalène	160	1130
Acénaphtène	15	260
Acénaphtylène	40	340
Fluorène	20	280

Anthracène	85	590
Phénanthrène	240	870
Fluoranthène	600	2850
Pyrène	500	1500
Benzo[a] anthracène	260	930
Chrysène	380	1590
Benzo[b] fluoranthène	400	900
Benzo[k] fluoranthène	200	400
Benzo [a] pyrène	430	1015
Di benzo [a,h] anthracène	60	160
Benzo [g,h,i] pérylène	1700	5650
Indéno [1,2,3-cd] pyrène	1700	5650

En conclusion, il faut mener une étude spécifique sur la sensibilité du milieu aux substances concernées avec au moins un test de lixiviation sur la toxicité globale du sédiment et une évaluation de l'impact prévisible sur le milieu.

I.5.3. Gestion et valorisation des sédiments

Selon L'Yavanc [24], en France, chaque année, en moyenne 50 millions de mètres cubes des sédiments sont dragués. Les volumes les plus importants des sédiments dragués se concentrent dans les grands ports. En 2011, les sept grands ports Maritimes (Dunkerque, La Havre, Rouen, Nantes, La Rochelles, Bordeaux, Marseille) ont compté à eux environ 88% du volume total [25]. Les trois principaux ports d'estuaires (Rouen, Nantes – Saint – Nazaire et Bordeaux) représentent annuellement en moyenne 25 millions de mètres cubes des sédiments dont 6,5 millions de mètres cubes de sables et 9,3 millions de mètres cubes de vases clapées. Les cinq grands ports maritimes (Dunkerque, Calais, Boulogne, La Havre et la Rochelle) draguent un volume moyen annuel de 6,2 millions de mètres cubes des sédiments qui se compose d'environ 20% de sables et 80% de vase.

Les sédiments, selon leur degré de pollution (teneur en métaux lourds, hydrocarbures : HAP, PCB,…), peuvent être considérés comme des déchets et posent des problèmes pour leur gestion [26].

- **Gestion des sédiments de dragage**

Dans le cas de non immersion (les concentrations des contaminants supérieures par rapport au seuil N2), il faut déposer les sédiments dans des zones de stockage, de manière permanente pour la part ultime, ou de manière temporaire dans le cadre du processus industriel de réutilisation des sédiments.

En effet, la classification européenne des déchets, en vigueur depuis 2002, a établi des critères d'admission relatifs aux déchets au centre de stockage des déchets (CsD) à partir des essais de lixiviation et de percolation (Conseil européen, 2002). Les déchets sont classés en fonction des

niveaux de concentration des contaminants dans les eaux de lixiviation et de percolation. Ils peuvent avoir les trois catégories suivantes :

- Déchets inertes (classe III) : tout déchet qui ne subit aucune modification physique, chimique ou biologique importante, qui ne se décompose pas, ne brûle pas, ne produit aucune réaction physique ou chimique, n'est pas biodégradable et ne détériore pas les matières avec lesquelles il entre en contact d'une manière susceptible d'entraîner des atteintes à l'environnement ou à la santé.
- Déchets non dangereux (classe II) : les déchets non inertes, non dangereux sont anciennement appelés les déchets industriels banals (DIB). Ils ne sont ni inertes, ni dangereux pour l'environnement ou la santé.
- Déchets dangereux (classe I) : Les déchets dangereux sont anciennement appelés des déchets industriels spéciaux (DIS) et contiennent des substances dangereuses pour l'environnement ou la santé.

Les valeurs limites des polluants sont présentées dans le tableau en $mg.kg^{-1}$ de matériau sec pour deux rapports Liquide/Solide (L/S : rapport entre la quantité de liquide (en litre) et de solide (en kilogramme). Par ailleurs, pour les déchets de catégorie de classe III, s'ajoutent aux valeurs seuils sur les lixiviats, des concentrations limites sur le matériau brut.

Tableau 1- 5 : Valeurs limites d'acceptation des déchets en ISDI, ISDND et ISDD

Composant	Valeurs seuils dans les lixiviats pour l'acceptation en CsD.									
	Classe III			Classe II			Classe I			
	L/S = 2L/Kg	L/S = 10L/Kg	CO percolation	L/S = 2L/Kg	L/S = 10L/Kg	CO percolation	Mâchefers L/S = 10 L/Kg	L/S = 2L/Kg	L/S = 10L/Kg	CO percolation
As	0,1	0,5	0,06	0,4	2	0,3	0,6	6	25	3
Ba	7	20	4	30	100	20	56	100	300	60
Cd	0,03	0,04	0,02	0,6	1	0,3	0,05	3	5	1,7
Cr total	0,2	0,5	0,1	4	10	2,5	2	25	70	15
Cu	0,9	2	0,6	25	50	30	50	50	100	60
Hg	0,003	0,01	0,002	0,05	0,2	0,03	0,01	0,5	2	0,3
Mo	0,3	0,5	0,2	5	10	3,5	5,6	20	30	10
Ni	0,2	0,4	0,12	5	10	3	0,5	20	40	12
Pb	0,2	0,5	0,15	5	10	3	1,6	25	50	15
Sb	0,02	0,06	0,1	0,2	0,7	0,15	0,7	2	5	1
Se	0,06	0,1	0,04	0,3	0,5	0,2	0,1	4	7	3
Zn	2	4	1,2	25	50	15	50	90	200	60
Chlorures	550	800	460	10000	15000	8500	10000	17000	25000	15000
Fluorures	4	10	2,5	60	150	40	60	200	500	120
Sulfates	560	1000	1500	10000	20000	7000	10000	25000	50000	17000

Phénols	0,5	1	0,3	/	/	/	/	/	/	/
COT sur éluats	240	500	160	380	800	250	800	480	1000	320
Fraction soluble	2500	4000	/	40000	60000	/	60000	70000	100000	/

- **Valorisation des sédiments de dragage**

Plusieurs filières de traitement et de valorisation sont étudiées et appliquées dans plusieurs domaines de génie civil. Nous pouvons citer ci-dessous certains domaines de valorisation des sédiments :

- Valorisation en technique routière en tant que couche de base ou couche de forme [27], [28–31]
- Fabrication des granulats artificiels [32, 33]
- Secteur briqueterie [34–36]
- Addition minérales [26, 37, 38]
- Matières premières dans la fabrication du ciment [36, 39]

II. Ciment : de la fabrication à l'hydratation

II.1. Définition, Histoire et Chiffres clés

Le ciment est le constituant principale du béton et le matériaux de construction le plus utilisé dans le monde [39]. Selon la norme européenne NF EN 197-1 [40], le ciment est un liant hydraulique, c'est -à-dire un matériau minéral finement moulu qui, gâché avec de l'eau, forme une pâte qui fait prise et durcit par suite de réaction et de processus d'hydratation et qui, après durcissement, conserve sa résistance et sa stabilité même sous l'eau.

Le ciment Portland a été inventé la première fois en 1824 en faisant une cuisson d'un mélange de calcaire et d'argile à 1200 °C [41]. Depuis le jour-là, les techniques de fabrication et les performances n'ont cessé de s'améliorer. En effet, la température proposée par Aspdin était plus faible que celle utilisée aujourd'hui dans l'industrie cimentaire (1450 °C). Comparant au premier liant hydraulique, l'utilisation d'une température de cuisson plus élevée permet une réduction du temps de calcination ainsi qu'une maitrise accrue de la prise et des résistances mécaniques développées par le liant [42].

La France se trouve comme 20ème producteur mondial de ciment avec une production de clinker de 14.2 Mt en 2012 et de 18 Mt de ciment. La France est également le premier producteur du ciment Portland en Europe.

II.2. Procédé cimentier

Le clinker, le constituant principal du ciment Portland est obtenu par la calcination, à haute température (1450 °C) dans un four rotatif, d'un mélange finement broyé composé de roches calcaires (80%) et d'argiles (20%) appelé le cru. Une fois le mélange cuit, il subit un refroidissement brutal à l'air (tremple) pour obtenir le clinker [43]. Le clinker se compose principalement de 4 phases minérales : l'alite (C_3S), la bélite (C_2S), l'aluminate de calcium (C_3A) et le ferro-aluminate de calcium (C_4AF). Le tableau 1-6 présente la formule chimique et la teneur des 4 phases minérales principales du clinker [44]

Tableau 1- 6 : Formule chimique et teneur des 4 phases minérales du clinker

Phase minérale	Nomenclature	Formule chimique	Teneur minimale (wt%)	Teneur maximale (wt%)	Teneur moyenne (wt %)
Alite	C_3S	Ca_3SiO_5	45.0	79.7	62
Bélite	C_2S	Ca_2SiO_4	5.7	29.8	22
Tricalcium aluminate	C_3A	$Ca_3Al_2O_5$	1.1	14.9	8
Alumino-tetracalcium ferrite	C_4AF	$Ca_4Al_2Fe_2O_{10}$	2.0	16.5	8

Généralement, le procédé cimentier se compose des 3 étapes principales suivantes :

- La préparation des matières premières.
- La cuisson du mélange (cru) aboutissant à la synthèse du clinker.
- Le broyage et l'ajout de constituant secondaire et le conditionnement du ciment.

II.2.1. Préparation des matières premières

Les matières premières telles que les roches de calcaires et d'argiles sont extraites des carrières naturelles. Elles se constituent des oxydes tels que CaO, SiO2, Al_2O_3 et Fe_2O_3 qui sont nécessaires à la fabrication du ciment. Le cru est finement broyé et homogénéisé afin de favoriser les

réactions chimiques entre les différents constituants lors de la cuisson. Actuellement, il existe 4 voies de préparation du mélange de cru [45].

- **La voie humide :** C'est la méthode la plus ancienne. Le principe est basé sur le mélange des calcaires et des argiles préalablement broyés avec une teneur en eau qui varie entre 25 et 40% de sorte à obtenir une pâte humide. Ensuite, cette pâte est directement injectée dans le four. Par conséquence, cette méthode provoque uneune importante consommation de quantité d'énergie pour éliminer l'eau excédentaire.
- **La voie semi-humide** : La préparation du mélange cru par la voie semi – humide est exactement la même que celle de la voie humique décrite ci-dessus. Cependant, le taux d'humidité n'excède pas les 15 % environ.
- **La voie sèche :** Le principe de cette méthode consiste à homogénéiser les matières premières préalablement broyées de sorte à obtenir un mélange des poudres pulvérulentes. Avant l'injection dans le four, le mélange est transporté dans une tour de préchauffage à cyclones. Des gaz circulant à sens inverse dans les cyclones, réchauffent la poudre. La température peut atteindre 800 °C et permet de perdre une partie de CO_2 et de l'eau contenue dans le mélange. La poudre est ensuite injectée dans le four. La figure 1 - 3 illustre le processus de la voie sèche [46].

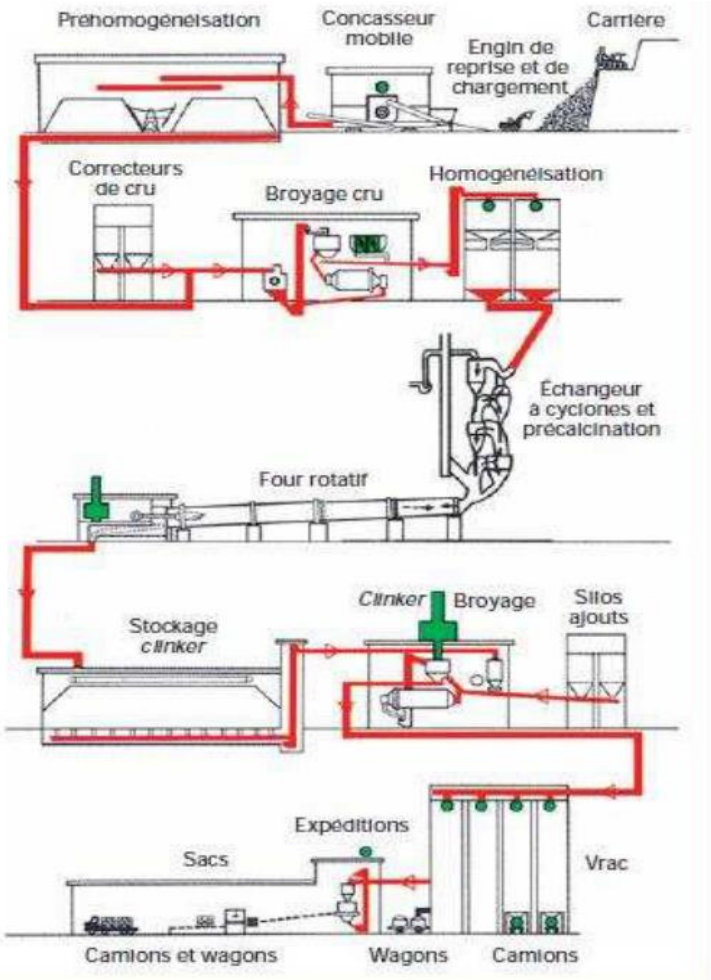

Figure 1- 3 Procédé cimentierpar voie sèche

- **La voie semi- sèche :** Le principe de cette méthode consiste à humidifier le mélange des matières premières préalablement broyées (son taux d'humidité est de 12% environ) afin d'obtenir des granules plus ou moins sphériques de 10 à 20 mm. Cette forme permet de favoriser l'écoulement des matières dans le four. Ces granules sont transportés vers une chambre de préchauffage, puis vers le four.

La voie sèche et la voie semi – sèche sont deux méthodes de préparation les plus utilisées dans l'industrie cimentaire grâce à leur consommation d'énergie la plus faible.
Les constituants sont dosés pour obtenir une composition régulière du ciment. Le tableau 1-7 donne la composition chimique en éléments majeurs recherchée pour un cru d'après CIMBETON.

Tableau 1- 7 : Composition chimique du cru (en % massique sur le mélange cru calciné)

Oxydes (% wt.)	CaO	SiO_2	Al_2O_3	Fe_2O_3
	65-70	18-24	4-8	1-6

Dans l'industrie cimentière, le dosage des constituants du mélange cru s'effectue à l'aide des modules suivants :

- **Lime Saturation Factor (LSF) :** La valeur LSF est calculée selon l'équation suivante :

$$LSF = \frac{100 * \%CaO}{2.8 * \%SiO2 + 1.18 * \%Al2O3 + 065 * \%Fe2O3}$$

Ce paramètre permet de déterminer la teneur optimale en chaux du cru afin d'obtenir la quantité souhaitée des phases silicates, et plus particulièrement en C_3S. Il permet également de contrôler le rapport entre les quantités de C_3S et C_2S comme indiqué dans la figure 1 - 4 [47], ainsi que la teneur en chaux libre du clinker. En général, la teneur en chaux libre du clinker est inférieure à 2% [36], par conséquent, la valeur LSF varie entre 95 et 97% [43].

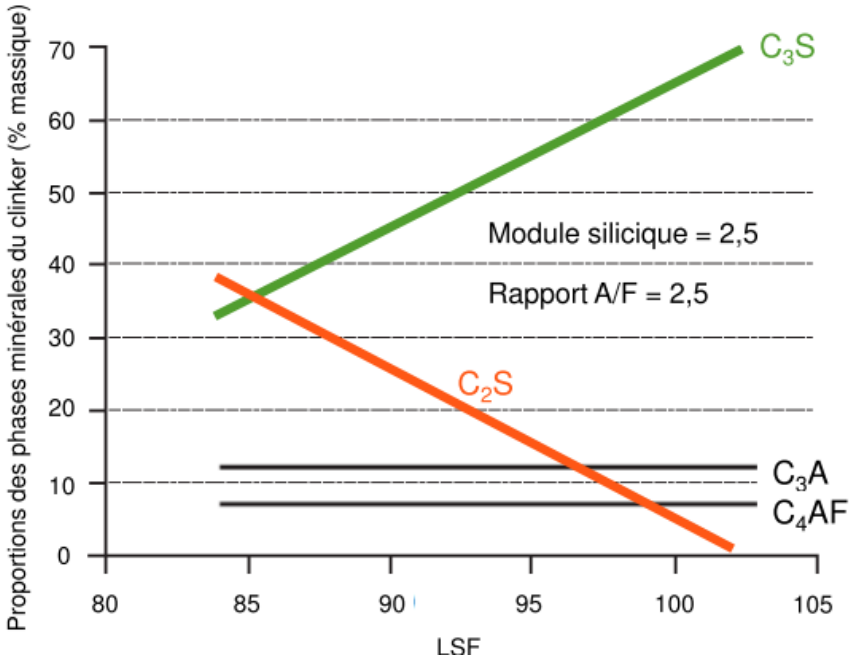

Figure 1- 4 Évolution des phases silicates en fonction de la valeur LSF

En outre, en présence de MgO, la valeur LSF s'écrit de la matière suivante :

$$LSF = \frac{100 * (\%CaO + 0.75\ MgO)}{2.8 * \%SiO2 + 1.18 * \%Al2O3 + 065 * \%Fe2O3}$$

- **Silica Ratio (SR) :** La valeur SR peut être calculée selon l'équation suivante :

$$SR = \frac{\%SiO2}{\%Al2O3 + \%Fe2O3}$$

Le module silicique (SR) permet de contrôler la proportion des phases silicatées dans le mélange par rapport aux phases interstitielles alumineuses et ferreuses. Ceci joue un rôle

important dans la facilité à cuire le mélange. Plus la valeur SR est élevée, plus c'est difficile à cuire le mélange du fait de richesse en silice et du faible teneur en liquide assurant les processus de diffusion à l'origine des réactions solide – liquide et liquide – liquide. Dans le cas du ciment Portland, la valeur SR est comprise entre 2 et 2.5.

- **Alumina Ratio (AR) :** Le module AR peut être calculé selon l'équation suivante :

$$AR = \frac{\%Al2O3}{\%Fe2O3}$$

Ce paramètre contrôle essentiellement la viscosité de la phase liquide ainsi que la vitesse de formation de la phase C_3A jusqu'à la température de 1338 °C. En effet, un rapport AR de 1.38 est connu pour maximiser le pourcentage de phase liquide à 1338 °C [44], et par conséquence, être favorable aux transformations chimiques pour lesquels, la présence d'une phase liquide est nécessaire. Cependant, la teneur en C_3A dans le clinker doit être limité, notamment pour la résistance vis-à-vis des sulfates [48].

Les gammes de valeurs des modules (LSF, SR, AR) pour le clinker Portland sont définies avec des variations selon différentes études présentées dans le tableau 1-8.

Tableau 1- 8 : Gammes de valeurs des modules pour le clinker

Module	Taylor [44]	Locher [49]
LSF	92 - 98	90 – 104
SR	2.0 – 3.0	1.6 – 4.1
AR	1.0 – 4.0	1.4 – 3.7

II.2.2. Cuisson du mélange cru

Après avoir été finement broyé et homogénéisé, le cru est transporté à une tour de préchauffage à cyclones où il est préchauffé à 800 °C. Cette étape permet d'éliminer l'eau dans le cru et d'éviter un choc thermique à son entrée dans le four. Ensuite, le cru est envoyé dans un four cylindrique, rotatif, et légèrement incliné dans lequel il va descendre grâce à sa gravité. Les matières sont chauffées progressivement par les gaz chauds circulant à contre courante jusqu'à atteindre la température de 1450 °C (la température de clinkérisation). Les matières sont cuites pendant environ 10 minutes à cette température. A la sortie du four, les nodules de clinker passent au travers d'un refroidisseur où leur température diminue rapidement jusqu'à atteindre la température ambiante. Ce processus de refroidissement est plus connu sous le nom de 'trempe'. Ce refroidissement joue un rôle important car il permet la stabilisation à la température ambiante des phases plus stables à hautes températures et d'empêcher la décomposition de l'alite en bélite et chaux libre [50]. Il existe trois types différents de refroidissement : le refroidissement au ballonnet, le refroidissement rotatif et le refroidissement à grille. Un ensemble complexe du processus physico – chimique se produit dans le four lors de la cuisson des matières est illustré dans la figure 1-5. Cependant, la transformation des matières dans le procédé cimentier peut être distinguée en trois phases.

- **En dessous de 1300 °C :**
  La décomposition des matières premières commence dès 600 °C. La décomposition de calcite pour donner de la chaux (CaO) et du CO_2 se produit entre 600 °C et 800 °C. En parallèle, les argiles se décomposent en oxydes libres telles que SiO_2, Al_2O_3, Fe_2O_3. Par conséquence, la bélite, les aluminates et les ferrites de calcium commencent à se former. À partir de 1300 °C, la bélite et la chaux libre sont partiellement dissoutes.
- **Entre 1300 °C et 1450 °C :**

A cet intervalle de température, la bélite et la chaux libre résiduelle réagissent pour former l'alite. Durant la cuisson, l'alite et la bélite continue de croître, ceci provoque un phénomène appelé 'cannibalisme' de la bélite par l'alite.

- **Refroidissement rapide :**
  En sortie du four, le clinker subit une trempe à l'air qui permet de diminuer rapidement sa température vers 100 °C. Ce changement rapide de température permet ainsi de stabiliser à la température ambiante les polymorphes des minéraux présents à hautes températures et de précipiter la phase interstitielle qui se forme autour des grains d'alite et de bélite [44].

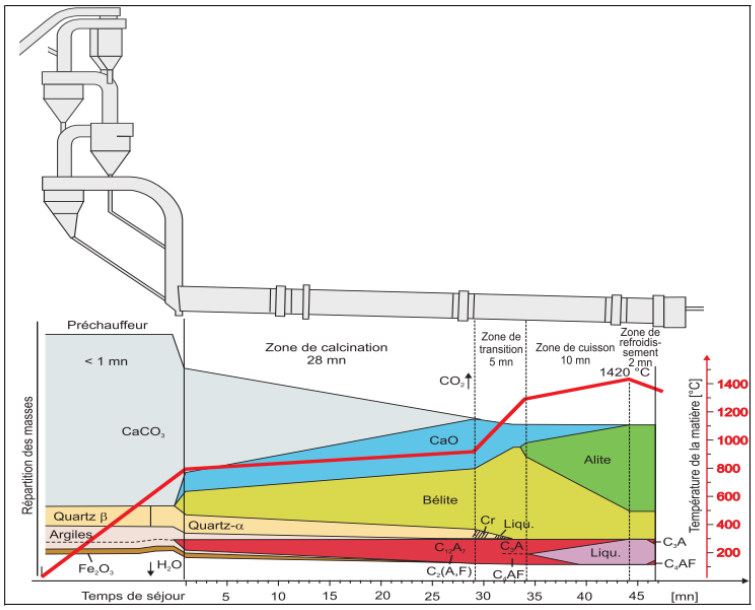

Figure 1- 5 : Transformation physico – chimique dans le four en fonction de la température [51]

II.2.3. Broyageet l'ajout de constituant secondaire et le conditionnement du ciment

Après avoir effectué le refroidissement, le clinker est finement broyé et des constituants secondaires sont ajoutés. En effet, la réactivité du ciment est optimale lorsque sa granulométrie est inférieure à 30 µm [52]. Le broyage peut être effectué selon deux procédés. Le premier procédé s'effectue en circuit ouvert dans lequel le réglage de la finesse est obtenu en ajustant le débit d'alimentation. Le deuxième procédé est de réaliser le broyage en circuit fermé où les particules insuffisamment broyées sont récupérées à l'aide d'un séparateur dynamique et renvoyées vers l'entrée du broyeur [43].
La variété de la nature et du taux d'induction des composants dans la formulation permet de proposer des divers types de ciments. La norme NF EN 197-1 [40] contient les notations utilisées pour les différents constituants du ciment qui sont décrits par la suite.

- **Clinker (K)** : le constituant de base du ciment. Il se forme à partir de la calcination à haute température de cru. Il est présent dans la composition de tous les ciments courants.
- **Laitier de haut fourneau (S) :** Le laitier de haut-fourneau est un sous-produit de l'industrie sidérurgique, et obtenu dans les hauts fourneaux lors de la fabrication de fonte. En effet, la production d'acier a pour étape essentielle le traitement thermique du minerai de fer à des températures comprises entre 1350 et 1550 °C. Après des heures, la fonte est récupérée en partie basse du haut-fourneau avec le laitier surnageant. Le laitier se sépare de la fonte en base grâce à la différence de densité. La technique de trempe à l'eau permet de figer le laitier sous la forme d'une phase non (ou peu) cristallisée. Le laitier sous la forme vitrifiée est utilisé comme addition minérale dans le ciment. La composition chimique du laitier est riche en oxyde de calcium, de silicium, de magnésium et

d'aluminium. Le tableau 1-9 présente la composition chimique moyenne des 27 laitiers de haut -fourneau produits en France et au Luxembourg en 1980.

Tableau 1- 9 : Composition chimique moyenne établie à partir de 27 laitiers produits en France et au Luxembourg en 1980 [44]

Oxyde	CaO	SiO_2	Al_2O_3	MgO	FeO	MnO	S	TiO_2	Na_2O	K_2O
% wt	42.24	33.48	13.29	5.95	1.24	0.64	0.94	0.55	0.39	0.70

En outre, la plupart des laitiers vitrifiés possèdent de 5 à 10% de phases cristallines telles que la solution solide d'akermanite ($Ca_2MgSi_2O_7$), de gehlénite $Ca_2Al_5(AlSi)O_7$ et de merwinite ($Ca_3MgSi_2O_8$). La norme NF EN 197-1 [40] définit trois différents types de ciments CEM III en fonction du pourcentage du clinker et du laitier.

- CEM III/A constitué de 35 à 64% de clinker et de 36 à 65% de laitier de haut – fourneau.
- CEM III/B constitué de 20 à 34% de clinker et de 66 à 80% de laitier de haut – fourneau.
- CEM III/C constitué de 5 à 19% de clinker et de 81 à 95% de laitier de haut – fourneau.

- **Pouzzolane (naturelle P ; Calciné Q) :** La pouzzolane naturelle a généralement l'origine de projection volcanique. Le caractère pouzzolanique des roches pyroclasiques est relié au refroidissement rapide du magma liquide ce qui conduit à la formation d'une matière vitreuse. La roche non volcanique présente une réactivité pouzzolanique peut être citée par exemple des diatomites qui sont obtenues par l'accumulation et cimentation de quelettes siliceux de diatomées.
  En outre, le traitement thermique par la calcination utilisé permet d'améliorer la réactivité pouzzolanique. Le tableau 1 - 10 présente la température optimale au traitement thermique des phases argileuses.

Tableau 1- 10 : Température optimale utilisée pour activer la réactivité des phases argileuses

Phases minerales	Température optimale
▪ **Illite :** $(K, H_3O)(Al, Mg, Fe)_2(Si, Al)4O10[(OH)_2, (H_20)] \rightarrow 3.5\ H_2O + (K)(Al, Mg, Fe)_2(Si, Al)_4O_{10.5}$	700°C [53] [54] 715°C [55] 850 °C [56]
▪ **Smectite:** $(K, Ca)(Si_4, Al)O_{10}(Al, Mg, Fe, Ti)(OH)_2 \rightarrow H_2O + (K,Ca)(Si_4, Al)O_{11}(Al, Mg, Fe, Ti)$	900°C [57] 930°C [58] 950°C [59]
▪ **Muscovite:** $K\,Al_2\,(Si_3\,Al)\,O_{10}\,(OH)_2 \rightarrow H_2O + KAl_2(Si_3Al)\,O_{11}$	850°C [60]
▪ **Chlorite:** $(Fe, Mg, Al)_6(Si, Al)_4O_{10}(OH)8 \rightarrow 4H_2O + (Fe, Mg, Al)_6(Si, Al)_4O_{14}$	800°C [61]

- **Cendres volantes (siliceuses V ; Calcique W) :**
  Les cendres volantes sont les sous-produits de l'industrie électrique, obtenues dans les centrales thermiques en faisant la combustion de charbon pulvérisé à des températures comprises entre 1100 et 1400 °C. Suivant le refroidissement, la teneur des phases amorphes est variable, comprise entre 60 et 90% [62]. Les phases cristallines dans les cendres volantes varient en fonction de la nature silico-alumineuse ou calcique des matières. Les phases cristallines habituellement identifiées dans les cendres volantes à faible teneur en calcium sont : le quartz, la mullite ($3Al_2O_3.2SiO_2$), l'hématite (Fe_2O_3) et la

magnétite (Fe_3O_4) [63]. Les cendres volantes riches en CaO possèdent plus de 4 phases cristallines. Les phases couramment identifiées sont : le silicate et aluminate de calcium (notamment C_2S et CA), l'alumino-silicate de calcium (C_2AS), le sulfate de calcium (CS, CSH_2) ou la ferrite (C_2F).
La norme NF EN 197-1 utilise la teneur en CaO réactif afin de différencier les types des cendres volantes : inférieure à 10% pour les cendres volantes siliceuses et supérieure à 10% pour les cendres volantes calciques.

- **Schiste calciné (T) :** Ils sont produits dans les fours spéciaux en calcinant à la température de 800 °C suivi d'un broyage fin. Les schistes calcinés présentent une forte réactivité pouzzolanique et hydraulique.

- **Fumée de silice (D) :** Les fumées de silice sont des co-produits de l'industrie de silicium et de des alliages. Elles se composent des particules sphériques très fines (environ 95% inférieures à 1 µm [64]) contenant au moins 85% de dioxyde de silice amorphe. Les fumées de silice présentent une surface spécifique BET élevée comprise entre 20 et 23 m2/g [65]. L'utilisation des fumées de silice comme une addition minérale présente un double effet : d'une part, une réactivité pouzzolanique élevée grâce à la silice amorphe, et d'autre part, un effet de filler du fait de sa finesse importante.

- **Calcaire (L ; LL si le COT < 0.2%) :** Il peut remplacer une proportion allant jusqu'à 35% de la masse totale du ciment. La présence des fillers de calcaire permet la formation du semi et monocarbonate et de stabiliser l'ettringite en comparant avec le ciment sans fillers calcaire.

$$C_3A + C\underline{c} + 11H \rightarrow C_4A\underline{c}H_{11}$$

$$C_3A + 0.5C\underline{c} + 0.5CH + 11.5H \rightarrow C_4A\underline{c}0.5H_{12}$$

$$2C_3A + C_6A\underline{s}3H_{32} + 4H \rightarrow 3CA\underline{s}H_{12}$$

- **Sulfate de calcium :** Il est présent sous la forme de gypse ($CaSO_4.2H_2O$) ou d'anhydrite ($CaSO_4$). L'ajout de sulfate de calcium est indispensable afin de contrôler la prise du ciment. En effet, l'hydratation de l'aluminate de calcium (C_3A) du ciment se produit très rapidement et ne peut pas être maîtrisée. Ceci conduit à la formation de C_4AH_{13} qui provoque une prise très rapide. De ce fait, le gypse ajouté dans le ciment va se dissoudre rapidement et libérer des ions sulfates dans la solution. Ces ions vont réagir avec les aluminates de calcium pour former à la surface de ce dernier une couche d'ettringite. Cette couche formée permet de ralentir l'hydratation des aluminates de calcium. Le taux du gypse à ajouter au clinker est très important car il va influencer sur le temps de prise et la résistance mécanique. En effet, le taux du gypse optimal dépend ce que l'on souhaite obtenir des résistances mécaniques élevées à court terme (2 jours) ou à long terme (28 jours) [66].

Les types de ciments courants dépendent de la nature du composant (décrit ci-dessus) et leur taux d'introduction dans la formulation. Le principe de substitution du clinker dans le ciment est illustré dans la figure 1-6.

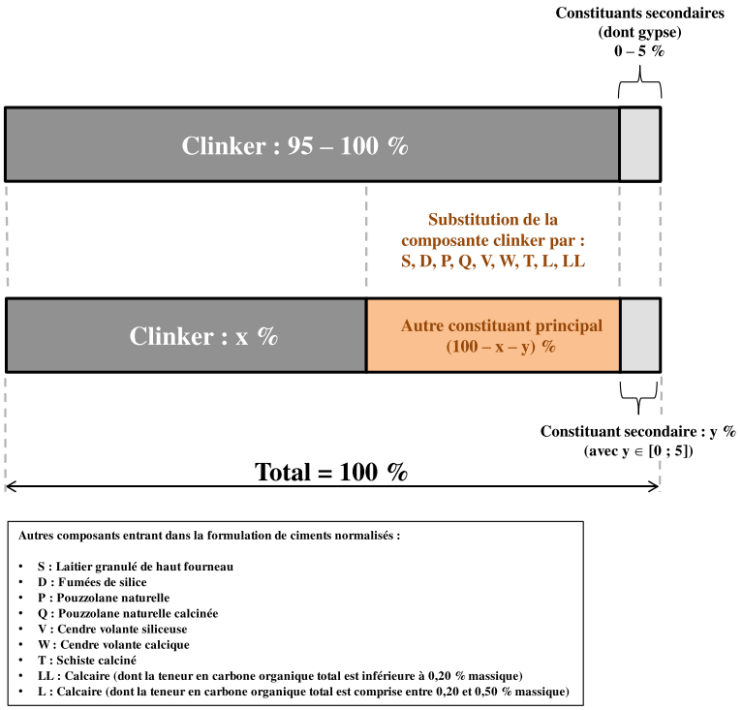

Figure 1- 6 : Principe de substitution du clinker par d'autres constituants principaux [39]

Le tableau 1-11 regroupe 5 grands types de ciments définis dans la norme NF EN 197-1.

Tableau 1- 11 : 5 grands types de ciments définis dans la norme NF EN 197-1

NF EN 197-1	Type de ciment
CEM I	Ciment Portland
CEM II	Ciment Portland composé
CEM III	Ciment de haut – fourneau
CEM IV	Ciment pouzzolanique
CEM V	Ciment composé

II.3. Les phases minérales du clinker

La formulation chimique et la teneur des 4 phases minérales du clinker ont été présentés dans le tableau 1-6. Cependant, le cru contient des éléments mineurs, les minéraux obtenus en sortie du four dans le clinker ne sont pas également purs. Dans cette partie, nous détaillons la forme morphologique, la réactivité et ainsi l'influence du refroidissement sur la forme des phases minérales du clinker.

II.3.1. Alite (C_3S)

L'alite est la phase majoritaire du clinker. Il présente 7 polymorphes différents dont la formation dépend de la température : trois polymorphes tricliniques (noté T1, T2 et T3), 3 polymorphes monocliniques (noté M1, M2 et M3) et un polymorphe rhomboédrique (noté R) [44]. Ce phénomène est appelé polymorphisme. La figure 1-7 présente 7 polymorphes de l'alite en fonction de la température

Figure 1- 7 : Polymorphes de l'alite en fonction de la température (source [67])

A la température ambiante, l'alite pur présente sous la polymorphe T1. Cependant, lors de la formation de l'alite au sein d'un clinker industriel, la présence des éléments mineurs permet la stabilisation de certains polymorphes monocliniques, principalement M1 et M3 [68] au détriment du polymorphe triclinique théorique. En outre, la présence de magnésium favorise à stabiliser le polymorphe M3, tandis que la présence de SO_3 favorise la formation du M1 [68]. La figure 1 - 8 présente la relation entre la teneur de SO_3, la teneur de MgO et les transformations des polymorphes de l'alite.

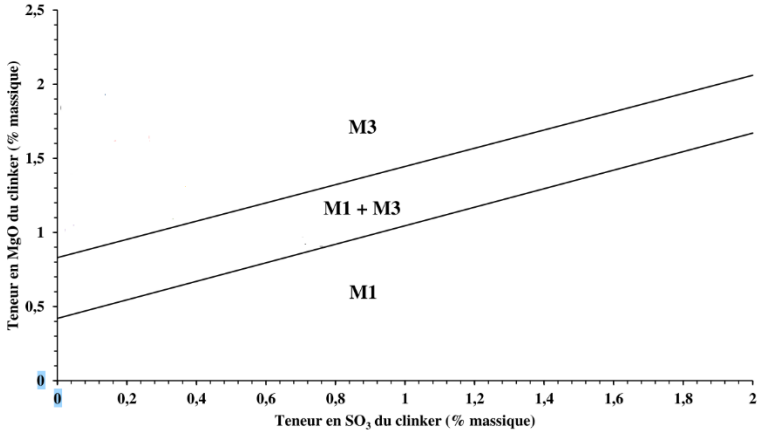

Figure 1- 8 : Relation entre la teneur de SO_3 et la teneur de MgO et les transformations des polymorphes de l'alite dans le clinker.

II.3.2. Bélite (C_2S)

La bélite ou le silicate bicalcique, est le deuxième constituant majoritaire du clinker. Elle possède 5 polymorphes différents dont la formation dépend également de la température : α (hexagonal), α'_H (orthorhombique), α'_L (orthorhombique), β (monoclinique) et ϒ (orthorhombique) [69]. La figure 1- 9 présente la relation entre la température et la formation de polymorphe de C_2S [44].

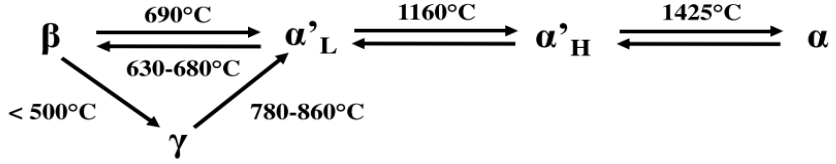

Figure 1- 9 : Relation entre la température et la formation de polymorphe de C_2S (source [67])

La structure de la bélite consiste à un assemblage de tétraèdres de SiO_4^{4-} reliés par des ions calciums Ca^{2+} en sites octaédriques [44, 69]. Les polymorphes α, α' et β sont relativement similaires et s'obtiennent par déplacement, en particulier par un changement d'orientation des tétraèdres de SiO_4^{4-} et des mouvements de la part des ions Ca^{2+} [43]. Le polymorphe ϒ résulte du refroidissement lent depuis α-C_2S. A la température ambiante, la structure ϒ - C_2S est la forme la plus stable, par conséquent, elle est peu réactive.
Dans le clinker industriel, la bélite est essentiellement sous la forme β et contient 4 à 6% d'éléments mineurs tels que l'aluminium, le fer et le potassium [43].

II.3.3. Aluminate tricalcique (C_3A)

L'aluminate tricalcique (C_3A) dans le cas d'un composé pur, ne possède pas de polymorphe liée à la température [44]. Le C_3A pur présente sous la forme cubique. Toutefois, l'insertion

d'éléments mineurs dans le réseau cristallin telles que le sodium, le fer et le silicium peut changer la symétrie du réseau cristallin. Le remplacement de Ca^{2+} par deux ions Na^{+} favorise le passage de système cubique à des systèmes monocliniques ou orthorhombiques en fonction du taux de substitution [70]. En effet, lorsque la teneur totale en alcalin est faible, le C_3A est sous la forme cubique. Par contre, lorsque la teneur totale en alcalin est plus élevée, c'est la forme orthorhombique qui prédomine. Cette forme peut contenir jusqu'à 20% d'éléments mineurs.

II.3.4. Aluminoferrite tétracalcique (C_4AF)

L'aluminoferrite tétracalcique doit être considérée comme une solution solide contenant C_2A et C_2F [69], dont la formulation chimique est $2CaO(AlxFe_{1-x})_2O_3$ avec $0 < x < 0.7$. La valeur limite de x égal à 0.7, du fait de l'instabilité de C_2A dans les conditions de pression [70]. Dans la structure cristalline, le fer et l'aluminium se partagent entre les sites tétraédriques et octatrédriques en fonction de la composition et les conditions de la formation de la phase. Cette phase, quant à elle, peut contenir jusqu'à environ 10% d'éléments mineurs [44].

II.3.5. Quantification des phases minérales dans le clinker – Formule Bogue

Le pourcentage massique en chacune des phases minérales du clinker peut être estimé en utilisant la formule Bogue [50] selon les équations suivantes :

$$C_3S = 4.07 * (CaO_{Total} – CaO_{\text{free lime}}) - 6.72 * Al_2O_3 – 1.43 * Fe_2O_3$$

$$C_2S = 8.60 * SiO_2 + 1.08 * Fe_2O_3 + 5.07 * Al_2O_3 - 3.07 * (CaO_{Total} – CaO_{\text{free lime}})$$

$$C_3A = 2.65 * Al_2O_3 – 1.69 * Fe_2O_3$$

$$C_4AF = 3.04 * Fe_2O_3$$

Une hypothèse fondamentale des équations dans la formule Bogue est la pureté des phases minérales du clinker et la non-incorporation des ions étrangers. Ceci explique pourquoi la somme massique des phases minérales en comptant également la teneur en chaux libre n'atteint pas 100%.

II.4. Hydratation du ciment

L'hydratation du ciment se produit dès sa mise en contact avec l'eau de gâchage selon différents processus de dissolution/précipitation. En effet, dans un premier temps, la solubilité des ciments anhydres est supérieure à celle des hydrates. Ainsi, l'hydratation du ciment consiste à une dissolution des phases anhydres du clinker. Ensuite, l'eau de gâchage s'enrichit progressivement en Ca^{2+}, $SiO_4H_2^{2-}$, SiO_4H^{3-}, sulfate et aluminium jusqu'à être saturée par rapport aux hydrates dont certains d'entre eux précipitent plus ou moins rapidement [43]. L'hydratation du ciment permet de former des hydrates qui vont par la suite conférer des propriétés mécaniques telles que la résistance en compression et en flexion, et des propriétés de durabilité telles que la résistance à la carbonatation, la résistance à la diffusion des ions sulfates et chlorures à la pâte de ciment durcie.
La réaction d'hydratation du ciment est un processus complexe qui dépend de plusieurs paramètres intrinsèques et extrinsèques du matériau [71].

II.4.1. Hydratation du ciment Portland

L'hydratation du ciment Portland se compose d'un ensemble de réactions chimiques des phases minérales du ciment telles que C_3S, C_2S, C_3A, C_4AF et gypse. Les équations d'hydratation couramment utilisées dans la littérature [44, 72] sont présentées ci-dessous :

$$C_3S + 5.3\ H \rightarrow C_{1.7}SH_4 + 1.3\ CH$$

$$C_2S + 4.3\ H \rightarrow C_{1.7}SH_4 + 0.3\ CH$$

$$C\overline{S} + 2\ H \rightarrow C\overline{S}H_2$$

$$C_3A + 6\ H \rightarrow C_3AH_6$$

$$C_3A + 3\ C\overline{S}H_2 + 26\ H \rightarrow C_6A\overline{S}_3H_{32}\ \text{(Ettringite)}$$

$$C_4AF + 3\ C\overline{S}H_2 + 30\ H \rightarrow C_6A\overline{S}_3H_{32} + CH + FH_3$$

$$2\ C_3A + C_6A\overline{S}_3H_{32} + 4H \rightarrow 3\ C_4A\overline{S}H_{12}$$

$$2\ C_4AF + C_6A\overline{S}_3H_{32} + 12\ H \rightarrow 3\ C_4A\overline{S}H_{12} + 2\ CH + 2\ FH_3$$

L'alite et la bélite s'hydratent afin de former des silicates de calcium hydratés (C-S-H) et de l'hydroxyde de calcium ou la portlandite ($Ca(OH)_2$-CH).
Le gypse ajouté dans le ciment va se dissoudre très rapidement conduisant à une solution saturée, réagit très vite avec les ions (Ca^{2+}, Al^{3+}) libérés à partir de la dissolution des phases interstitielles pour former un trisulfoaluminate de calcium hydraté ($C_6A\overline{S}_3H_3$) appelé ettringite (Aft). Cependant, la quantité du gypse dans le ciment est souvent insuffisante pour que la totalité de C_3A réagisse. Par conséquence, l'ettringite est partiellement transformée en $C_6A\overline{S}_3H_3$ ou monosulfoaluminate de calcium hydraté (Afm).
Après plusieurs mois d'hydratation, une pâte de ciment se compose de 40 – 60% C-S-H, 15 -20 % de $Ca(OH)_2$, 10 – 20% d'ettringite et/ou monosulfoaluminate de calcium hydraté, 10 -20% des pores et de 0 -5% de composés mineurs [44].

II.4.2. Hydratation du ciment composé

- **Hydratation du ciment au laitier de haut – fourneau (ciment CEM III)**

  La réaction d'hydratation du laitier nécessite un milieu basique, et la solubilisation du laitier est optimale dans le milieu où le pH est supérieur à 12. En effet, les composés les plus basiques du laitier peuvent être dissouts par l'eau mais la vitesse de dissolution est beaucoup plus lente que pour des solutions basiques [73]. Dans le cas du ciment au laitier, l'hydratation se produit une fois que l'hydratation du clinker a commencé.

  L'hydratation du ciment au laitier produit, principalement, les mêmes types d'hydrates que ceux formés par l'hydratation du clinker. Parmi les hydrates formés lors d'hydratation du ciment au laitier, on peut citer : le silicate de calcium hydraté (C-S-H), la portlandite, l'ettringite, Afm et l'hydrogrenat (C_3AH_6/C_3ASH_4). D'autres hydrates sont également présents dans les pâtes de CEM III : l'hydrotalcite C_6AH_{13} ou la stratlingite C_2ASH_8. Contrairement à l'hydratation du ciment CEM I, la portlandite formée dans le ciment CEM III est consommée au moins partiellement au cours du temps afin d'hydrater le laitier.

  En outre, la quantité d'aluminium incorporée dans la structure de C-S-H est faible dans le cas du ciment CEM I. Cependant, cette quantité est plus élevée dans le cas des additions cimentaires riches en aluminium. Les hydrates sont notés C-A-S-H et leurs propriétés chimiques et leur structure sont modifiées par rapport à celle de C-S-H.

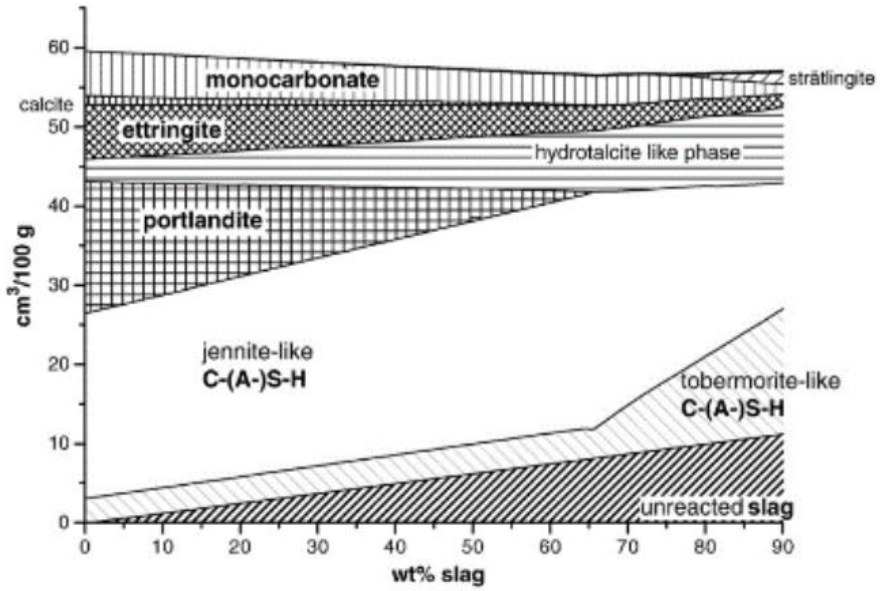

Figure 1- 10 : Simulation de la quantité des hydrates formés lors de l'hydratation d'un ciment au laitier [74]

La figure 1- 10 illustre les principaux hydrates présents dans les pâtes de ciment CEM III en fonction de la quantité du laitier (la modélisation réalisée en supposant que la totalité du ciment portland ainsi que 75 % du laitier ont réagi). Lors d'hydratation du ciment CEM III, les phases C-A-S-H, l'ettringite, Afm, l'hydrotalcite sont identifiées. En outre, deux types de C-A-S-H sont différenciés en fonction de leur structure (jennite et tobermorite). Lorsque la teneur du laitier est supérieure à 65%, la portlandite est absente dans le milieu. Pour une teneur en laitier supérieure à 80%, la stratlingite se forme.

Le degré d'hydratation du ciment CEM III est influencé par plusieurs facteurs tels que : l'origine du laitier, la composition chimique, la température d'hydratation, l'origine du clinker.

- **Hydratation du ciment composé – Système ciment/Métakaolin (AS_2)**

  Le métakaolin est une pouzzolane synthétisée en faisant la calcination de la kaolinite selon l'équation suivante :

  $$Al_2O_3.2SiO_2.2H_2O \rightarrow Al_2O_3.2SiO_2 \text{ (amorphe)} + 2H_2O$$

  Les hydrates formés lors de l'hydratation du ciment contenant du métakaolin sont les suivants : l'aluminate tétracalcique hydraté (C_4AH_{13}), l'hydrogrenat (C_3AH_6), Stratlingite (C_2ASH_8) et C-S-H. Murat a établi plusieurs réactions pouzzolaniques en fonction du rapport CH/AS2.

$CH/AS_2 = 1$	$AS_2 + 3CH + 6H \rightarrow C_2ASH_8 + C\text{-}S\text{-}H$
$CH/AS_2 = 1.67$	$AS_2 + 5CH + 3H \rightarrow C_3AH_6 + C\text{-}S\text{-}H$
$CH/AS_2 = 2$	$AS_2 + 6CH + 9H \rightarrow C_4AH_{13} + C\text{-}S\text{-}H$

Cependant, certains de ces hydrates sont stables au cours du temps, d'autres moins, tels que les gels silico calciques. La présence des hydrates en fonction du rapport CH/AS_2 et du temps d'hydratation est présentée dans les tableaux suivants (Tableau 1-12 et Tableau 1- 13).

Tableau 1- 12 : Hydrates stables en fonction du rapport CH/AS_2 après 90 jours.

CH/AS_2	$0.4 < CH/AS_2 < 1.5$	$0.4 < CH/AS_2 < 1.5$

Hydrates présentes à 90 jours	C_2ASH_8, C-S-H	C_2ASH_8, C-S-H, C_4AH_{13} (traces)

Tableau 1- 13 : Hydrates stables en fonction du temps d'hydratation

Échéance (jours)	J < 7	7 < J < 28	28 < J
Hydrates formés ($CH/AS_2 > 7$)	C_4AH_{13}, C_2SH_y	C_2ASH_8, C_2SH_y	$C_3AS_{0.3}H_{5.4}$, C_2SH_y

Comme le cas du ciment au laitier, le métakaolin peut consommer la portlandite pour réagir lui – même et produit le C-S-H, CASH, CAH. La figure 1- 11 illustre la teneur la portlandite en fonction de la teneur du métakaolin et du temps d'hydratation. On remarque que plus la teneur du métakaolin augmente, plus la porlandite est consommée rapidement.

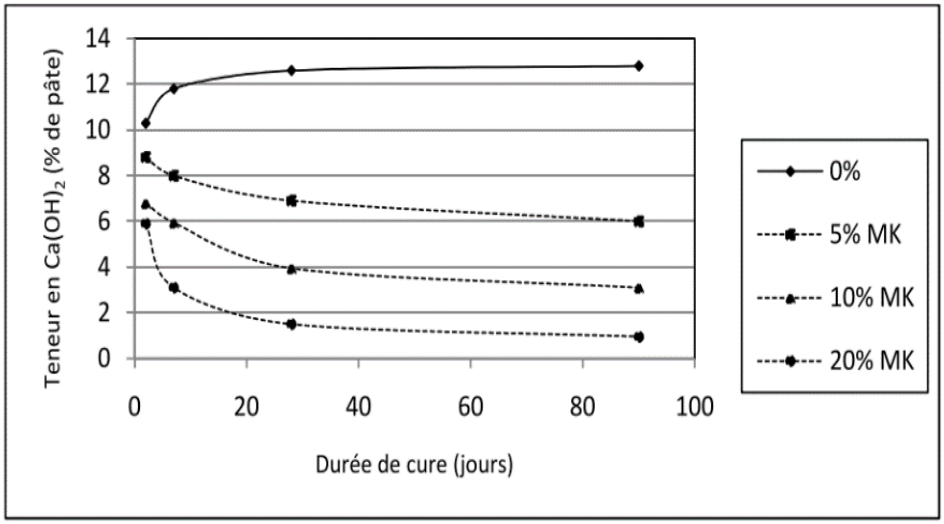

Figure 1- 11 : Teneur de portlandite dans la pâte de ciment en fonction de la teneur de métakaolin et du temps d'hydratation

II.5. Caractéristiques des produits d'hydratation

La formation de différents hydrates lors de l'hydratation du ciment constitue un assemblage de diverses phases plus ou moins cristallisées à la température et la pression ambiante. Parmi ces hydrates, la portlandite, l'ettringite et le monosulfoaluminate de calcium hydraté sont les mieux cristallisés. Par contre, le C-S-H a une structure faiblement cristallisée, voire amorphe. Cette partie présente la structure et les propriétés des hydrates formés lors d'hydratation du ciment.

- **Silicate de calcium hydraté (C-S-H)**

  Le silicate de calcium hydraté (C-S-H) est le principal hydrate constituant de la phase liante de la pâte de ciment. Il contribue de manière significative aux macros – propriétés du béton telles que la résistance et la durabilité [75, 76]. La structure de C-S-H se présente sous la forme de particules nanométriques agrégées les unes aux autres. La taille de ces particules varie en fonction du rapport Ca/Si : d'environ 60 * 60 * 5 nm^3 pour 1 < Ca/Si < 1.5 et de 60 * 30 * 5 nm^3 pur 1.7 < Ca/Si < 2 [77].

  La stœchiométrie de C-S-H dépend au rapport W/C, de la température et de la composition du ciment [78–80]. Elle est également liée à la composition de la solution interstitielle avec laquelle le C-S-H est à l'équilibre. Plus la solution interstitielle est concentrée en calcium (ou faible en silicium), plus le rapport C/S de C-S-H est élevé.

- C-S-H (α): 0.66 < C/S < 1 formée pour une concentration de [Ca^{2+}] inférieure à 2 mmol/l.
- C-S-H (β): 1 < C/S < 1.5 formée pour une concentration de [Ca^{2+}] entre 2 et 22 mmol/l.
- C-S-H (Υ): C/S = 1.7 formée pour une concentration de [Ca^{2+}] supérieure à 22 mmol/l.

Le C-S-H possède une structure lamellaire, composé d'une couche d'oxyde de calcium avec des chaînes de silicates organisées en structure 'dreierketten' [81] (Figure 1-12). Les inter-feuillets se composent des ions calcium et des molécules d'eau. Les chaînes de silicate sont constituées à partir des dimères de silicates reliés parfois entre eux par un tétraèdre, appelé tétraèdre pontant, formant des pentaèdres [82] (Figure 1-13).

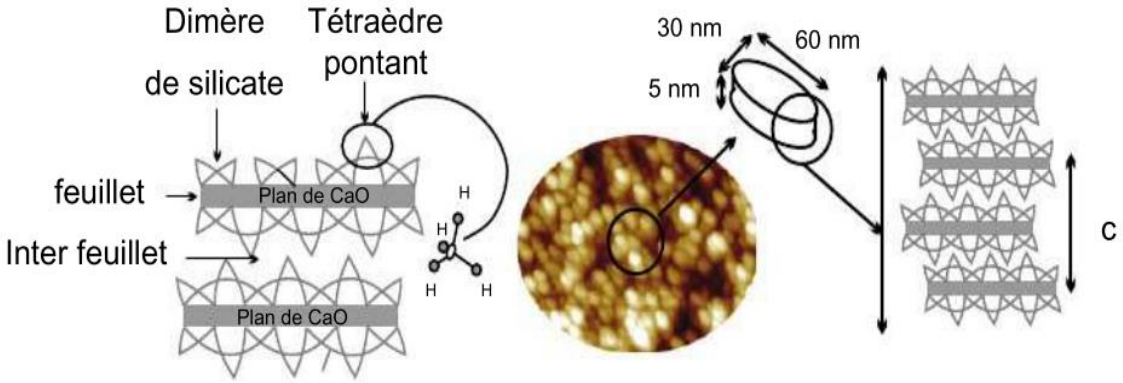

Figure 1- 12 : La structure cristalline du C-S-H

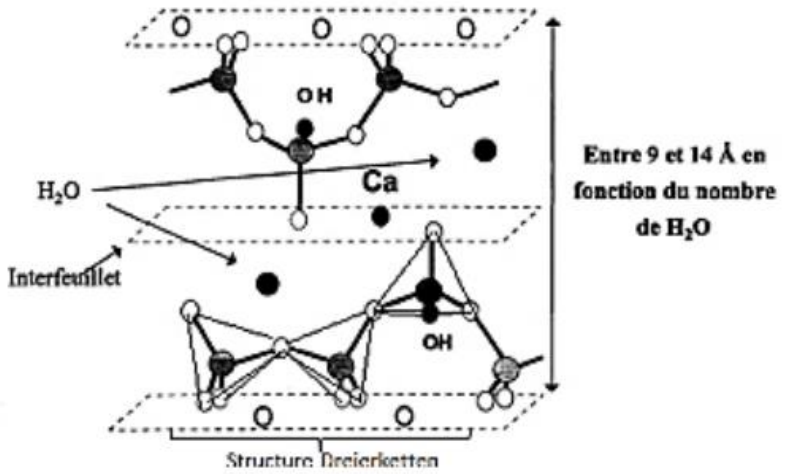

Figure 1- 13 : Structure d'inter – feuillet du C-S-H

Cependant, la structure atomique du C-S-H dépend également du rapport C/S. En effet, pour le C-S-H ayant un faible rapport C/S (0.7 < C/S < 1.5), sa structure atomique est proche de la tobermorite [83]. Le C-S-H ayant un rapport C/S supérieur à 1.5, la structure n'est pas encore bien définie et est en discussion. Les études précédentes indiquent que ce C-S-H semblerait à garder une structure proche de celle de la tobermorite [84, 85]. En outre, une diminution du rapport C/S entraîne un allongement des chaînes (Figure 1-14) [86].

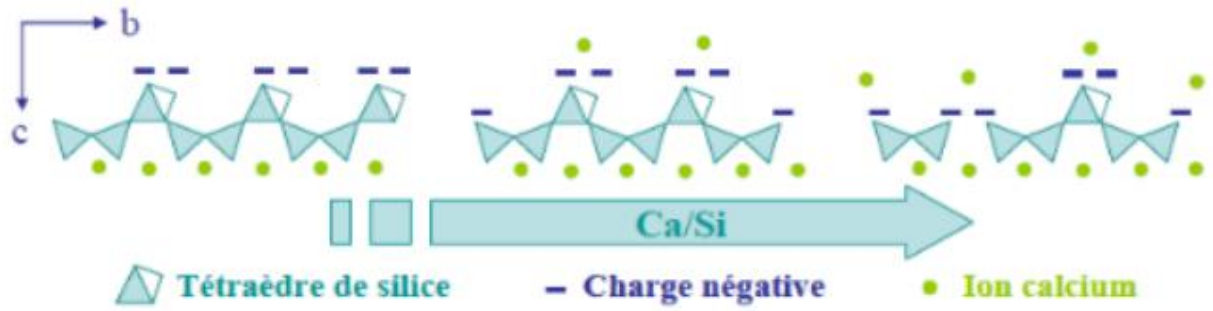

Figure 1- 14 : Structure simplifiée du C-S-H en fonction du rapport C/S

- **L'hydroxyde de calcium (Portlandite)**
  La portlandite est également un principal hydrate de l'hydratation du ciment CEM I. Elle se présente sous une forme d'un empilement de feuillets. L'arrangement des cristaux dans ces feuillets est sous la forme d'une structure hexagonale où le calcium est en site octaédrique et l'oxygène en site tétraédrique [81]. La figure 1-15 présente la structure de la portlandite.

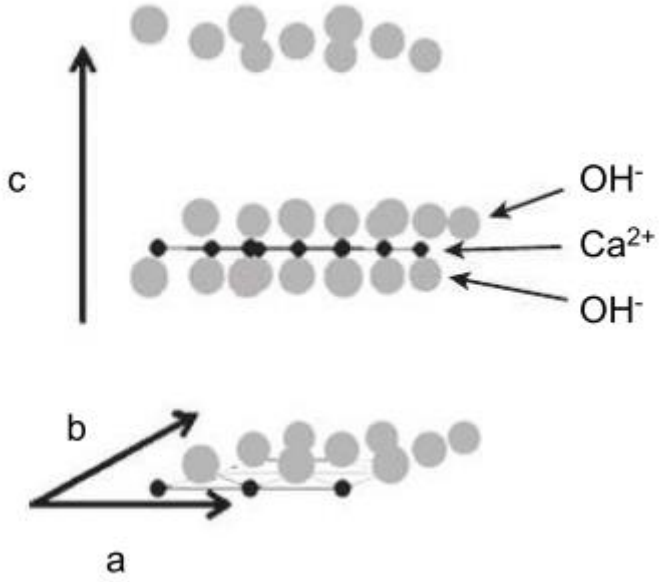

Figure 1- 15 : Structure de la portlandite [81]

- **Ettringite (Aft)**
  L'ettringite ou Aft est également un principal hydrate formé suite à l'hydratation du ciment CEM I. Elle provient essentiellement de l'hydratation du C_3A avec le régulateur de prise (le gypse) et cristallise sous la forme d'aiguilles. Sa formule s'écrit $[Ca_3Al(OH)_6.12H_2O.(SO_4)_3.nH2O]$ avec $0 \leq n \leq 2$. La structure de l'ettringite se compose de colonnes de cations coordinés par les oxygènes des hydroxydes et des molécules d'eau (Figure 1-16). Les ions sulfates servent à assurer l'électroneutralité du système [81].

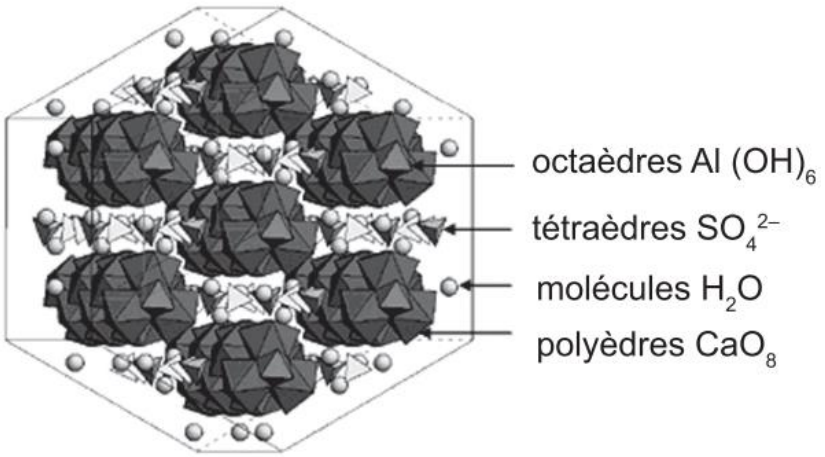

Figure 1- 16 : Structure cristalline de l'ettringite

Cet hydrate est stable à la température ambiante mais est très sensible à l'augmentation de la température. Zhou et al [87] ont montré que l'ettringite commence à se dégrader et à perdre son eau liée à partir de 50 °C.

- **Monosulfoaluminate de calcium hydraté (Afm)**
  Le monosulfoaluminate de calcium hydraté (Afm) provient de la réaction entre la phase C_3A en excès avec l'ettringite. La formule cristallographique de cette phase est $[Ca_2Al(OH)_6.2H_2O]_2.SO_4.nH_2O$ avec $0 \leq n \leq 2$. Il cristallise sous la forme de feuillets avec une structure hexagonale. Dans la structure de cet hydrate, certains ions calcium (Ca^{2+}) sont remplacés par des ions trivalents, majoritairement des ions aluminium (Al^{3+}) et minoritairement des ions ferrique (Fe^{3+}). Ce remplacement entraîne un excès de charges positives compensé par la présence d'anions dans l'inter-feuillet. Ces ions peuvent être : OH^- et SO_4^{2-}. La figure 1-17 illustre la structure du monosulfoaluminate de calcium hydraté.

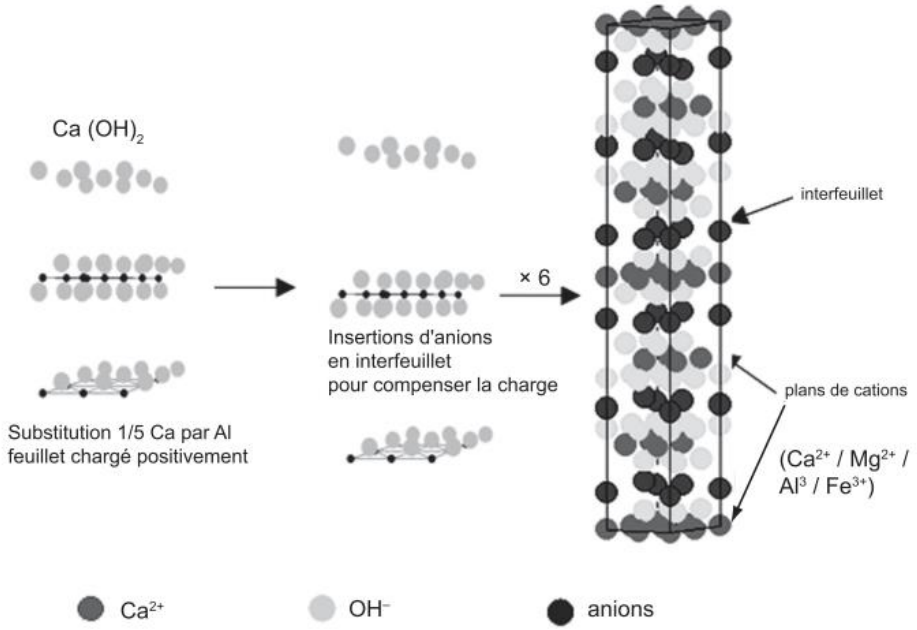

Figure 1- 17 : Structure du monosulfoaluminate de calcium hydraté [81]

II.6. Cinétique d'hydratation

L'hydratation du ciment se produit selon plusieurs étapes dues à la différence notable en termes de vitesse d'hydratation des différentes phases du ciment. En effet, les phases interstitielles, plus

particulièrement le C_3A sont extrêmement réactives dès le contact avec l'eau de gâchage. La réaction commence dès les premières minutes. Un ralentissement important de la vitesse d'hydratation est rapidement observé. Ce phénomène est lié principalement à la réaction entre le C_3A et le gypse qui conduit à la formation de l'ettringite. Une fois tout le gypse est consommé, une diminution de la quantité d'ettringite formée et une accélération de l'hydratation du C_3A sont observées. Les phases silicates de calcium réagissent avec l'eau de manière différente. Le C_3S commence à réagirquelques heures après la mise en contact du ciment avec l'eau. Cette réaction génère dans le premier temps le C-S-H puis la portlandite. Le C_2S est la dernière phase à réagir (après quelques jours) pour former le C-S-H et la portlandite. La figure 1-18 illustre l'évolution des hydrates formés en fonction du temps d'hydratation du ciment.

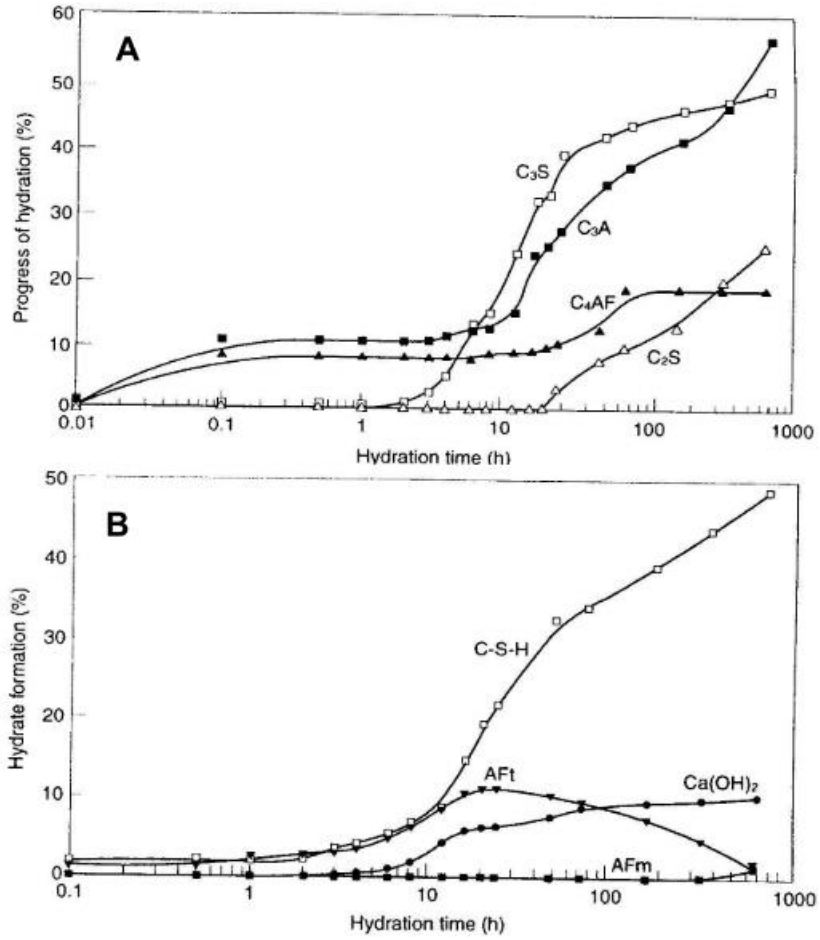

Figure 1- 18 : Évolution des phases lors de l'hydratation du ciment A) Anhydres, B) Hydrates [88] (source d'image [43]).

L'hydratation de la pâte de ciment suivie par la calorimétrie se compose de 5 étapes consécutives (Etape (I) à Etape (V))(Figure 1-19).

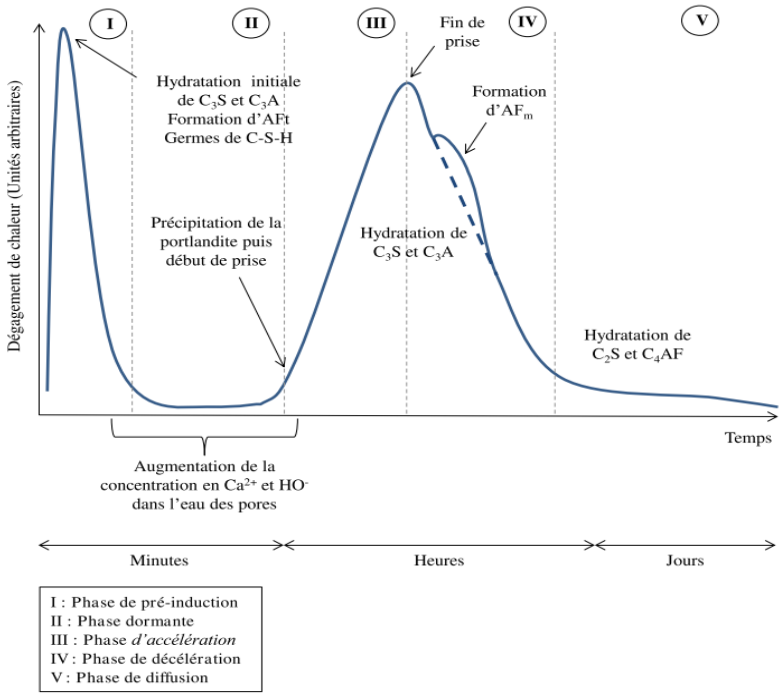

Figure 1- 19 : Chaleur dégagée de l'hydratation du ciment portland (Source d'image [67])

- **Etape I : Phase de pré-induction**

Dans cette phase, l'hydratation du ciment génère une quantité importante de chaleur, liée notamment à l'hydratation de la phase C_3A.

- **Etape II : Phase dormante ou Phase d'induction**

Pendant cette période, la vitesse des réactions d'hydratation (formation de C-S-H et d'ettringite) diminue, de même que le flux de chaleur observé en calorimétrie [67].

- **Etape III : Phase d'accélération**

Dans cette période, les ions Ca^{2+} et OH^- dans la solution précipitent afin de former de la portlandite. Les ions en solution consommés vont permettre une dissolution accrue de tous les composants du ciment, puis une précipitation, notamment sous la forme de silicate de calcium hydraté. La formation de C-S-H et leur connectivité conduisent également à une diminution de la plasticité et une rigidification du matériau [67].

- **Etape IV : Phase de décélération (ou de durcissement)**

Cette phase commence après que le flux de chaleur ait atteint son maximum. La vitesse des réactions d'hydratation diminue progressivement dans cette période. La précipitation de C-S-H continue encore, cependant, le mode de formation ainsi que la morphologie diffèrent comparativement à la phase d'accélération [67]. En effet, dans la phase précédente, le C-S-H formée se trouve à l'extérieur des grains de ciment. Ce dernier formé dans cette période précipite à l'intérieur même des gangues précédemment formées. Les propriétés mécaniques du matériau s'accroissent au cours de cette période grâce à la formation de liaison entre les particules hydratées.

- **Etape V : Phase de ralentissement (ou de diffusion)**

La dernière phase consiste à un ralentissement des réactions d'hydratation. Dans cette période, la vitesse d'hydratation est principalement gouvernée par la vitesse de diffusion de l'eau et celle des ions dissous au travers des hydrates déjà formés [43].

II.7. Degré de l'hydratation du ciment et la méthode de détermination du degré de l'hydratation

II.7.1. Degré de l'hydratation du ciment

Le degré de l'hydratation d'un matériau cimentaire est défini comme étant le rapport de la quantité de ciment hydraté à celle du ciment anhydre initial [71]. Il existe plusieurs approches expérimentales afin de déterminer la quantité de ciment hydraté :

- Analyse thermique (ATG)
- Analyse des images à la microscopie électronique (MEB-BSE)
- Analyse de la diffraction des rayons X (Méthode Rietveld)
- Résonance magnétique nucléaire (RMN)
- Calorimétrie

Le principe de ces méthodes consiste à déterminer la quantité des hydrates formés ou des anhydres restants dans un matériau cimentaire hydraté. Dans cette partie, nous détaillons les méthodes habituellement utilisées pour mesurer le degré de l'hydratation du ciment.

- **Méthode de quantification de la portlandite par l'analyse thermique ATG :**

Cette méthode est utilisée par plusieurs auteurs [71, 89, 90] afin de déterminer le degré de l'hydratation en mesurant la quantité de la portlandite formée lors de l'hydratation du ciment. Le principe de cette méthode est basé sur le fait que le degré de l'hydratation croît linéairement avec la quantité de la portlandite formée. La masse de la porlandite est mesurée par l'analyse ATG à l'aide d'une plage de température correspondante à la déshydratation de la portlandite. Le degré de l'hydratation est calculé selon l'équation suivante :

$$\alpha(t) = \frac{m\ Ca(OH)2}{mC\ .\Upsilon 0} * 100$$

Avec :

α(t) : Degré de l'hydratation du ciment à l'instant t.

$m_{Ca(OH)_2}$: Masse de $Ca(OH)_2$ formée.

m_C : Masse du ciment

$\Upsilon 0$: Quantité de la portlandite formée pour l'hydratation complète du ciment. Cette valeur dépend de la composition chimique du ciment.

La masse du ciment est calculée selon l'équation suivante :

$$m_c = \frac{m\ échantillon}{\left(1+\frac{E}{c}\right).(1+LOI)}$$

Avec :

Méchantillon : Masse de l'échantillon

E/C : Rapport Eau/Ciment

LOI : Perte de masse du ciment

La quantité de la portlandite mesurée à l'aide de l'analyse ATG peut être calculée selon l'équation suivant :

$$m_{Ca(OH)_2} = \frac{\Delta m\ 450°C-550°C(t).MCa(OH)2}{MH2O}$$

Avec :

$M_{Ca(OH)_2}$: Masse molaire de la Portlandite

MH2O : Masse molaire de l'eau

$\Delta m\ 450°C - 550°C(t)$: Perte de masse entre 450 et 550 °C de l'échantillon

Cependant, la difficulté de cette méthode réside dans la détermination des intervalles de température de déshydratation de la portlandite. En effet, plusieurs plages de température pour la portlandite ont été proposées par plusieurs auteurs (Figure 1-20).

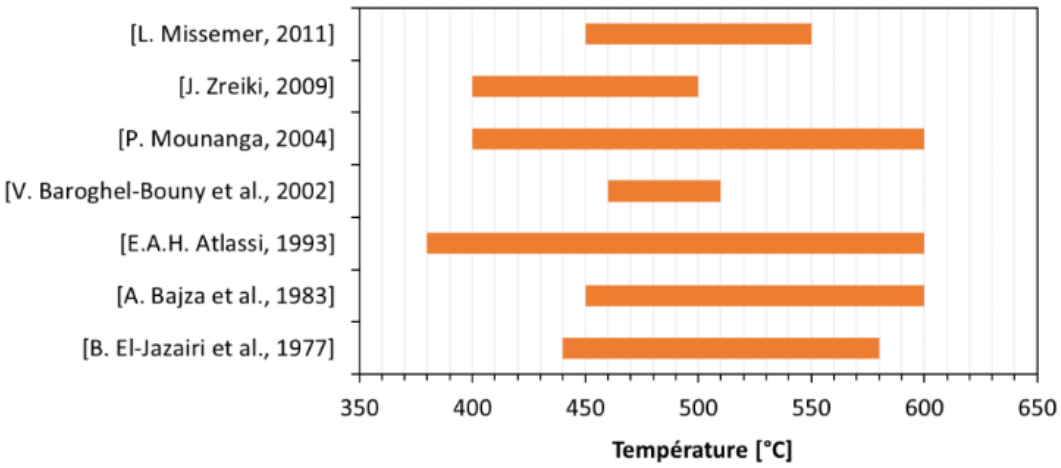

Figure 1- 20 : Intervalles de température de déshydroxylation de la portlandite selon différents auteurs (Source d'image [71])

La différence des intervalles de température entre les auteurs pourrait provenir de la différence de la méthode de calcul de perte de masse. En effet, il existe deux méthodes différentes pour le calcul de la perte de masse dans la littérature :

- **Méthode de la « tangente » :**

Le principe de cette méthode consiste à un changement de pente de la courbe ATG pour déterminer le début et la fin de la plage de température (Figure 1-21). Ensuite, des tangentes sont tracées de chaque point le long de la courbe ATG. Une ligne verticale est ensuite tracée sur le point d'inflexion de la courbe ATG. Cette ligne coupe les deux tangentes en deux points A et B. La différence de masse entre ces deux points A et B présente la perte de masse correspondant à la déshydratation de la portlandite.

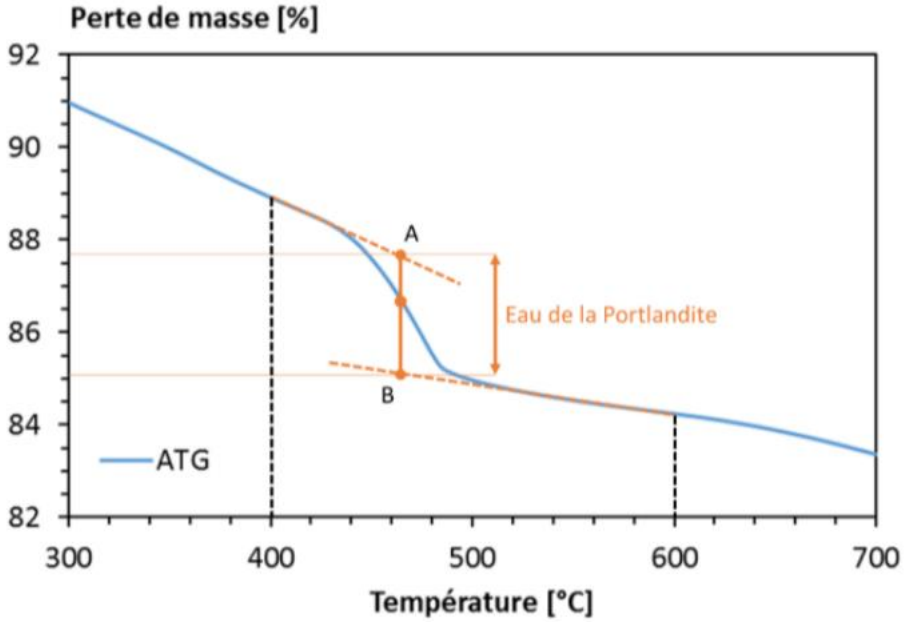

Figure 1- 21 : Détermination de la plage de température de déshydratation par la méthode de la tangente (Source d'image [71])

- **Méthode de la dérivée :**

Le principe de cette méthode consiste à tracer la courbe de la dérivée première (DTG) afin de trouver le début et la fin du pic de la dérivée (respectivement le point A et B) et à mesurer la perte de masse correspondante (Figure 1-22).

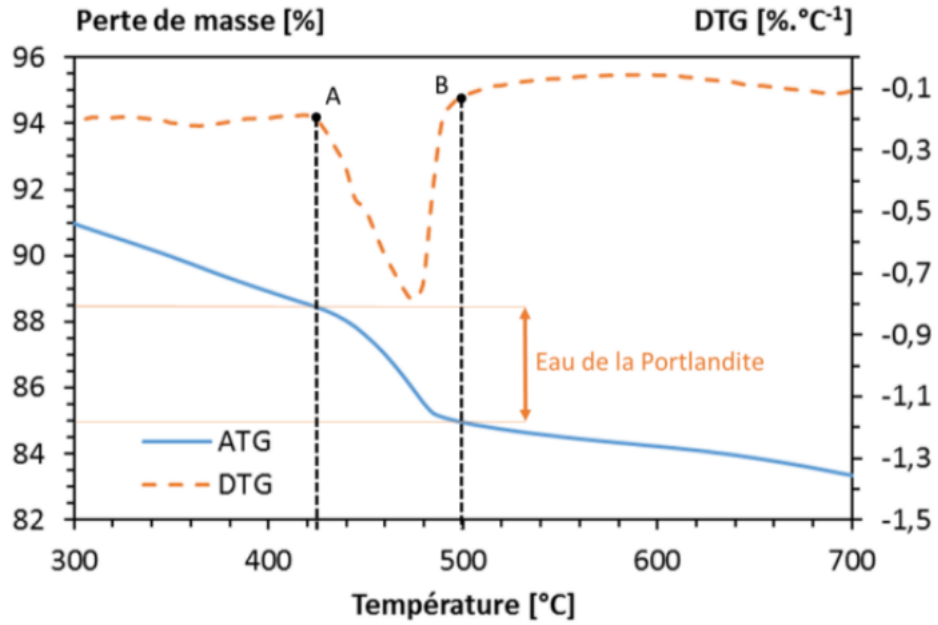

Figure 1- 22 : Détermination de la plage de température de déshydratation de la portlandite par la méthode de la dérivée (Source d'image [71])

Les études précédentes [91, 92] ont comparé deux méthodes de calcul afin de déterminer le degré de l'hydratation de ses matériaux. Les résultats montrent que le degré de l'hydratation mesuré par la méthode de la tangente était largement inférieur à celui mesuré par la méthode de la dérivée. Cependant, la méthode de la dérivée a donné la valeur de l'hydratation supérieure à 1.

- **Méthode de quantification de l'eau liée par analyse ATG**

Le principe de cette méthode est basé sur la détermination de la teneur de l'eau liée (l'eau des hydrates formés lors de l'hydratation du ciment) en comparant avec la teneur de l'eau liée produite pour unehydratation complète du ciment. Le degré de l'hydratation mesuré par la méthode de quantification de l'eau liée peut être calculé selon l'équation suivante :

$$\alpha(t) = \frac{Wn\,(t)}{Wn(\infty)} * 100$$

Avec :
α(t) : Degré de l'hydratation à l'instant t.
Wn(t) : Quantité de l'eau liée de l'échantillon à l'instant t.
Wn (∞) : Quantité de l'eau liée lors de l'hydratation complète du ciment. Cette valeur dépend également de la composition chimique du ciment.
La difficulté de cette méthode est la détermination de la température pour la perte de l'eau liée. En effet, entre 25 °C et 400 °C, il y a grand nombre de déshydratations simultanées telles que la déshydratation de l'ettringite, ou du C-S-H et la perte de masse liée à l'eau libre. Dans les études précédentes [44, 90], la quantité de l'eau liée dans la pâte de ciment hydraté est calculé selon l'équation suivante :

$W_n(t) = [\Delta m\ (145\ °C – 1000\ °C) - \Delta m\ (600\ °C – 880\ °C) – m_c * PAF]/m_c$

Avec :
Δm (145 °C – 1000 °C) : Perte de masse de l'échantillon entre 145 °C et 1000 °C.
Δm (600 °C – 880 °C) : Perte de masse de l'échantillon entre 600 °C et 880 °C.
m_c : Masse du ciment.
PAF : Perte au feu du ciment.

- **Méthode de l'analyse des images (MES – BSE)**

Un inconvénient de la méthode de quantification de la portlandite dans la détermination du degré de l'hydratation du ciment n'est pas appliqué dans le cas d'un matériau cimentaire contenant des additions pouzzolanique dû à la consommation de la portlandite par ces additions. Par conséquence, la méthode de l'analyse des images SEM – BSE a été utilisée [93–95] afin de déterminer le degré de l'hydratation ainsi que la quantité des phases dans un matériau cimentaire hydraté. Le processus de cette méthode se compose de 3 étapes principales suivantes :

- Choix du grossissement et de la résolution des images.
- Segmentation des phases grâce aux seuils en fonction des niveaux de gris.
- Quantification des phases dans la zone analysée.

Le choix du grossissement et de la résolution des images joue un rôle important dans ce processus. En effet, plus le grossissement est élevé, plus la résolution de l'image est élevée mais plus le nombre d'images nécessaires et le temps d'analyse sont importants.
La segmentation des phases est effectuée par les seuils en fonction de niveau de gris et permet de distinguer les phases telles que : les pores, les hydrates et les anhydres (Figure 1-23).

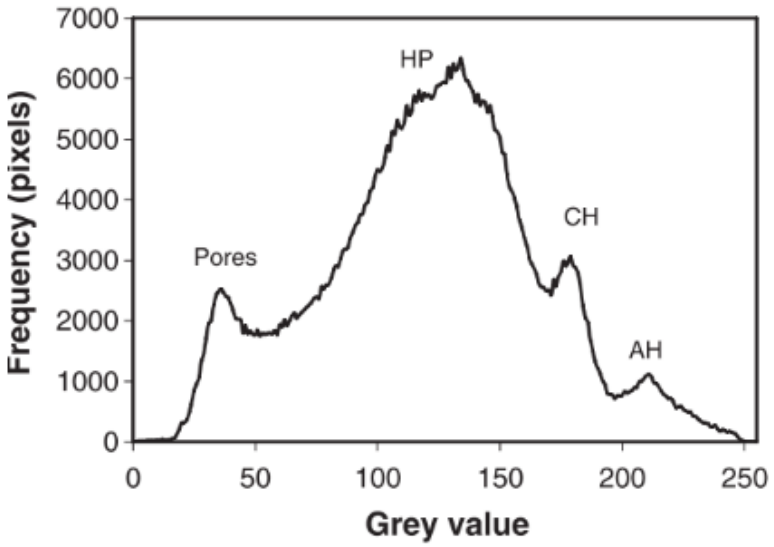

Figure 1- 23 : Histogramme du mortier [95]

Les seuils peuvent être déterminés en utilisant les points d'inflexion sur le graphe de l'aire cumulée en fonction du seuil de gris [95] (Figure 1-24).

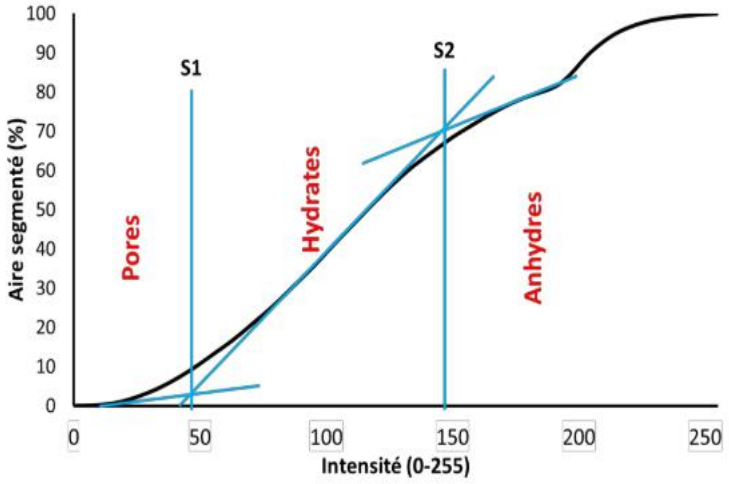

Figure 1- 24 : Estimation des seuils par la méthode de Wong et al [95] (Source d'image [93])

Enfin, la quantification des phases est effectuée et permet de calculer le degré de l'hydratation du ciment selon l'équation suivante :

$$\alpha(t) = \frac{V\ anhydre\ (t)}{V\ anhydre\ (t=0)} * 100$$

Avec :
V anhydre (t) : Volume de l'anhydre à l'instant (t) correspondant à la surface du pic de l'anhydre calculée.
V anhydre (t = 0) : Volume de l'anhydre à l'instant t = 0.
Le volume initial du ciment peut être calculé selon l'équation suivante :

$$V\ anhydre\ (t = 0) = \frac{1}{p\ (ciment\ ) * \left(\frac{E}{C}\right) + 1} * 100$$

Avec :
Pc : Densité spécifique du ciment.
E/C : Rapport E/C de la pâte de ciment.

II.8. Modélisation de l'hydratation

L'hydratation des matériaux cimentaires est un processus physico – chimique complexe. Par conséquence, une compréhension et une analyse numérique de ce processus au cours du temps d'hydratation sont très utiles pour connaître l'état du matériau ainsi que suivre l'évolution des phases dans le temps d'hydratation.
Dans la littérature, il existe 4 grandes familles de modèles de modélisation de l'hydratation des matériaux cimentaires :

- Modèles analytiques
- Modèles semi – analytiques
- Modèles thermodynamiques
- Modèles associés au développement de la microstructure.

II.8.1. Modèles analytiques

Dans cette famille de modélisation, il existe 3 différents types qui permettent de donner le degré de l'hydratation dans le temps.

- **Nucléation – Croissance**

  Ce modèle considère la vitesse de nucléation et la vitesse de croissance des hydrates selon l'équation suivante [96] :

$$\frac{d\alpha}{dt} = G(t)\frac{dN(t)}{dt}$$

Avec :
G(t) : Vitesse de croissance du système.
dN(t)/dt : Vitesse de nucléation du système.
L'équation de type Avrami [97] est principalement utilisée afin de modéliser la nucléation – croissance du système :

$$\frac{d\alpha}{dt} = (1-\alpha) * nkt^{(n-1)}$$

Pour chaque phase anhydre, les valeurs n, k doivent être ajuster expérimentalement [98].

- **Dispersion**

Knudsen [99] a proposé le modèle de dispersion qui prend en compte l'effet de la finesse des grains sur la cinétique de l'hydratation. L'hydratation du ciment peut être calculée selon l'équation suivante :

$$\alpha(r, t) = e^{(-\frac{r}{kt^n})}$$

Avec :
r : Rayon moyen des grains du ciment.
k : Coefficient à ajuster expérimentalement.

- **Diffusion ionique à travers les couches d'hydrates**

Lors de l'hydratation du ciment, le C-S-H formé sur la surface des grains de ciment modifierait considérablement le processus de l'hydratation du ciment. En effet, le processus de nucléation – croissance s'arrête et l'hydratation est contrôlée par la diffusion des ions à travers les couches d'hydrates. En outre, le changement de taille des grains du ciment doit être pris en compte. Pour prendre en compte le changement de rayon des grains du ciment, Fujii et al [100] ont proposé le modèle suivante :

$$-\frac{dr}{dt} = \frac{D}{r^D - r}$$

Avec :
D : Coefficient de diffusion ionique à travers les couches des hydrates.
r^D : Rayon du grain du ciment pour t = t^D.
Le degré de l'hydratation du ciment peut être calculé selon l'équation suivante :

$$\alpha = 1 - (\frac{r}{R})\hat{}3$$

Avec :
R : Rayon initial du grain du ciment.

- **Modèle semi-analytique**

Ce modèle donne le degré de l'hydratation du ciment à partir du degré de l'hydratation de chaque phase du clinker. Mounanga et al [90] ont utilisé ce modèle pour mesurer le degré de l'hydratation du ciment CEM I selon l'équation suivante :

$$\alpha(t) = \alpha_{C3S}(t) * [\%C_3S] + \alpha_{C2S}(t) * [\%C_2S] + \alpha_{C3A}(t) * [\%C3A] + \alpha_{C4AF}(t) * [\%C_4AF]$$

Avec:
α(t): Degré de l'hydratation du ciment à l'instant t.
$\alpha_{C3S}(t)$, $\alpha_{C2S}(t)$, $\alpha_{C3A}(t)$, $\alpha_{C4AF}(t)$: Degré de l'hydratation de C_3S, C_2S, C_3A et C_4AF respectivement à l'instant t.
[%C_3S], [%C_2S], [%C_3A], [%C_4AF] : Proportion massique initiale de C_3S, C_2S, C_3A et C_4AF respectivement.

- **Modèle thermodynamique**

Le principe de ce modèle est basé sur l'interaction entre les particules en solution et à l'équilibre chimique. La compatibilité des phases est déterminée afin de prédire la composition de la solution interstitielle et la formation des principaux hydrates du ciment hydraté [101].

- **Modèle associé au développement de la microstructure**

Le principe de ce modèle consiste à une représentation géométrique du système pour calculer les principales propriétés physiques et mécaniques du matériau hydraté. Nous pouvons citer certains codes de calcul utilisant ce modèle tels que : HYMOSTRUC et CEMHYD3D.

- **HYMOSTRUC**

Ce code de calcul développé par Breugel [102] permet de modéliser l'hydratation du ciment à partir des données d'entrées telles que : le rapport E/C, la granulométrie du ciment, la composition chimique du ciment.

- **CEMHYD3D**

Ce code développé par Bentz au NIST (National Institute of Standards and Technology) se compose de trois versions [103–105]. Il utilise une approche géométrique tridimensionnelle afin de modéliser le processus de l'hydratation du ciment ainsi que des propriétés de la microstructure [106–108]. Dans ce code, chaque voxel (un volume cubique de 1 μm^3) est attribué à une phase telle que : anhydre (C_3S, C_2S, C_3A, C_4AF, Gypse), hydrates (C-S-H, $Ca(OH)_2$, etc (Figure 1-25).

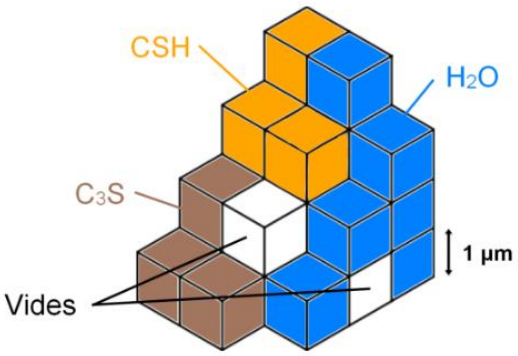

Figure 1- 25 : Présentation des voxels attribués aux phases dans le code CEMHYD3D (Source d'image [71])

Un processus composant 3 étapes consécutives permet de modéliser l'hydratation d'un matériau cimentaire et d'obtenir une microstructure de la pâte de ciment hydratée (Figure 1-26).

- **Étape 1** : Dans la première étape, le code permet de placer aléatoirement dans un volume cubique fini (en général, 100 * 100 * 100 μm^3) des particules monophasiques de clinker et des particules du gypse à partir des données expérimentales telles que : la granulométrie du ciment, la teneur volumique du gypse, le rapport volumique (E/C) de la pâte de ciment.
- **Étape 2** : Dans cette étape, les particules monophasiques du clinker sont divisées en différentes phases du clinker telles que C_3S, C_2S, C_3A et C_4AF grâce à des données expérimentales de la proportion volumique de ces phases dans le clinker.
- **Étape 3** : Dans la dernière étape, la modélisation de l'hydratation de la pâte de ciment sera effectuée dans les conditions contrôlées sous forme de cycle de dissolution – diffusion – précipitation. La modélisation de l'hydratation s'arrête si l'ensemble des

phases anhydres est hydraté ou après un certain nombre de cycles défini par l'utilisateur.

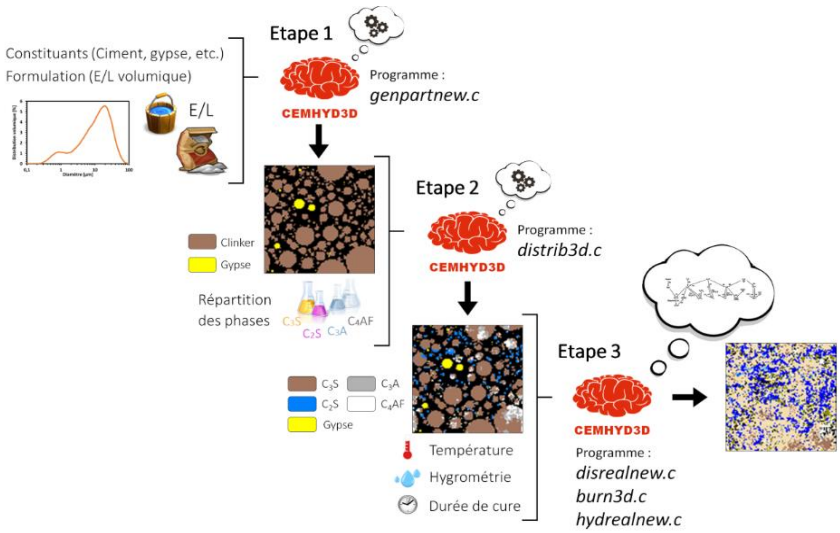

Figure 1- 26 : Étapes principales du processus de la modélisation de l'hydratation dans le code CEMHYD3D (Source d'image [71])

III. Méthode de Calcination Flash

III.1. Présentation de la méthode de calcination Flash

La méthode de calcination Flash est une technique de traitement thermique des matériaux fins à la température élevée pendant un temps très court. Cette technique a été initialement utilisée pour activer certaines argiles telles que le kaolinite [109],et les phases argileuses des sédiments [26]. Le principe de cette méthode consiste à éliminer l'eau interfoliaire par la calcination. En effet, les techniques de cuisson reposées sur l'utilisation de fours conventionnels rotatifs permettent d'aboutir à une activation des argiles. Malgré que ces cuissons soient efficaces, mais le temps du processus est important. De plus, les coûts énergétiques de cette méthode sont très élevés. Par conséquence, l'utilisation d'une autre méthode de calcination plus d'économie est encouragée.

La méthode de calcination Flash est une cuisson brutale et très rapide sous un transport aéraulique qui optimise la consommation énergétique et provoque la formation des phases métastables ou de morphologie complexe (grains multiphasique). En outre, le choc thermique pourrait provoquer des défauts de surface des cristallites ce qui crée un nombre de sites réactifs. Dans cette méthode, deux paramètres sont prépondérants : le temps d'exposition et la température de cuisson [26].

III.2. Étapes du processus de la calcination Flash

L'unité de calcination Flash utilisée dans cette thèse est le four de calcination Flash installé au centre de recherche (CERI MP) de l'IMT – Nord – Europe (Figure 1 – 27). Le four permet de calciner environ 25 kg du matériau par heure à une température allant jusqu'à 900 °C.

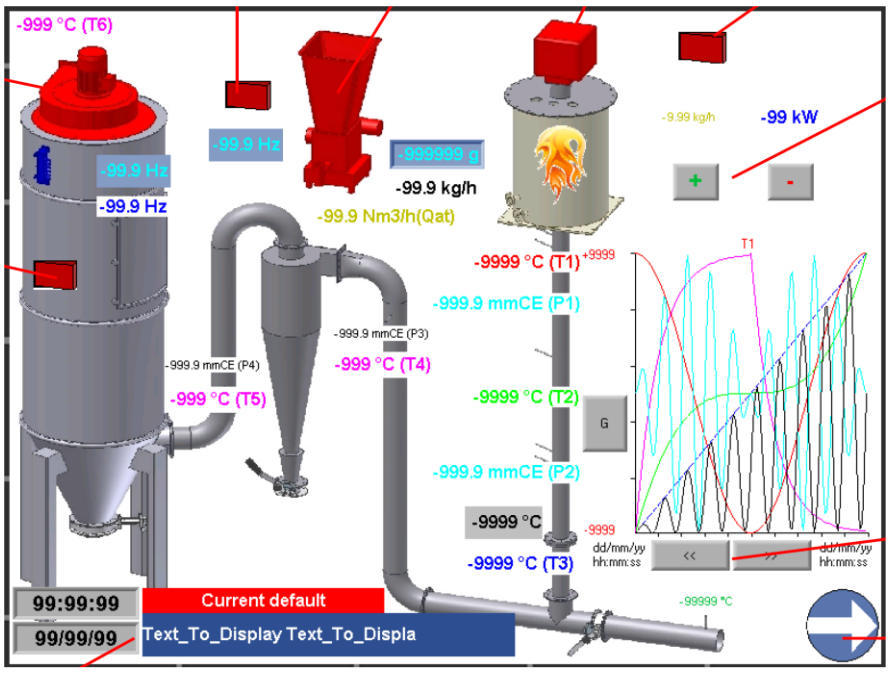

Figure 1- 27 : Schéma du four de calcination Flash (IMT Nord – Europe)

Les étapes principales du processus de calcination Flash sont les suivantes :

- **Préparation du matériau** : Avant d'introduir le matériau dans le four de calcination Flash, il doit être séché et finement broyé. En effet, la finesse des matériaux est un paramètre majeur pour leur future réactivité.
- **Introduction du matériau :** Le matériau est introduit dans la chambre de combustion grâce à un courant d'air comprimé. Ensuite, les particules du matériau sont cuites à haute température pendant quelque dixième de seconde.
- **Récupération du matériau :** Le matériau calciné est récupéré dans un cyclone en bas grâce à la gravité du matériau.

Conclusion et perspectives en vue du travail de thèse

Cette étude bibliographique permet de mettre en évidence plusieurs points importants :

- Le ciment Portland est un matériau complexe malgré que sa fabrication soit connue depuis plusieurs siècles. La valorisation des déchets dans le processus de fabrication du clinker est l'origine de la difficulté d'obtention d'un ciment ayant une composition régulière dans le temps. Un changement des matières premières pourrait provoquer un changement de la structure de phases formées dans le processus de clinkérisation.
- L'hydratation du ciment est un processus physico – chimique complexe qui dépend de plusieurs paramètres. Il existe plusieurs modèles qui permettent de modéliser l'hydratation du ciment. Cependant, il existe encore certaines divergences entre les modèles disponibles dans la littérature.
- Le sédiment est un matériau très hétérogène qui se compose de matières organiques, de matières inorganiques, d'eau, ect. Le sédiment a été valorisé avec succès dans plusieurs études mais la plupart de ces études sont à échelle laboratoire.

Dans ce contexte, cette thèse qui rentre dans le cadre d'un projet industriel vise à mettre en évidence un certain nombre d'interrogations :

- Quels sont les effets de l'incorporation d'un sédiment sur la formation des phases minérales du clinker ?
- Quelle méthode fiable pour mesurer le degré de l'hydratation ?
- Quelles sont les possibilités de modélisation numérique de l'hydratation des ciments en utilisant le code CEMHYD3D afin de mieux comprendre la cinétique d'hydratation du ciment à base sédiment ?
- Quel est la température optimale dans le processus de calcination Flash pour activer la réactivité pouzzolanique du sédiment ?
- Quels sont les effets du remplacement du laitier par le sédiment calciné dans la fabrication du ciment CEM III ?
- Quels sont les effets des taux de substitution du sédiment sur la cinétique d'hydratation, la performance mécanique ainsi que la structure des phases formées ?

Références:

1. Meyer, C.: The greening of the concrete industry. Cem. Concr. Compos. 31, 601–605 (2009). https://doi.org/10.1016/j.cemconcomp.2008.12.010
2. Mamindy-pajany, Y.: Traitement de sédiments portuaires méditerranéens contaminés en arsenic et en métaux : Géochimie et écotoxicologie, (2010)
3. M.BOUTOUIL: Traitement des vases de dragage par stabilisation / solidification à base de ciment et additifs, (1998)
4. Beauchamp, J.: « Sédiments et roches sédimentaires, cours de sédimentologie »
5. Schneider, G.: Boue de curage des cours d'eau. Le courrier de l'environnement de l'INRA.
6. LIFE, 2002.: Méthodes de gestion et de réutilisation des sédiments pollués. Agence de l'eau Picardie. Pôle de Compétence des sites et sols pollués. Etude réalisée par In Vivo, France, p. 126.
7. Ujevic, I., Odzak, N., Baric, A.: Trace metal accumulation in different grain size fractions of the sediments from a semi-enclosed bay heavily contaminated by urban and industrial wastewaters. Water Res. 24, 3055–3061 (2000)
8. Lin, J.-G., Chen, S.-Y., 1998.: The relationship between adsorption of heavy metal and organic matter in river sediments. Environment International 24, 345-352.
9. Gosselin, A.: Protocole d'évaluation de latraitabilité des sédiments, des sols et de boues à l'aide des technologies minéralurgiques. , Canada (1999)
10. Geffard, O.: Toxicité potentielle des sédiments marins et estuariens contaminés: évaluation chimique et biologique, biodisponibilité des contaminants sédimentaires. Thèse de doctorat., (2001)
11. Proulhac, N.: Schéma directeur du traitement des vases portuaires. , France (2006)
12. Grosdemange, D.: Guide pour la gestion des opérations de dragage. Fédération Française des Ports de Plaisance. (2005)
13. Cazalet, M.L.: Caractérisation physico-chimique d'un sédiment marin traité aux liants hydrauliques – Évaluation de la mobilité potentielle des polluants inorganiques . Hal. 239 (2012)
14. Hlavackova, P.: Evaluation du comportement du cuivre et du zinc dans une matrice de type sol à l'aide de différentes méthodologies., (2005)
15. Bonnet, C.: Développement de bioessais sur sédiments et applications à l'étude, en laboratoire, de la toxicité de sédiments dulçaquicoles contaminés., (2000)
16. MUSTIN, M.: Le compost : gestion de la matière organique. , Paris (1987)

17. Silitonga, E.: Valorisation des sédiments marins contaminés par solidification / stabilisation à base de liants hydrauliques et de fumée de silice. Thèse Dr. Univ. Caen/Basse Normandie. 229 (2010)
18. Hecho, L.: Etat de l'art des tests de traitabilité - Technique d'une pollution. (1998)
19. Luoma, S.N., Philip S. Rainbow: METAL CONTAMINATION IN AQUATIC ENVIRONMENTS. SCIENCE AND LATERAL MANAGEMENT. (2009)
20. Alzieu, C.: L'étain et les organoétains en milieu marin : biogéochimie et écotoxicologie. Repères océan (Ifremer), 15, 104p. (1999)
21. Calmano, W.: Mobilization and Scavenging of Heavy Metals Following Resuspension of Anoxic Sediments from the Elbe River. Environmental Geochemistry of Sulfide Oxidation. (1994)
22. Chapman, Peter, M., Wang, F., Janssen, C., Persoone, G., Herbert, E.A.: Ecotoxicology of metals in aquatic sediments: binding and release, bioavailability, risk assessment, and remediation. J. Can. des Sci. halieutiques Aquat. (1998)
23. C.Benoit-Bonnemason: Evolution des métaux et de leurs formes chimiques dans des vases portuaires stockées à terre. Ultra Traces Analyses Aquitaine (UT2A). (2007)
24. L'YAVANC, J., Alzieu, C., Mauvais, J.-L.: Les dragages sur le littoral français. In: Dragage et environnement marin : état des connaissances. (1999)
25. Egiseau: Bonnes pratiques pour la caractérisation des matériaux en vue d ' une opération de dragage et d ' immersion en milieu marin et estuarien. (2016)
26. Amar, M.: Étude expérimentale et numérique de la valorisaion des sédiments de dragage dans les matrices cimentaires - Thèse de doctorat, (2017)
27. Dubois, V.: Etude du comportement physico-mécanique et caractérisation environnementale des sédiments marins – Valorisation en technique routière - Thèse de doctorat, (2006)
28. Scordia, P.: Caractérisation et valorisation de sédiments fluviaux pollués et traités dans les matériaux routiers, (2008)
29. Tribout, C.: Valorisation de sédiments traités en techniques routières : contribution à la mise en place d'un protocole d'acceptabilité. Thèse de doctorant de l'Université Toulouse III, (2010)
30. Miraoui M.: Mise en œuvre d'une démarche de prétraitement et de traitement des sédiments de dragage en vue d'une valorisation dans le génie civil - Thèse de doctorat
31. DIA, M.: Traitement et Valorisation de Sédiments de Dragage Phosphatés en Technique Routière. thèse Dr. Univ. d'Artois. 072, 169 (2013)
32. S.Brakni: Première approche vers une valorisation de granulats artificiels à base de sédiments de dragage - Thèse de doctorat, (2008)
33. Ennahal, I., Maherzi, W., Benzerzour, M., Mamindy, Y., Abriak, N.E.: Performance of Lightweight Aggregates Comprised of Sediments and Thermoplastic Waste. Waste and Biomass Valorization. (2020). https://doi.org/10.1007/s12649-020-00970-1
34. DUAN, Z., LAFHAJ, Z., BEL HADJ ALI, I., DUCELLIER, S.: Valorisation des sédiments fluviaux traités en vue d'une utilisation en génie civil. Rev. Paralia. 6, 5.1-5.12 (2013). https://doi.org/10.5150/revue-paralia.2013.005
35. M.Samara: Valorisation des sédiments traités dans les bétons autoplaçants. XXVIe. In: Rencontres Universitaires de Génie Civil. , Nancy (2008)
36. Anger, B.: Caractérisation des sédiments fins des retenues hydroélectriques en vue d ' une orientation vers des filières de valorisation matière, (2014)
37. Benzerzour, M., Maherzi, W., Amar, M.A.A., Abriak, N.E., Damidot, D.: Formulation of mortars based on thermally treated sediments. J. Mater. Cycles Waste Manag. 20, 592–603 (2018). https://doi.org/10.1007/s10163-017-0626-0

38. Safhi, A. el M., Benzerzour, M., Rivard, P., Abriak, N.E., Ennahal, I.: Development of self-compacting mortars based on treated marine sediments. J. Build. Eng. 22, 252–261 (2019). https://doi.org/10.1016/j.jobe.2018.12.024
39. Faure, A.: Capacité d ' un sédiment à se substituer à la fraction argileuse de la matière première de l ' industrie des liants hydrauliques - Thèse de doctorat, (2017)
40. Association Française de Normalisation (AFNOR): NF EN 197-1: Composition, spécifications et critères de conformité des ciment courant.
41. Renaut, M.: Calcination des déchets industriels : synthèse de ciment et stabilisation / solidification des résidus de combustion - Thèse de doctorat, (2017)
42. Gani, M.: Cement and Concrete. Londres: Chapman & Hall. 224 p. ISBN : 978- 0412790508. (1997)
43. Gineys, N.: Influence de la teneur en éléments métalliques sur les propriétés techniques et environnementales du ciment Portland, (2011)
44. Taylor HFW: Cement chemistry. (1997)
45. Seidel G., Huckauf H., S.J.: Technologies des ciments, plâtres et chaux, Septima, Paris, 1980, 230 p.
46. Abdo, J.: Ciments. C920 V2. Saint-Denis: Techniques de l'Ingénieur. 16 p.
47. G.K.Moir: Advanced Concrete Techbology. (2003)
48. Lawrence, C. D., 2004b.: The Constitution and Specification of Portland Cements. Dans: P. C. Hewlett, éd. Lea's Chemistry of Cement and Concrete. Quatrième éd. Oxford: Butterworth- Heinemann, pp. 130-193. ISBN: 0750662565.
49. F.W.Locher: Cement principles of production and use. (2006)
50. Bogue, R.H., Lerch, W.: Hydration of Portland Cement Compounds. Ind. Eng. Chem. 26, 837–847 (1934). https://doi.org/10.1021/ie50296a007
51. Humblodt K.D.H, W.A.G.: L'évolution technologique du four rotatif avec préchauffeur à cyclones vers le four court, Pyrorapid, 1986. Ishikawa.
52. Lea: Lea's chemistry of cement and concrete. Elsevier. (2003)
53. Hirono, T., Tanikawa, W.: Implications of the thermal properties and kinetic parameters of dehydroxylation of mica minerals for fault weakening, frictional heating, and earthquake energetics. Earth Planet. Sci. Lett. 307, 161–172 (2011). https://doi.org/10.1016/j.epsl.2011.04.042
54. Jiang, T., Li, G., Qiu, G., Fan, X., Huang, Z.: Thermal activation and alkali dissolution of silicon from illite. Appl. Clay Sci. 40, 81–89 (2008). https://doi.org/10.1016/j.clay.2007.08.002
55. Konan, K.L., Peyratout, C., Smith, A., Bonnet, J.P., Magnoux, P., Ayrault, P.: Surface modifications of illite in concentrated lime solutions investigated by pyridine adsorption. J. Colloid Interface Sci. 382, 17–21 (2012). https://doi.org/10.1016/j.jcis.2012.05.039
56. Habert, G., Choupay, N., Escadeillas, G., Guillaume, D., Montel, J.M.: Clay content of argillites: Influence on cement based mortars. Appl. Clay Sci. 43, 322–330 (2009). https://doi.org/10.1016/j.clay.2008.09.009
57. Garg, N., Skibsted, J.: Pozzolanic reactivity of a calcined interstratified illite/smectite (70/30) clay. Cem. Concr. Res. 79, 101–111 (2016). https://doi.org/10.1016/j.cemconres.2015.08.006
58. He, C., Makovicky, E., Osbæck, B.: Thermal stability and pozzolanic activity of raw and calcined mixed-layer mica/smectite. Appl. Clay Sci. 17, 141–161 (2000). https://doi.org/10.1016/S0169-1317(00)00011-9
59. Buchwald, A., Hohmann, M., Posern, K., Brendler, E.: The suitability of thermally activated illite/smectite clay as raw material for geopolymer binders. Appl. Clay Sci. 46, 300–304 (2009). https://doi.org/10.1016/j.clay.2009.08.026
60. Toledo Filho, R.D., Gonçalves, J.P., Americano, B.B., Fairbairn, E.M.R.: Potential for use of

crushed waste calcined-clay brick as a supplementary cementitious material in Brazil. Cem. Concr. Res. 37, 1357–1365 (2007). https://doi.org/10.1016/j.cemconres.2007.06.005
61. Villiéras, F., Yvon, J., François, M., Maurice^Cases, J., Lhote, F., Uriot, J.P.: Micropore formation due to thermal decomposition of hydroxide layer of Mg-chlorites: interactions with water. Appl. Clay Sci. 8, 147–168 (1993). https://doi.org/10.1016/0169-1317(93)90034-X
62. Gambhir, M.: Concrete Technology - Theory and Practice. Quatrième éd. New Delhi: Tata McGraw Hill Education Private Limited. 716 p. ISBN : 978-0-07-015136-9. (2009)
63. Joshi, R. C. & Lohtia, R. P., 1997.: Fly Ash in Concrete: Production, Properties and Uses. Amsterdam: Gordon and Breach Science Publishers. 128 p. ISBN : 90-5699-580-4.
64. Siddique, R. & Khan, M. I., 2011.: Supplementary Cementing Materials. Berlin: Springer-Verlag. 287 p. ISBN : 978-3-642-17865-8.
65. Ramachandran, V., Paroli, R., Beaudoin, J. & Delgado, A., 2002.: Handbook of thermal analysis of construction materials. Norwich: Noyes Publications / William Andrew Publishing. 680 p. ISBN : 0-8155-1487-5. Ramaroson,.
66. Barnes P., Ghose A., M.A.L.: Cement tubules: another look, Cement and Concrete Research, Vol. 10, 1980, p. 639-645.
67. Faure, A.: Capacité d ’ un sédiment à se substituer à la fraction argileuse de la matière première de l ’ industrie des liants hydrauliques - Thèse de doctorat, (2017)
68. Maki, I., Goto, K.: Factors Influencing the Phase Constitution of Alite. Cem. 12, 301–308 (1982)
69. Kurdowski, W., 2014.: Cement and Concrete Chemistry. Dordrecht: Springer. 700 p. ISBN : 978-94-007-7944-0.
70. Bye, G.C.: Portland cement: Composition, production and properties. (1999)
71. Bordy, A.: Influence des conditions thermo-hydriques de conservation sur l ’ hydratation de matériaux cimentaires à base d ’ une fine recyclée. 1–155 (2016)
72. Younsi, A.: Carbonatation de bétons à forts taux de substitution du ciment par des additions minérales, (2012)
73. Berthomier, M.: Etude de la lixiviation de l’aluminium de matériaux cimentaires à base de CEM III utilisés dans les canalisations d’eau potable : approche expérimentale et numérique. (2020)
74. Lothenbach, B., Scrivener, K., Hooton, R.D.: Supplementary cementitious materials. Cem. Concr. Res. 41, 1244–1256 (2011). https://doi.org/10.1016/j.cemconres.2010.12.001
75. Tang, S., Wang, Y., Geng, Z., Xu, X., Yu, W., A, H., Chen, J.: Structure, fractality, mechanics and durability of calcium silicate hydrates. Fractal Fract. 5, (2021). https://doi.org/10.3390/fractalfract5020047
76. Wang, L., Guo, F., Lin, Y., Yang, H., Tang, S.W.: Comparison between the effects of phosphorous slag and fly ash on the C-S-H structure, long-term hydration heat and volume deformation of cement-based materials. Constr. Build. Mater. 250, 118807 (2020). https://doi.org/10.1016/j.conbuildmat.2020.118807
77. S. Gauffinet, E. Finot, E. Lesniewska, et A.N.: Observation directe de la croissance d’hydrosilicate de calcium sur des surfaces d’alite et de silice par microscopie à force atomique ».
78. Richardson, I.G.: Nature of C-S-H in hardened cements. Cem. Concr. Res. 29, 1131–1147 (1999). https://doi.org/10.1016/S0008-8846(99)00168-4
79. Escalante-Garcia, J.I., Sharp, J.H.: Variation in the composition of C-S-H gel in portland cement pastes cured at various temperatures. J. Am. Ceram. Soc. 82, 3237–3241 (1999). https://doi.org/10.1111/j.1151-2916.1999.tb02230.x
80. Richardson, I.G.: The calcium silicate hydrates. Cem. Concr. Res. 38, 137–158 (2008).

https://doi.org/10.1016/j.cemconres.2007.11.005
81. Nonat, A.: Chapitre2: L'hydratation des ciments- La durabilité des bétons. (2008)
82. P. Faucon: « Durabilité du béton : Physico-chimie de l'altération par l'eau », Université de Cergy Pontoise, 1997.
83. Renaudin, G., Russias, J., Leroux, F., Cau-dit-Coumes, C., Frizon, F.: Structural characterization of C-S-H and C-A-S-H samples-Part II: Local environment investigated by spectroscopic analyses. J. Solid State Chem. 182, 3320–3329 (2009). https://doi.org/10.1016/j.jssc.2009.09.024
84. Lothenbach, B., Nonat, A.: Calcium silicate hydrates: Solid and liquid phase composition. Cem. Concr. Res. 78, 57–70 (2015). https://doi.org/10.1016/j.cemconres.2015.03.019
85. Kovačević, G., Persson, B., Nicoleau, L., Nonat, A., Veryazov, V.: Atomistic modeling of crystal structure of Ca1.67SiHx. Cem. Concr. Res. 67, 197–203 (2015). https://doi.org/10.1016/j.cemconres.2014.09.003
86. J. Haas: « Etude expérimentale et modélisation thermodynamique du système CaO-SiO2-(Al2O3)-H2O » Université de Bourgogne, Dijon, 2012.
87. Zhou, Q., Glasser, F.P.: Thermal stability and decomposition mechanisms of ettringite at <120°C. Cem. Concr. Res. 31, 1333–1339 (2001). https://doi.org/10.1016/S0008-8846(01)00558-0
88. F.M., L.: Chemistry of cement and concrete, 4th edition, John Wiley and Sons Inc., New York, Toronto, 1988, 1092 p.
89. Elkarim, M., Bulteel, D., Potier, G., Michel, F., Zhao, Z., Courard, L.: Use of grinded hardened cement pastes as mineral addition for mortars. (2020). https://doi.org/10.1016/j.jobe.2020.101863
90. Mounanga, P., Khelidj, A., Loukili, A., Mounanga, P., Khelidj, A., Loukili, A., Predicting, V.B.: Predicting Ca (OH) 2 content and chemical shrinkage of hydrating cement pastes using analytical approach To cite this version : HAL Id : hal-01007190. (2004)
91. Kocaba, V.: Development and Evaluation of Methods to Follow Microstructural Development of Cementitious Systems Including Slags Development and Evaluation of Methods to Follow Microstructural Development of Cementitious Systems Including Slags
92. Namoulniara, D.K., Kevin, D., Etude, N.: Etude expérimentale de la diffusion du CO2 et des cinétiques de carbonatation de matériaux cimentaires à faible dosage en clinker To cite this version : HAL Id : tel-01279105 Etude expérimentale de la diffusion du CO 2 et des cinétiques de carbonatation d. (2016)
93. LE, T.: Influence de l'humidité des granulats de béton recyclé sur le comportement à l'état frais et durcissant des mortiers, (2015)
94. Kocaba, V., Gallucci, E., Scrivener, K.L.: Methods for determination of degree of reaction of slag in blended cement pastes. Cem. Concr. Res. 42, 511–525 (2012). https://doi.org/10.1016/j.cemconres.2011.11.010
95. Wong, H.S., Head, M.K., Buenfeld, N.R.: Pore segmentation of cement-based materials from backscattered electron images. Cem. Concr. Res. 36, 1083–1090 (2006). https://doi.org/10.1016/j.cemconres.2005.10.006
96. Powers: Structure and Physical Properties of Hardened Portland Cement Paste. Journal of the American Ceramic Society, 41(1958), p.1 (1958).
97. M. Avrami: Kinetics of Phase Change. I General Theory. The Journal of Chemical Physics, 7(12) (1939).
98. I. Odler, J. Schüppstuhl: Early hydration of tricalcium silicate III. Control of the induction period. Cement and Concrete Research, 11(5), pp.765–774 (1981).
99. T. Knudsen: The dispersion model for hydration of portland cement I. General concepts. Cement and Concrete Research, 14, pp.622–630 (1984).

100. K. Fujii, W.K.: Kinetics of the Hydration of Tricalcium Silicate. Journal of the American Ceramic Society, 57(11), pp.492–497 (1974).
101. B. Lothenbach, F. Winnefeld, C. Alder, E. Wieland, P. Lunk: Effect of temperature on the pore solution, microstructure and hydration products of Portland cement pastes. Cement and Concrete Research, 37, pp.483–491 (2007).
102. K. Van Breugel: Simulation of hydration and formation of structure in hardening cement-based materials. TU Delft, Delft University of Technology. (1991).
103. Bentz, D.P.: Guide to Using CEMHYD3D: A Three-Dimensional Cement Hydration and Microstructure Development Modelling Package. (1997)
104. NIST: Guide to using CEMHYD3D Version 3.0.
105. Bentz, D.P.: CEMHYD3D : A Three-Dimensional Cement hydratation and Microstructure Development Modelling Package Version 2.0.
106. Kamali, S., Moranville, M., Garboczi, E., Prené, S., Gérard, B.: Hydrate dissolution influence on the Young's modulus of cement pastes. Proc. 5th Int. Conf. Fract. Mech. Concr. Concr. Struct. 12–16 (2004)
107. Analysic of CCRL proficiency cements 135 and 136 usiNG CEMHYD3D.
108. Guillon, E.: Durabilité des matériaux cimentaires : modélisation de l ' influence des équilibres physico-chimiques sur la microstructure et les propriétés mécaniques résiduelles, (2004)
109. San Nicolas, R.: Approche performantielle des bétons avec métakaolins obtenus par calcination flash. (2011)

Partie I : Valorisation des sédiments dans la fabrication du ciment

Cette partie présente, sous forme de plusieurs articles, les études menées pour la formulation de ciments pour lesquels le sédiment est directement intégré dans le cru. Les différents impacts sur l'ensemble des propriétés des matériaux finaux et les résultats obtenus y sont détaillés. Dans cette partie deux chapitres y sont présenté, l'un avec une approche laboratoire et numérique, le second avec une approche tenant en compte les contraintes industrielles.

Chapitre 2 : Valorisation du sédiment contaminé dans le cru – Impact de la teneur élevée du sédiment incorporé sur la formation des phases et la performance du ciment produit.

I. Introduction du chapitre

Dans ce chapitre, d'une part, nous présentons les résultats de la valorisation du sédiment dans la fabrication du ciment CEM I et d'autre part, les effets de l'incorporation du sédiment sur la formation des phases minérales du clinker. En outre, le code CEMHYD3D a été utilisé afin de modéliser l'hydratation des ciments synthétisés. Ceci permet de prédire égalementl'évolution des phases du ciment au cours du temps d'hydratation et de confirmer le comportement d'hydratation du ciment à base du sédiment. Nous présentons également les résultats de l'étude de comparaison du degré de l'hydratation du ciment déterminé par trois différentes méthodes (Méthode de quantification de la Portlandite – Méthode de quantification de l'eau liée – Méthode de l'analyse des images SEM –BSE). L'objectif de cette étude est d'évaluer la fiabilité de chaque méthode. Par la suite, la méthode retenue sera utilisée afin déterminer les valeurs du degré de l'hydratation des ciments synthétisés dans cette thèse et ces valeurs seront également utilisées pour être comparées avec les valeurs prédites par le code CEMHYD3D. De plus, cette étude permettera d'évaluer la fiabilité de la méthode d'analyse des images SEM – BSE qui pourrait être utilisée dans le cas des ciments contenant des additions pouzzolaniques.

Les objectifs de ce chapitre sont les suivants :

- Évaluation de la qualité du processus de cuisson des mélanges crus et le processus de broyage des clinkers à l'échelle laboratoire.
- Étude de l'influence d'une teneur élevée de sédiment sur la formation des phases minérales du clinker, sur la cinétique de l'hydratation et sur les performances mécaniques du ciment à base de sédiment.
- Étude de la fiabilité des différentes méthodes de détermination du degré de l'hydratation du ciment.
- Modélisation numérique de l'hydratation des ciments synthétisés au laboratoire en utilisant le code CEMHY3D

Les résultats de ce chapitre sont présentés dans deux articles ci-dessous (article 1 et article 2).

II. Démarche expérimentale

Dans la première partie de ce chapitre, deux formulations de cru ont été préparées. Les clinkers et les ciments synthétisés ont été caractérisés afin de comprendre les effets du sédiment sur les propriétés du ciment. La quantité de chaque matière première dans le cru de chaque formulation a été calculée en utilisant les valeurs des modules LSF, AR, SR qui sont utilisées habituellement dans l'industrie cimentière. Ensuite, l'ensemble des matières premières ont été mélangées en ajoutant de l'eau afin d'obtenir un mélange plus homogène. Pour faciliter la cuisson dans le four,

des pastilles ont été confectionnées. Elles ont été ensuite cuites dans le four selon le programme suivant :

- Cuisson à 200 °C pendant 20 minutes
- Augmentation de la température jusqu'à 1450 °C avec une rampe de 7 °C/min,
- Palier de 15 minutes à 1450 °C
- Refroidissement dans le four jusqu'à la température ambiante.

Le processus expérimental de cette partie est présenté ci-dessous :

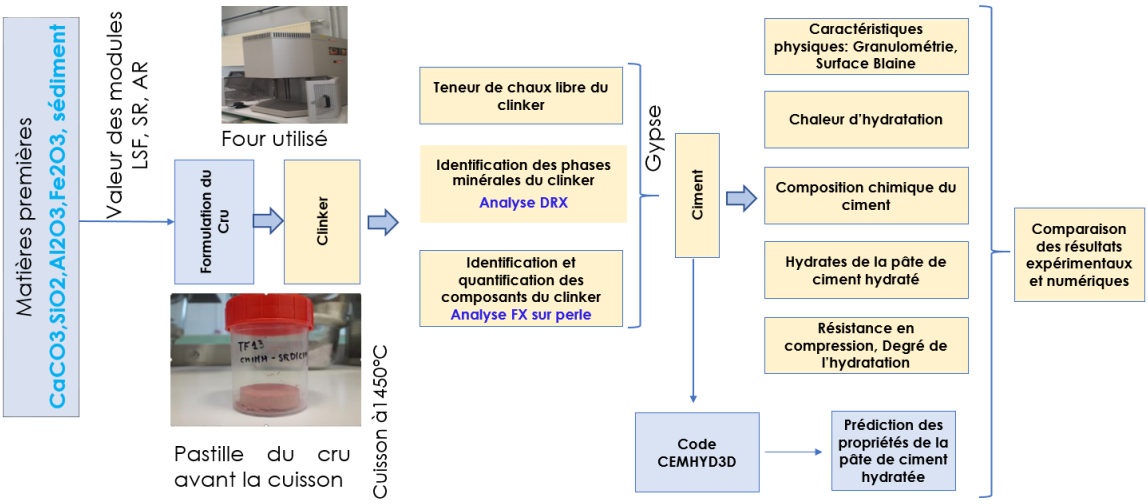

Les résultats de cette étude sont présentés dans l'article 1.

Dans la deuxième partie de ce chapitre, nous nous intéressons à évaluer les méthodes habituellement utilisées dans la littérature pour la détermination du degré de l'hydratation du ciment CEM I. Le ciment utilisé est le ciment de référence synthétisé dans la première partie de ce chapitre (OPC 97TM). Ce choix permet de limiter l'incorporation des éléments mineurs dans les phases minérales du clinker ainsi que les hydrates de la pâte de ciment hydratée. La pâte de ciment a été confectionnée avec un rapport E/C = 0.5. Puis, les pâtes ont été préservées dans une solution saturée en chaux jusqu'à maturation (2 et 28 jours). Ce choix permet d'éviter le phénomène de carbonatation de l'échantillon qui peut influencer sur le résultat. Pour l'analyse des images SEM–BSE, on doit faire un arrêt d'hydratation avant l'acquisition des images. Plusieurs images ont été prises dans les différentes zones de l'échantillon. Le logiciel Origine Pro a été utilisé afin de quantifier les phases sur l'histogramme de l'image.

La composition chimique des phases minérales du clinker et de la phase C-S-H de la pâte de ciment hydratée a été mesurée en utilisant l'analyse MEB – EDS. Pour cette analyse, environ 100 points ont été mesurés sur les différentes zones de l'échantillon.

Le processus expérimental de cette étude est présenté ci-dessous :

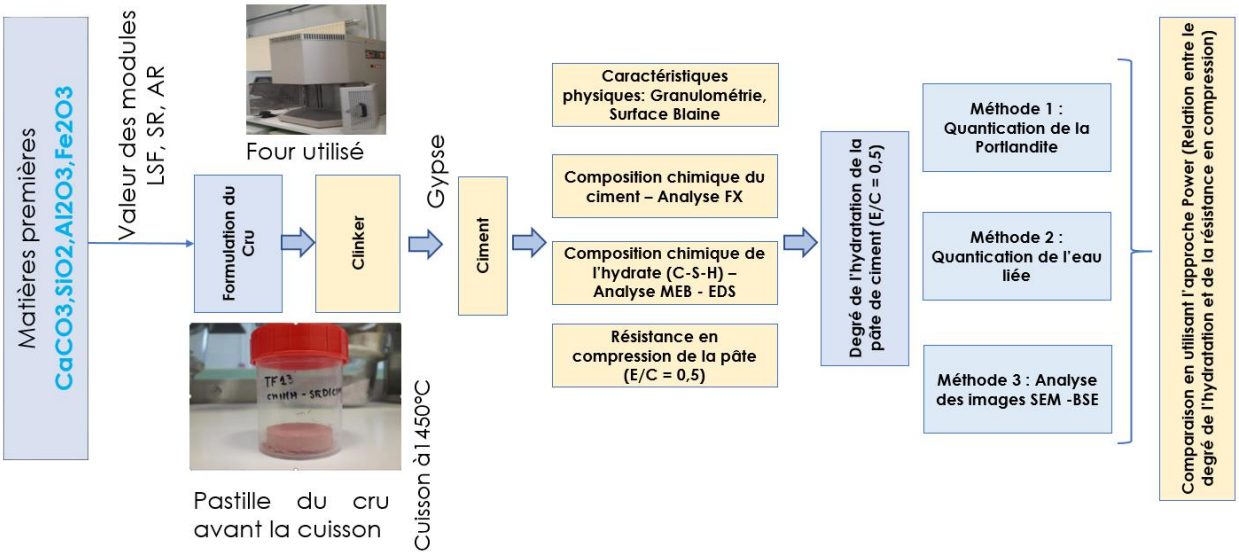

Les résultats de cette étude sont présentés dans l'article 2.

III. Résultat du chapitre

Les résultats des travaux effectués dans cette partie sont présentés dans l'article 1 et l'article 2 ci-après.

Article 1: Recycling of dredged sediment as a raw material for the manufacture of Portland cement – Numerical modeling of the hydration of synthesized cement using the CEMHYD3D code

Synthèse : Dans cette étude, deux ciments ont été synthétisés au laboratoire. Les caractéristiques du ciment OPC 97 (32% wt du sédiment incorporé dans le cru) ont été comparées aux ceux du ciment OPC TM (ciment de référence, sans sédiment dans le cru). Les caractéristiques du ciment OPC 97 ont été comparées aux ceux du ciment OPC TM. Le degré de l'hydratation des ciments a été déterminé en utilisant la méthode de quantification de l'eau dans les hydrates à l'aide de l'analyse ATG après 2 et 28 jours de l'hydratation. La résistance en compression a été mesurée sur les échantillons de la pâte (E/C = 0.5) de 1 * 1 *1 cm^3. En outre, les caractéristiques de deux ciments ont été utilisées comme les données d'entrée du code CEMHYD3D. La modélisation de l'hydratation est effectuée dans les conditions similaires à celles dans les analyses expérimentales.

Les résultats montrent que :

- Le sédiment pourrait être utilisé comme matière première dans la fabrication du ciment.
- La présence de MgO et du SO_3 favorise la formation du polymorphe M3 de l'Alite dans le clinker à base du sédiment
- Le sédiment ne modifie pas la formation des phases minérales dans le clinker. Cependant, la présence des éléments mineurs pourrait provoquer une teneur Ca/Si plus élevée dans la phase C_3S par rapport au clinker de référence.
- Le ciment à base du sédiment présente un comportement similaire au ciment Portland ordinaire lorsque l'on mesure la chaleur d'hydratation, le degré d'hydratation et le développement de la résistance en compression en fonction du temps.

- Le logiciel CEMHYD3D a été utilisé pour modéliser l'hydratation du ciment et suivre l'évolution des phases dans le temps. Le code a simulé parfaitement l'hydratation des ciments en comparant les résultats numériques et les résultats expérimentaux. La modélisation confirme le comportement expérimental du ciment à base sédiment.

Date de soumission	
Statut	Accepté et publié
Journal	Journal of Building Engineering https://doi.org/10.1016/j.jobe.2021.103871

Article 1: Recycling of dredged sediment as a raw material for the manufacture of Portland cement – Numerical modeling of the hydration of synthesized cement using the CEMHYD3D code

Duc Chinh CHU[(1)(*)], Joelle KLEIB[(1)], Mouhamadou AMAR[(1)], Mahfoud BENZERZOUR[(1)], Nor-Edine ABRIAK[(1)]

[(1)] Univ.Lille, IMT Lille Douai, Univ.Artois, Yncrea Hauts-de-France, ULR 4515-LGCgE, 6 Laboratoire de Génie civil et géo-Environnement, F-59000, Lille, France

[(*)] **Corresponding author: Duc Chinh CHU**

Email: duc.chinh.chu@imt-lille-douai.fr

ABSTRACT

Around 56 million m^3 of sediments are dredged in France per year to maintain the access to ports and waterways. Sediments are considered as waste regarding regulations and cause environmental, ecological and economic issues. This paper aims to use dredged sediments as raw material to replace traditional materials in Portland clinker production. Two clinkers are produced at the laboratory scale: a reference with chemical reagents $CaCO_3$, SiO_2, Al_2O_3 and Fe_2O_3 and a second clinker with sediment as a partial substitution for chemical reagents while controlling all the three cementitious modulus.

The synthetized cements were characterized by X-ray diffraction; X-ray fluorescence and scanning electron microscopy in order to identify their mineralogical and chemical composition as well as their microstructure. The reactivity of the synthesized cements was followed by isothermal calorimetry and the mechanical strength of cement pastes was measured at 2, 15 and 28 days. The CEMHYD3D code was used to numerically modelling the hydration of synthesized cements in order to follow the evolution of phases and to predict the properties of hydrated cements.

The results demonstrate the potentiality of reuse sediments in the cement manufacturing with a high rate of sediment incorporation without affecting the phase assemblage.

Keywords: Recycling, sediment, clinker, hydration, CEMHYD3D

Graphical abstract

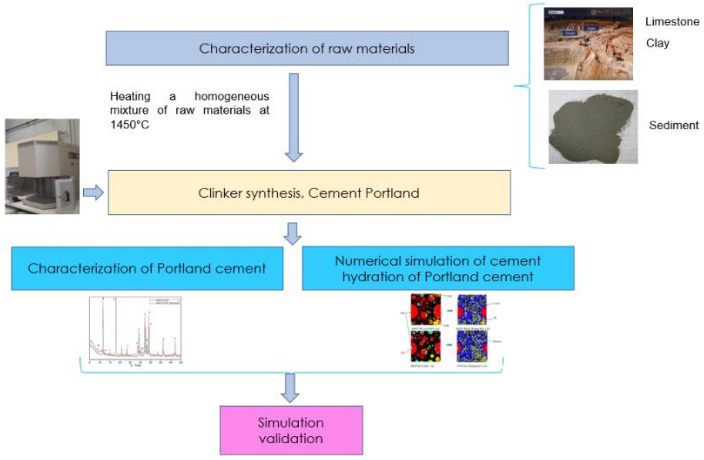

1. Introduction

In 2016, the French cement industry produced around 17 million tons of cement and represents the leader in producing Portland cement in the European Union [1]. However, the production of cement has a considerable impact on the environment related to the extraction of natural resources and the CO_2 emissions [2]. In 2012, around 800 million tons of raw materials were extracted in France where 50% are allocated for the production of construction materials [3]. Consequently, the valorization of industrial by-products and waste as raw materials in the manufacture of cement became a trend for reserving natural resources. Previous studies [4–9], have demonstrated the effectiveness of using wastes by partial replacing some of the raw materials in the manufacture of cement.

In France, around 56 Mm^3 of sediments (marine and river sediments) are dredged annually to restore acceptable navigation thresholds, to avoid flooding and to improve the quality of the environment. After dredging, sediments are either immersed in the sea, remained in the land (in general polluted sediment), or recovered in different sectors such as construction and agriculture. Several treatments and recovery methods for sediments have been studied and applied in various fields of civil engineering. Among these, the re-use of sediments in road engineering as a base layer or a form layer [10–14], manufacture of artificial aggregates [15] and as a mineral addition in mortars [16, 17]. In the most of these applications, sediments should be treated before recovery.

In addition to the above applications of sediments, some studies showed that the latter could replace some of the raw materials in the manufacture of cement due to its chemical composition that contains the main components ($CaCO_3$, SiO_2, Al_2O_3 and Fe_2O_3) for clinker production. In fact Portland cement contains about 95% of clinker and 5% of secondary constituents [18]. The clinker results from burning at high temperature (1450°C) of the raw mixture generally containing 80% of limestone, as a source of calcium oxide, and 20% of clay as a source of silica and alumina and iron oxide. At high temperature, the chemical elements recombine to form four main mineral phases: Tri-calcium silicate (C_3S: $3CaO.SiO_2$), Di-calcium silicate (C_2S: $2CaO.SiO_2$), Tricalcium aluminate (C_3A: $3CaO.Al_2O_3$) and Alumino-tetracalcium ferrite (C_4AF: $4CaO.Al_2O_3.Fe_2O_3$) (Table 1) [18].

Table 1 Main phases of Portland clinker according to the cement nomenclature

Mineral phases	Cement nomenclature	Full chemical formula	Minimum content (wt%)	Maximum content (wt%)
Alite	C_3S	Ca_3SiO_5	45.0	79.7
Belite	C_2S	Ca_2SiO_4	5.7	29.8
Tricalcium aluminate	C_3A	$Ca_3Al_2O_5$	1.1	14.9
Alumino-tetracalcium ferrite	C_4AF	$Ca_4Al_2Fe_2O_{10}$	2.0	16.5

Dalton et al. [19] have synthesized clinkers at a laboratory and industrial scale, with raw materials extracted from quarries and with a contaminated sediment from New York/New Jersey Port. Different formulations with variable sediment substitution rates from 1% to 12% were tested. The authors noted that the Alite/Belite ratio in the synthesized clinkers decreased when the sediment content in the clinker was greater than 6.5% on the laboratory and industrial scale. The compressive strength of these cements was slightly lower than that of the reference Portland cement. Therefore, they conclude that cooling is necessary to prevent the decomposition of alite into belite and free lime.

Aouad et al [20] used the lower fraction (2 mm) of a heavy metal contaminated river sediment from a canal in northern France, to synthesize a clinker in the laboratory with 39.1% of sediment. The authors showed that the four mineral phases of the cement were obtained without appearance of secondary phases. The compressive strength of the synthesized cement paste was 20% higher compared to that of the reference cement paste (CEM I 52.5) at 56 days.

The fine sediments (<200µm) from French hydroelectric reservoirs has been used by Faure et al. [21], [22] as a raw material in the raw meal for Portland clinker production. The sediments replaced all or a part of the silico-aluminous raw materials in the raw mix. The mixtures were burned in a static furnace at 1450°C for 45 minutes and subjected to rapid air quench cooling. The Portland cement produced from clinker incorporating 11.3% of sediment has satisfactory properties in accordance with NF EN 197-1 standard. Compared with the reference cement, it has a higher reactivity and develops a higher mechanical performance.

Therefore, the objectives of this study are, first to synthesize a clinker in the laboratory scale with the highest possible content of the river sediment Noyelle - Sous -Lens (NSL) from the Haut de France. The cements containing sediment have been characterized and compared to those synthesized from pure raw materials in order to study the substitution impacts of the sediment on the property of the cements. Second the hydration of synthesized cements was modeled using the CEMHYD3D code.

2. Materials and research methods

The raw materials used in this study for clinker's manufacturing are chemical reagents $CaCO_3$, SiO_2, Al_2O_3, Fe_2O_3, in addition to the sediment.

The sediment used is river sediment collected from the Noyelles-Sous-Lens (NSL) disposal site in the Haut de France region, France. This sediment was homogenized and dried in the oven at 40°C to reach a constant weight, then grounded.

2.1. Results of the sediment characterization

Different characterizations were conducted on the sediment before using it in the raw meal for clinker production.

The physical characterization consists to determine: the particle size distribution of the sediment using the COULTER laser granulometer type LS 13320 after a liquid dispersion, the organic matter content (OM) by measuring the weight loss at 550°C for 2 hours , the density by a helium pycnometer of Accupyc 1330 type [23], the value with methylene blue (VBS) [24], the fineness of sediment by the Brunauer-Emmett-Teller (BET) method, and the Blaine method [25].

The chemical composition of the sediment was identified using X-ray fluorescence analysis.

The mineralogical composition of the sediment was analysed by XRD analysis (using a Bruker D2 Advance device equipped with a Cu anticathode, λ = 1.5406 Å) with the angle 2θ from 5° to 80° and a step size of 0.02. In order to complete the sediment's characterization a thermogravimetric analysis TGA/DTA (using a Netzsch STA 409 device) was carried out on 100 mg of dried fine sediment (particle size less than 40 µm) with a heating rate of 10 °C/min and temperature range from 40°C to 1000°C.

The mobility of the metallic trace elements (MMTE) and the anionic elements of the raw sediment were measured after the leaching of the sample using a liquid/solid ratio of 10 and an equilibrium time of 24 hours according to the standard NF EN 12457-2 [26] using an Inductively Coupled Plasma Optical Emission Spectrometer (ICP-OES 5100 Agilent Technologies). The leaching limit values for inert waste (IW) and non-hazardous waste (NHW) specified in Directive 1999/31/EC were used to verify material compliance.

2.1.1. The physical characteristics of the sediment

The results of the physical characterization are shown in the Table 2. The NSL sediment has an organic matter content of 16.1%. The loss on ignition at 950°C is due to the decomposition of the limestone in the sediment.

The Blaine surface of the sediment is higher than that of commercial Portland cement (the value of 3800 cm^2/g). The value of the BET surface of the sediment is more important than that of Blaine because it is more influenced by the roughness of the surface and the open porosity [18].

Table 2 Physical characteristics of the sediment

Property	NSL
Density (g/cm^3)	2.43
BET (cm^2/g)	43765
Blaine surface (cm^2/g)	6562
OM content (wt%)	16.1
LOI 950°C/1h (%)	27.63
d_{10} (µm)	1.39
d_{50} (µm)	10.16
d_{90} (µm)	47.90

The particle size distribution of the sediment presented in Fig. 1 shows that approximately 99.7% of the particles have a particle size less than 200 µm. This result is in accordance with the particle size required for the raw materials in the cement industry [27].

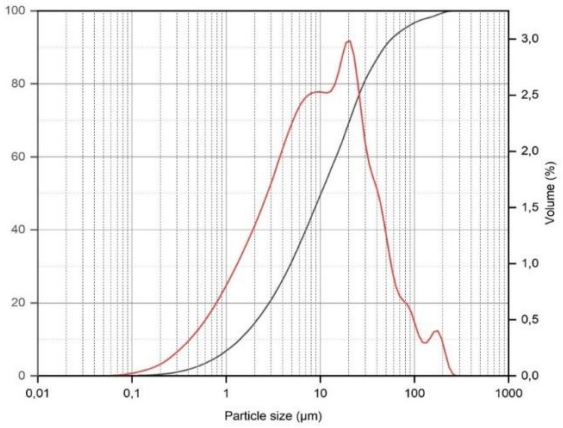

Fig. 1 Particle size distribution of the NSL sediment

2.1.2. Chemical and mineral characteristics

Table 3 shows the chemical composition of the sediment as well as for the other raw materials. The four main oxides of the sediment are SiO_2, CaO, Al_2O_3 and Fe_2O_3. In addition, minor oxides such as MgO, ZnO, Na_2O and K_2O are detected and their presence could have impacts on the clinker. The chemical composition shows that the sum of oxides ($CaO + SiO_2 + Al_2O_3 + Fe_2O_3$) of the calcined sediment is equal to 89.75% which is in accordance with the agreement between French cement industry groups signed in 2001 in order to define the limits of acceptability of the entry of the mineral waste used as raw materials into the plant [28]. According to this agreement, calcined waste must comply with the following composition:

$$CaO + SiO_2 + Al_2O_3 + Fe_2O_3 \geq 80\%$$

Table 3 Chemical compositions of raw materials

Oxides (wt. %)	NSL	Limestone	Iron oxide	Sand	Alumina oxide
SiO_2	39.62	0	0	98.5	0
Al_2O_3	9.64	0	0	0.6	100
Fe_2O_3	5.12	0	96	0.1	0
CaO	10.57	55	0	0	0
MgO	0.88	0	0	0	-
Na_2O	0.69	0	0	0	-
K_2O	1.84	0	0	0	-
SO_3 total	0.22	0	0	0	-
TiO_2	0.60	0	0	0	-

P_2O_5	2.10	0	0	0	-
ZnO	0.27	0	0	0	-
L.O.I 950°C	27.63	45	0	0	-
Total	99.17	100	96	99.2	100

The results of the mineralogical analysis (Fig.2) show that the main phases of the sediment are quartz, calcite, brushite, and muscovite. These results are in accordance with previous studies conducted on the same sediment [10], [16], [21].

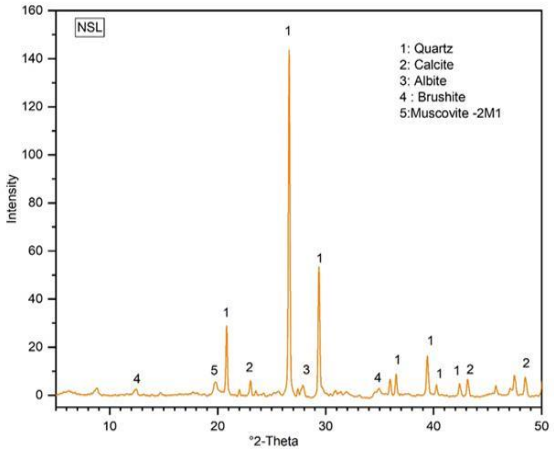

Fig. 2 X-ray diffraction (XRD) of the NSL sediment

The TGA-DTA analysis of NSL sediment (Fig.3) shows three main peaks related to three main weight losses.

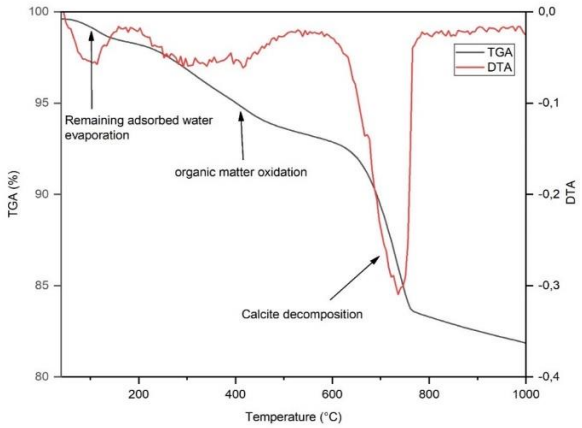

Fig. 3 TGA/DTA analysis of the NSL sediment

The results are summarized in the Table 4.

Table 4 Weight losses at the different degradation temperatures for NSL sediment

Temperature range (°C)	Weight loss (wt. %)	Attributed reaction

105°C – 150°C	0.65	Remaining adsorbed water evaporation
212°C – 550 °C	4.89	Organic matter, clay phase decomposition
615°C – 850 °C	9.72	Calcite decomposition
40°C – 1000 °C	17.74	Total mass loss

2.1.3. Environmental characteristics

The result of the leaching analysis shows the presence of metallic trace elements as well as anionic elements in sediments (Table 5). The content of certain metallic trace elements in the NSL sediment exceeds the value specified for inert waste (IW), in particular, the content of zinc. Nevertheless these values are below the acceptable limits of heavy metals in the common agreement between the French cement industries [28].

Table 5 Metallic trace elements in sediment (mg/kg)

Elements	NSL	IW	NHW
As (mg/kg)	< 0.08	**0.5**	**2**
Ba (mg/kg)	1.4912	**20**	**100**
Cd (mg/kg)	<0.008	**0.04**	**1**
Cr (mg/kg)	<0.03	**0.5**	**10**
Cu (mg/kg)	2.0509	**2**	**50**
Mo (mg/kg)	0.5538	**0.5**	**10**
Ni (mg/kg)	0.4799	**0.4**	**10**
Pb (mg/kg)	0.0447	**0.5**	**10**
Sb (mg/kg)	-	**0.06**	**0.7**
Se (mg/kg)	0.1019	**0.1**	**0.5**
Zn (mg/kg)	7.8518	**4**	**50**

2.2. Clinker and cement synthetizing method

From the result of the analysis of the material's chemical composition, the different formulations of the raw meal were set up based on the following modulus usually used in the cement industry: the Lime Saturation Factor (LSF), the Silica Ratio (SR) and the Alumina Ratio (AR) [18]. These are the main parameters to control the quality of the clinker [29]. The calculations of LSF, SR and AR are presented by the equations below:

$$LSF = \frac{100 * \%CaO}{2.8 * \%SiO2 + 1.18 * \%Al2O3 + 065 * \%Fe2O3} \quad \text{Eq (1)}$$

$$SR = \frac{\%SiO2}{\%Al2O3+\%Fe2O3} \quad \text{Eq (2)}$$

$$AR = \frac{\%Al2O3}{\%Fe2O3} \quad \text{Eq(3)}$$

The LSF ensures good stoichiometry between calcium oxide and the other three main oxides. A higher LSF value corresponds to higher calcium silicate content, but the burning will be more difficult and may cause volume instability of the hydrated cement (high content of free lime). In addition, the LSF modulus helps to control the relationship between the quantity of C_3S and C_2S [30]. The value of LSF is usually considered between 95 and 97 [31] but technically the range of LSF can vary from 90 to 104 [32]. The SR modulus allows the determination of the relative proportion between the silicate phases and the aluminate phases. A high value of SR will cause difficulty in the clinkerization process due to a lack of fluxing agents. This modulus affects also the properties of clinker including the setting and durability. The value of SR is between 2.0 and 3.0 [18] but in the more restrictive and optimized field, it is taken between 2.4 and 2.6 [31]. The AR modulus expresses the ratio between the mineral phases C_3A and C_4AF. A high value of AR will provoke the formation of significant content of C_3A in the clinker and this affects the resistance to sulphates [33]. The appropriate value for AR is between 1.5 and 1.8 [31].

In this study, the objective is to synthesize a Portland clinker using a maximum amount of sediment as a raw material.

After the sediment characterization, two clinkers where synthetized. First, a reference clinker, CP 97TM, is produced using pure chemical reagents, $CaCO_3$, SiO_2, Fe_2O_3 and Al_2O_3 (without sediment). The choice of using pure materials aims to study the influence of the components of the sediment on the synthesized clinker. Then, a second clinker, CP97, with sediment was produced. The modulus applied for both clinkers are LSF = 97, SR = 2.6 and AR = 1.45. The choice of value LSF = 97 is to avoid the significant presence of non-combined CaO and to have a significant content of C_3S in the clinker. In order to calculate the mass percentage of each component in the raw meal for the two formulations, as well as the maximum amount of sediment in the formulation CP97, solver function was used (Table 6).

Table 6 Mix design for the production of the two clinkers

Formula	NSL (wt. %)	Limestone (wt. %)	Alumina oxide (wt. %)	Iron oxide (wt. %)	Sand (wt. %)
CP 97TM	0	79.99	3.17	2.32	14.52
CP 97	31	67.61	0	0.5	0.89

For each raw meal formulation, the raw materials were first mixed by adding water with a water/material ratio = 0.6 in order to have good homogeneity. After drying at 105°C, pellets (with a diameter of 40mm and a height of 15mm) are formed using a press and a force of 5 KN.

The pellets were burned in a static furnace at 200°C for 20 minutes, then the temperature increases to 1450°C with a heating rate of 7°C/minute, and kept at this temperature for 15 minutes. After clinkerization, the obtained clinkers were cooled in the furnace to reach the room temperature.

The cements were produced by mixing pure gypsum ($CaSO_4.2H_2O$) with clinkers after grinding. The addition of gypsum plays a very important role in controlling the setting of the cement. Indeed, the reaction of C_3A with water is very violent and immediately stiffens the cement paste [34]. This phenomenon is due to the formation of hydrated calcium aluminates in plaques, according to Eq (4), which are distributed in the space filled with the mixing water and constitute bridges between the particles of the cement causing a rapid setting.

$$C_3A + 21H \rightarrow C_2AH_8 + C_4AH_{13} \rightarrow C_3AH_6 \qquad Eq(4)$$

In addition, the presence of sulphate increases the hydration of C_3S, which requires an improvement in the development of compressive strength [35] and a stability control of the volume of the paste [18]. However, an excess of sulfate can cause swelling by the late reaction with tricalcium aluminate [36] which increases the rate of degradation and deterioration of concrete [37]. The standard EN 197-1 [38] specify the limit content of SO_3 at 3.5%. Based on Day's hypothesis which assumed that there would be delayed ettringite formation only for an SO_3/Al_2O_3 ratio greater than 0.7, in this study, gypsum was added ensuring the SO_3/Al_2O_3 ratio equal to 0.6. These mixtures were ground in a centrifugal ball mill to reach the Blaine surface at 3500 cm^2/g. Table 7 shows the mass proportion of the constituents of the cement.

Table 7 Compositions of the OPC 97TM, OPC97 cements

Component	OPC 97TM	OPC 97
Clinker (%)	95.67	95.16
Gypsum (%)	4.33	4.84

2.3. Characterization method of the produced clinkers and cements

Several tests have been used in order to characterize the raw meals, clinkers and cement pastes. The results of the experimental chemical composition of raw meals determined by XRF allow verifying that the values of the modulus are reached. The mineral phases of the clinkers were identified by XRD. The polymorphs of crystalline phases in clinkers have also been detailed in order to highlight the influence of the sediment on the formation of crystalline phases. The modified Bogue's formula [7] was used to quantify the crystalline phases in the clinkers. This method takes into account the content of non-combined lime in the clinker.

The content of free lime, in the clinker, is an important parameter to evaluate the quality of the clinker produced. In general, a content of free lime less than 2% is acceptable in the cement industry [39]. The content of non-combined lime in clinkers was measured using the Schlafer-Bukokowski method.

In order to study the microstructure of the synthetized clinkers and to observe the effect of sediment substitution, the optical microscope Leica was used after immersing clinkers in a solution containing 95% HNO_3 acid and 5% ethanol.

The chemical composition of the clinker phases has been studied on polished sections with a Hitachi S-4300 SE/N scanning electron microscope operating in backscattered electron mode (20 keV) and equipped with an energy dispersive X-ray spectrometer (EDS).

The reactivity of the cement pastes was followed using the isothermal calorimetry test carried at 20 °C. Based on a previous study [40], 8 g of cement and 4 g of water previously stored at 20 °C were used. The calorimeter was a home-made calorimeter using fluxmeters the allowed the calorimeter to equilibrate in less than 5 min.

The degree of hydration of cement pastes (with W/C = 0.5) was determined by measuring the amount of bound water using TGA analysis [41]. After 24 hours, the sample was removed from the moulds and then stored in saturated lime solution at 20 °C. The degree of hydration of the cement was determined according to the following formula:

$$\alpha(t) = \frac{Wn\,(t)}{Wn(\infty)} \qquad \text{Eq(5)}$$

With:

$\alpha(t)$: Degree of hydration of the sample at time t.

$W_n(t)$: Amount of bound water at time t (in gram of water per 100 g of anhydrous cement).

$W_n(\infty)$: Amount of bound water after a total hydration of the cement paste (in gram of water per 100 g of anhydrous cement).

The value of $W_n(t)$ can be determined experimentally using the formula in Eq (6) if the two following conditions are met:

- No carbonation in the cement paste.
- Low weight loss of anhydrous cement before 1000° C

$$W_n(t) = \frac{\Delta m\ sample\ (105\ °C - 1000\ °C)(t)}{m\ sample\ (1000°C)(t)} * 100 \qquad \text{Eq(6)}$$

In order to determine the $W_n(\infty)$ value, NIST provides an approximate theoretical estimation of the amount of bound water produced for the five main mineral phases of cement when hydration is complete [42].

The compressive strength was measured on small cubes of the cement paste of dimension 1 x 1 x 1 cm^3. A mixture of cement and water with a W/C ratio equal to 0.5 was mixed manually for a few minutes. The installation method is similar to that carried out in the studies [20],[43]. The samples were stored in the saturated lime solution until testing time (2, 15 and 28 days). The tests were carried out at a constant stress of 0.3 MPa/s using a uniaxial press.

2.4. Modeling of cement hydration using the CEMHYD3D code

2.4.1. CEMHYD3D code

The CEMHYD3D code developed by Dale P.Bentz at NIST (National Institute of Standards and Technology) has been used successfully in several previous studies [44],[45],[46]. It allows the user to digitally generate and hydrate a 3D microstructure of the cement paste from the phase composition, particle size and W/C volume ratio, under controlled hydration conditions [47]. The model does not use a classical chemical point of view with the equilibrium of species in solution and the resolution of the associated systems of equations, but uses a completely original mechanism of reaction between species using cellular automata [48]. A list of the chemical equations taken into account in order to carry out the hydration of the cement numerically is detailed by Dale P.Benzt [49]. A 3D microstructure consists of micro cubes of 1 μm^3, called voxels, each representing a phase: solid (C_3S, C_2S, C_3A, C_4AF, Gypsum, etc.), liquid (saturated porosity).

The advantage of using the CEMHYD3D code is to allow the user to access all the information on the properties of the material such as the amount of the different phases, the amount of porosity, etc.

The compressive strength in the model is estimated using the Powers's empirical relation [49] :

$$\sigma_c(t) = \sigma_0(X(t))^n \quad \text{Eq (7)}$$

With:

$\sigma_c(t)$: Mechanical resistance to compression at time t.

σ_0 : Mechanical resistance to compression when capillary porosity is zero. It is calibrated on the basis of determination of resistance at 28 days.

n : Value taken between 2.6 and 3.0. In general, a value equal to 2.6 is applied for CEM I.

X(t): Ratio of hydrate gel-space. In the CEMHYD3D, X(t) is determined as follows:

$$X(t) = \frac{Number\ of\ hydrate\ pixels}{Number\ of\ hydrate\ pixels + Number\ of\ porosity\ pixels} \quad \text{Eq (8)}$$

We also have:

$$X(t) = \frac{0.68\ \alpha(t)}{0.32\alpha(t) + \frac{W}{C}} \quad \text{Eq(9)}$$

With:

α(t): hydration degree for a sample at time t.

W/C: water/cement ratio

The porosity of the microstructure in the CEMHYD3D model is limited to the capillary porosity. The finer porosities are not taken into account because of the size of the voxels composed of 1 μm^3.

2.4.2. Determination of time constant

The time constant (β) is used to convert times/cycles in the CEMHYD3D code. The value should be determined experimentally by the user depending on the type of cement used. The formula showing the relationship between time and the number of cycles is as follows:

$$t = \frac{\beta}{K} * c^2 \quad \text{Eq (10)}$$

With:

t: Time of hydration in hours.

c: Number of hydration cycles performed by the program in the CEMHYD3D.

β: Conversation factor cycles/time in hour/$(cycles)^2$.

K: Speed coefficient for the cycle.

The value of K is determined by the following formula:

$$K = e^{\frac{E}{8.314}\left(\frac{1}{298.15} - \frac{1}{T°+273.15}\right)} \quad \text{Eq (11)}$$

With:

E: Activation energy of the cement in KJ/mol.

T°: Temperature of the system in °C.

To determine the β value, the degree of hydration of the cement paste should be used. The value of the coefficient K is calculated according to Eq (12) with the activation energy of the cement E = 40 (KJ/mol) and gives a result of K = 0.9997.
Knowing the experimental value of the degree of hydration of the cement paste at a given time, the user determines the number of hydration cycles for which the program reaches the same value as the experimental α(t) [48]. In this study, the bound water measurement method was used to determine the degree of hydration of the cement paste.

3. Results and discussion

3.1. Characterization of clinkers

3.1.1. Mineral and chemical composition of CP 97TM and CP 97 formulation

The raw meals (before clinkerization) for the two formulations CP 97TM and CP 97 were analyzed by XRF in order to determine experimental content of main oxides (Table 8).

Table 8 Chemical composition of CP 97TM and CP 97 raw meals

Oxide (wt. %)	CP 97TM		CP 97	
	Theoretical	Experimental	Theoretical	Experimental
SiO_2	14.30	13.8	13.19	12.9
Al_2O_3	3.26	2.8	3.00	3.05
Fe_2O_3	2.25	2.1	2.07	2.07
CaO	43.99	43.8	40.58	40.26
MgO	0.00	0.00	0.27	0.33
Na_2O	0.00	0.00	0.21	Traces
K_2O	0.00	0.00	0.57	0.59
SO_3 total	0.00	0.00	0.07	0.12
TiO_2	0.00	0.00	0.19	0.17
P_2O_5	0.00	0.00	0.65	0.56
ZnO	0.00	0.00	0.08	0.1
LOI 950°C	35.99	36.88	39.10	39.4
Total	99.79	99.38	100.00	99.55
LSF	97.00	101.1	97.00	98.04
SR	2.60	2.81	2.60	2.52
AR	1.45	1.33	1.45	1.47

CaO/SiO_2	3.08	3.17	3.08	3.12

The experimental results were compared to the theoretical results in order to check the values of the modules used. A good compatibility was observed in particular in the case of the CP 97 formulation between the experimental and theoretical composition. However, an increase in LSF in the case of the CP 97TM formula was noted. This increase could cause the risk of a higher free lime content in the CP 97TM clinker.

The free lime content in the clinker of the two formulations CP97TM and CP97 was measured and corresponds to 1.287% and 0.786% respectively. The difference can be explained by the actual value of LSF = 101.1 in CP 97TM compared to LSF = 98.04 in CP 97 clinker. The values are obviously below the acceptable threshold for free lime content in the cement industry (2% wt).

Table 9 shows the proportion of the crystalline phases of the clinker calculated by the modified Bogue's formula.

Table 9 Mineral phases content in the two clinkers CP 97TM and CP 97

Mineral phases	CP 97TM	CP 97
C_3S	76.83	66.99
C_2S	4.96	10.69
C_3A	6.16	7.59
C_4AF	10.15	10.41
CaO free	1.287	0.786

In order to identify the mineralogical assemblage of the two produced clinkers, an XRD analysis was performed. The results are represented in the Fig.4 and confirm the presence of the four crystalline phases C_3S, C_2S, C_3A and C_4AF as well as the peak of calcium oxide. In addition, we note that there is no secondary phase in the CP 97TM and CP 97 clinker.

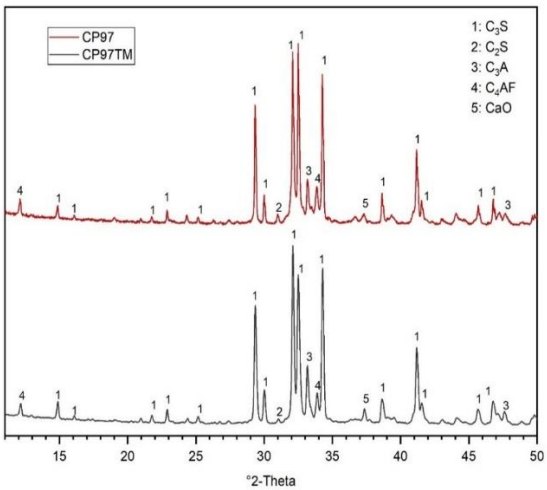

Fig. 4 X-ray diffraction (XRD) of the CP 97TM and CP 97 clinker

In order to highlight the impacts of the incorporation of the sediment on the morphology of the crystalline phases formed in the synthetized clinkers, the different angular ranges 2θ were examined (Table 10).

Table 10 The angular range 2θ for the different mineral phases

Mineral phases	C_3S	C_2S	C_3A
Angle 2θ	[36°-38°] [55.5°-57.5°]	[30.5°-32°] [32.7°-33.7°]	[47°-48°]

We note that the XRD curve of the CP 97TM clinker is more "smooth" than that of the CP97 clinker. This may be due to the purity of the raw mix of CP 97TM which does not contain minor oxide. Concerning the morphology of C_3S in the clinker, Fig.5 indicated the formation of the M3 polymorph in the clinker CP 97. In fact this could be related to the presence of MgO in the CP 97 raw meal which can promote the formation of M3 polymorph [50].

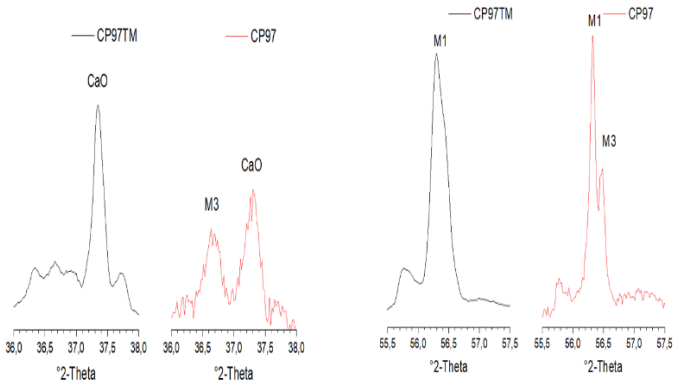

Fig. 5 M1 and M3 polymorph of C_3S of the clinker CP 97TM and CP 97

Concerning the C_2S polymorph, it can be seen from the Fig. 6 that the incorporation of sediment in the raw meal did not affect the formation of C_2S. The results show also that the polymorph β-C_2S is the most common in the two synthetized clinkers (with or without sediment).

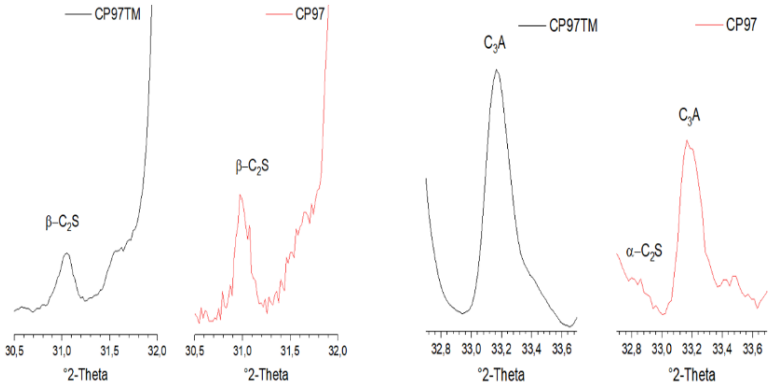

Fig. 6 β-C2S and α-C_2S polymorph of the clinker CP 97TM and CP 97

The formation of orthorhombic C_3A (Fig.7) was observed in the CP 97 clinker. This could be due to the presence of Na^+ ions that replace Ca^{2+} ions and leads to the change from the cubic system to the orthorhombic system [51].

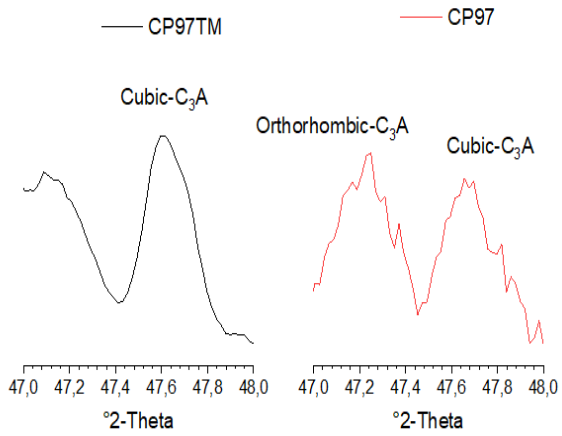

Fig. 7 C_3A polymorph of the clinker CP 97TM and CP 97

Fig. 8 shows micrographs of polished sections of CP 97TM and CP 97 clinkers by optical microscopy.

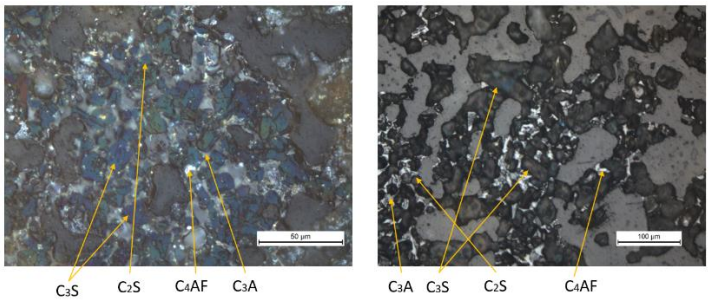

Fig. 8 Observation by optical microscope on the polished section of clinker CP 97TM (left) and CP 97 (right)

The four typical phases of clinker were observed.

A good distribution of silicate phases and interstitial phases in the two clinkers. The presence of polygonal alite and round form belite is well defined.

The presence of sulfur (SO_3) in the CP 97 clinker reduces the viscosity and surface tension of the liquid phase, and promotes the formation of alite crystals larger than those of reference clinker CP 97TM [52].

3.1.2. Chemical composition of mineral phases of clinkers (Result SEM-EDS)

In order to study the influence of the incorporation of sediments on the chemical composition of the mineral phases of the clinkers, the SEM - EDS analysis was carried out on the three clinkers. Approximately, 30 points were measured for each phase.

Fig.9 and Fig.10 show the result of the analysis on the silicate phases of the CP 97TM and CP 97 clinkers.

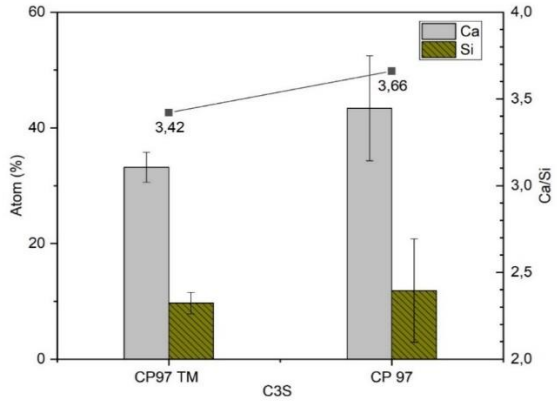

Fig. 9 Chemical composition and the ratio of major elements in C_3S

The result of the analysis on the C_3S phase showed that:

- The C/S (CaO/SiO_2) ratio of the two clinkers is higher than the theoretical value (C/S = 3). This difference can be due to the EDS points made and to the size of diffusion bulb which analyzes an area and not a point [53].
- C_3S incorporates a certain amount of secondary species, including aluminum in varying amounts. The measurement showed the Al/Si (Al_2O_3/SiO_2) ratio equal to 0.07 for the two clinkers. This value is higher than that in the Taylor's study which gave an Al/Si ratio equal to 0.04.
- For the minor elements in the C_3S phase, the CP 97TM and CP 97 clinkers contain 1.14%, 2% respectively.

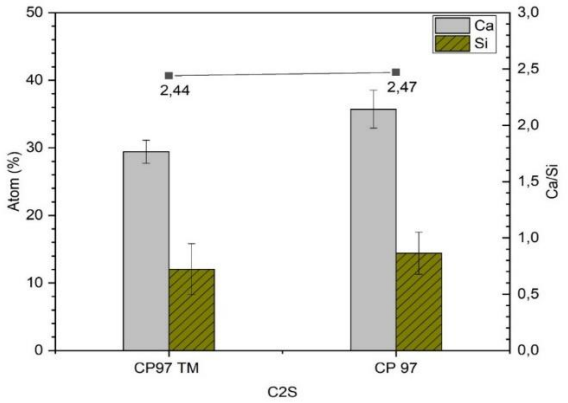

Fig. 10 Chemical composition and the ratio of major elements in C_2S

The results of the EDS analysis on the C_2S phase show the following:

- The C/S ratio of the three clinkers is more than the theoretical value of the C_2S phase (C/S = 2).
- Same as the C_3S phase, the C_2S phase contains a certain amount of secondary species. The Al/Si ratio is equal to 0.07 for the two clinkers, this value is relatively similar to that in the Taylor study (Al/Si = 0.077).
- C_2S incorporates 1.42%, 3.03% respectively of the minor elements in the clinkers CP 97TM and CP 97.

Fig.11 and Fig.12 show the results of the SEM-EDS analysis at the interstitial phases.

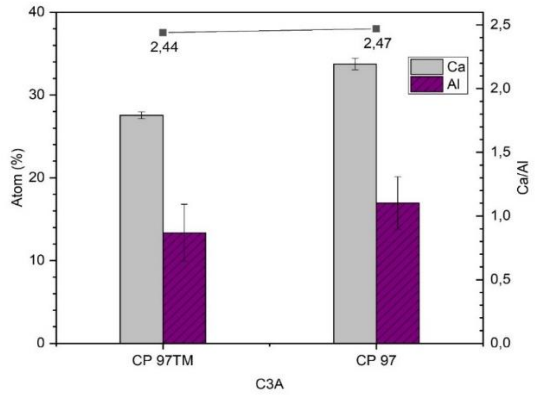

Fig. 11 Chemical composition and the ratio of the major elements of the phase C_3A

From the result illustrated in Fig.11, some conclusions can be made:

- The C/A (CaO/Al_2O_3) ratio in the two clinkers is higher than the theoretical value (Ca/Al = 1.5) of this phase. However, this ratio is relatively similar for the two clinkers.
- The content of secondary elements in the CP 97TM, CP 97 clinkers is 3.42%, 4.55% respectively.

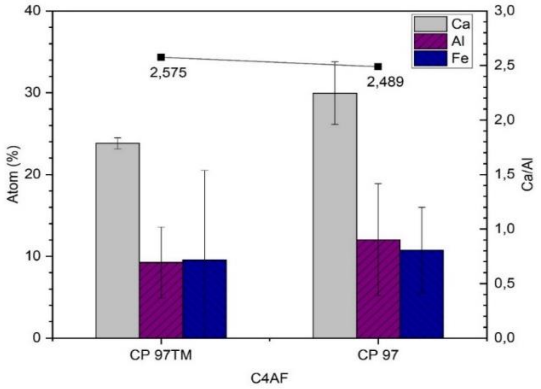

Fig. 12 Chemical composition and the ratio of the major elements of the phase C_4AF

The result of the SEM-EDS analysis of the phase C_4AF (Fig.12) showed that:

- The Ca/Al (CaO/Al_2O_3) ratio in the two clinkers is higher than the theoretical value of this phase (Ca/Al = 2).
- The Al/Fe ratio of the two clinkers CP 97TM, CP 97 is 0.99, 1.12, which is relatively close to the theoretical value (Al/Fe = 1).

3.2. Characterization of cements

3.2.1. Chemical composition of cements

Table 11 shows the chemical composition of cements measured by XRF analysis.

Table 11 Chemical composition of the OPC 97TM, OPC97 cements

Elements (%)	OPC 97TM	OPC 97
SiO_2	20.5	19.7
Al_2O_3	4.7	5

Fe_2O_3	3.1	3.1
CaO	65.5	62.4
MgO	ND	0.6
Na_2O	ND	ND
K_2O	ND	0.5
SO_3	1.9	2.5
TiO_2	ND	0.3
P_2O_5	ND	0.9
ZnO	ND	0.2
L.O.I	3.6	4.0
Total	99.2	99.0

3.2.2. Heat of hydration of cements

The hydration of the cement is an exothermic process, the analysis of the heat released makes it possible to provide information on the kinetics of the hydration of each constituent of the cement, in particular of C_3S because it is mainly responsible for the compressive strength from early age [54]. The cement hydration heat curves shown in Fig.13 indicates the peak delay due to C_3S hydration of OPC 97 cement pastes compared to OPC 97TM paste. This could be due to the higher reactivity of the M1 form compared to the M3 form in C_3S. Indeed, OPC 97TM cement contains mainly M1 form while OPC 97 cements contain mainly the M3 polymorph.

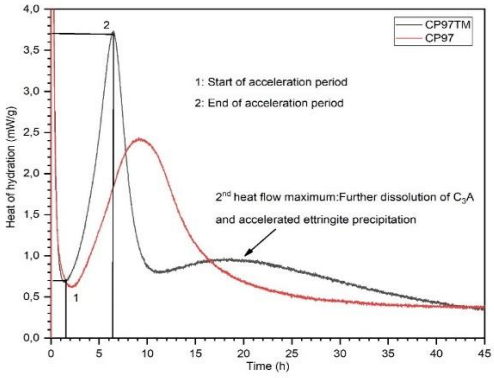

Fig. 13 Heat of hydration of cement pastes (W/C = 0.5)

Compressive strength is an important indicator to assess the quality of cement. Fig. 14 shows the compressive strength of cement pastes after 2, 15 and 28 days of hydration.

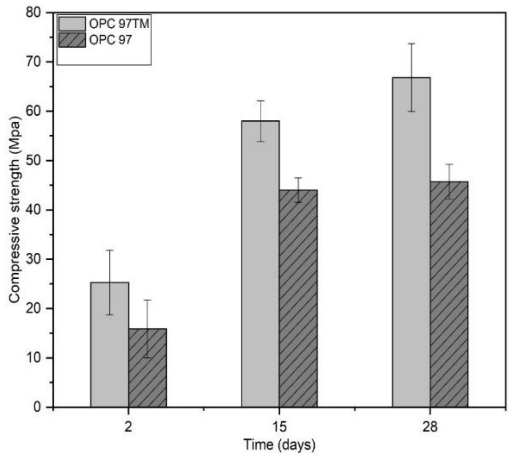

Fig. 14 Compressive strength of cement pastes over time of hydration

OPC 97TM shows higher compressive strength than the OPC 97 cements in the early age and long term. The observed difference in compressive strength could be explained by:

- The delay in the hydration of C_3S observed by the isothermal calorimetry test (Fig. 13) of OPC 97 cement. This causes less development at an early age.
- The C_3S content in OPC 97TM cement is higher than that in OPC 97 cement (Table 9) because C_3S is mainly responsible for the mechanical development of the cement matrix.

3.2.3. Degree of hydration of cements

The degree of hydration of hydrated pastes can allow:

- Highlight the delay in hydration of OPC 97 cement compared to OPC 97TM cement.
- Establish the relation with the compressive strength.

Table 12 shows the theoretical amount of water bound to two cements for complete hydration.

Table 12 Determination of $W_n(\infty)$ from the mineral composition of the cement and the theoretical values of bound water produced for the major phases of the cement at complete hydration

Phase	Coefficient proposed by NIST	Mineral composition of cements (wt.%)		Mass of bound water to complete hydration (g/100 g of anhydrous cement	
		OPC 97TM	OPC 97	OPC 97TM	OPC 97
C_3S	0.24	73.96	66.33	17.75	15.92
C_2S	0.21	4.77	10.58	1.00	2.22
C_3A	0.4	5.93	7.51	2.37	3.00
C_4AF	0.37	9.77	10.31	3.62	3.814
Lime	0.33	1.24	0.78	0.408	0.257
Total (%)		95.67	95.51	25.148	25.22

The degree of hydration of the cements was calculated according to Eq (6) and Eq (7) from the result of the TGA analysis shown in Fig.15.

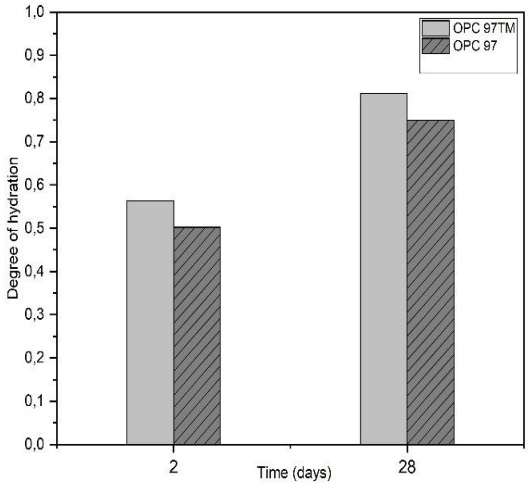

Fig. 15 Degree of hydration of cement pastes (W/C = 0.5)

The result of the degree of hydration of the cements shows that the OPC 97TM cement has a higher reactivity than the OPC 97 cement. This result is consistent with that of heat from hydration by the isothermal calorimetry test.

The $Ca(OH)_2$ content formed in hydrated pastes was also measured by TGA analysis. Table 13 presents the $Ca(OH)_2$/initial cement's mass ratio as a function of the hydration time.

Table 13 $Ca(OH)_2$/initial cement's mass ratio over time of hydration

Time (days)	OPC 97TM	OPC 97
2 days	20.15 (%)	16.31 (%)
28 days	29.04 (%)	25.33 (%)

The results show that the OPC 97TM cement is more reactive than the OPC 97 cement and well consistent with the result of degree of hydration and heat of hydration.

Fig.16 - 17 show the XRD analysis on cement pastes after 28 days of hydration. The result shows clearly a decrease in anhydrous phases as well as the formation of hydrate phases such as portlandite and ettringite in hydrated cements.

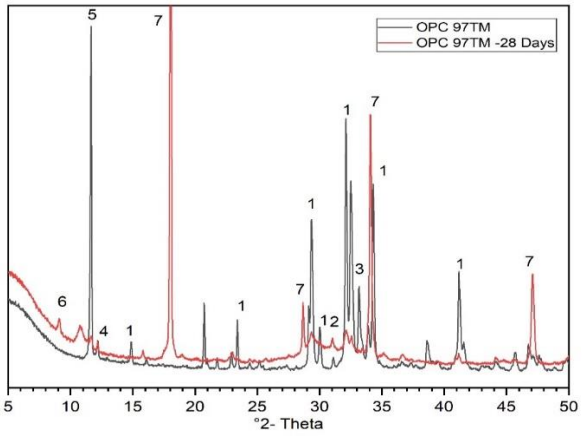

Fig. 16 X-ray diffraction (XRD) of OPC 97TM over time of hydration (1: C_3S, 2: C_2S, 3: C_3A, 4: C_4AF, 5: Gypsum, 6: Ettringite (Aft), 7: Portlandite)

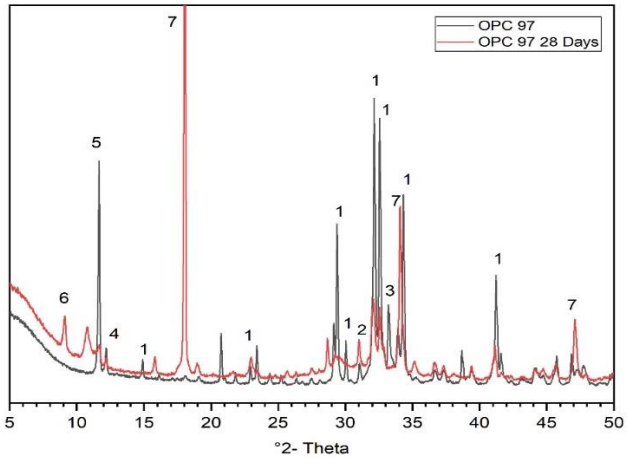

Fig. 17 X-ray diffraction (XRD) of OPC 97 over time of hydration (1: C_3S, 2: C_2S, 3: C_3A, 4: C_4AF, 5: Gypsum, 6: Ettringite (Aft), 7: Portlandite)

3.3. Modeling of cement hydration

The hydration of the synthesized cements OPC 97TM and OPC 97 is numerically modeled using the CEMHYD3D code and compared with the experimental results. The experimental characteristics of the two cements were used as the input data for the CEMHYD3D code.

3.3.1. Particle size distribution of cements

The particle size distribution of the cements was determined by the COULTER laser granulometer type LS 13320. Tables 14 - 15 present the experimental and numerical results of the OPC 97TM and OPC 97 cements respectively.

The result shows that the particle size distribution of the cements used in the CEMHYD3D code was relatively similar with the experimental result.

Table 14 Particle size distribution of OPC 97TM cement (Experimental and numerical result)

Diameter of particles (µm)	Mass fraction (%) (Exp)	Mass fraction (%) (CEMHYD3D)
1	12.805	12.236
3	4.056	3.874
5	6.023	5.756
7	6.443	6.176
9	6.163	5.909
11	5.662	5.328
13	5.127	4.898
15	4.644	4.611
17	4.259	3.944
19	3.982	3.805
21	3.736	3.820
23	3.490	3.297
25	3.241	2.116
29	5.808	6.639
33	7.257	4.854
37	4.199	6.886
49	10.860	12.851
73	2.250	3.000
Total	100.00	100

Table 15 Particle size distribution of OPC 97 cement (Experimental and numerical result)

Diameter of particles (µm)	Mass fraction (%) (Exp)	Mass fraction (%) (CEMHYD3D)
1	11.3487	10.9460
3	3.8930	3.7573
5	5.9458	5.7252

7	7.0075	6.7446
9	7.2094	6.9749
11	6.9718	6.7212
13	6.4481	6.1794
15	5.8153	5.5849
17	5.1927	5.3073
19	4.6175	4.8009
21	4.0419	3.8550
23	3.5097	3.3277
25	3.0766	2.1353
29	5.2911	6.7007
33	6.7252	4.8991
37	3.9203	6.9499
41	6.5334	6.3905
53	1.6881	3.01
57	0.7630	-
Total	99.9993	100.0000

3.3.2. Mineral composition of cements

The CEMHYD3D code uses the volume fraction of mineral phases as input data. By applying the densities values of the mineral phases proposed by NIST [55], Table 16 shows the experimental and numerical result of the volume fraction of two cements OPC 97TM and OPC 97 as well as the W/C ratio.

The result demonstrated a good coherence between the experimental and numerical result on the fraction of the phases as well as the W/C ratio.

Table 16 Volume fraction of cements OPC 97TM and OPC 97 (Experimental and numerical result)

Phases	OPC 97 TM cement			OPC 97 cement		
	Exp (%)	CEMHYD3D code		Exp (%)	CEMHYD3D code	
		Pixels	% Volume		Pixels	% Volume
C_3S	74.693	289811	74.617209	66.64	257381	66.267505
C_2S	4.719	18378	4.7317564	10.41	39609	10.198071

C_3A	6.344	24902	6.411481	8	30572	7.8713275
C_4AF	8.492	32944	8.4820429	8.91	34026	8.7606238
Gypsum	5.75	22362	5.757511	6.04	23235	5.982281
Total	99.998	388397	100	100	384823	99.0798
W/C	0.5	0.4999		0.5	0.5	

3.3.3. Determination of the β value in the CEMHYD3D code

In order to determine the β value in the CEMHYD3D code, the values of the degree of hydration of OPC 97TM and OPC 97 cement pastes at 2 days of hydration were used as the calibration values. In fact, we run a simulation of 1000 cycles with any β value, then we look for the value of the number of cycles that allows to reach a degree of hydration corresponding to the experimental value of the degree of hydration at 2 days.

The β value is determined according to Eq (11) and Eq (12) with the cycle values found above. In our case, the β values are 0.00008742 for OPC 97TM cement and 0.00011186 for OPC 97 cement.

3.3.4. Results of the modeling of cement hydration in the CEMHYD3D code

The hydration of the two cements OPC 97TM and OPC 97 was numerically modeled in the code CEMHYD3D at a constant temperature of 20 °C and in the saturated condition, which are similar with the conditions of the experimental hydration. The modeling results are presented in the following figures and compared with the experimental results.

a) Degree of hydration of cement pastes

Fig. 18 shows the degree of hydration estimated by the CEMHYD3D code by comparing with the experimental values measured at 2 and 28 days of hydration. A good consistency between the numerical and experimental values was observed. The result in the code also showed a higher degree of hydration of OPC 97TM cement compared to OPC 97 cement.

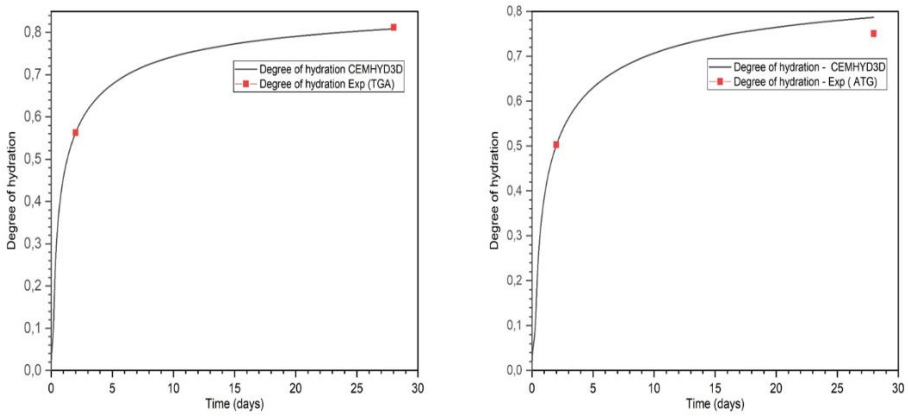

Fig. 18 Degree of hydration of OPC 97 TM (left) and OPC 97 (right) cements (Experimental and numerical result)

Fig. 19 shows the microstructure generated in the CEMHYD3D code from the input data and the microstructure after 28 days of hydration.

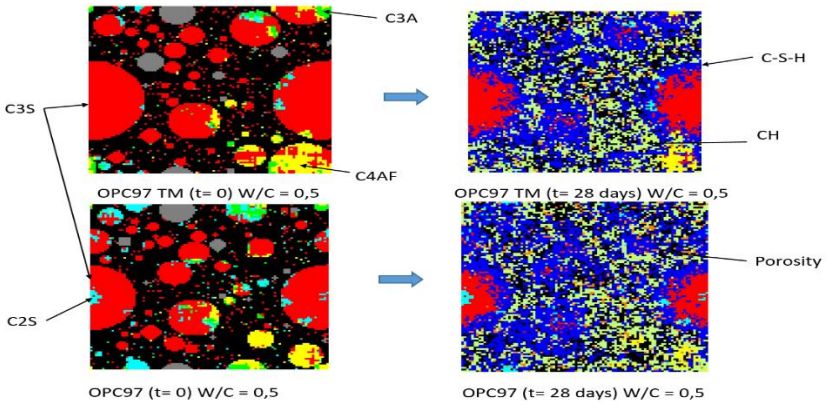

Fig. 19 Microstructure generated in the CEMHYD3D code of OPC 97TM and OPC 97 cements in the initial state (left) and after 28 days of hydration

b) Compressive strength of cement pastes

The code uses Eq (8) to estimate the compressive strength by taking an experimental value as the calibration value. The numerical and experimental result of the compressive strength is presented in Fig. 20. The compressive strength estimated by the CEMHYD3D code is quite consistent with the experimental results.

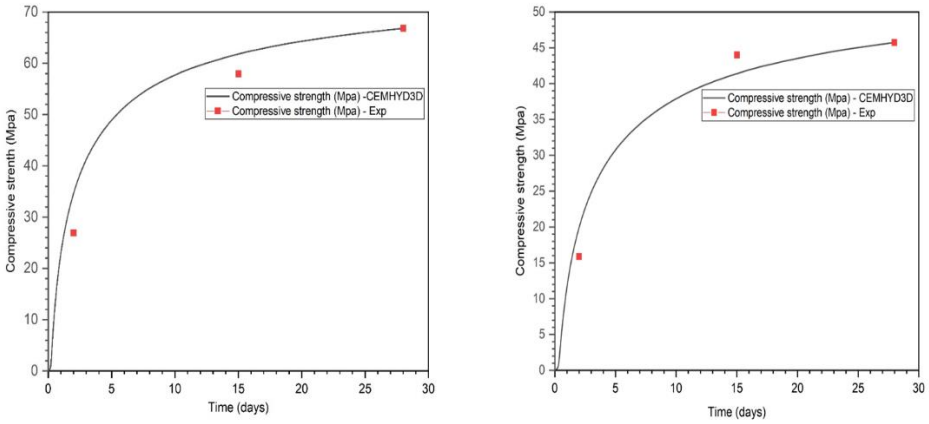

Fig. 20 Numerical and experimental result of the compressive strength of OPC 97TM (left) and OPC 97 (right) cements

c) Mass ratio of hydrates

Given the $Ca(OH)_2$ is a data relatively to be determined thanks to the TGA analysis, we chose to compare the numerical and experimental quantity of this hydrate to evaluate the relevance of the CEMHYD3D code in our study. CEMHYD3D code gives the volume of $Ca(OH)_2$ over time of hydration, a portlandite's density value of 2.24 (g/cm^3) is used to convert from volume fraction to mass fraction. Fig. 21 shows the CH/ initial cement mass ratio of two cements over the time of hydration.

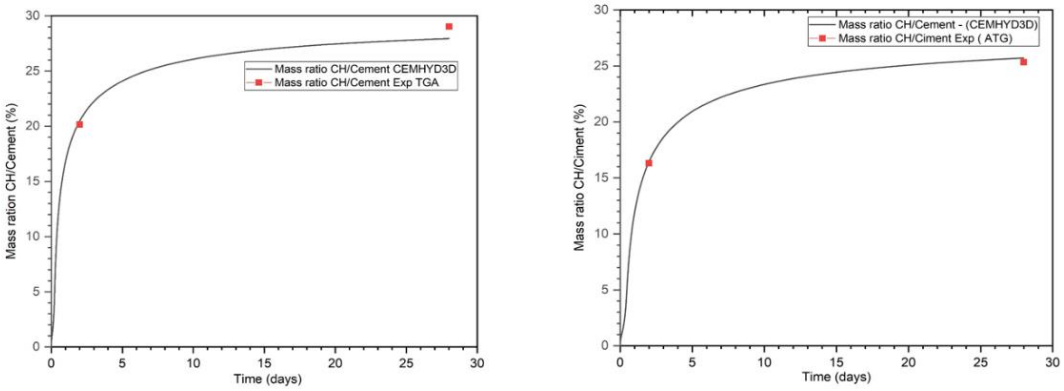

Fig. 21 CH/initial cement mass ratio of OPC 97TM (left) and OPC 97 (right) cement paste

Indeed, the code gave good consistency with the experimental results for the two cements. In addition, the CEMHYD3D code also makes it possible to monitor the evolution of the anhydrous phases as well as the hydrates over time of hydration. This is interesting because it is difficult to follow the evolution of phases by experimental test, for example C-S-H. This phase is responsible for the development of mechanical resistance in the cement matrix. Following the evolution of C-S-H could help understand the development of mechanical strength. In this study, we present the numerical result of the evolution of C-S-H over time of hydration in the CEMHYD3D code (Fig. 22).

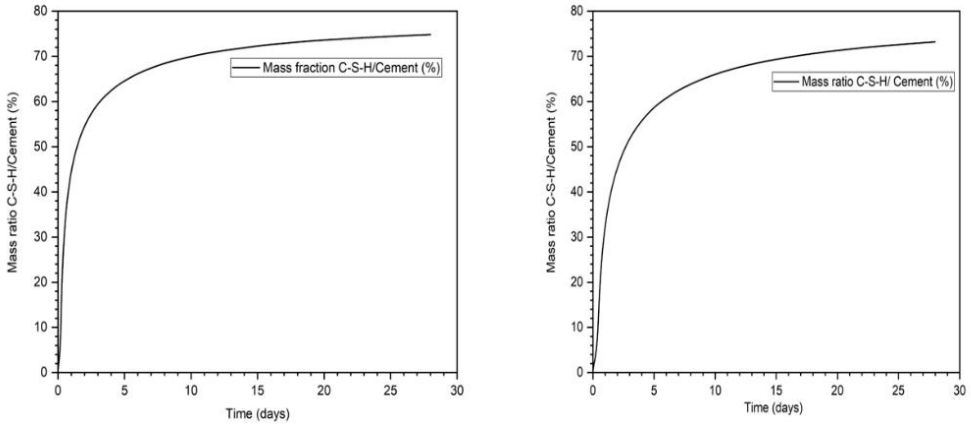

Fig. 22 C-S-H/Initial cement mass ratio measured by CEMHYD3D code for OPC 97TM (left) and OPC 97 (right) cement pastes

From the result of the mass ratio C-S-H/initial cement mass ration, we can extract the following conclusions:

- OPC 97TM gives a higher C-S-H/ initial cement mass ratio than OPC 97 cement at early age (2 days). This may explain the greater early-age mechanical development of OPC 97TM compared to OPC 97.
- At 28 days of hydration, this ratio is relatively similar for the two cements, however the compressive strength of the OPC 97TM is higher than the compressive strength of the OPC 97. This may be due to the presence of the elements miners integrated into C-S-H which influence mechanical performance.

4. Conclusion

The objective of this study is to recycle the maximum possible of the NSL river sediment as a raw material in the cement manufacturing. The following main results are obtained:

- The NSL sediment contains the 4 main oxides, CaO SiO_2, Al_2O_3 and Fe_2O_3 needed to produce a Portland clinker.
- 31 wt. % of NSL sediment can be recycle in the raw meal with $CaCO_3$ and correction agents SiO_2, Al_2O_3 and Fe_2O_3 for the formulation with LSF = 97, SR = 2.6 and AR = 1.45.
- In all synthetized clinkers (the reference and the clinker with sediment) the 4 mains crystalline phases of an ordinary Portland cement C_3S, C_2S, C_3A and C_4AF are obtained in addition to the free lime. The XRD analysis indicated that the incorporation of the sediment promotes the formation of an alite M3 polymorph and an orthorhombic polymorph - C_3A due to the presence of minor oxides such as MgO, Na_2O.
- The free lime content and the identification of the crystalline phases of the clinkers show that the cooling process used in this study did not cause a negative effect such as the decomposition of alite.
- The typical form of alite and belite crystals has been well identified. The presence of SO_3 in CP97 clinkers promotes the formation of larger crystals of alite than those in the reference clinker CP 97TM.
- The atomic ratio estimated from the SEM-EDS analysis of the major elements in the main phases of the two clinkers is higher than the theoretical values. This ratio of C_2S, C_3A, C_4AF phases are relatively similar, however this ratio of C_3S phase is higher in sediment-based clinkers.
- Cements based on sediments show a development of mechanical resistance over time of hydration. However, the mechanical performance of cement decreases with the rate of sediment. This can be explained by the formation of the M3 polymorph form of C_3S less reactive than the M1 polymorph form in sediment-based clinkers.
- The CEMHYD3D code was used to model the hydration of OPC 97TM and OPC 97 cements. The numerical and experimental results are quite consistent. This code also allows you to visually follow the evolution of all phases over time of hydration. This is interesting because the hydration of the cement is a complex process and difficult to follow all the evolutions by the experimental tests. In addition, based on the result of the modeling, several studies on the microstructure can be investigated as leaching in coupling with other computer code.

Author statement

Duc Chinh CHU: Conceptualization, Methodology, Investigation, Visualization, Writing-original draft
Joelle KLEIB: Methodology, Conceptualization, Supervision, Validation, Writing-review & Editing
Mouhamadou AMAR: Methodology, Conceptualization, Supervision, Validation, Writing-review & Editing
Mahfoud BENZERZOUR: Methodology, Conceptualization, Supervision, Validation, Writing-review & Editing, Resources
Nor-Edine ABRIAK: Methodology, Conceptualization, Supervision, Validation, Writing-review & Editing, Resources

Funding
No applicable

Declarations of Competing Interest

The authors declare that they have no known competing financial interests or personal relationships that could have appeared to influence the work reported in this paper.

Availability of data and material:

We confirm that all results are available in the database. If necessary, please contact us at the address: duc.chinh.chu@imt-lille-douai.fr

Code availability: CEMHYD3D: A Three-Dimensional Cement Hydration and Microstructure Development Modelling Package. Version 2.0 | NIST

Acknowlegments

The authors wish to acknowledge the SEDICIM project and the FEDER funds.

Reference

1. INSEE: https://www.insee.fr/fr/statistiques/3589283
2. Kajaste, R., Hurme, M.: Cement Industry Greenhouse Gas Emissions - Management Options and Abatement Cost. J. Clean. Prod. 112, 4041–4052 (2015)
3. Ademe: Déchet, Chiffres-clés. (2015)
4. Pan, J.R., Huang, C., Kuo, J.J., Lin, S.H.: Recycling MSWI bottom and fly ash as raw materials for Portland cement. Waste Manag. 28, 1113–1118 (2008). https://doi.org/10.1016/j.wasman.2007.04.009
5. Ferreira, C., Ribeiro, A., Ottosen, L.: Possible applications for municipal solid waste fly ash. J. Hazard. Mater. 96, 201–216 (2003). https://doi.org/10.1016/S0304-3894(02)00201-7
6. Mukiza, E., Zhang, L.L., Liu, X., Zhang, N.: Utilization of red mud in road base and subgrade materials: A review. Resour. Conserv. Recycl. 141, 187–199 (2019). https://doi.org/10.1016/j.resconrec.2018.10.031
7. De Larrard, F., Colina, H.: Le béton recyclé. (2018)
8. Chen, G., Lee, H., Young, K.L., Yue, P.L., Wong, A., Tao, T., Choi, K.K.: Glass recycling in cement production-an innovative approach. Waste Manag. 22, 747–753 (2002). https://doi.org/10.1016/S0956-053X(02)00047-8
9. Renaut, M.: Calcination des déchets industriels : synthèse de ciment et stabilisation / solidification des résidus de combustion - Thèse de doctorat, (2017)
10. Dubois, V.: Etude du comportement physico-mécanique et caractérisation environnementale des sédiments marins – Valorisation en technique routière - Thèse de doctorat, (2006)
11. Scordia, P.: Caractérisation et valorisation de sédiments fluviaux pollués et traités dans les matériaux routiers, (2008)
12. Tribout, C.: Valorisation de sédiments traités en techniques routières : contribution à la mise en place d'un protocole d'acceptabilité. Thèse de doctorant de l'Université Toulouse III, (2010)
13. Miraoui M.: Mise en œuvre d'une démarche de prétraitement et de traitement des sédiments de dragage en vue d'une valorisation dans le génie civil - Thèse de doctorat
14. M.Dia: Traitement et valorisation de sédiments de dragage phosphatés en technique routière - Thèse de doctorat, (2013)
15. S.Brakni: Première approche vers une valorisation de granulats artificiels à base de sédiments de dragage - Thèse de doctorat, (2008)
16. Amar, M.: Étude expérimentale et numérique de la valorisaion des sédiments de dragage dans les matrices cimentaires - Thèse de doctorat, (2017)
17. Zhao, Z., Benzerzour, M., Abriak, N.E., Damidot, D., Courard, L., Wang, D.: Use of

uncontaminated marine sediments in mortar and concrete by partial substitution of cement. Cem. Concr. Compos. 93, 155–162 (2018). https://doi.org/10.1016/j.cemconcomp.2018.07.010
18. Taylor HFW: Cement chemistry. (1997)
19. Dalton, J.L., Gardner, K.H., Seager, T.P., Weimer, M.L., Spear, J.C.M., Magee, B.J.: Properties of Portland cement made from contaminated sediments. Resour. Conserv. Recycl. 41, 227–241 (2004). https://doi.org/10.1016/j.resconrec.2003.10.003
20. Aouad, G., Laboudigue, A., Gineys, N., Abriak, N.E.: Dredged sediments used as novel supply of raw material to produce Portland cement clinker. Cem. Concr. Compos. 34, 788–793 (2012). https://doi.org/10.1016/j.cemconcomp.2012.02.008
21. Faure, A., Smith, A., Coudray, C., Anger, B., Colina, H., Moulin, I., Thery, F.: Ability of Two Dam Fine-Grained Sediments to be Used in Cement Industry as Raw Material for Clinker Production and as Pozzolanic Additional Constituent of Portland-Composite Cement. Waste and Biomass Valorization. 8, 2141–2163 (2017). https://doi.org/10.1007/s12649-017-9870-8
22. Faure, A., Coudray, C., Anger, B., Moulin, I., Colina, H., Izoret, L., Théry, F., Smith, A.: Beneficial reuse of dam fine sediments as clinker raw material. Constr. Build. Mater. 218, 365–384 (2019). https://doi.org/10.1016/j.conbuildmat.2019.05.047
23. Association Française de Normalisation (AFNOR): NF EN 1097-7 : Détermination de la masse volumique absolue du filler - Méthode au pycnomètre. (2008)
24. NF P94-068 : Mesure de la capacité d'adsorption de bleu de méthylène d'un sol ou d'un matériau rocheux - Détermination de la valeur de bleu de méthylène d'un sol ou d'un matériau rocheux par l'essai à la tache.
25. Association Française de Normalisation (AFNOR): NF EN 196-6 : Méthodes d'essai des ciments - Détermination de la finesse. (2018)
26. NF EN 12457-2. Leaching-Compliance Test for LeachingofGranular Waste Materials and SludgesPart 2: One Stage Batch Test at a Liquid to Solid Ratio of10 l/kgfor Materials with Particle Size Below 4 mm (without or with Size Reduction); BSI: London, UK, 2002.
27. Centre d'information sur le ciment et ses appications: Ciments et Bétons.
28. ANGER, B., THERY, F., LEVACHER, D.: Caractérisation des sédiments fins des retenues hydroélectriques en vue d'une pré-orientation vers des filières de valorisation matière. 97–102 (2015). https://doi.org/10.5150/cmcm.2015.020
29. Lea: Lea's chemistry of cement and concrete. Elsevier. (2003)
30. G.K.Moir: Advanced Concrete Techbology. (2003)
31. G.K.Moir; Mineralised high alite cement. World Cem. 13, 374 (1982)
32. F.W.Locher: Cement principles of production and use. (2006)
33. Lawrence, C.D.: The Constitution and Specification of Portland Cements. (2004)
34. Neville, A.: Propriétés des Bétons, édition Eyrolles, Translated by CRIB. (2000)
35. Hill, L., Fulvio, T.: Manufacturing solutions for concrete performance, World cement.
36. Baron, J., Ollivier, J.-P.: Les Bétons. (1997)
37. Zayed, A.: Effect of sulfur trioxide content on concrete structures using Florida Materials, Research report, University of south Florida. (2004)
38. Association Française de Normalisation (AFNOR): NF EN 197-1: Composition, spécifications et critères de conformité des ciment courant.
39. Faure, A.: Capacité d ' un sédiment à se substituer à la fraction argileuse de la matière première de l ' industrie des liants hydrauliques - Thèse de doctorat, (2017)
40. Kleib, J., Aouad, G., Khalil, N., Zakhour, M.: Incorporation of zinc in calcium sulfoaluminate cement clinker. Adv. Cem. Res. 1–7 (2020). https://doi.org/10.1680/jadcr.19.00125
41. NIST: Technical Note VCCTL-04.

42. NIST: Technical Note VCCTL-01.
43. Joelle Kleib: Ecoconception des ciments : synthèse , hydratation et durabilité-Thèse doctorant IMT Lille Douai et L'Université Libanaise, (2018)
44. Bentz, D.P.: Incorporation of Fly Ash into a 3-D Cement Hydration Microstructure Model Nistir 6050. (1997)
45. Bentz, D.P.: Modeling the influence of limestone filler on cement hydration using CEMHYD3D. Cem. Concr. Compos. 28, 124–129 (2006). https://doi.org/10.1016/j.cemconcomp.2005.10.006
46. Kamali, S., Moranville, M., Garboczi, E., Prené, S., Gérard, B.: Hydrate dissolution influence on the Young's modulus of cement pastes. Proc. 5th Int. Conf. Fract. Mech. Concr. Concr. Struct. 12–16 (2004)
47. NIST: Guide to using CEMHYD3D Version 3.0.
48. Bresciani, C.: Simulation numérique de l ' hydratation et du développement des propriétés physiques et mécaniques d ' une pâte de ciment afin de sélectionner de nouveaux ajouts minéraux., (2009)
49. Bentz, D.P.: Guide to Using CEMHYD3D: A Three-Dimensional Cement Hydration and Microstructure Development Modelling Package. (1997)
50. Maki, I., Goto, K.: Factors Influencing the Phase Constitution of Alite. Cem. 12, 301–308 (1982)
51. Bye, G.C.: Portland cement: Composition, production and properties. (1999)
52. Clark, M.: Petcoke and Nodulisation. Int. Cem. Rev. 39 (2003)
53. Berthomier, M.: Etude de la lixiviation de l'aluminium de matériaux cimentaires à base de CEM III utilisés dans les canalisations d'eau potable : approche expérimentale et numérique. (2020)
54. Gineys, N., Aouad, G., Damidot, D.: Managing trace elements in Portland cement - Part I: Interactions between cement paste and heavy metals added during mixing as soluble salts. Cem. Concr. Compos. 32, 563–570 (2010). https://doi.org/10.1016/j.cemconcomp.2010.06.002
55. Bentz, D.P.: CEMHYD3D : A Three-Dimensional Cement hydratation and Microstructure Development Modelling Package Version 2.0.

***Article 2**: Determination of the degree of hydration of Portland cement using three different approaches: Scanning electron microscopy (SEM-BSE) and Thermogravimetric analysis (TGA)*

Synthèse : Dans cette étude, le ciment synthétisé au laboratoire OPC 97 TM a été utilisé pour évaluer la fiabilité des trois méthodes utilisées dans la détermination du degré de l'hydratation. Les trois méthodes utilisées sont : Quantification de Portlandite, Quantification de l'eau liée et Analyse des images SEM-BSE.
Les résultats montrent que :

- Le rapport de CaO/SiO_2 de la phase C-S-H mesuré par l'analyse MEB –EDS est plus élevé que la valeur théorique habituelle utilisée dans les équations d'hydratation d'un ciment CEM I (la valeur théorique de la phase C-S-H : $CaO/SiO_2 = 1.7$).
- La méthode de quantification de l'eau liée semble présenter des valeurs intéressantes lorsqu'on utilise l'approche de Power : relation entre la résistance à la compression et le degré de l'hydratation.
- La méthode de l'analyse des images SEM –BSE présente un résultat similaire à celui de la méthode de quantification de la Portlandite. Cette méthode démontre la pertinence de l'utiliser comme méthode fiable pour la détermination du degré de l'hydratation, en particulier dans le cas du ciment contenant des additions minérales pouzzolaniques. Cependant, il est nécessaire d'améliorer certains paramètres tels que le nombre d'unités-image (pixels) observées et la résolution des images afin d'augmenter la précision de l'analyse.

Date de soumission	
Statut	Accepté et publié
Journal	Case Studies in Construction Materials https://doi.org/10.1016/j.cscm.2021.e00754

Article 2 : Determination of the degree of hydration of Portland cement using three different approaches: Scanning electron microscopy (SEM-BSE) and Thermogravimetric analysis (TGA)

Duc Chinh CHU[(1)], Joelle KLEIB[(1)], Mouhamadou AMAR[(1)], Mahfoud BENZERZOUR[(1)], Nor-Edine ABRIAK[(1)]

[(1)] Univ.Lille, IMT Lille Douai, Univ.Artois, Yncrea Hauts-de-France, ULR 4515-LGCgE, 6 Laboratoire de Génie civil et géo-Environnement, F-59000, Lille, France

[(*)] Corresponding author: Duc Chinh CHU
Email: duc.chinh.chu@imt-lille-douai.fr
Univ.Lille, IMT Lille Douai, Univ.Artois, Yncréa Hauts-de-France, ULR 4515-LGCgE, 6 Laboratoire de Génie civil et géo-Environnement, F-59000, Lille, France

Abstract

Cement paste hydration is a complex physical-chemical process. The aim of this paper is to use three approaches to determine the degree of hydration: portlandite quantification, scanning electron microscopy and bound water quantification. In order to investigate the physical-chemical and mechanical properties, as well as the hydrates generated. Portland cement was synthesized and characterized in the laboratory. At all hydration durations, the portlandite quantification method and SEM-BSE image analysis show similar results. The method of SEM images analysis requires time to gather and process images, but is unaffected by the type of hydrates produced. The bound water quantification method gives a lower degree of hydration than two other methods at all hydration times. To test the reliability of these procedures, the compressive strength was calculated based on the degree of hydration. The results indicate that the portlandite quantification method and SEM-BSE image analysis are more accurate than the bound water quantification approach in terms of reproducing the experimental results.

Keywords: Cement, Hydration, Portlandite, Bound water, SEM-BSE, Compressive strength.

I. Introduction

Portland cement is a mixture of clinker and calcium sulfate in a ratio of approximately 95:5% [1]. Cement is one of the essential constituents in the manufacture of concrete; the most widely used building material in the world. The mineralogical composition of clinker consists of alite (C_3S: Ca_3SiO_5), belite (C_2S: Ca_2SiO_4), tricalcium aluminate (C_3A: $Ca_3Al_2O_6$) and tetra-calcium aluminoferrite (C_4AF: $Ca_4Al_2O_{10}Fe_2$). During hydration, the cement reacts with water resulting in the formation of different hydrates. Ettringite is formed from the reaction of calcium sulfate, tricalcium aluminate and water. The reaction of the silicates leads to the formation of portlandite (CH) and a Calcium Silicate Hydrate (C-S-H).

Previous studies [2, 3] have shown that C-S-H is the main hydrate of hydrated cement paste and contributes significantly to macro-properties of concrete such as strength and durability.

The composition of the C-S-H, depends on the water to cement ratio (w/c ratio), the temperature as well as the composition of the cement [4–6]. Indeed, in the literature, there are three distinct phases C-S-H depending on the C/S (CaO/SiO_2) ratio:

- C-S-H (α): 0.66 < C/S < 1 formed when the $[Ca^{2+}]$ concentration is less than 2 mmol/l.
- C-S-H (β): 1 < C/S < 1.5 formed when the $[Ca^{2+}]$ concentration is between 2 and 22 mmol/l.
- C-S-H (ϒ): C/S = 1.7 formed when the $[Ca^{2+}]$ concentration is greater than 22 mmol/l.

In addition, Phung et al [7] have shown that the C/S molar ratio of the cement paste was critical in determining the microstructure of C-S-H and the decrease in the C/S ratio can alter the microstructure of C-S-H.

The amount of hydrates formed during hydration depends on the degree of hydration which is defined as a ratio of the amount of hydrated cement to that of the initial anhydrous cement. There are several experimental approaches to determine the degree of hydration of cement such as:

- Scanning electron microscopy (SEM-BSE) [8, 9].
- X-ray diffraction (XRD) [10].
- Thermogravimetric analysis (TGA) [11].
- Measurement of the heat of hydration by isothermal calorimetry [9, 12].
- Nuclear magnetic resonance (NMR) [3, 13].
- Compressive strength [14].

Several studies have employed the thermal analysis method (TGA) to determine the degree of hydration of cement. The basic idea is to use the following simplified equations ((Eq1) -> (Eq8)) to measure the portlandite amount (CH) [10, 11] and chemically bound water [12] generated during hydration [15–17].

$$C_3S + 5.3\ H \rightarrow C_{1.7}SH_4 + 1.3\ CH \quad (1)$$

$$C_2S + 4.3\ H \rightarrow C_{1.7}SH_4 + 0.3\ CH \quad (2)$$

$$C\bar{S} + 2\ H \rightarrow C\bar{S}H_2 \quad (3)$$

$$C_3A + 6\ H \rightarrow C_3AH_6 \quad (4)$$

$$C_3A + 3\ C\bar{S}H_2 + 26\ H \rightarrow C_6A\bar{S}_3H_{32}\ (\text{Ettringite}) \quad (5)$$

$$C_4AF + 3\ C\bar{S}H_2 + 30\ H \rightarrow C_6A\bar{S}_3H_{32} + CH + FH_3 \quad (6)$$

$$2\ C_3A + C_6A\bar{S}_3H_{32} + 4H \rightarrow 3\ C_4A\bar{S}H_{12} \quad (7)$$

$$2\ C_4AF + C_6A\bar{S}_3H_{32} + 12\ H \rightarrow 3\ C_4A\bar{S}H_{12} + 2\ CH + 2\ FH_3 \quad (8)$$

In a recent study, Lei et al [3] used the $Ca(OH)_2$ quantification method measured by TGA analysis and the NMR method for the determination of the degree of hydration of cement paste (W/C = 0.3). The ^{29}Si NMR and ^{27}Al NMR is used to quantify the phases containing these elements in a cementitious material. Good consistency between the two methods was observed (74.0% for the $Ca(OH)_2$ quantification method at 28 days and 78.4% for the NMR method at 28 days). However, in his study, the degree of hydration was calculated according to the equation (Eq9):

$$\alpha(t) = \frac{m\ Ca(OH)2}{25\ wt.\%} * 100 \quad (9)$$

Knowing that the 25% value is not always constant because the mineral composition of cement is always variable. In addition, the NMR method is a complicated method (long analysis time, 1 day for ^{29}Si NMR analysis), therefore, in this study, three methods used are: Method 1: Portlandite quantification method, Method 2: Bound water of quantification method, Method 3: SEM-BSE image analysis method.

The first approach for evaluating the degree of hydration is to use the following equations to calculate the $Ca(OH)_2$ amount estimated from the TGA analysis according to (Eq10):

$$m_{Ca(OH)2} = \frac{\Delta m\ 450°C-550°C(t).MCa(OH)2}{MH2O} \quad (10)$$

with:

$m_{Ca(OH)2}$: Amount of $Ca(OH)_2$.

$\Delta m\ 450°C - 550°C(t)$: The mass loss of the samples between 450 °C and 550 °C from the TGA analysis.

$M_{Ca(OH)2}$: Molar mass of $Ca(OH)_2$ equal to 74.09 g/mol.

M_{H2O}: Molar mass of water equal to 18 g/mol.

Then the degree of hydration of the cement can be calculated using the equation below (Eq11):

$$\alpha(t) = \frac{m\ Ca(OH)2}{mC\ .\Upsilon 0} * 100 \quad (11)$$

The mass of the sample can be calculated using the equation (Eq12):

$$m_c = \frac{m\ sample}{\left(1+\frac{w}{c}\right).(1+LOI)} \quad (12)$$

with:

α(t): Degree of hydration of the cement at time t.

m_{sample}: Mass of the samples.

m_c: Mass of the initial cement.

Υ_0: Amount of $Ca(OH)_2$ produced upon complete hydration of the cement. This value depends on the composition of the cement as well as the stoichiometry of the C-S-H gel of the cement hydration reactions (Eq(1) -> Eq(8)).

w/c: the water to cement ratio of the paste.

LOI: loss of cement on ignition.

The second experimental approach for determining the degree of hydration of cement recommended by the National Institute of Standards and Technology (NIST) consists in determining the amount of water chemically bound according to the following equation (Eq13):

$$\alpha(t) = \frac{Wn\ (t)}{Wn(\infty)} * 100 \quad (13)$$

with:

α(t): degree of hydration of the sample at time t.

$W_n(t)$: amount of bound water for a sample at time (in gram of water per 100 g of anhydrous cement).

$W_n(\infty)$: amount of water bound for a completely hydrated sample (in gram of water per 100 g of anhydrous cement).

The $W_n(t)$ value can be determined experimentally by (Eq14) if the two following conditions are met:

- No carbonation in the cement paste.
- Low weight loss of anhydrous cement before 1000° C

$$W_n(t) = \frac{\Delta m\ sample\ (105\ °C - 1000\ °C)(t)}{m\ sample\ (1000°C)(t)} * 100 \quad (14)$$

In order to determine the $W_{n(\infty)}$ value, NIST provides an approximate theoretical estimation of the amount of bound water produced for the five main mineral phases of cement after hydration is complete [18].

The third method consists of the SEM-BSE image analysis technique to study the distribution of phases in the observation area. Indeed, this technique has been frequently applied to examine the cementitious material's microstructure [19]. In an SEM-BSE image, the backscatter coefficient increases monotonically with the average atomic number of each phase [20]. This allows differentiating and quantifying of each crystalline phases in the analysis area. However, in cement-based materials, the backscattering coefficients of numerous hydration products (C-S-H,

Ettringite, etc.) are too similar to be separated individually on the histogram [19]. Because the epoxy backscatter coefficient is substantially lower than the other phases, the pores may be easier to segment [19].

The SEM-BSE image analysis has been used to quantify phases of hydrated cement paste [21], to study the phase distribution in the mortar interphase zone [22], and to estimate the reaction fraction of mineral additions in the cement matrix [9]. The three steps in this approach are as follows:

- Choice of magnification and resolution of the image.
- Phase segmentation by gray level thresholds.
- Quantification of phases in the analysis area.

Table 1 summarizes the advantages and disadvantages of the three methods of determining the degree of hydration used in this study.

Table 1

Advantages and disadvantages of the three methods (Method 1: $Ca(OH)_2$ quantification method, Method 2: Bound water of quantification method, Method 3: SEM-BSE image analysis method).

Method	Method 1	Method 2	Method 3
Advantages	• Ease of sample preparation. • Ease of processing the result.	• Ease of sample preparation. • Ease of processing the result.	• Apply cement containing a pozzolanic mineral addition, a slag.
Disadvantages	• Do not apply cement containing a pozzolanic mineral addition.	• An adequate analysis program to avoid the loss of bound water.	• Difficulty of sample preparation • Difficulty of processing the result.

There have been no researches published to far that compare the various methods for determining the degree of hydration of CEM I cement. Therefore, the purpose of this study is to compare the feasibility and reliability of the SEM –BSE image analysis approach for estimating the degree of hydration of cement with two other methods using the thermogravimetric analysis (TGA).

II. Material and method

II.1. Method of characterization of the synthesized clinker and cement

The clinker cement (OPC 97TM) used in this study was synthesized in the laboratory by burning a mixture of limestone ($CaCO_3$), silica oxide (SiO_2), aluminum oxide (Al_2O_3) and iron oxide (Fe_2O_3). The proportion of components was calculated using the modulus usually used in the cement industry: the Lime Saturation Factor (LSF), the Silica Ratio (SR) and the Alumina Ratio (AR). The calculations of modulus (LSF, SR and AR) are presented by the equations below ((Eq15) -> (Eq17)):

$$LSF = \frac{100 * \%CaO}{2.8 * \%SiO2 + 1.18 * \%Al2O3 + 065 * \%Fe2O3} \quad (15)$$

$$SR = \frac{\%SiO2}{\%Al2O3+\%Fe2O3} \quad (16)$$

$$AR = \frac{\%Al2O3}{\%Fe2O3} \quad (17)$$

In this study, the values LSF = 97, SR = 2.6 and AR = 1.45 were used for the formulation of mixture. Table 2 shows the composition of the components of the formulation.

Table 2

Mix design for the production of the clinker cement OPC 97TM.

Formula	Limestone (wt. %)	Alumina oxide (wt. %)	Iron oxide (wt. %)	Silica oxide (wt. %)
OPC 97TM	79.99	3.17	2.32	14.52

The raw materials were first mixed by adding water with a water/material ratio = 0.6 in order to have good homogeneity. After drying at 105°C, pellets (with a diameter of 40 mm and a height of 15 mm) are formed using a press and a force of 5 KN. The pellets were burned in a furnace at 200°C for 20 minutes, then the temperature increases to 1450°C with a heating rate of 7°C/minute, and kept at this temperature for 15 minutes. After clinkerization, the obtained clinkers were cooled in the furnace to reach the room temperature. Portland cement was produced by adding gypsum ($CaSO_4.2H_2O$) to ground clinker in order to have an SO_3/Al_2O_3 molar ratio of 0.6.

The content of free lime in the clinker was determined by the Schlafer-Bukokowski method. Indeed, cement manufacturers consider that a clinker, whose composition is perfectly dosed, has a CaO_{free} content of less than 2% wt. [23]. Therefore, in this study, the maximum acceptable CaO_{free} content is set at 2%.

The mineralogical composition of the clinker was identified by X-ray diffraction (XRD) and quantified according to the Bogue modified formula, which takes into account the presence of CaO_{free} [24].

The chemical composition of the clinker and hydrated cement paste phases was analyzed on the polished sections using a Hitachi S-4300 SE/N scanning electron microscope operating in backscattered electron mode (20 keV) and equipped with an energy dispersive X-ray spectrometer (EDS). For the measurement, the points were carried out on several zones.

The particle size distribution of the OPC 97TM cement was measured using the Beckman Coulter – LS13 320 type device after dispersing in an ethanol solution. The absolute density of the OPC 97TM cement was carried out using an Accupyc 1330 helium pycnometer. The Blaine specific surface of the cement was measured according to standard NF EN 196-6 [25]. In this study, the Blaine surface of the cement is between 3500 and 4000 cm^2/g.

The chemical composition of the synthetized cement was verified by X-Ray fluorescence (XRF). The mineralogy of cement and hydrated cement paste was analyzed by X-ray diffraction (XRD) using a BRUKER D2 Advance device equipped with a Cu anticathode, λ = 1.5406 Å with the angle 2θ from 5° to 80° and a step of 0.02.

II.2. Method for determining the degree of hydration

In this study a cement pastes with a w/c ratio of 0.5 was used to determine the degree of hydration. After three minutes of mixing, the paste was introduced into the polytetrafluotethylene molds for measuring the degree of hydration, and into the 1x1x1 cm^3 size molds for the measurement of compressive strength. The cement pastes were demolded after 24 hours and stored in the saturated lime solution.

Based on previous studies [23, 26–29], the compressive strength of the cement paste was measured on the cube of dimension 1x1x1 cm^3 under a constant stress of 0.3 MPa/s using a uniaxial press at 2, 15 and 28 days of hydration. For each measurement, 6 samples were tested.

II.2.1. Determination of the degree of hydration by thermogravimetric analysis (TGA)

To prevent carbonation of the cement paste, in this study, no method of stopping hydration was used. The cement paste for the TGA analysis was analyzed immediately upon reaching the desired hydration time. The device used is the NETZSCH STA 409 type with the following experimental conditions:

- During the analysis the sample is kept under a flow of Argon at a flow rate of 75 ml/min.
- The temperature increases from 30 °C to 105 °Cat a rate of 2 °C/min, then maintained at 105 °C for 1 hour before increasing to 1100 °C at a rate of 3 °C/min.

II.2.2. Determination of the degree of hydration by the SEM-BSE image analysis method

To stop the hydration, the samples for image analysis were submerged in an acetone solvent solution. Indeed, drying samples at 105 °C has the potential to alter the microstructure of the cement paste [30] and so impair image analysis results. A JEOL scanning electron microscope operating in backscattered electron mode (15 keV) with a magnification of 500 and a resolution of 1280 x 960 pixels was used to capture images of the sample. For the measurement, around 20 pictures were taken at various positions throughout the sample.

III. Results

This part presents, on the one hand, the result of characterization of the cement (OPC 97TM) and the cement paste in order to assess the quality of the cement synthesized in the laboratory, and on the other hand, the results of the degree of hydration of the paste determined by three different methods.

III.1. Characterization of clinker and synthesized cement

The CaO_{free} content of the clinker measured according to the Schlafer-Bukokowski method is 1.287%, which is less than the limit value (2%). This indicates that the clinker's composition is well dosed.

Table 3 and Table 4 show the chemical composition of the mineral phases of the clinker identified by SEM-EDS analysis. Approximately 30 points were measured for each phase in different areas.

Table 3

Results of the SEM-EDS analysis on the silicate phases of the synthesized clinker.

Mineral phase	Formula	CaO/SiO_2 (Theoretical ratio)	CaO/SiO_2 (SEM-EDS results)
Alite	Ca_3SiO_5	3	3.42
Belite	Ca_2SiO_4	2	2.44

Table 4

Results of the SEM-EDS analysis on the interstitial phases of the synthesized clinker.

Mineral phase	Formula	CaO/Al_2O_3 (Theoretical ratio)	CaO/Al_2O_3 (SEM-EDS results)
Tricalcium aluminate	$Ca_3Al_2O_6$	1.5	2.44
Calcium aluminoferrite	$Ca_4Al_2O_{10}Fe_2$	2	2.575

The results of SEM-EDS analysis showed that the ratio of the main oxides in the four phases was higher than the theoretical value. A similar result was found in Gineys's et al. research on clinker synthesized in the laboratory [23]. The difference between the theoretical and experimental values could be due to the presence of minor elements in the mineral phases, for example, Al and Fe in the C_3S and C_2S phases. This could influence the ratio of major elements in these phases. Table 5 show the physical characteristics of OPC 97TM cement. The Blaine surface of the cement reaches 3800 cm^2/g, which respects the values of the Blaine surface targeted between 3500 and 4500 cm^2/g.

Table 5

Physical characteristics of OPC 97TM cement synthesized in the laboratory.

Cement	Density (g/cm^3)	Blaine surface (cm^2/g)	BET surface (m^2/g)	d10 (µm)	d90 (µm)
OPC 97TM	3.15	3800	1.224	0.72	43.31

The chemical composition of OPC 97TM cement is also presented in Table 6.

Table 6

Chemical composition of OPC 97TM cement.

Element	SiO_2	Al_2O_3	Fe_2O_3	CaO	SO_3	LOI at 950 °C	Total
(wt.%)	20.5	4.7	3.1	65.5	1.90	3.6	99.2

The chemical composition of the main elements of the hydrated calcium silicate by the SEM-EDS analysis measured on the sample of the hydrated cement paste at 2 days is presented in the Fig.1. Around 100 points were measured in four different areas. The $CaO\text{-}SiO_2\text{-}Al_2O_3$ ternary diagram is superimposed on the ternary diagram produced by Lothenbach [31]. This diagram shows the positions of the main cement hydrates: $Ca(OH)_2$, C-S-H (with two C/S ratios) or even C-A-S-H. The diagrams show that the hydrated calcium silicates are mainly concentrated in areas where the C/S ratio is greater than 1.7. A similar results have been found in previous studies on CEM I [11, 32]. Fig.2 illustrates the C/S and Al_2O_3/SiO_2 ratios of the different measured points.

The result show that:

- The C/S ratio (CaO/SiO_2) obtained in the C-S-H phase varies from 2.5 to 3.5 but is always higher than the value of 1.7 used in the equations for the description of cement hydration (Eq1), (Eq2). This difference can be due to the EDS points made

and to the size of the diffusion bulb which analyzes an area and not a point. Typically, the diffusion bulb's size is 1 μm^3 and the resolution of a SEM 20 kV tungsten filament is 3 nm. Thus, other hydrates are analyzed and will have an influence on the C/S and Al_2O_3/SiO_2 ratios, in particular, the C/S ratio [32].

- The average value of the Al_2O_3/SiO_2 ratio of hydrates measured is equal to 0.14 and this value is very consistent with the initial value of the Al_2O_3/SiO_2 ratio in the anhydrous OPC 97TM cement (the Al_2O_3/SiO_2 ratio in the cement is equal to 0.137). This result means that all of the aluminum in the cement is found in the C-A-S-H and C-S-H phases. The incorporation of aluminum into the C-S-H phase has been demonstrated in research by Richardson et al [33]. This study showed an Al/Si ratio equal to 0.25, corresponding to the maximum aluminum that can be incorporated into C-S-H.

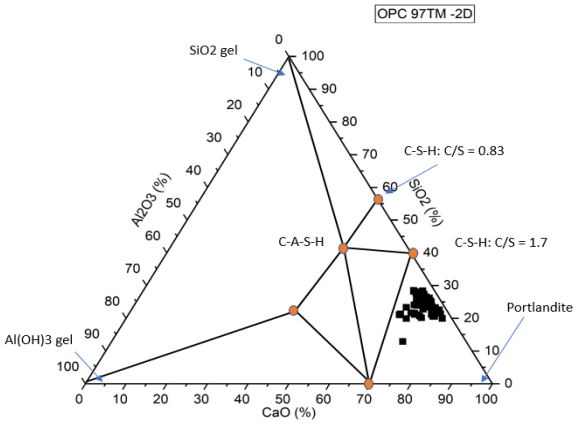

Fig. 1 $CaO\text{-}SiO_2\text{-}Al_2O_3$ ternary diagram obtained for the cement paste after 2 days of hydration.

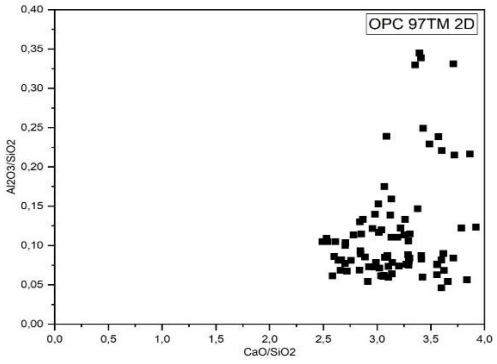

Fig. 2 Ratio of the principal elements of hydrated calcium silicate measured by SEM-EDS analysis on the sample of the cement paste after 2 days of hydration.

The evolution of the mineral phases over time of hydration identified by the XRD analysis is presented in Fig.3.

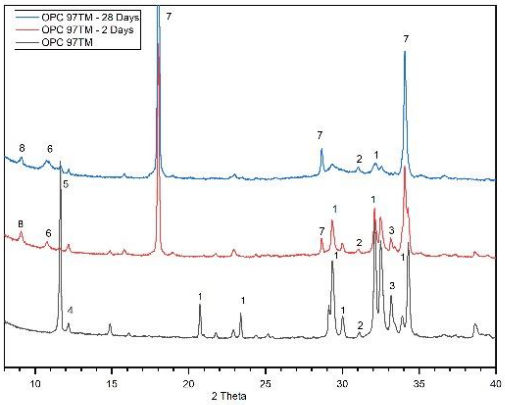

Fig. 3 X-Ray diffraction of OPC 97TM over time of hydration (1: C_3S, 2: C_2S, 3: C_3A, 4: C_4AF, 5: Gypsum, 6: Afm, 7: $Ca(OH)_2$), 8: Ettringite (Aft).

The formation of additional phases such as ettringite and portlandite in the hydrated cement paste has been observed. These hydrates formed correspond to the products described in equations (Eq 1) -> (Eq 8). However, the presence of hydrated calcium silicate (C-S-H) is difficult to detect due to its amorphous nature.

The compressive strength of the cement paste is presented in the Table 7. This result is consistent with the previous XRD result showing the transformation of anhydrous phases to hydrates in hydrated cement paste, which is the origin of resistance development.

Table 7

Compressive strength of the cement paste over the time of hydration.

Time (days)	Compressive strength (Mpa)	Deviation (%)
2 days	25.26	6.5
15 days	57.98	9.5
28 days	66.61	8.5

III.2. Degree of hydration of cement by portlandite quantification analysis by TGA analysis

The amount of portlandite produced during cement hydration was estimated by TGA analysis on cement pastes at 2 and 28 days of hydration. Table 8 shows the mineral composition of the cement and the $Ca(OH)_2$ amount produced during complete hydration, according to the calculation from the simplified equations (Eq1) -> (Eq8). Indeed, the results of the SEM-EDS analysis on the clinker and the cement paste showed a different element ratio than the theoretical ratios used in these equations.

Table 8

$Ca(OH)_2$ production for a complete hydration of cement of OPC 97TM cement.

Anhydrous phases	Mass content in cement (%)	CH mass for 1 g of anhydrous cement (g/g of cement)
C_3S	73.96	0.312

C_2S	4.77	0.0062
C_3A	5.93	0
C_4AF	9.77	0.0147
CaO_{free}	1.24	0
Gypsum	4.33	0
Total	100	0.3329

Fig.4 shows the TGA analysis curve of the cement paste after 2 days of hydration.

- Zone (I): the temperature increases from 30 °C to 105 °C to remove evaporable water.
- Zone (II): the temperature is maintained at 105 °C for 1 hour to remove the rest of evaporable water.
- Zone (III): the temperature between 650 °C and 800 °C corresponds to the decomposition of calcite temperature. In this case, the loss of weight of the sample is very low, this means that the protocol allows avoiding the phenomenon of carbonation and the quantity of $Ca(OH)_2$ determined between 450 °C and 560 °C is the totality of the $Ca(OH)_2$ produced during the hydration of the cement.

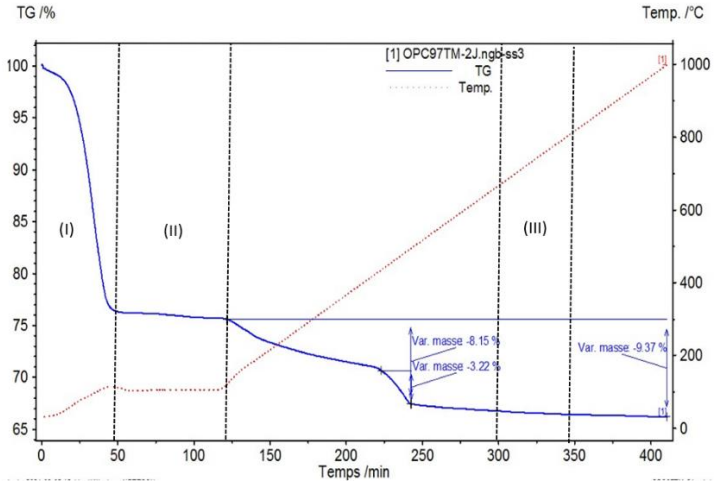

Fig. 4 TGA analysis of the cement paste (w/c = 0.5) after 2 days of hydration.

Table 9 shows the amount of portlandite as well as the degree of hydration calculated according to (Eq10), (Eq11) and (Eq12) taking the value Υ_0 (total amount of Portlandite produced when the hydration is completed) equal to 0.3329 (Table 8).

Table 9

Quantity of $Ca(OH)_2$ and the degree of hydration of the cement paste over the time of hydration.

Time (days)	Portlandite mass (g/100 g of pastes)	Degree of hydration (%)
2 days	13.24	60.09
28 days	20.44	92.16

III.3. Degree of hydration of cement by quantification of chemically bound water by TGA analysis

This approach determines the degree of hydration of the cement according to (Eq13) and (Eq14) using TGA analysis. The $W_n(\infty)$ value is calculated based on a theoretical approximation of the amount of chemically bound water for the five main phases of cement upon complete hydration. Table 10 shows the theoretical amount of water in the cement for complete hydration.

Table 10

Theoretical amount of water bound for complete hydration of OPC 97TM cement.

Anhydrous phases	Masse content in cement (wt.%)	Quantity of bound water produced in g of water/g of phase in the cement	Mass of water related to complete hydration (g)
C_3S	73.96	0.24	17.75
C_2S	4.77	0.21	1.00
C_3A	5.93	0.40	2.372
C_4AF	9.77	0.37	3.614
CaO_{free}	1.24	0.33	0.409
Gypsum	4.33	0	0
Total	100		25.145

From Table 10, we conclude that the $W_n(\infty)$ = 25.145 (g).
From the result of the TGA analysis (Fig.4), we then obtain:
$\Delta m\ sample\ (105\ °C - 1000\ °C)(2\ days)$ = 9.37 (g).
$m\ sample\ (1000°C)(2\ days)$ = 66.21 (g).

$$w_n(2\ days) = = \frac{\Delta m\ sample\ (105\ °C - 1000\ °C)(t)}{m\ sample\ (1000°C)(t)} * 100 = \frac{9.37}{66.21} * 100 = 14.152\ (g).$$

The degree of hydration of the cement within 2 days of hydration was calculated using (Eq13):

$$\alpha(t) = \frac{Wn\ (t)}{Wn(\infty)} = \frac{14.152}{25.145} * 100 = 56.28\ (\%).$$

Table 11 shows the degree of hydration of the cement paste calculated according to the method of quantification of water bound over time of hydration.

Table 11

Degree of hydration of OPC 97TM cement estimated by the bound water quantification method.

Time (days)	Degree of hydration (%)
2 days	56.28
28 days	80.85

III.4. Degree of hydration of cement by SEM-BSE image analysis method

Fig.5 shows the essential steps applied in this study to quantify the cement phases over time of hydration.

- Step 1: Acquisition of SEM-BSE images of the sample.
- Step 2: Acquisition of histogram of SEM-BSE images of the sample using Matlab software.
- Step 3: Quantification of phases on the diagram of histogram using Origin pro software.

The segmentation of the pores from an image with gray levels (0-255), first requires the setting of a threshold value [34]. In the literature, many methods exist for determining this threshold value, which is very important for quantification with better precision, for example it corresponds to the point of intersection of the tangents to the peak curves of the pores and of the peaks of the hydrated phases (HP) (Fig.5). This threshold level of pore segmentation is around 50 for the cement paste in this study. After setting the threshold level, the deconvolution method was applied using the Origin Pro 8.5 software for phase quantification. The quantity of phases from the analysis of the images corresponds to the volume fraction of these phases in the cement paste and the degree of hydration of the cement is estimated according to the following equation (Eq18):

$$\alpha(t) = \frac{V\ anhydrous\ cement\ (t)}{V\ anhydrous\ cement\ (t=0)} * 100 \qquad (18)$$

The cement paste made with a W/C ratio equal to 0.5 corresponds to an initial volume fraction of the cement equal to 38.83%.

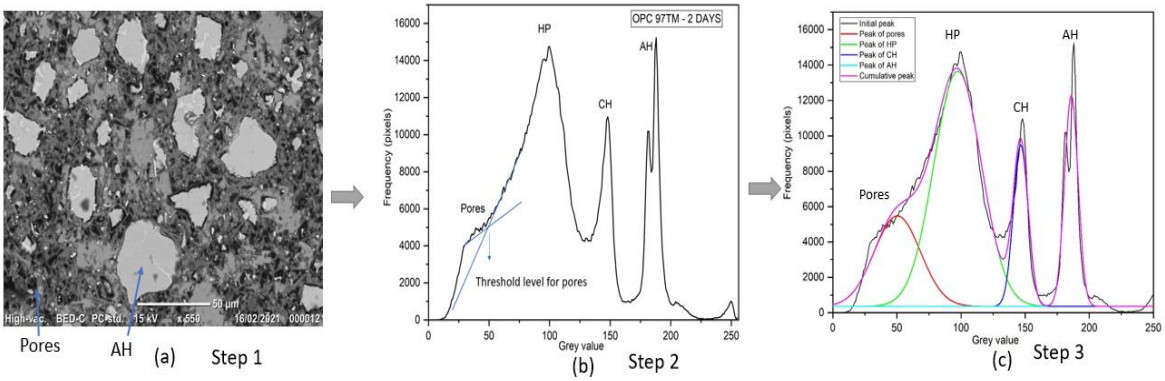

Fig. 5 Methodology of phase quantification using image analysis technique (cement paste after 2 days of hydration)

Several images were analyzed and the Table 12 shows the result of the degree of hydration of the cement over time of hydration by the method of SEM – BSE image analysis.

Table 12

Degree of hydration of cement estimated by the SEM – BSE image analysis method.

Time (days)	Amount of anhydrous cement (%)	Degree of hydration (%)	Deviation (%)
2 days	14.35	63.04	7.80
28 days	2.46	93.66	8.40

III.5. Assessment of the relevance of method for determining the degree of hydration

Table 13 shows the degree of the OPC 97TM cement paste determined by three different methods.

Table 13

Degree of hydration of the OPC 97TM cement paste determined by three different methods.

Method	Degree of hydration (%)	
	2 Days	28 Days
Method 1	60.09	92.16
Method 2	56.28	80.85
Method 3	63.04	93.66

The deviation of the degree of hydration estimated by different methods was observed. In order to assess the relevance of these methods, the Power's approach (Eq19) was used [35] which presents a model for estimating compressive strength as a function of the degree of hydration.

$$\sigma_c(t) = \sigma_0(X(t))^n \quad (19)$$

with:

$\sigma_c(t)$: Compressive strength at time t.

σ_0: Compressive strength when capillary porosity is zero. It is calibrated on the basis of determination of resistance at 2 days.

n: Value taken between 2.6 and 3.0. In general, a value equal to 2.6 is applied for CEM I.

X(t): Ratio of hydrate gel-space, is determined as following equation (Eq20):

$$X(t) = \frac{0.68\,\alpha(t)}{0.32\alpha(t)+\frac{W}{C}} \quad (20)$$

with:

α(t): Degree of hydration of sample at time t.

W/C: water/cement ratio.

From the relationship between the compressive strength and the degree of hydration (Eq19) and (Eq20), the experimental value of the compressive strength was used to assess the suitability of the three methods. The principle is to determine the degree of hydration at 28 days from the hydration at 2 days in order to achieve desired compressive strength. The degree of hydration at 28 days is calculated using the following equation (Eq21):

$$\alpha(28\text{ days}) = \frac{0.5}{\left(\frac{0.32\alpha(2\text{days})/100+0.5}{\alpha(2\text{ days})/100} * \sqrt[2.6]{\frac{\sigma c(2\text{ days})}{\sigma c(28\text{ days})}} - 0.32\right)} \quad (21)$$

with:

σ_c (2 days): Compressive strength at 2 days (Mpa).

σ_c (28 days): Compressive strength at 28 days (Mpa).

α (2 days): Degree of hydration at 2 days (%).

α (28 days): Degree of hydration at 28 days calculated from the degree of hydration at 2 days to reach the desired resistance value at 28 days (%).

Table 14 shows the value of the degree of hydration calculated according to (Eq21) from the degree of hydration at 2 days determined according to the three methods.

Table 14

Degree of hydration at 28 days calculated from (Eq21) according to three methods, Method 1: Portlandite quantification method, Method 2: Bound water of quantification method, Method 3: SEM-BSE image analysis method.

Degree of hydration	Method 1	Method 2	Method 3
α (28 days) (%) (Eq21)	102.9	97.6	111.9
α (28 days) (%) (Experimental)	92.16	80.85	93.66
Deviation (%)	11.65	20.71	19.47

The result shows that:

- $Ca(OH)_2$ quantification method seems to give a better result compared to two other methods with the smallest deviation. However, the degree of hydration at 28 days calculated from method 1 and method 3 exceeds 100%. In addition, Zhang et al [36] found that the degree of hydration of CEM I cement paste varies between 55 and 80 % at 28 days depending on the W/C ration (W/C ration between 0.3 and 0.7).
- Comparing with Zhang's result, method 2 seems to present a reasonable result. However, it should be noted that some phases (Ettringite, C-S-H) start dehydroxylation at a lower temperature than 105 °C [11].

In addition, we chose to compare the experimental quantities of $Ca(OH)_2$ to evaluate the methods' relevance in our study because $Ca(OH)_2$ is a relatively easy data set to determine thanks to TGA analysis. The SEM-BSE image analysis presents the volume of $Ca(OH)_2$ over time of hydration. We convert from volume fraction to mass fraction using a $CaOH)_2$ density of 2.24 (g/cm^3). The $Ca(OH)_2$/initial cement mass ratio measured by the SEM-BSE images analysis method is calculated according to the following equation (Eq22):

$$\frac{Ca(OH)2\ (t)\ mass}{initial\ cement\ mass} = \frac{V\ Ca(OH)2\ (t)}{V\ anhydrous\ cement\ (t=0)} * \frac{2.24}{3.15} * 100 \qquad (22)$$

With:
$Ca(OH)_2$(t) mass: Masse of $Ca(OH)_2$ at time t.
$V_{Ca(OH)2}$ (t) : Volume of $Ca(OH)_2$ at time t.
$V_{anhydrous\ cement\ (t=0)}$: Initial volume of anhydrous cement.
$Ca(OH)_2$ density : 2.24 g/cm^3.
Cement density: 3.15 g/cm^3 (Table 5).
The result of three methods is presented in the Table 15.

Table 15

$Ca(OH)_2$/initial cement mass ratio measured by three methods.

$\frac{Ca(OH)2\ (t)\ mass}{initial\ cement\ mass}$ (%)	Method 1	Method 2	Method 3
2 Days	20.27	20.15	21.25
28 Days	30.68	29.03	31.18

The result shows that:

- Method 1 and method 3 seem to present the result consistent with method 2 by presenting a higher ration. But the deviation is small.

IV. Conclusion

The objective of this study is to estimate the degree of hydration of cement synthesized in the laboratory by three different approaches: method of quantification of portlandite, method of quantification of chemically bound water and method of image analysis. The results showed that:

- The C/S ratio in the alite and the belite in the clinker measured by the SEM-EDS analysis are higher than the theoretical ratio equal to 3 and 2 respectively. The CaO/Al_2O_3 and CaO/Fe_2O_3 ratios in C_3A and C_4AF are also higher than the theoretical value of 1.5 and 2 respectively. The difference between the theoretical and experimental values could be due to the presence of minor elements in the mineral phases, for example, Al and Fe in the C_3S and C_2S phases. This could influence the ratio of major elements in these phases.
- The C/S ratio in the hydrated calcium silicate (C-S-H) phase measured by the SEM-EDS analysis on the hydrated cement paste at 2 days is also higher than the theoretical value of 1.7 used in the equations of cement hydration. This difference can be due to the EDS points made and to the size of the diffusion bulb which analyzes an area and not a point. In addition, the incorporation of aluminum in this phase has been detected. This could have an influence on the C/S ratio.
- The bound water quantification method seems to present a reasonable result using the Power's approach and using the result in the literature.
- The $Ca(OH)_2$ quantification method seems to overestimate the degree of hydration. The result also depends on the temperature range of $Ca(OH)_2$ quantification on the TGA curve.
- The SEM – BSE image analysis method presents relatively similar results with the results by the $Ca(OH)_2$ quantification method. This method demonstrates the feasibility used as a reliable method to determine the degree of hydration, the amount of hydrates in a cementitious material. However, it is necessary to improve the number of images and the resolution to increase the precision.

Declaration of competing interest:

The authors declare that they no known competing financial interests or personal relationships that could have appeared to influence the work reported in this paper.

Acknowledgments:

The authors wish to acknowledge the SEDICIM project and the FEDER funds.

Reference

1. Nonat, A.: Chapitre2: L'hydratation des ciments- La durabilité des bétons. (2008)
2. Tang, S., Wang, Y., Geng, Z., Xu, X., Yu, W., A, H., Chen, J.: Structure, fractality, mechanics and durability of calcium silicate hydrates. Fractal Fract. 5, (2021). https://doi.org/10.3390/fractalfract5020047
3. Wang, L., Guo, F., Lin, Y., Yang, H., Tang, S.W.: Comparison between the effects of phosphorous slag and fly ash on the C-S-H structure, long-term hydration heat and volume deformation of cement-based materials. Constr. Build. Mater. 250, 118807 (2020). https://doi.org/10.1016/j.conbuildmat.2020.118807
4. Richardson, I.G.: Nature of C-S-H in hardened cements. Cem. Concr. Res. 29, 1131–1147 (1999). https://doi.org/10.1016/S0008-8846(99)00168-4
5. Escalante-Garcia, J.I., Sharp, J.H.: Variation in the composition of C-S-H gel in portland cement pastes cured at various temperatures. J. Am. Ceram. Soc. 82, 3237–3241 (1999). https://doi.org/10.1111/j.1151-2916.1999.tb02230.x

6. Richardson, I.G.: The calcium silicate hydrates. Cem. Concr. Res. 38, 137–158 (2008). https://doi.org/10.1016/j.cemconres.2007.11.005
7. Phung, Q.T., Maes, N., Jacques, D., Perko, J., De Schutter, G., Ye, G.: Modelling the evolution of microstructure and transport properties of cement pastes under conditions of accelerated leaching. Constr. Build. Mater. 115, 179–192 (2016). https://doi.org/10.1016/j.conbuildmat.2016.04.049
8. Snellings, R., Vayghan, A.G., Horckmans, L., Snellings, R., Peys, A., Teck, P., Maier, J., Friedrich, B., Klejnowska, K.: Use of Treated Non-Ferrous Metallurgical Slags as Supplementary Cementitious Materials in Cementitious Mixtures Use of Treated Non - Ferrous Metallurgical Slags as Supplementary Cementitious Materials in Cementitious Mixtures. (2021). https://doi.org/10.3390/app11094028
9. Kocaba, V., Gallucci, E., Scrivener, K.L.: Methods for determination of degree of reaction of slag in blended cement pastes. Cem. Concr. Res. 42, 511–525 (2012). https://doi.org/10.1016/j.cemconres.2011.11.010
10. Lu, X., Ye, Z., Wang, S., Du, P., Li, C., Cheng, X.: Study on the preparation and properties of belite-ye'elimite-alite cement. Constr. Build. Mater. 182, 399–405 (2018). https://doi.org/10.1016/j.conbuildmat.2018.06.143
11. Cassagnabère, F., Mouret, M., Escadeillas, G.: Early hydration of clinker-slag-metakaolin combination in steam curing conditions, relation with mechanical properties. Cem. Concr. Res. 39, 1164–1173 (2009). https://doi.org/10.1016/j.cemconres.2009.07.023
12. Bentz, D.P., Barrett, T., De la Varga, I., Weiss, W.J.: Relating Compressive Strength to Heat Release in Mortars. Adv. Civ. Eng. Mater. 1, 20120002 (2012). https://doi.org/10.1520/acem20120002
13. Ha, B.T.T.: Evolution physico-chimique des liants bas PH hydratés Influence de la température et mécanisme de rétention des alcalins - Thèse doctorante, (2010)
14. Benzerzour, M., Maherzi, W., Amar, M.A.A., Abriak, N.E., Damidot, D.: Formulation of mortars based on thermally treated sediments. J. Mater. Cycles Waste Manag. 20, 592–603 (2018). https://doi.org/10.1007/s10163-017-0626-0
15. Bordy, A.: Influence des conditions thermo-hydriques de conservation sur l ' hydratation de matériaux cimentaires à base d ' une fine recyclée. 1–155 (2016)
16. Elkarim, M., Bulteel, D., Potier, G., Michel, F., Zhao, Z., Courard, L.: Use of grinded hardened cement pastes as mineral addition for mortars. (2020). https://doi.org/10.1016/j.jobe.2020.101863
17. Bresciani, C.: Simulation numérique de l ' hydratation et du développement des propriétés physiques et mécaniques d ' une pâte de ciment afin de sélectionner de nouveaux ajouts minéraux., (2009)
18. NIST: Technical Note VCCTL-01.
19. Wong, H.S., Head, M.K., Buenfeld, N.R.: Pore segmentation of cement-based materials from backscattered electron images. Cem. Concr. Res. 36, 1083–1090 (2006). https://doi.org/10.1016/j.cemconres.2005.10.006
20. P.J. Goodhew, J. Humphreys, R.B.: Electron Microscopy and Analysis, 3rd edition. aylor Fr. London, 2001, 251 pp. (2001)
21. Scrivener, K.L., Patel, H.H., Pratt, P.L., And, Parrott, L.J.: Analysis of Phases in Cement Paste using Backscattered Electron Images, Methanol Adsorption and Thermogravimetric Analysis.
22. LE, T.: Influence de l'humidité des granulats de béton recyclé sur le comportement à l'état frais et durcissant des mortiers, (2015)
23. Gineys, N.: Influence de la teneur en éléments métalliques sur les propriétés techniques et environnementales du ciment Portland, (2011)

24. Bogue, R.H., Lerch, W.: Hydration of Portland Cement Compounds. Ind. Eng. Chem. 26, 837–847 (1934). https://doi.org/10.1021/ie50296a007
25. Association Française de Normalisation (AFNOR): NF EN 196-6 : Méthodes d'essai des ciments - Détermination de la finesse. (2018)
26. Aouad, G., Laboudigue, A., Gineys, N., Abriak, N.E.: Dredged sediments used as novel supply of raw material to produce Portland cement clinker. Cem. Concr. Compos. 34, 788–793 (2012). https://doi.org/10.1016/j.cemconcomp.2012.02.008
27. Joelle Kleib: Ecoconception des ciments : synthèse , hydratation et durabilité-Thèse doctorant IMT Lille Douai et L'Université Libanaise, (2018)
28. Kleib, J., Aouad, G., Abriak, N.E., Benzerzour, M.: Production of Portland cement clinker from French Municipal Solid Waste Incineration Bottom Ash. Case Stud. Constr. Mater. 15, e00629 (2021). https://doi.org/10.1016/j.cscm.2021.e00629
29. Kleib, J., Aouad, G., Khalil, N., Zakhour, M.: Incorporation of zinc in calcium sulfoaluminate cement clinker. Adv. Cem. Res. 1–7 (2020). https://doi.org/10.1680/jadcr.19.00125
30. Zhang, J., Scherer, G.W.: Comparison of methods for arresting hydration of cement. Cem. Concr. Res. 41, 1024–1036 (2011). https://doi.org/10.1016/j.cemconres.2011.06.003
31. Lothenbach, B., Scrivener, K., Hooton, R.D.: Supplementary cementitious materials. Cem. Concr. Res. 41, 1244–1256 (2011). https://doi.org/10.1016/j.cemconres.2010.12.001
32. Berthomier, M.: Etude de la lixiviation de l'aluminium de matériaux cimentaires à base de CEM III utilisés dans les canalisations d'eau potable : approche expérimentale et numérique. (2020)
33. Richardson, I. G.A. R. Brough, et al: Location of Aluminum in substituted calcium silicate hydrate, C-S-H, gels as determined by 29Si and 27Al NMR and EELS. 1993.
34. Zined, B.: Influence de la microstructure sur le transport diffusif des pâtes, mortiers et bétons à base de CEM I avec ajout de fumée de silice, (2016)
35. Bentz, D.P.: Guide to Using CEMHYD3D: A Three-Dimensional Cement Hydration and Microstructure Development Modelling Package. (1997)
36. Zhang, S., Zhang, M.: Hydration of cement and pore structure of concrete cured in tropical environment. Cem. Concr. Res. 36, 1947–1953 (2006). https://doi.org/10.1016/j.cemconres.2004.11.006

Chapitre 3 : Valorisation du sédiment dans le cru – Application dans un projet industriel – Projet SEDICIM

L'objectif dans ce chapitre est d'évaluer la qualité des ciments à base sédiments, synthétisés au laboratoire en respectant les critères industriels.

Pour cela, dans un premier temps, nous avons caractérisé au total 7 sédiments différents afin de trouver le sédiment le plus adapté en termes de priorités physico-chimiques. Les essais ont été effectués en tandem aux seins du laboratoire IMT Nord – Europe et du laboratoire EQIOM afin de comparer les résultats.

Dans le chapitre 2, les résultats de caractérisation des ciments synthétisés au laboratoire ont permis d'obtenir les points importants suivants :

- Le processus de cuisson au laboratoire permet d'obtenir les ciments avec une bonne qualité (la teneur de chaux libre dans les clinkers inférieure à la valeur limite de 2% wt).
- La faisabilité d'utilisation du sédiment en tant que la matière première dans la fabrication du ciment avec une teneur élevée jusqu'à 32% wt.

I. Introduction

Sur la base des résultats obtenus dans le chapitre 2, on s'intéresse ici à la valorisation du sédiment dans le mélange cru en respectant des critères industriels tels que la viscosité du mélange. Contrairement au chapitre 2, les matières premières utilisées dans ce chapitre sont les matières utilisées chez EQIOM pour la fabrication du ciment (trois types de calcaire, deux types d'argile, l'oxyde de fer, le sable). Le résultat de ce chapitre servira pour la formulation du mélange de cru à l'échelle industrielle.

L'objectif ici est la valorisation du sédiment pour la fabrication de deux types de ciment : CEM I 52.5 et CEM III 42.5.

- CEM I 52.5 : Deux formulations de cru ont été confectionnées. La première est la formulation de référence qui est constituée des calcaires, d'argiles, du sable et d'oxyde de fer. La deuxième formulation a une teneur de 2% wt. de sédiment pour remplacer une partie des matières premières et des calcaires, des argiles et de l'oxyde de fer.
- CEM III 42.5 : Trois ciments CEM III ont été confectionnés. Les compositions de ces ciments sont les suivantes :
    - CEM III de référence : Clinker (sans sédiment dans le mélange cru) + Laitier + Gypse.
    - CEM III 2% ASL : Clinker (2% wt du sédiment dans la formulation cru) + Laitier + Gypse.
    - CEM III 10% SF : Clinker (sans sédiment dans le mélange cru) + Laitier + 10% sédiment calciné + Gypse.

La liste des essais de caractérisation des sédiments est présentée ci-aprés :

Caractérisation		IMT					EQIOM				
		DKS	DKV	NSL	LM	ASL	DKS	DKV	NSL	LM	ASL
Caractérisations physiques	Masse volumique spécifique	✓	✓	✓	✓	✓	X	X	X	X	X
	Teneur en matières organiques	✓	✓	✓	✓	✓	✓	✓	✓	✓	X
	Granulométrie Laser et Tamis	✓	✓	✓	✓	✓	✓	✓	✓	✓	X
	Granulométrie Voie humide	✓	✓	✓	✓	✓	✓	✓	✓	✓	X
	Surface spécifique BET/Blaine	✓	✓	✓	✓	✓	X	X	X	X	X
	Perte au feu P.A.F 950°C	✓	✓	✓	✓	✓	✓	✓	✓	✓	X
	Valeur VBS	✓	✓	✓	✓	X	X	X	X	X	X
Caractérisations chimiques et minéralogiques	Analyse FX (sur pastilles)	✓	✓	✓	✓	✓	✓	✓	✓	✓	X
	Analyse FX (Sur perle)	✓	✓	✓	✓	✓	✓	✓	✓	✓	X
	Diffractométrie DRX standard	✓	✓	✓	✓	✓	✓	✓	✓	✓	X
	Diffractométrie DRX (5°-80°)	✓	✓	✓	✓	✓	✓	✓	✓	✓	X
	Analyse themogravimétrique (ATG-ADT)	✓	✓	✓	✓	✓	X	X	X	X	X
Caractérisation environnementale	Lixiviation	✓	✓	✓	✓	✓	✓	✓	✓	✓	X

II. Démarche expérimentale

Les matières premières et le sédiment ont été caractérisés afin de déterminer leur composition chimique et leur composition minérale. Ensuite, les matériaux ont été broyés finement pour obtenir une granulométrie inférieure à 200 µm. Le dosage des composants dans la formulation a été calculé en utilisant les valeurs des modules LSF, AR, SR qui sont utilisées habituellement dans l'industrie cimentière. L'ensemble des matières premières ont été mélangées en ajoutant de l'eau afin d'obtenir un mélange plus homogène. Pour faciliter la cuisson dans le four, les pastilles ont été confectionnées. Elles ont été ensuite cuites dans le four selon le programme suivant : la cuisson à 200 °C pendant 20 minutes, puis, la température augmentée jusqu'à 1450 °C avec une vitesse de chauffage de 7 °C/min, la température maintenue à 1450 °C pendant 15 minutes, enfin le refroidissement dans le four jusqu'à la température ambiante. La méthodologie suivie dans ce chapitre est détaillée ci-dessous :

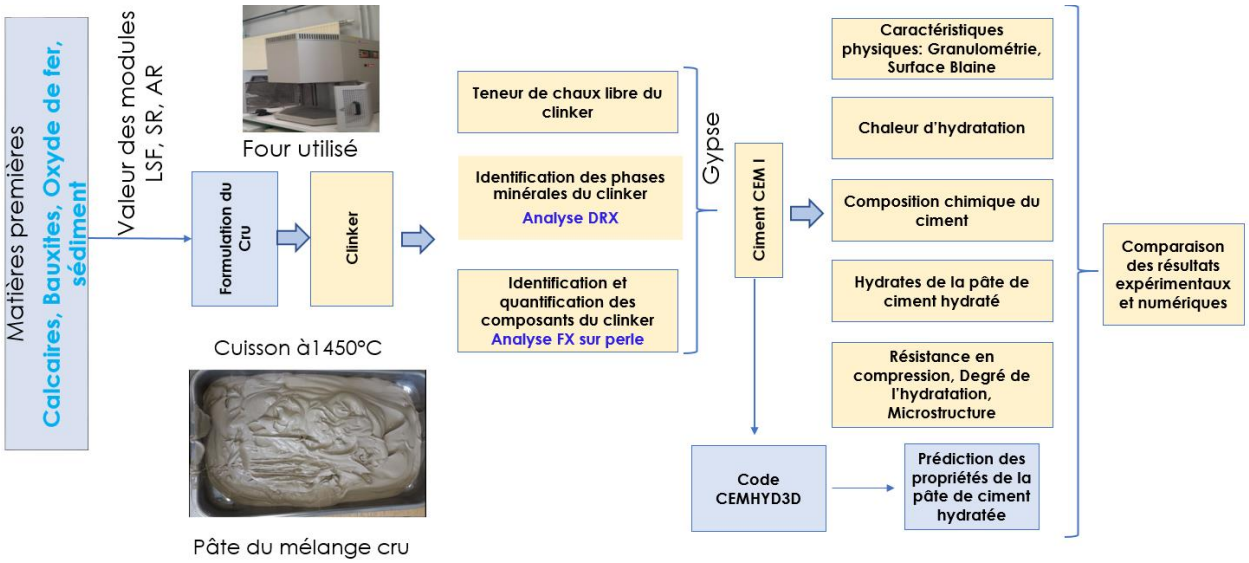

Les deux clinkers obtenus ont été caractérisés afin de vérifier la composition chimique, la teneur en chaux libre et la composition minérale.

Les ciments sont obtenus en broyant le clinker avec les autres composants tels que le gypse, le laitier et le sédiment calciné en fonction du type de ciment. La réactivité des ciments a été évaluée en mesurant la chaleur de l'hydratation de la pâte de ciment par analyse de calorimétrie

isotherme et le degré de l'hydratation de la pâte de ciment à l'aide de la méthode de quantification de l'eau liée. Contrairement au ciment étudié dans le chapitre 2, dans ce chapitre, la résistance en compression des ciments a été mesurée sur les mortiers normalisés selon la norme NF EN 196-1.
La microstructure a été évaluée en mesurant la porosité au mercure des échantillons de mortiers. Enfin, la composition chimique des phases minérales et des hydrates de la pâte de ciment a été identifiée à l'aide de l'analyse MEB-EDS. Pour chaque phase, environ 100 points ont été mesurés sur différentes zones.
Les caractéristiques des ciments CEM I sont également utilisées comme données d'entrée du code CEMHYD3D pour modéliser l'hydratation du ciment CEM I.

III. Résultat du chapitre

Les résultats de ce chapitre sont présentés dans les articles 3 (pour le CEM I) et l'article 4 (pour le CEM III).

Article 3: Valorization of sediments as raw material in the manufacture of Portland cement – Numerical modeling of the hydration of synthesized cements

---

Synthèse : Dans cette étude, le ciment témoin a été fabriqué à partir des matières premières d'extraction issue du gisement de l'industriel. Un ciment contenant 2% de sédiment (fluvial) en masse a été aussi produit en respectant le critère de la viscosité du mélange à l'usine (fabrication par voie humide). Les principaux résultats sont les suivants :

- Le sédiment ne modifie pas la composition des phases minérales du clinker
- Le ciment à base de sédiment a une hydratation similaire au ciment de référence sans sédiment.
- Les deux ciments présentent des résistances en compression supérieures à 52.5 MPa mesurées sur le mortier normalisé à 28 jours.
- CEMHYD3D a été utilisé pour modéliser l'hydratation du ciment et suivre l'évolution des phases dans le temps. Les résultats numériques sont cohérents avec les résultats expérimentaux.
- CEMHYD3D permet de prédire égalementl'évolution de la microstructure d'une matrice cimentaire telle que la porosité en comparant les résultats numériques avec les résultats expérimentaux de la porosité au mercure.

Date de soumission	8 octobre 2021
Statut	With editor
Journal	Construction and Building Materials https://www.editorialmanager.com/conbuildmat/default1.aspx

Article 3 : Valorization of sediments as raw material in the manufacture of Portland cement – Numerical modeling of the hydration of synthesized cements

Duc Chinh CHU[(1)], Joelle KLEIB[(1)], Mouhamadou AMAR[(1)], Mahfoud BENZERZOUR[(1)], Jaouad NADAH[(2)], Nor-Edine ABRIAK[(1)]

[(1)] Univ.Lille, IMT Lille Douai, Univ.Artois, Yncrea Hauts-de-France, ULR 4515-LGCgE, 6 Laboratoire de Génie civil et géo-Environnement, F-59000, Lille, France

[(2)] EQIOM Le LAB, CRT 1 Parc Vendôme – 460 Allée de l'Innovation, 59810 LESQUIN, France.

[(*)] **Corresponding author:**

duc.chinh.chu@imt-nord-europe.fr

Abstract

The valuation of sediments in the manufacture of cement could have benefits. The first is that it could solve the problem of sediment management. Second, it helps to reserve natural resources and reduce the impact on the environment due to the extraction of raw materials. This research aims at the use of sediment as a raw material while respecting specific criteria in the cement industry. The sediment-based cement was characterized by X-Ray Diffraction (XRD), X-Ray Fluorescence (XRF), and Scanning Electron Microscope with Energy Dispersive X-Ray Spectroscopy (SEM - EDS) to verify the mineralogical and chemical composition of the phases. The reactivity was followed by isothermal calorimetry, the degree of hydration in the hydration time. The compressive strength was measured on the mortar sample and the microstructure of the hydrated cement was investigated by measuring the mercury porosity. By comparing with the reference cement (without sediment), the result shows that the sediment-based cement would have the same characteristics as the reference cement and the use of the sediment did not modify the composition of the phases and the hydration behavior of the cement.

In addition, the hydration of the synthesized cements was numerically modeled using the CEMHYD3D model (NIST). Numerical modeling makes it possible to better understand the hydration of cement and to quickly follow the evolution of phases and hydrates over time. The experimental and numerical results confirm the success of the recovery of the sediment in the manufacture of Portland cement.

Keyword: Sediment, Cement, Valorization, Hydration, CEMHYD3D.

I. Introduction

The cement industry is one of the most polluting industries. In 2019, French cement industry produced 2.9% of the country's carbon dioxide emissions [1]. In addition, the extraction of raw materials from quarries can have negative impacts on the environment. Indeed, this extraction and the construction of the roads necessary for their transport can modify the landscapes and have an impact on the use of the land [2]. The use of material recovery at different stages of the cement process becomes a challenge to preserve the natural resource. This will have two interests, on the one hand, reducing the extraction of raw materials, and on the other hand, solving the problem of waste storage. In 2014, French cement industry recycled 2.6 Mt of mineral materials, of which 0.6 Mt recovered in the preparation of raw material [3].

In France, approximately 56 million m^3 of sediments (marine and river) are dredged each year in order to ensure acceptable navigation thresholds, avoid flooding and improve the quality of the environment [4]. These sediments are then either submerged in the sea or deposited in landfields. However, according to European Directive 2008/98/EC, landfields sediment with specific thresholds could be considered as inert or dangerous wastes [5]. Consequently, it is necessary to find adequate solutions for the recovery of these sediments. In the literature, sediments have been recycled as the foundation layer in road construction [6–8], the mineral

addition replaces part of the cement [9, 10] or the replacement of part of the raw materials in the manufacture of clinker [11–13]. Anger [14] has evaluated the potential of the recovery of sediments for several applications. The results showed that replacing part of the raw materials with sediment seemed to be the most promising solution. In 2015, 12.5 Mt of clinker was produced in France [15] and the required annual amount of raw material can be reached at 21.3 Mt.

The objective of this research is first to assess the impact of the use of sediments as raw materials on the formation of clinker phases. Then, the properties of hydrated cement were also evaluated by experimental tests such as isothermal calorimetry and compressive strength. Finally, the CEMHYD3D model was used to simulate the hydration behavior of the synthesized cement and to monitor the evolution of the phases over time of hydration. The experimental results and the results of the numerical modeling of cement hydration are compared to assess the reliability of the model. Numerical modeling also provides a better understanding of the hydration behavior of synthesized cements and to reduce the number of experimental tests.

II. Materials and methods

II.1. Raw materials

The sediment used in this research is the fluvial sediment collected at the Air sur Lys (ASL) depot site in the Haut de France region, France. It was then homogenized and dried to a constant mass at 40 ° C.

The limestone, clay, sand and iron oxide extracted from the deposit were supplied by the cement company EQIOM. These materials were also dried to constant mass and ground to a particle size of less than 200 µm.

Table 1 presents the nomenclature of materials used in the research.

Table 1

The nomenclature of materials in the research

Sediment	Limestone 1	Limestone 2	Limestone 3	Clay 1	Clay 2	Sand	Iron oxide	Gypsum
ASL	LIM 1	LIM 2	LIM 3	CLY 1	CLY 2	SAN	IRO	GYP

II.2. Raw material characterization method

The particle size distribution of the raw materials in this study was measured using the BECKMAN COULTER type LS13 320 device. To do this, approximately 2 grs of powder was immersed in 50 ml of acetone solution and dispersed using the ultrasound machine for 2 minutes. For the sediment, the particle size was measured in two different fractions. A fraction greater than 80 µm was measured using wet sieves, and a fraction less than 80 µm was measured using the laser diffraction particle size analyzer. This choice allows a more precise evaluation of the particle size of the sediment because the analyzer can only measure up to 2000 µm diameter. Fig.1 illustrates the particle size distribution of two fractions of the sediment.

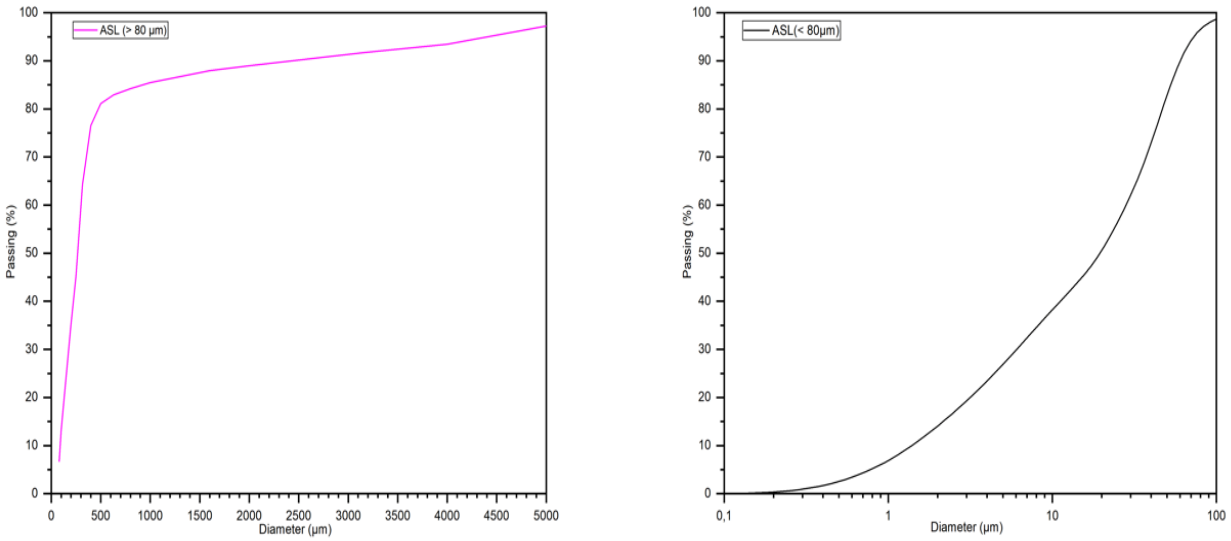

Fig. 1 Particle size distribution of the two fractions of sediment

Table 2 shows the density of the raw materials used in the research.

Table 2

Density of the raw materials

Density (g/cm^3)	ASL	LIM 1	LIM 2	LIM 3	CLY 1	CLY 2	SAN	IRO	GYP
	2.65	2.76	2.76	2.76	2.65	2.65	2.63	3.99	2.36

The chemical composition was determined by X-Ray Fluorescence (XRF) using an S4 - PIONEER apparatus equipped with a 4 -kW generator and an Rh anode. The beads were prepared by mixing 2 grs of the material analyzed with 10 grs of melting agent (mass ratio 1: 5). Table 3 shows the result of the chemical analysis of the materials. The main oxides of the materials are SiO_2, Al_2O_3, Fe_2O_3 and CaO. These are the main oxides constituting the phases of the cement

Table 3

Chemical composition of materials

Oxide (%)	ASL	LIM 1	LIM 2	LIM 3	CLY 1	CLY 2	SAN	IRO	GYP
SiO_2	65.15	5.3	9.5	6.0	48.7	60.6	88.3	2.2	1.95
Al_2O_3	7.35	1.9	3.7	1.2	20.6	14.9	4.8	0.3	0.33
Fe_2O_3	3.1	0.6	1.3	0.6	10.7	7.9	1.2	70.6	0.28
CaO	7.55	49.8	45.8	50.0	1.1	2.3	2.1	13.5	32.85
MgO	0.7	0.4	0.6	0.4	1.1	0.8	ND	2.2	0.34
Na_2O	0.85	ND	ND	ND	ND	ND	ND	ND	0
K_2O	1.65	0.4	0.9	0.2	1.5	1.3	0.3	0.1	0.08
SO_3	0.1	ND	ND	ND	ND	ND	ND	0.2	38.58

TiO_2	0.65	ND	0.1	ND	0.7	0.7	0.9	ND	0
P_2O_5	0.25	ND	ND	0.2	0.3	0.2	ND	ND	0
Mn_2O_3	ND	ND	ND	ND	ND	0.2	ND	0.7	0
ZnO	0.1	ND	ND	ND	ND	ND	0.1	ND	0
LOI	12.1	40.9	37.5	40.9	14.6	10.5	1.9	1.2	24.85
Total	99.5	99.3	99.4	99.5	99.3	99.4	99.6	98.7	99.28

Note: ND = not detected.

X-ray diffraction (XRD) was used to identify the mineralogical phases using a Bruker D2 Advance type apparatus equipped with a Cu anode, λ = 1.5406 Å, with the recording angle 2θ of the diffraction from 5° to 80° and a step size of 0.02. Table 4 presents the main mineral phases identified in the materials.

Table 4

The main mineral phases of materials identified by X-ray diffraction (XRD)

Materials	Phases
ASL	• Quartz (SiO_2) • Calcite ($CaCO_3$) • Muscovite ($KAl2(AlSi_3O_{10})(F,OH)2$) • Albite • Montmorillonite (Clay) ($(Na, Ca)_{0.3}(Al, Mg)_2(Si_4O_{10}(OH)_2.nH2O$). • Orthoclase
LIM 1	• Calcite ($CaCO_3$)
LIM 2	• Calcite ($CaCO_3$)
LIM 3	• Calcite ($CaCO_3$)
CLY 1	• Quartz (SiO_2) • Montmorillonite (Clay) • Iron aluminum oxide hydroxide • Kaolinite ($Al_2O_3.2SiO_2.2H_2O$)
CLY 2	• Quartz (SiO_2) • Montmorillonite (Clay) • Kaolinite ($Al_2O_3.2SiO_2.2H_2O$)
SAN	• Quartz (SiO_2) • Calcite ($CaCO_3$)
IRO	• Magnetite ($FeO.Fe_2O_3$) • Calcite ($CaCO_3$) • Wustite (FeO)

GYP	• Gypsum ($CaSO_4.2H_2O$)

Thermogravimetric analysis (TGA) was used to measure the loss of mass of materials through temperature. Certain mineral phases such as limestone and clay can be quantified by TGA analysis. The device used is the Netzsch STA 409 type with a heating rate of 10 °C/min and the temperature increased from 40 °C to 1000 °C. Table 5 shows the result of the TGA analysis of materials and the associated phenomena as a function of temperature. The result showed the presence of organic matter, clay phases and limestone in the sediment. Indeed, the mass loss observed between 450 and 600 ° C is most likely due to hydroxylation of the clay phases [16, 17]. However, Fernandez et al [18] showed that the hydroxylation of montmorillonite occurs at a higher temperature between 400 °C and 800 °C with slow removal of water up to 800 °C. The decomposition of calcite mainly occurs between 650 °C and 850 °C [19]. The mass loss observed between 850 °C and 1000 °C is most likely due to recrystallization [20].

Table 5

Material mass loss between 105 °C and 1000 °C, as well as associated phenomena

Temperature °C	Attributed phenomenon	Mass loss (wt %)							
		ASL	LIM 1	LIM 2	LIM 3	CLY 1	CLY2	SAN	IRO
105 – 150	Evaporable water	0.48	0.25	0.14	0.23	0.14	0.02	0.07	0.02
150 – 450	Organic matter oxidation	2.22	0.03	0.19	0.06	4.31	2.92	0.45	3.15
450 - 650	Dehydroxylation of clay	1.73	1.14	0.96	0.91	4.74	3.25	1.19	1.69
650 – 850	Decomposition of calcite	5.36	36.47	36.56	36.54	0.80	1.37	0.46	4.30
850 – 1000	Dehydroxylation of montmorillonite, Recrystallization	0.81	0.14	0.15	0.14	0.33	0.38	0.14	2.39
105 - 1000	Total mass loss	10.60	38.03	38.00	37.88	10.33	7.94	2.32	11.55

Finally, the mobility of the metallic trace elements (MTE) and the anionic elements of the sediment were measured after the leaching of the sample using a liquid/solid ratio of 10 and an equilibrium time of 24 hours [21], Inductively Coupled Plasma Optical Emission Spectrometer (ICP-OES 5100 Agilent Technologies) was used for the analysis. The leaching limit values for inert waste (IW) and non-hazardous waste (NHW) specified in Directive 1999/31/EC were used to verify material compliance. In addition, the acceptable values for the content of heavy metals in waste required by all French cement industrial groups in 2001 were lower [14], were used to assess the possibility of recycling the waste. The result of the sediment leaching analysis is shown in Table 6. The sediment is classified as inert class-non-hazardous. The content of heavy metals (As + Ni + Co + Se + Ti + Cr + Pb + Sn + V) < 10000 mg/kg, which meets the requirements of French cement industry groups on waste recovery.

Table 6

Metallic trace elements of ASL sediment

Sample	Concentration (mg/kg)										
ASL	As	Ba	Cd	Cr	Cu	Mo	Ni	Pb	Sb	Se	Zn
	< 0.1	0.14	<0.008	<0.005	0.18	0.10	0.04	<0.03	0.06	0.1	0.14
IW	**0.5**	**20**	**0.04**	**0.5**	**2**	**0.5**	**0.4**	**0.5**	**0.06**	**0.1**	**4**
NHW	**2**	**100**	**1**	**10**	**50**	**10**	**10**	**10**	**0.7**	**0.5**	**50**

The characterization result shows that:

- The main oxides of the sediment are SiO_2, Al_2O_3, Fe_2O_3 et CaO. These are major oxides constituting phases of cement.
- The sediment used in the research is inert and non-hazardous.
- Heavy metal content in the sediment meets the requirements of French cement manufactures for waste recovery.

II.3. Cement synthesis method

II.3.1 Formulation method

Unlike previous research [11, 12, 22], the recovery of waste has occurred at the laboratory scale. The objective of this research is to assess the feasibility of recovering waste in the manufacture of cement on an industrial scale. Therefore, the formulations must meet the following specifics:

- The viscosity of the raw mixture (water/material ratio given) must meet the requirements of the cement manufacturer EQIOM to avoid risks of clogging of the basin and segregation of the paste. Knowing that the higher the water/material ratio, the higher the viscosity of the mixture, the greater the energy consumption.
- The chemical composition of the clinker must meet the requirements of the desired content of the main oxides.

The analysis of the viscosity of the raw material paste mixture was carried out at the EQIOM cement company according to its protocol. The result shows that:

- The viscosity of the mixture decreases with the increase in the content of the incorporated sediment.
- The flocculation of the paste appears from 2% of sediment incorporated into the mixture

Consequently, the maximum possible content of the sediment incorporated in the raw mixture according to the viscosity criterion is 2% wt but should be 7% wt a dry process was used. Also, the total cement produced by the manufacturer which is more than 10 000 tons per day should be taken into account.

For the criterion of the chemical composition of the clinker, from the result of the analysis of the materials chemical composition, the different formulations of the raw meal were set up based on the following modulus usually used in the cement industry: the Lime Saturation Factor (LSF), the Silica Ratio (SR) and the Alumina Ratio (AR) [23]. These are the main parameters to control the quality of the clinker [24]. The calculations of LSF, SR and AR are presented by the equations below (Eq(1) -> Eq(3)):

$$LSF = \frac{100 * \%CaO}{2.8 * \%SiO2 + 1.18 * \%Al2O3 + 065 * \%Fe2O3} \quad (1)$$

$$SR = \frac{\%SiO2}{\%Al2O3+\%Fe2O3} \quad (2)$$

$$AR = \frac{\%Al2O3}{\%Fe2O3} \quad (3)$$

The LSF ensures good stoichiometry between calcium oxide and the other three main oxides. A higher LSF value corresponds to higher calcium silicate content, but the burning will be more difficult and may cause volume instability of the hydrated cement (high content of free lime). In addition, the LSF modulus helps to control the relationship between the quantity of C_3S and C_2S [25]. The LSF value is usually considered between 95 and 97 [26] but technically the range of LSF can vary from 90 to 104 [27]. The SR modulus allows the determination of the relative proportion between the silicate phases and the aluminate phases. A high value of SR will cause difficulty in the clinkerization process due to a lack of fluxing agents. This modulus affects also the properties of clinker including the setting and durability. The SR value is between 2.0 and 3.0 [23] but in the more restrictive and optimized field, it is taken between 2.4 and 2.6 [26]. The AR modulus expresses the ratio between the mineral phases C_3A and C_4AF. A high value of AR will provoke the formation of significant content of C_3A in the clinker and this affects the resistance to sulphates [28]. The appropriate value for AR is between 1.5 and 1.8 [26].

To comply with the criterion of the viscosity of the mixture and the composition of the clinker, in this research, two formulations were established using the following values: LSF = 98, SR = 2.5, AR = 1.65, and maximum content of 2% wt of the sediment. The first is the reference clinker noted OPC TM using only components (LIM 1, LIM 2, LIM 3, CLY 1, CLY 2, SAN and IRO). The second formulation, denoted OPC 2% ASL, consists of the components (LIM 1, LIM 2, LIM 3, CLY 1, CLY 2, SAN, IRO, and ASL) with a substitution rate of the sediment equal to 2% wt. Table 7 shows the composition of the components of two formulations of the clinker.

Table 7

Composition of the components of two clinker formulations

Formula	ASL (wt %)	LIM1 (wt %)	LIM2 (wt %)	LIM3 (wt %)	CLY1 (wt %)	CLY2 (wt %)	SAN (wt %)	IRO (wt %)
OPC TM	0	52.08	17.36	17.36	3.18	4.78	4.31	0.93
OPC 2%ASL	2	51.87	17.29	17.29	2.98	4.47	3.17	0.93

Based on previous studies [11, 22], all the components are mixed with water to better homogenize them. The mixture is then dried at 105 °C and pressed at 5 kN into pellets. Then, the pellets are burned at 200 °C for 20 minutes, then at 1450 °C with a speed of 7 °C/min. After 15 min of burning at the clinkering temperature (1450 °C), the clinker was cooled in the furnace to reach room temperature.

Cement is produced by blending the clinker with gypsum. The addition of gypsum plays a very important role in controlling the setting time of the cement. Indeed, the reaction of C_3A with water is very violent and immediately stiffens the cement paste [29]. This phenomenon is due to the formation of hydrated calcium aluminate in plates, according to Eq (4), which is distributed in the space filled with the mixing water and constitutes the bridges between the cement particles, causing a setting fast.

$$C_3A + 21H \rightarrow C_2AH_8 + C_4AH_{13} \rightarrow C_3AH_6 \quad (4)$$

In addition, the presence of sulphate increases the hydration of C_3S, which requires an improvement in the development of compressive strength [30] and a stability control of the volume of the paste [23]. However, an excess of sulfate can cause swelling by the late reaction with tricalcium aluminate [31] which increases the rate of degradation and deterioration of concrete [32]. In this research, the content of gypsum was added to obtain an SO_3 content of 3.6% wt in the cement. Table 8 shows the composition of the components of the two cements. The components were ground together to reach the Blaine specific surface of 4500 cm^2/g.

Table 8

Composition of the components of two cements

Cement	Clinker (wt. %)	Gypsum (wt. %)
OPC TM	90.71	9.29
OPC 2%ASL	90.64	9.36

II.3.2 Characterization methods of clinker and cement

Several experimental tests were carried out to characterize the properties of the product and to assess the quality of the cooking process in the laboratory.

The specific density of clinkers and cements was measured using the ACCUPYC 1330 Helium Pycnometer according to the standard NF EN 1097-7 [33]. The specific surface of the cement was estimated by measuring the specific surface area Brunauer-Emmett-Teller (BET) [34] and the Blaine specific surface [35]. The particle size distribution of the cement was measured using the BECKMAN COULTER type LS13 320 device. X-Ray Fluorescence (XRF) was used to verify the chemical composition of raw mixes, clinkers and cements. The mineral composition was identified by X-Rays Diffraction (XRD). All the processes are identical with the processes used in the raw material characterization part.

The Rietveld analysis was also performed using TOPAS software to quantify the crystal phases of the clinker.

The content of free lime (CaO_{free}) in the clinker is an important parameter to assess the quality of the clinker and of the firing process in the laboratory. In general, a free lime content of less than 2% is acceptable in the cement industry [36]. In this research, Schlafer-Bukolowki method [37] was used to estimate the free lime content in the clinker. The content of mineral phases(C_3S, C_2S, C_3A, C_4AF) can be estimated using the Bogue formula [14] according to the following equations (Eq (5) -> Eq (8)):

$$C_3S = 4.07 * (CaO_{Total} – CaO_{free\ lime}) - 6.72 * Al_2O_3 – 1.43 * Fe_2O_3 \quad (5)$$

$$C_2S = 8.60 * SiO_2 + 1.08 * Fe_2O_3 + 5.07 * Al_2O_3 - 3.07 * (CaO_{Total} – CaO_{free\ lime}) \quad (6)$$

$$C_3A = 2.65 * Al_2O_3 – 1.69 * Fe_2O_3 \quad (7)$$

$$C_4AF = 3.04 * Fe_2O_3 \quad (8)$$

To study the effect of the substitution of the sediment on the mineral phases of the clinker, an analysis of the chemical compositions of the mineral phases was carried out on the polished section of the clinker using a Hitachi S-4300 SE/N Scanning Electron Microscope operating in backscattered electron mode (20 KeV) and equipped with an energy dispersive X-ray spectrometer (EDS). For each phase, around 100 points were measured in four different zones.

The setting start time was measured using a Vicat device after determining the water demand of the cement which allows it to reach the normal consistency according to NF EN 196-3 [38].

The isothermal calorimetry analysis performed at 20 °C was used to monitor the reactivity of the cement paste. Based on previous research [39], the paste was made with 8 grs of cement and 4 grs of water that had been previously stored at 20 °C (W/C = 0.5). The calorimeter is a homemade type using flowmeters that allowed the calorimeter to equilibrate in less than 5 min. In addition, the reactivity of cement over time can be estimated using the notion of the degree of hydration of the cement, which expresses the fraction of the anhydrous reacting. In the literature, there are several methods for determining the degree of hydration of cement, such as:

- Scanning electron microscopy (SEM-BSE) [40, 41]
- X-ray diffraction (XRD) [42]
- Thermogravimetric analysis (TGA) [43]
- Measurement of the heat of hydration by isothermal calorimetry [41, 44]
- Nuclear magnetic resonance (NMR) [45]
- Compressive strength [9]

In this research, the degree of cement was determined by measuring the amount of water bound in the cement paste (with W/C = 0.5) by thermogravimetric analysis (TGA). To avoid the phenomenon of carbonation, the pastes after demolding were stored in the saturated lime solution until the day of the test (2, 15 and 28 days).

The degree of hydration of the cement was determined according to the following formula in Eq (9):

$$\alpha(t) = \frac{Wn\,(t)}{Wn(\infty)} \quad (9)$$

With:

α(t): Degree of hydration of the sample at time t.

$W_n(t)$: Amount of bound water at time t (in gram of water per 100 g of anhydrous cement).

$W_n(\infty)$: Amount of bound water after a total hydration of the cement paste (in gram of water per 100 g of anhydrous cement).

The value of $W_n(t)$ can be determined experimentally using the following formula in Eq (10):

$$W_n(t) = \frac{\Delta m\ sample\ (105\ ^\circ C - 1000\ ^\circ C)(t)}{m\ sample\ (1000\ ^\circ C)(t)} * 100 \quad (10)$$

In order to determine the $W_n(\infty)$ value, NIST (National Institute of Standards and Technology) provides an approximate theoretical estimation of the amount of bound water produced for the five main mineral phases of cement when hydration is complete [46].

The compressive strength was measured on 4 * 4 * 16 cm^3 mortars according to the standard NF EN 196-1 [47]. The mortars were demolded after 24 hours, then stored in the saturated lime solution until the days of the test (1, 2 and 28 days of curing). The objective is the determination of the cement class according to standard NF EN 197-1 [48].

The porosity and the pore distribution of the mortars were measured using Mercury Intrusion Porosimetry (MIP) technique (Micromertitics Autopore IV type). Based on previous research [49], the sample is first immersed in acetone solution to stop hydration, then dried to a constant mass at 40 °C. Indeed, drying at a higher temperature can cause a modification of the pores in the porous structure.

To study the effect of incorporating the sediment into the raw mixture, scanning electron microscopy was used to observe hydrates formed from the cement paste. To do this, the dried

sample must be coated with carbon on the surface and observed using a scanning electron microscope (SEM).

II.3.3 Modeling of cement hydration using the CEMHYD3D model

CEMHYD3D model

The CEMHYD3D code developed by Dale P.Bentz at NIST has been used successfully in several previous studies [50–52]. It allows the user to numerically generate and hydrate a 3D microstructure of the cement paste from the phase composition, particle size distribution and W/C volume ratio, under controlled hydration conditions [53]. The model does not use a classical chemical standpoint the equilibrium of species in solution and the resolution of the associated systems of equations, but uses a completely original mechanism of the reaction between species using cellular automata [54]. A list of the chemical equations taken into account to carry out the hydration of the cement numerically is detailed by Dale P.Benzt [55]. A 3D microstructure consists of micro cubes of 1 μm^3, called voxels, each representing a phase: solid (C_3S, C_2S, C_3A, C_4AF, Gypsum, etc.), liquid (saturated porosity). The advantage of using the CEMHYD3D code is to allow the user to access all the information on the properties of the material such as the amount of the different phases, the amount of porosity.

The compressive strength in the model is estimated using the Power's empirical relation [55] :

$$\sigma_c(t) = \sigma_0(X(t))^n \quad (11)$$

With:

$\sigma_c(t)$: Mechanical resistance to compression at time t.

σ_0: Mechanical resistance to compression when capillary porosity is zero. It is calibrated on the basis of determination of resistance at 28 days.

n: Value taken between 2.6 and 3.0. In general, a value equal to 2.6 is applied for CEM I.

X(t): Ratio of hydrate gel-space. In the CEMHYD3D model, X(t) is determined as follows (Eq (12):

$$X(t) = \frac{Number\ of\ hydrate\ pixels}{Number\ of\ hydrate\ pixels + Number\ of\ porosity\ pixels} \quad (12)$$

We have:

$$X(t) = \frac{0.68\ \alpha(t)}{0.32\alpha(t) + \frac{W}{C}} \quad (13)$$

With:

α(t): Hydration degree of sample at time t.

W/C: Water/cement ratio

The porosity of the microstructure in the CEMHYD3D model is limited to the capillary porosity. The finer pores are not taken into account because of the size of the voxels composed of 1 μm^3.

Determination of time constant

The time constant (β) is used to convert times/cycles in the CEMHYD3D model. The value should be determined experimentally by the user depending on the type of cement used. The formula showing the relationship between time and the number of cycles is as follows (Eq(14)):

$$t = \frac{\beta}{K} * c^2 \quad (14)$$

With:

t: Time of hydration in hours.

c: Number of hydration cycles performed by the program in the CEMHYD3D.

β: Conversation factor cycles/time in hour/(cycles)^2.
K: Speed coefficient for the cycle.

The value of K is determined by the following formula:

$$K = e^{\frac{E}{8.314}\left(\frac{1}{298.15} - \frac{1}{T°+273.15}\right)} \quad (15)$$

With:
E: Activation energy of the cement in KJ/mol.
T°: Temperature of the system in °C.

To determine the β value, the degree of hydration of the cement paste should be used. The value of the coefficient K is calculated according to Eq(15) with the activation energy of the cement E = 40 (KJ/mol) and gives a result of K = 0.9997.

Knowing the experimental value of the degree of hydration of the cement paste at a given time, the user determines the number of hydration cycles for which the program reaches the same value as the experimental α(t) [54]. In this study, the bound water measurement method was used to determine the degree of hydration of the cement paste.

III. Results and discussions

III.1. Characterization of clinkers

The chemical composition and the values (LSF, SR, AR) of two formulations analyzed by XRF are presented in Table 9. Good consistency between the experimental values and the theoretical values was observed.

Table 9

The chemical composition and values (LSF, SR and AR) of two formulations analyzed by XRF

Oxide (wt. %)	OPC TM		OPC 2% ASL	
	Theory	Exp	Theory	Exp
SiO_2	13.72	13.55	13.71	13.4
Al_2O_3	3.42	3.5	3.41	3.5
Fe_2O_3	2.07	2.1	2.07	2.1
CaO	42.93	41.9	42.87	41.9
MgO	0.48	0.5	0.48	0.5
Na_2O	0.00	ND	0.02	ND
K_2O	0.52	0.6	0.54	0.6
SO_3	0.00	ND	0.00	ND
TiO_2	0.00	0.2	0.00	0.2
P_2O_5	0.00	0.1	0.06	0.1
Mn_2O_3	0.00	ND	0.00	ND
ZnO	0.01	ND	0.00	ND

LOI	36.03	36.45	36.05	37.1
Total	99.24	99.65	99.24	99.4
LSF	98	96.47	98	97.41
SR	2.5	2.42	2.5	2.40
AR	1.65	1.67	1.65	1.67

Table 10 shows the free lime content and the content of the mineral phases of two clinkers, OPC TM and OPC 2% ASL, determined by the Schlafer-Bukolowki method-Bogue formula and by the Rietveld method. The results from the two methods are very similar. The free lime content in the two clinkers is below the limit value of 2%, which means that the two clinkers have a good dosage and the clinkerization process in the laboratory does not cause the C_3S phase to decompose into C_2S and CaO.

Table 10

Content of mineral phases in the two clinkers OPC TM and OPC 2%ASL

Method	Clinker	C_3S (wt. %)	C_2S (wt. %)	C_3A (wt. %)	C_4AF (wt. %)	CaO free (wt. %)
Schlafer-Bukolowki method – Bogue formula	OPC TM	61.63	15.76	9.14	9.18	1.60
	OPC 2% ASL	63.98	12.23	10.06	9.25	1.65
Rietveld method	OPC TM	64.87	12.47	8.83	9.04	1.19
	OPC 2% ASL	66.23	12.90	9.61	8.64	1.48

The result of the analysis of the composition of the mineral phases of the clinkers by the SEM-EDS analysis has been presented in the following figures. Fig.2 and Fig.3 illustrate the composition and atomic ratio of two main components in the silicate phases (C_3S and C_2S) of OPC TM and OPC 2% ASL clinkers.

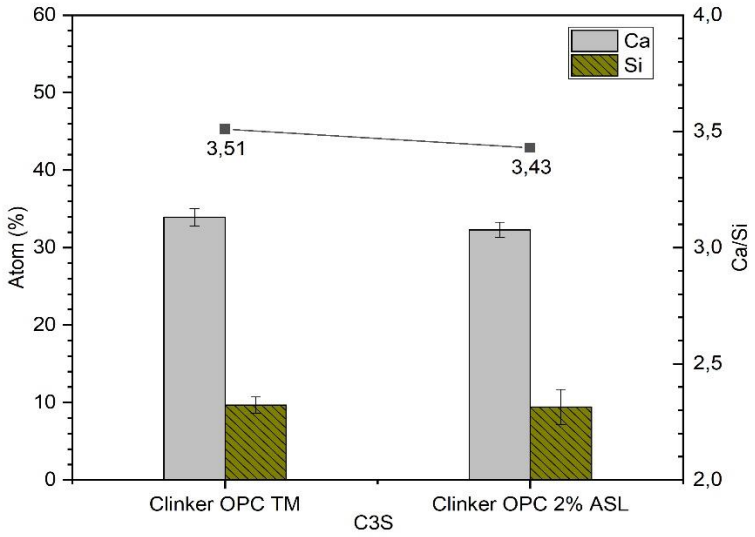

Fig. 2 Composition and atomic ratio of the C_3S phase's two main components

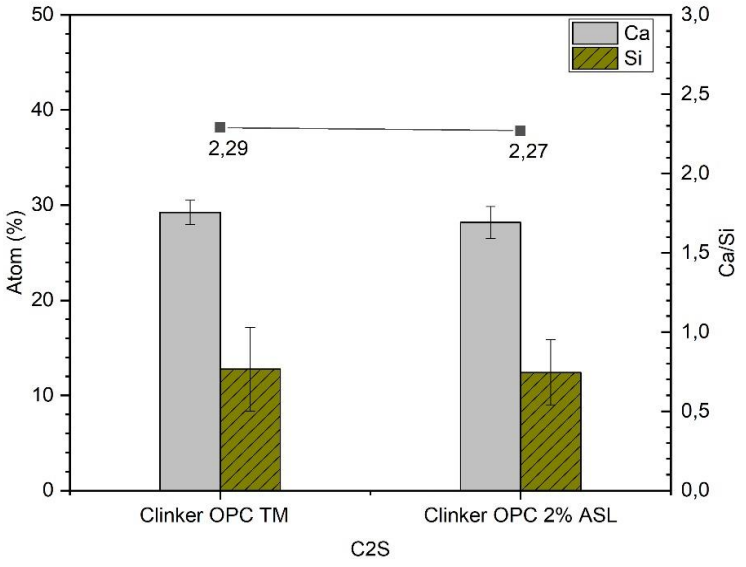

Fig. 3 Composition and atomic ratio of the C_2S phase's two main components

The result shows that:

- The main elements of the silicate phases are Ca and Si. The experimental atomic ratio (Ca/Si) in these phases is higher than the theoretical ratio (Ca/Si = 3 in C_3S and Ca/Si = 2 in C_2S).
- The atomic ratio (Ca/Si) of the C_3S phase in the OPC 2% ASL clinker is slightly lower than in the OPC TM clinker, but this difference is small.

The major elements and the atomic ratio of these elements in the aluminate phases (C_3A and C_4AF) are shown in Fig.4 and Fig.5.

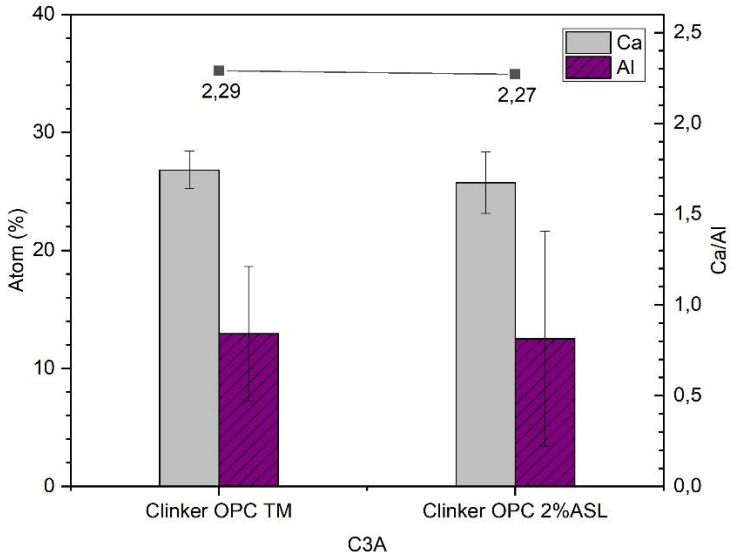

Fig. 4 The major elements and atomic ratio (Ca/Al) of the C_3A phase

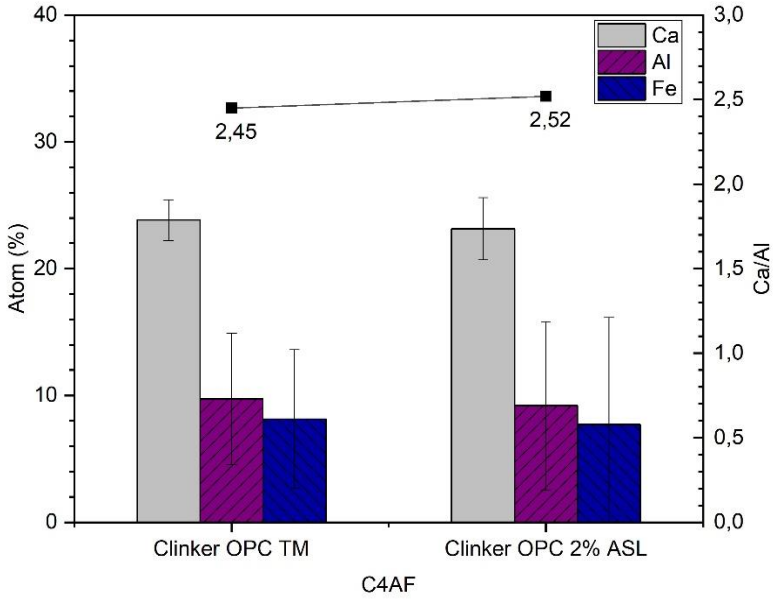

Fig. 5 The major elements and the atomic ratio (Ca/Al) of the C_4AF phase

The result shows that:

- The major elements in the aluminate phases are Ca, Al and Fe. The experimental atomic ratio (Ca/Al and Ca/Fe) in these phases is higher than the theoretical atomic ratio (Ca/Al = 1.5 in phase C_3A and Ca/Al = 2, Ca/Fe = 2 in the C_4AF phase).
- Substitution of the sediment also does not cause the modification of the atomic ratio of the main elements in the aluminate phases.

The distribution and the morphology of the mineral phases of the OPC TM and OPC 2% ASL clinkers have been illustrated in Fig.6. The result shows that:

- The four typical mineral phases of clinker have been identified in the two clinkers OPC TM and OPC 2% ASL. The phase distribution is similar in the two clinkers.
- Substitution of the sediment does not change the morphology of the silicate phases (C_3S and C_2S).

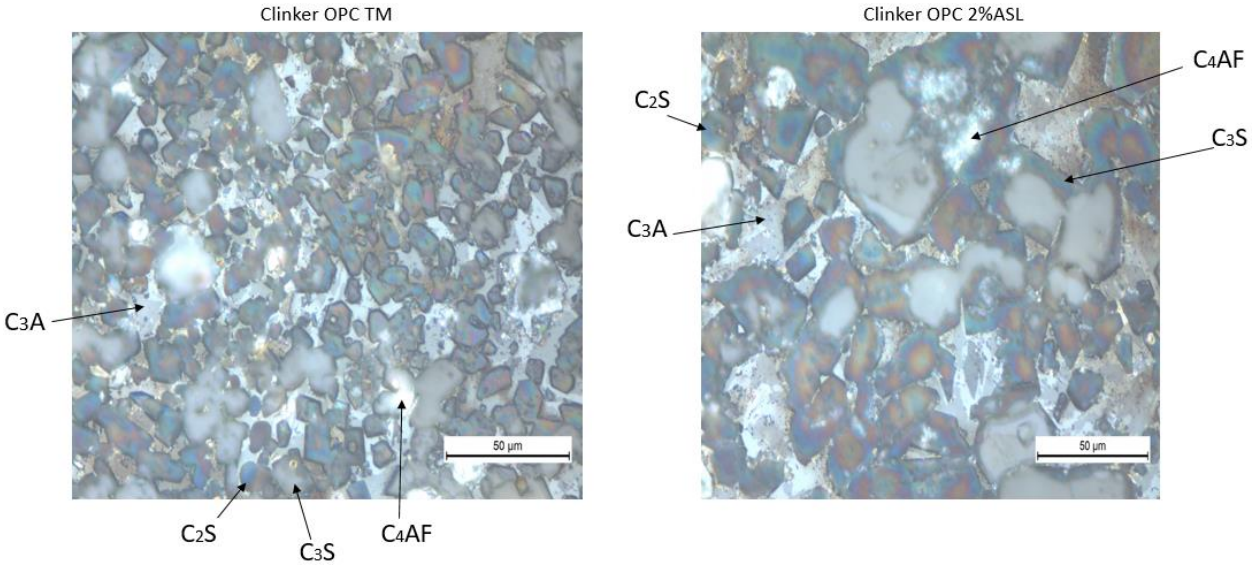

Fig. 6 Distribution of mineral phases typical of OPC TM and OPC 2%ASL clinkers

III.2. Characterization of cement

The characteristics of OPC TM and OPC 2%ASL cements have been presented in Table 11.

Table 11

Physical characteristics of OPC TM and OPC 2% ASL cements

Property	OPC TM	OPC 2% ASL
Density (g/cm^3)	3.1	3.1
Blaine specific surface (cm^2/g)	4450	4460
BET specific surface (m^2/g)	1.46	1.47
Water demand (%)	30.03	30.05
Setting time (minutes)	180	180

OPC TM and OPC 2% ASL cements have very similar Blaine specific surface and BET specific surface. This is important when comparing the reactivity of the two types of cements because the fineness of the cement is one of the important parameters influencing the reactivity of the cement.

III.2.1 Heat of hydration

The reactivity of the cement followed by the isothermal calorimetry was presented in Fig.7. OPC 2% ASL cement exhibits hydration behavior similar to that of the OPC TM cement because the shape of the heat of hydration curves is identical. However, the heat flux released during the hydration of the OPC 2% ASL cement occurred somewhat earlier than the OPC TM cement. This may be due to the fineness of OPC cement 2% ASL higher than that of OPC TM cement.

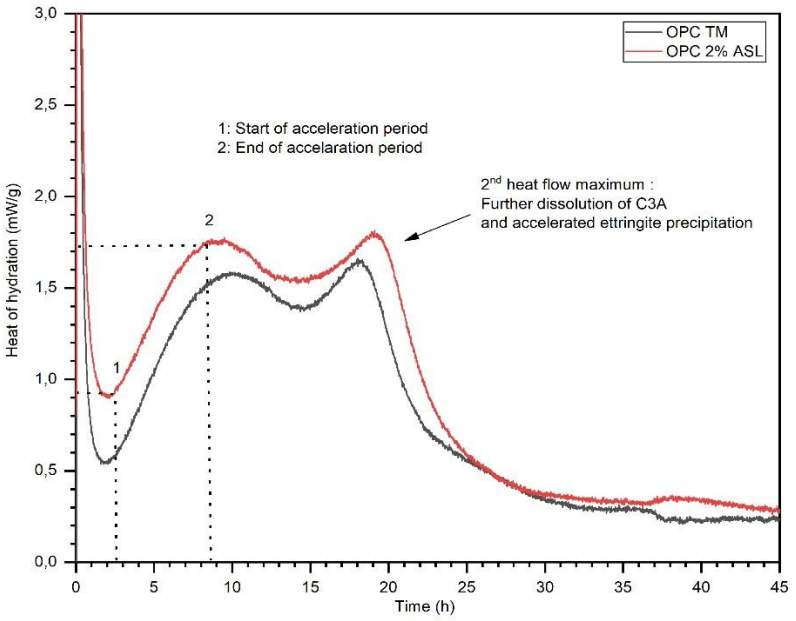

Fig. 7 Heat of hydration of cements pastes (W/C = 0.5) generated during the hydration

III.2.2 Degree of hydration of cement

The degree of hydration of the cements was measured using the bound water quantification method using thermogravimetric analysis (TGA). Fig.8 shows the TGA curve of the OPC TM cement paste after 2 days of hydration.

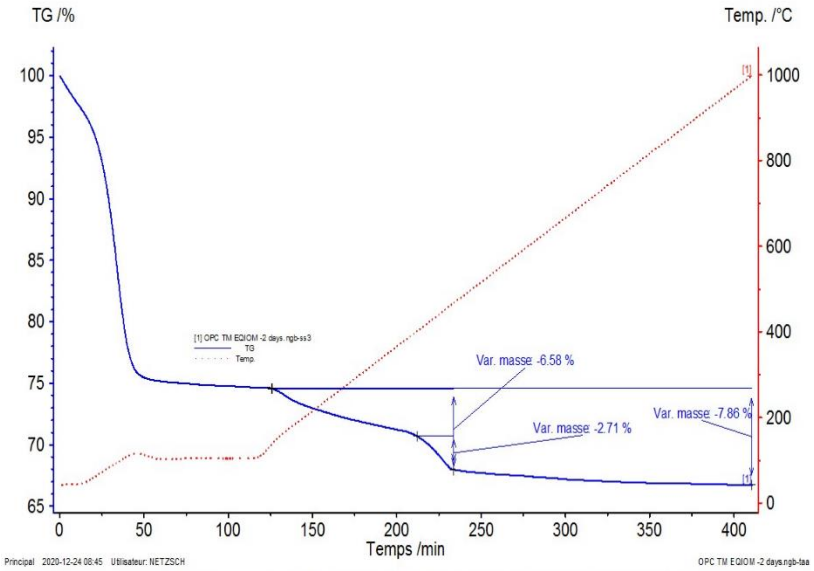

Fig. 8 TGA curve of the OPC TM cement paste after 2 days of hydration

The bound water content W_n(2days) is calculated according to Eq(10):

$$W_n(2\ days) = \frac{\Delta m\ sample\ (105\ °C - 1000\ °C)(2\ days)}{m\ sample\ (1000°C)(2\ days)} * 100 = \frac{7.86}{66.73} * 100 = 11.78\ (g)$$

Table 12 shows the $W_{n(\infty)}$ value during complete hydration of OPC TM and OPC 2% ASL cements.

Table 12

Determination of $W_{n(\infty)}$ from the mineral composition of the cement and the theoretical values of bound water produced for the major phases of the cement at complete hydration

Phase	Coefficient proposed by NIST	Mineral composition of cements (% Mass)		Mass of bound water to complete hydration (g/100 g of anhydrous cement	
		OPC TM	OPC 2%ASL	OPC TM	OPC 2%ASL
C_3S	0.24	57.45	59.68	13.79	14.32
C_2S	0.21	14.69	11.41	3.08	2.39
C_3A	0.4	8.52	9.38	3.41	3.75
C_4AF	0.37	8.56	8.63	3.16	3.19
Lime	0.33	1.49	1.54	0.49	0.51
Gypsum	-	9.29	9.36	-	-
Total (%)		100	100	23.93	24.17

The degree of hydration of the OPC TM cement after 2 days of hydration is calculated according to Eq (9):

$$\alpha(2\ \text{days}) = \frac{Wn\ (2\ days)}{Wn(\infty)} = \frac{11.78}{23.93} = 0.492$$

Table 13 shows the degree of hydration of OPC TM and OPC 2% ASL cements measured after 2, 15 and 28 days of hydration. The result shows that OPC 2% ASL cement is more reactive than OPC TM cement. This result is consistent with the result of the heat of hydration test by isothermal calorimetry.

Table 13

Degree of hydration of OPC TM and OPC 2%ASL cements

Time (days)	OPC TM	OPC 2% ASL
2 Days	0.492	0.52
15 Days	0.735	0.736
28 Days	0 .808	0.815

III.2.3 X-ray diffraction of cement paste

The mineral phases and hydrates formed over the hydration time of the two OPC TM and OPC 2% ASL cements identified by XRD analysis were shown in Fig.9 and Fig.10 respectively. The result shows that:

- All the typical mineral phases of cement such as C_3S, C_2S, C_3A, C_4AF and gypsum have been identified in both OPC TM and OPC 2% ASL cements.
- The hydrates formed are the common hydrates identified in Portland cement, such as portlandite ($Ca(OH)_2$) and Ettringite. However, the presence of C-S-H was not detected by XRD analysis due to its amorphous.

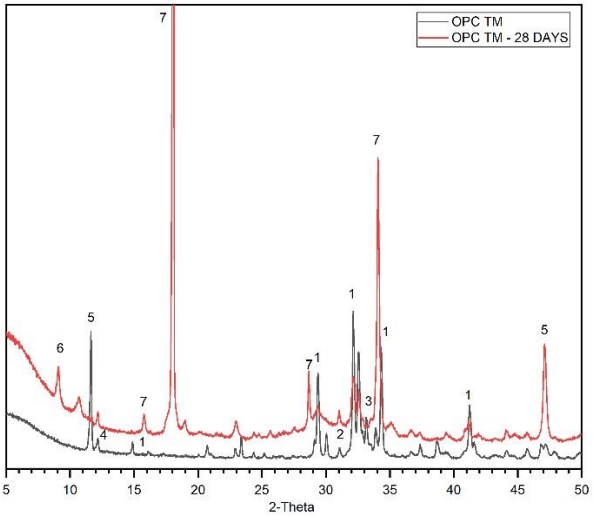

Fig. 9 Mineral composition and hydrates formed during the hydration of OPC TM cement (1: C_3S, 2: C_2S, 3:C_3A, 4: C_4AF, 5: Gypsum, 6: Ettringite, 7: Portlandite)

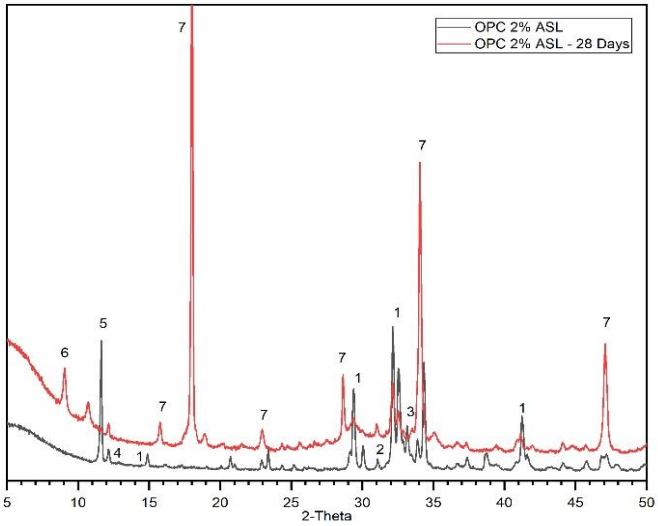

Fig. 10 Mineral composition and hydrates formed during the hydration of OPC 2% ASL cement (1: C_3S, 2: C_2S, 3:C_3A, 4: C_4AF, 5: Gypsum, 6: Ettringite, 7: Portlandite)

The presence of the mineral phases of the OPC TM and OPC 2% ASL cements pastes observed using electron microscopy on the surface of the hydrated pastes is presented in Fig.11. The morphology and distribution of the hydrates formed in the OPC TM and OPC 2% ASL cements pastes are identical.

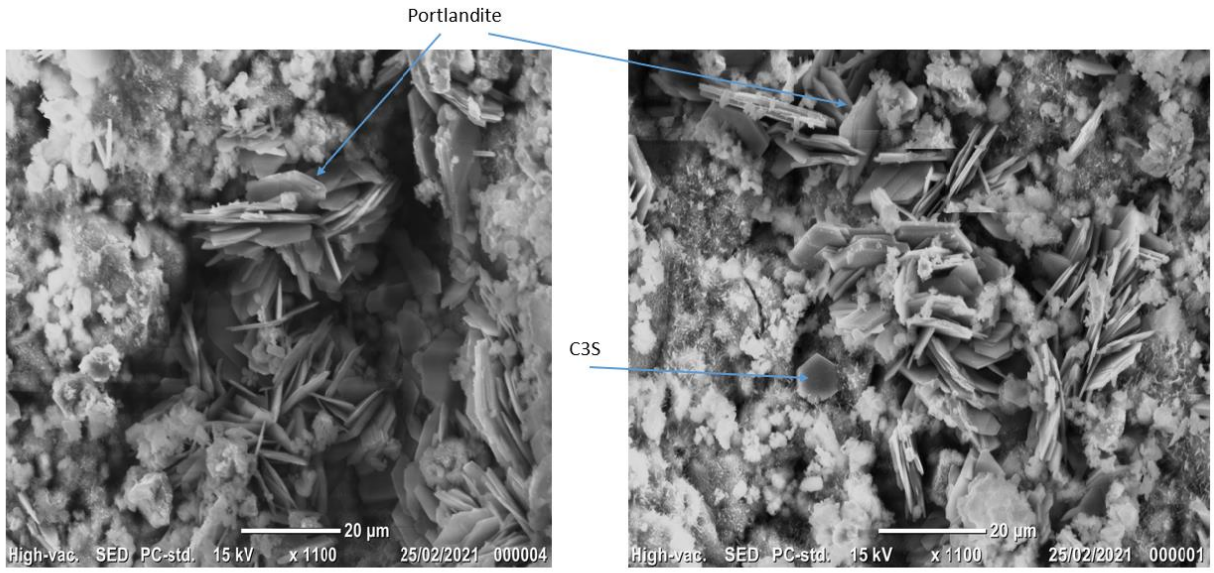

Fig. 11 Observation of hydrates by electron microscopy on the surface of hydrated cements pastes

III.2.4 Compressive strength of mortar

The compressive strength of the OPC TM and OPC 2% ASL cements measured on the mortar sample was presented in Table 14. The compressive strength of the two cements was similar at all times of the test. According to standard NF EN 197-1, the two cements are classified CEM I 52.5 grade.

Table 14

Compressive strength of the OPC TM and OPC 2%ASL cements

Time (Days)	OPC TM (Mpa)	OPC 2%ASL (Mpa)
1 Day	19.20	20.86
2 Days	32.24	33.99
28 Days	55.08	56.57

The total porosity of OPC TM and OPC 2% ASL mortars measured after 1 and 28 days of hydration is shown in Table 15. The result shows that the two cements have similar porosity at all times of the test. A decrease in porosity over time of hydration has been observed. This is due to the formation of hydrates which fill voids and reduce porosity.

Table 15

Total porosity of the OPC TM and OPC 2%ASL mortars measured by MIP

Time (Days)	OPC TM (%)	OPC 2% ASL (%)
1 Day	16.049	16.78
28 Days	12.763	12.88

The pore size distribution of OPC TM and OPC 2% ASL mortars after 1 and 28 days of hydration was shown in Fig.12 and Fig.13 respectively.
The result shows that:

- The pore size distribution of OPC TM and OPC 2% ASL mortars is similar at all times of the test.
- The pore size decreases over time of hydration on the OPC TM and OPC 2% ASL mortars.

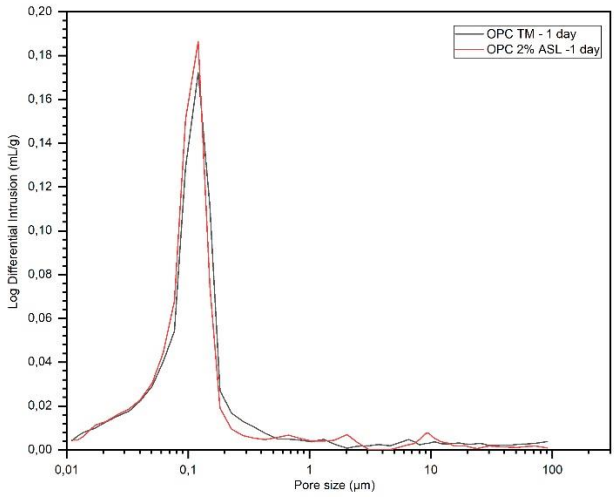

Fig. 12 Pore size distribution of OPC TM and OPC 2%ASL mortars after 1 day of hydration measured by MIP

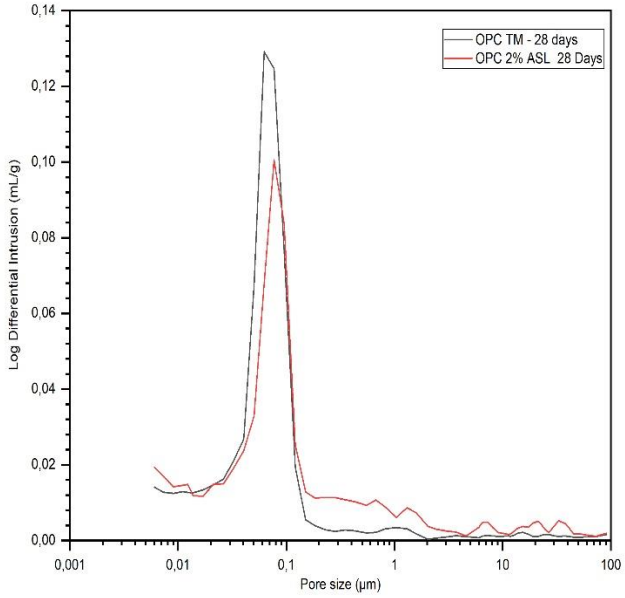

Fig. 13 Pore size distribution of OPC TM and OPC 2%ASL mortars after 28 days of hydration measured by MIP

III.3. Cement hydration modeling

In this part, we present the results of hydration modeling of OPC TM and OPC 2% ASL cements using the CEMHYD3D model. The characteristics of the cement were used as the input data for the model.

III.3.1 Particle size distribution of cement

The particle size distribution of the cement is one of the input data of the model, and it plays an important role and can directly influence the precision of the model result. Table 16 and Table 17 present the experimental and numerical results of the particle size distribution of OPC TM and OPC 2% ASL cements.

Table 16

Experimental and numerical results of the particle size distribution of OPC TM cement

Diameter of particles (μm)	Mass fraction (%) (Exp)	Mass fraction (%) (CEMHYD3D)
1	10.480	10.660
3	2.450	2.492
5	5.360	5.447
7	7.270	7.386
9	8.020	8.124
11	8.070	8.282
13	7.640	7.874
15	7.000	7.299
17	6.230	6.502
19	5.460	5.647
21	4.730	5.038
23	4.140	4.893
25	3.710	4.186
29	6.500	6.568
33	7.250	9.604
37	3.010	0.000
49	2.65	0.000
Total	99,97	100

Table 17

Experimental and numerical results of the particle size distribution of OPC 2%ASL cement

Diameter of particles (μm)	Mass fraction (%) (Exp)	Mass fraction (%) (CEMHYD3D)
1	10.49	10.262
3	2.29	2.243
5	5.46	5.339
7	7.40	7.243
9	8.15	8,018
11	8.17	8,086
13	7.76	7,564
15	7.14	6,837
17	6.37	6,497
19	5.64	5,642
21	5.01	5,034
23	4.55	4,888
25	4.18	4,182
29	7.29	6,562
33	7.01	4,798
37	2.11	6,806
49	0.97	0,000
Total	99.99	100

The result shows that:

- Good consistency between the experimental and numerical results for the two cements, OPC TM and OPC 2% ASL.
- A difference between the experimental and numerical results at the coarser fraction (between 33 μm and 49 μm) for the two cements. However, this difference is small.

III.3.2 Mineral composition of cement in the CEMHYD3D model

The composition of the mineral phases of cement is also one of the input data sets for the CEMHYD3D model. The volume fraction of the mineral phases was used in the model to construct a numerical cement that has a composition similar to that of real cement. The volume fraction of the phases was calculated using the density values of the mineral phases proposed by NIST [56]. Table 18 shows the experimental and numerical volume fraction of the mineral phases of OPC

TM and OPC 2% ASL. Good consistency between the experimental result and the result of the model of the two cements was observed. In addition, the W/C ratio modeled in the CEMHYD3D model is approximately equal to the experimental ratio.

From the results of numerical modeling of the particle size and composition of the mineral phases, we can conclude that the CEMHYD3D model approximately modeled the OPC TM and OPC 2% ASL cements used in the experimental tests.

Table 18

Experimental and numerical volume fraction of the mineral phases of OPC TM and OPC 2% ASL cements

Phases	OPC TM			OPC 2%ASL		
	Exp (%)	CEMHYD3D		Exp (%)	CEMHYD3D	
		Pixels	% Volume		Pixels	% Volume
C_3S	0.5708	223945	0.5704	0.5924	235642	0.5943
C_2S	0.1428	56692	0.1444	0.1108	43963	0.1109
C_3A	0.0897	35493	0.0904	0.0986	38991	0.0983
C_4AF	0.0731	28712	0.0731	0.0737	29362	0.0740
Gypsum	0.1234	47776	0.1217	0.1244	48572	0.1225
Total	1.00	392618	1.00	1.00	396530	1.00
W/C	0.5	0.499		0.5	0.491	

III.3.3 Determination of the constant of time β in the CEMHYD3D model

In order to determine the β value in the CEMHYD3D model, the values of the degree of hydration of OPC TM and OPC 2%ASL cement pastes after 2 days of hydration were used as the calibration values. In fact, we run a simulation of 1000 cycles with any β value, then we look for the value of the number of cycles that allows reaching a degree of hydration corresponding to the experimental value of the degree of hydration at 2 days.

The β value is determined according to Eq (14) and Eq (15) with the cycle values found above. In our case, the β values are 0.0001062 for OPC TM and 0.00008742 for OPC 2%ASL.

III.4. Results of the modeling of cement hydration in the CEMHYD3D model

The hydration of the two cements OPC TM and OPC 2%ASL was numerically modeled in the CEMHYD3D model at a constant temperature of 20 °C and in the saturated conditions, which are similar to the conditions of the experimental hydration. The modeling results are presented in the following figures and compared with the experimental results.

III.4.1 Degree of hydration of cement

The degree of hydration of OPC MT and OPC 2% ASL pastes (W/C = 0.5) estimated by the CEMHYD3D model is shown in Fig.14 and Fig.15 respectively. By comparing the experimental result and the numerical result, good consistency was observed. The CEMHYD3D model seems to present the higher hydration values at the experimental values. This could be explained by the numerical cements is thinner than the actual cements, therefore the reactivity is higher. However, this difference is very small and negligible.

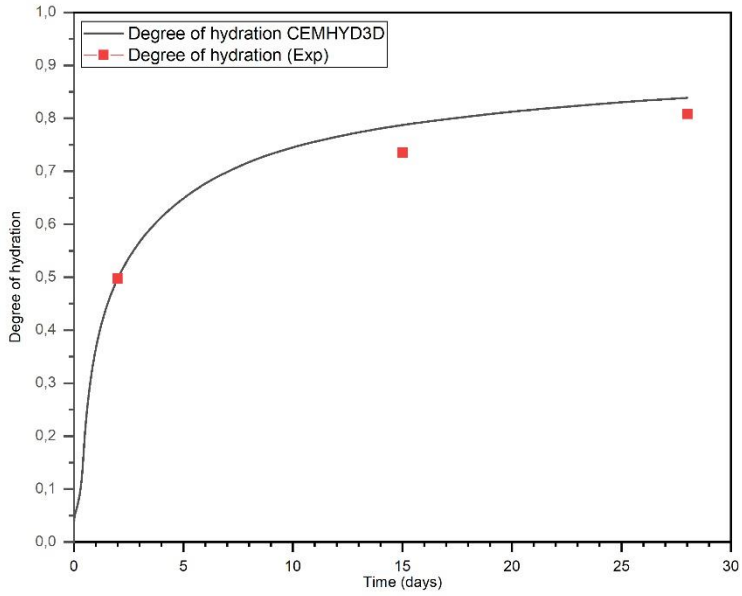

Fig. 14 Degree of hydration of the OPC TM paste over time of hydration

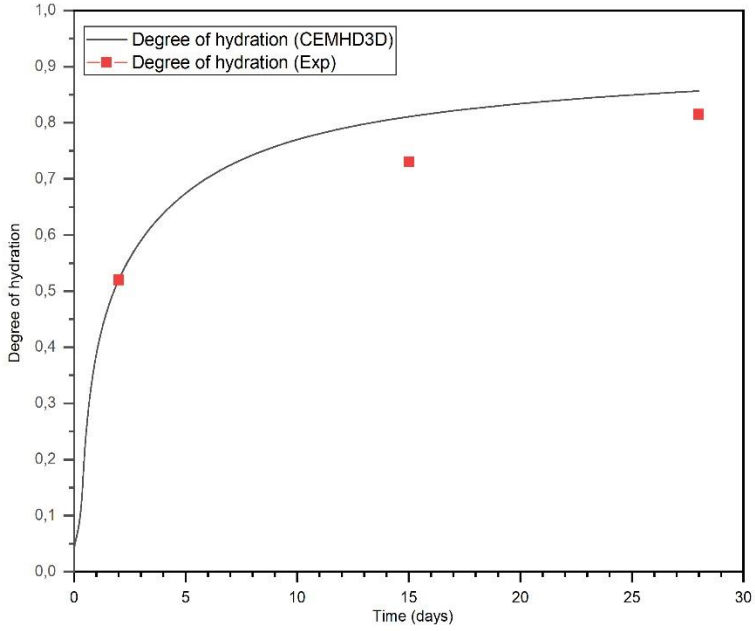

Fig. 15 Degree of hydration of the OPC 2%ASL paste over time of hydration

The hydration of OPC TM and OPC 2% ASL cement pastes modeled by the CEMHYD3D model is presented in Fig.16. In the initial state (t = 0), all the phases of the cements are present and the fraction of the phases is following the volume fraction presented in Table 18. After 28 days of hydrations, the decrease in the fraction of anhydrous and the formation of hydrates (CSH, Portlandite) around the anhydrous were observed. This modeling is similar to the real

phenomenon of hydration of cement paste. A decrease in the porosity of the cement pastes was also observed on the numerically hydrated paste.

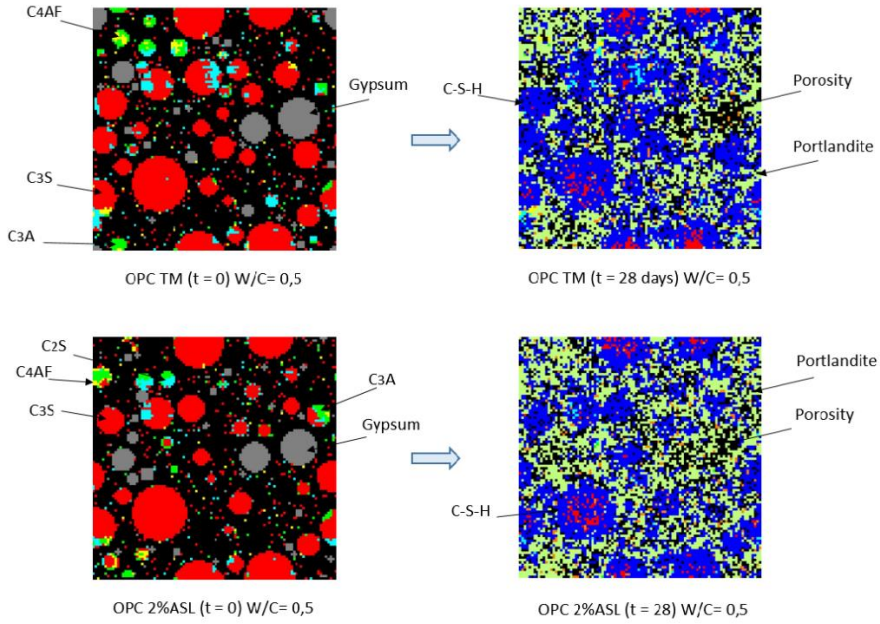

Fig. 16 Hydration of OPC TM and OPC 2%ASL cement pastes modeled by the CEMHYD3D model

III.4.2 Mass ratio of hydrates

Given the $Ca(OH)_2$ is a data relatively to be determined thanks to the TGA analysis, we chose to compare the numerical and experimental quantity of this hydrate to evaluate the relevance of the CEMHYD3D model in our study. CEMHYD3D model gives the volume of portlandite over time of hydration, a portlandite's density value of 2.24 (g/cm^3) is used to convert from volume fraction to mass fraction. Fig.17 shows the CH/Cement initial mass ratio of two types of cement over the time of hydration.

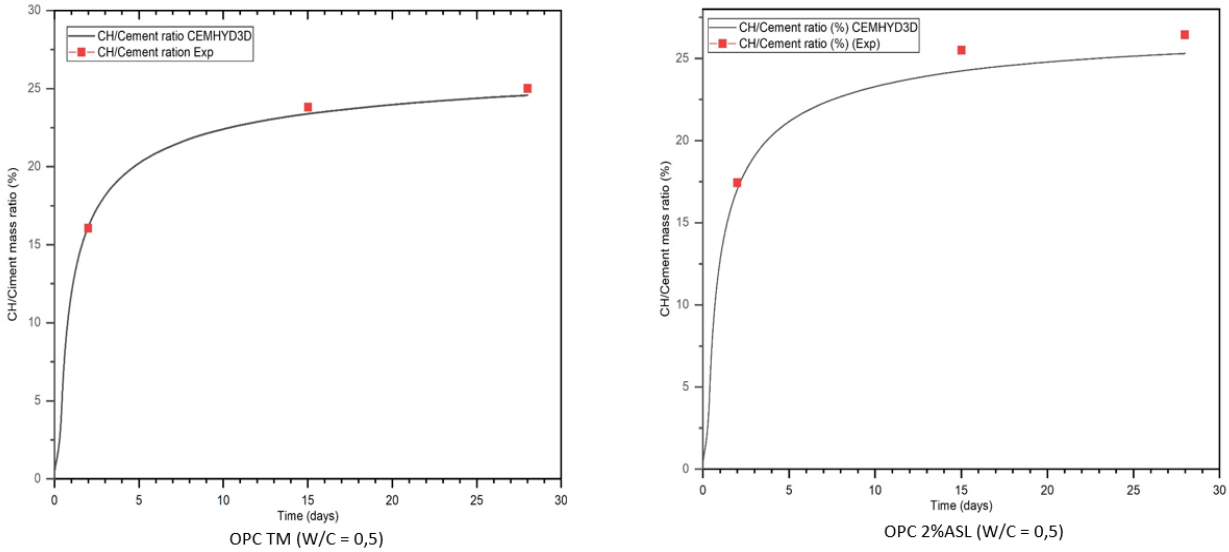

Fig. 17 $Ca(OH)_2$/cement initial mass ratio of OPC TM and OPC 2%ASL cement pastes over time of hydration

The CEMHYD3D model presents a numerical result of the $Ca(OH)_2$/cement initial mass ratio similar to the experimental result. OPC 2% ASL cement has a higher ratio than OPC TM cement at all times of the test. This can be explained by the higher content of C_3S in the OPC 2% ASL cement, which allows more portlandite to be formed.

III.4.3 Porosity of mortars

The CEMHYD3D model makes it possible to estimate the porosity of hydrated cement by considering the porosity equal to the fraction of water remaining in the sample. It does not count the intrinsic porosity of the C-S-H phase.
Table 19 shows the components and their volumes in the formulations of the mortars used in the compressive strength test.

Table 19

Components and their volumes in the formulations of the mortars used in the compressive strength test

Sample	Mass (g)			Volume (cm^3)				% Volume		
	Cement	Sand	Water	Cement	Sand	Water	Total	Cement	Sand	Water
OPC TM Mortar	450	1350	225	145.16	509.43	225	879.6	16.5	57.92	25.58
OPC 2%ASL Mortar	450	1350	225	145.16	509.43	225	879.6	16.5	57.92	25.58

We assume the initial porosity of the mortar (t = 0) is equal to the initial volume fraction of water (25.58%). The evolution of the porosity of OPC TM and OPC 2% ASL mortars over time of hydration followed by the experimental test (MIP) and numerical modeling is illustrated in Fig.18 and Fig.19 respectively.

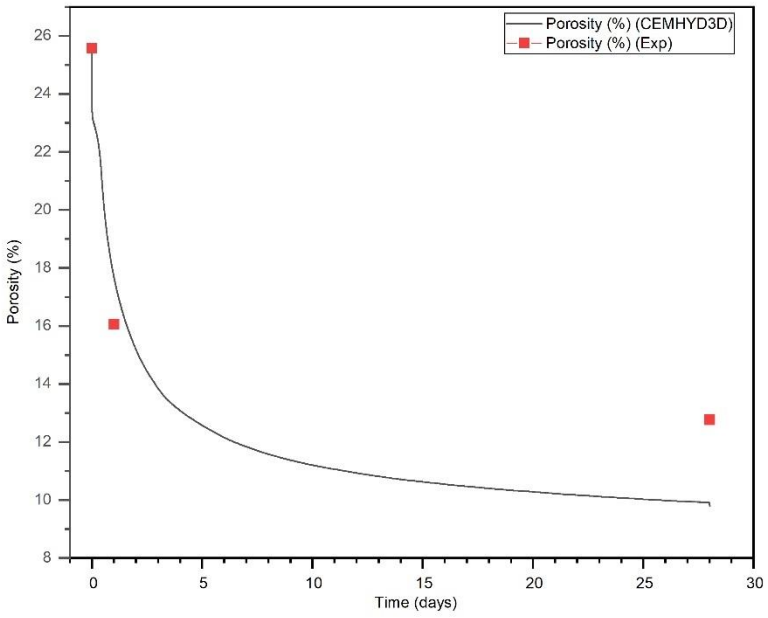

Fig. 18 Evolution of the porosity of the OPC TM mortar over time of hydration followed by the experimental test (MIP) and numerical modeling

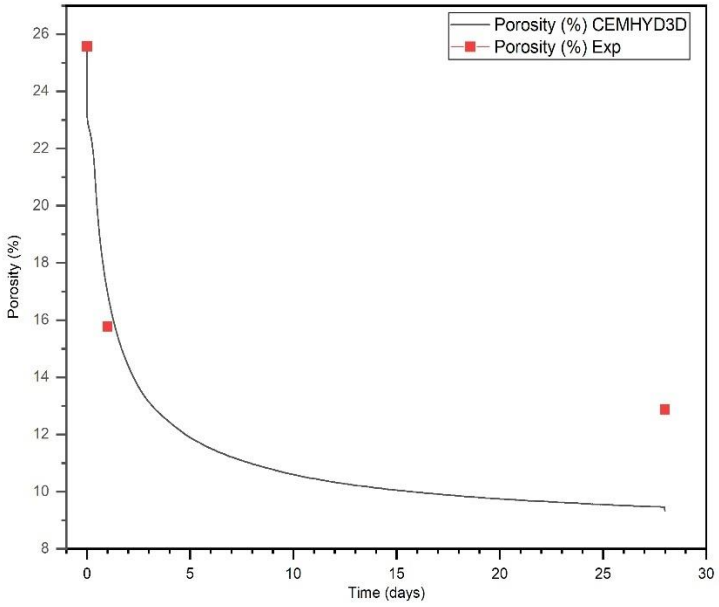

Fig. 19 Evolution of the porosity of the OPC 2%ASL mortar over time of hydration followed by the experimental (MIP) test and numerical modeling

The result shows that:

- The initial porosity (t = 0) measured by experimental and numerical analysis is identical. This is because the CEMHYD3D model perfectly modeled the volume fraction of the components.
- At 1 day of hydration, the experimental and numerical results are identical for the two mortars, OPC TM and OPC 2% ASL. At 28 days, the experimental test exhibits a higher porosity than the CEMHYD3D model. The difference between the experimental and numerical results can be explained by the size of the pixels used in the CEMHYD3D model being equal to 1 µm. The model counts the pores at around 1 µm. In fact, the pores in the cement matrix can be smaller than 1 µm (Fig.12 and Fig.13). However, the trend in the evolution of porosity presented by experimental testing and numerical modeling is similar.

III.4.4 Compressive strength

The CEMHYD3D model estimates the compressive strength using the Power's approach according to Eq(11), Eq(12) and Eq(13). The experimental and numerical results of the compressive strength of OPC TM and OPC 2% ASL mortars are presented in Fig.20. The CEMHYD3D model seems to present the compressive strength a little more than the experimental compressive strength. However, the difference is relatively small, and the shape of the resistance curve is relatively similar.

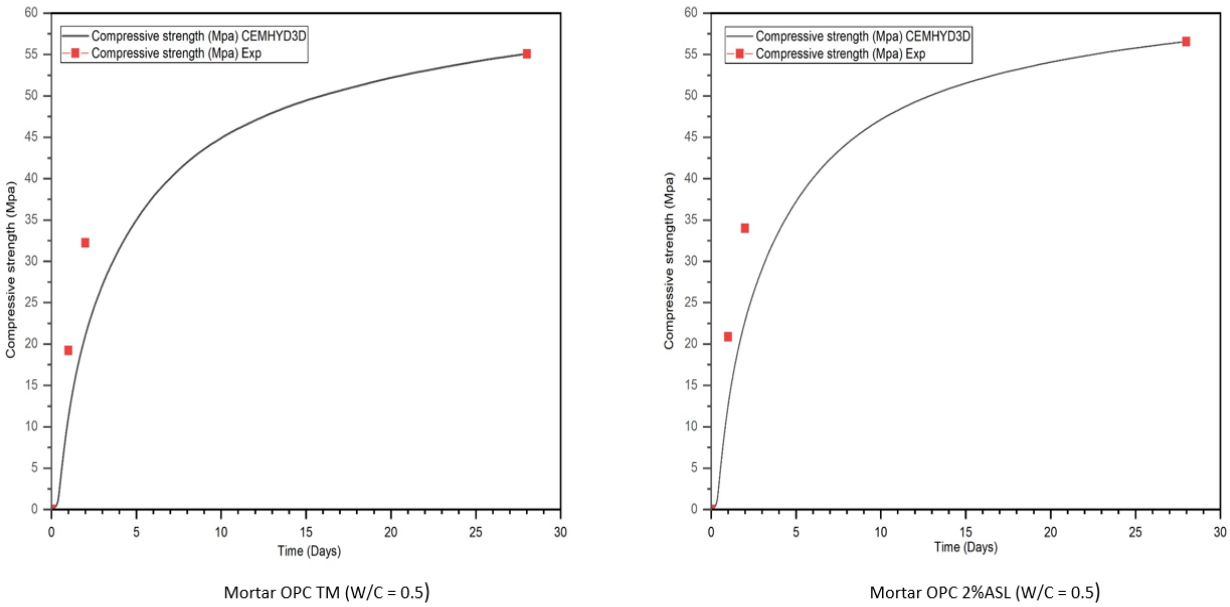

Fig. 20 Compressive strength of OPC TM and OPC 2%ASL mortars measured by experimental test and numerical modeling

IV. Conclusion

The objective of this research is to assess the feasibility of recovering sediment from the manufacture of cement in order to apply it to an industrial project. The main results are obtained:

- The sediment contains the four main oxides (CaO, SiO_2, Al_2O_3 and Fe_2O_3) which are needed to make Portland cement.
- A maximum content of 2%. wt of the sediment can be recycled to ensure the viscosity of the mix.
- The two cements, OPC TM and OPC 2% ASL, have been successfully synthesized in the laboratory. The free lime content in the two clinkers is below the threshold (2% wt).
- The four main mineral phases (C_3S, C_2S, C_3A and C_4AF) have been identified and quantified. The values of the modulus (LSF, SR, AR) are similar to the theoretical values used for the formulation.
- Substitution of the sediment does not modify the chemical compositions in the mineral phases of the clinker. This was demonstrated in the SEM-EDS analysis.
- The sediment-based cement exhibits similar hydration behavior to the reference cement (OPC TM).
- The development of the compressive strength between the two cements is very similar. They are classified CEM I 52.5 grade.
- The CEMHYD3D model has been used successfully to model the hydration of synthesized cements. The results of numerical modeling are consistent with the experimental results.
- The CEMHYD3D model also makes it possible to quickly assess the hydration behavior of cement and to visually follow the evolution of anhydrous hydrates formed over time of hydration. This can make it possible to reduce the number of experimental tests.
- The result of the numerical modeling can be used to study the leaching behavior by coupling with other computer models.

Author statement

Duc Chinh CHU: Conceptualization, Methodology, Investigation, Visualization, Writing-original draft

Joelle KLEIB: Methodology, Conceptualization, Supervision, Validation, Writing-review & Editing

Mouhamadou AMAR: Methodology, Conceptualization, Supervision, Validation, Writing-review & Editing
Mahfoud BENZERZOUR: Methodology, Conceptualization, Supervision, Validation, Writing-review & Editing, Resources
Jaouad NADAH: Methodology, Conceptualization, Supervision, Validation.
Nor-Edine ABRIAK: Methodology, Conceptualization, Supervision, Validation, Writing-review & Editing, Resources

Funding
No applicable

Declarations of Competing Interest

The authors declare that they have no known competing financial interests or personal relationships that could have appeared to influence the work reported in this paper.

Availability of data and material:

We confirm that all results are available in the database. If necessary, please contact us at the address: duc.chinh.chu@imt-nord-europe.fr

Code availability: CEMHYD3D: A Three-Dimensional Cement Hydration and Microstructure Development Modelling Package. Version 2.0 | NIST

Acknowlegments

The authors wish to acknowledge the SEDICIM project and the FEDER funds.

Bibliography

1. https://www.actu-environnement.com/ae/news/Bilan-carbone-ciment-filiere-changer-33280.php4#:~:text=La%20production%20de%20ciment%20est,gaz%20%C3%A0%20effet%20de%20serre.&text=%22Pour%20une%20tonne%20de%20ciment, des%20liants%20hydrauliques%20(ATILH).: Bilan carbone du ciment : comment la filière veut changer la donne
2. Richaud Moreau: Ciment et Béton. (2005)
3. Raoul, P.: L'industrie cimentière française et la réduction des émissions de CO2.
4. Ministry of Ecology, Energy, Sustainable Development and Territorial Planning, Circulaire du 04/07/08 relative à la procédure concernant la gestion des sédiments lors de travaux ou d'opérations impliquant des dragages ou vurages maritimes et fluviaux, Off.
5. Directive 2008/98/EC of the European Parliament and of the Council of 19 November 2008 on waste and repealing certain Directives, O.J.L 312-3, 2008.
6. Dubois, V.: Etude du comportement physico-mécanique et caractérisation environnementale des sédiments marins – Valorisation en technique routière - Thèse de doctorat, (2006)
7. Scordia, P.Y.: Caractérisation et valorisation des sédiments fluviaux pollués et traités dans les matériaux routiers - Thèse de doctorat, Ecole centrale de Lille. (2008)
8. M.Dia: Traitement et valorisation de sédiments de dragage phosphatés en technique routière - Thèse de doctorat, (2013)
9. Benzerzour, M., Maherzi, W., Amar, M.A.A., Abriak, N.E., Damidot, D.: Formulation of mortars based on thermally treated sediments. J. Mater. Cycles Waste Manag. 20, 592–603 (2018). https://doi.org/10.1007/s10163-017-0626-0
10. BENZERZOUR, M., Mouhamahou, A., ABRIAK, N.-E.: New experimental approach of the reuse of dredged sediments in a cement matrix by physical and heat treatment. 140, 432–444 (2017)
11. Aouad, G., Laboudigue, A., Gineys, N., Abriak, N.E.: Dredged sediments used as novel

supply of raw material to produce Portland cement clinker. Cem. Concr. Compos. 34, 788–793 (2012). https://doi.org/10.1016/j.cemconcomp.2012.02.008
12. Faure, A., Coudray, C., Anger, B., Moulin, I., Colina, H., Izoret, L., Théry, F., Smith, A.: Beneficial reuse of dam fine sediments as clinker raw material. Constr. Build. Mater. 218, 365–384 (2019). https://doi.org/10.1016/j.conbuildmat.2019.05.047
13. Dalton, J.L., Gardner, K.H., Seager, T.P., Weimer, M.L., Spear, J.C.M., Magee, B.J.: Properties of Portland cement made from contaminated sediments. Resour. Conserv. Recycl. 41, 227–241 (2004). https://doi.org/10.1016/j.resconrec.2003.10.003
14. Anger, B.: Caractérisation des sédiments fins des retenues hydroélectriques en vue d ' une orientation vers des filières de valorisation matière, (2014)
15. Cimbéton, Infociments 2016. L'essentiel, 2016
16. Fernandez, R.: Calcined clayey soils as a potential replacement for cement in developing countries. Ph.D Thesis, Ecole Polytechnique Fédérale de Lausanne, (2009)
17. Skibsted, J., Snellings, R.: Reactivity of supplementary cementitious materials (SCMs) in cement blends. Cem. Concr. Res. 124, 105799 (2019). https://doi.org/10.1016/j.cemconres.2019.105799
18. Fernandez, R., Martirena, F., Scrivener, K.L.: The origin of the pozzolanic activity of calcined clay minerals: A comparison between kaolinite, illite and montmorillonite. Cem. Concr. Res. 41, 113–122 (2011). https://doi.org/10.1016/j.cemconres.2010.09.013
19. Dang, T.A., Kamali-Bernard, S., Prince, W.A.: Design of new blended cement based on marine dredged sediment. Constr. Build. Mater. 41, 602–611 (2013). https://doi.org/10.1016/j.conbuildmat.2012.11.088
20. Danner, T., Norden, G., Justnes, H.: Characterisation of calcined raw clays suitable as supplementary cementitious materials. Appl. Clay Sci. 162, 391–402 (2018). https://doi.org/10.1016/j.clay.2018.06.030
21. NF EN 12457-2. Leaching-Compliance Test for LeachingofGranular Waste Materials and SludgesPart 2: One Stage Batch Test at a Liquid to Solid Ratio of10 l/kgfor Materials with Particle Size Below 4 mm (without or with Size Reduction); BSI: London, UK, 2002.
22. Kleib, J., Aouad, G., Abriak, N.E., Benzerzour, M.: Production of Portland cement clinker from French Municipal Solid Waste Incineration Bottom Ash. Case Stud. Constr. Mater. 15, e00629 (2021). https://doi.org/10.1016/j.cscm.2021.e00629
23. Taylor HFW: Cement chemistry. (1997)
24. Lea: Lea's chemistry of cement and concrete. Elsevier. (2003)
25. G.K.Moir: Advanced Concrete Techbology. (2003)
26. G.K.Moir; Mineralised high alite cement. World Cem. 13, 374 (1982)
27. F.W.Locher: Cement principles of production and use. (2006)
28. Lawrence, C.D.: The Constitution and Specification of Portland Cements. (2004)
29. Neville, A.: Propriétés des Bétons, édition Eyrolles, Translated by CRIB. (2000)
30. Hill, L., Fulvio, T.: Manufacturing solutions for concrete performance, World cement.
31. Baron, J., Ollivier, J.-P.: Les Bétons. (1997)
32. Zayed, A.: Effect of sulfur trioxide content on concrete structures using Florida Materials, Research report, University of south Florida. (2004)
33. NF EN 1097-7. Tests for Mechanical and Physical Properties of Aggregates—Part 7: Determination of the Particle Density of Filler— Pyknometer Method; BSI: London, UK, 2008.
34. ISO 18757. Fine Ceramics (Advanced Ceramics, Advanced Technical Ceramics)—Determination ofSpecific Surface Area ofCeramic Powders by Gas Adsorption Using the BET Method; ISO: Geneva, Switzerland, 2003.
35. Association Française de Normalisation (AFNOR): NF EN 196-6 : Méthodes d'essai des ciments - Détermination de la finesse. (2018)
36. Faure, A.: Capacité d ' un sédiment à se substituer à la fraction argileuse de la matière première de l ' industrie des liants hydrauliques - Thèse de doctorat, (2017)

37. P. Schläpfer, R. Bukowski, Untersuchungen über die Bestimmung des freien Kalkes und des Kalziumhydroxydes in Zement-klinkern, Zementen, Schlacken und abgebundenen hydraulischen Mörteln, Eidgenössische Materialprüfungsanstalt an der E.T.H. in Zürich. 63.
38. AFNOR: NF EN 196-3. Methods of testing cements. Part 3 – Determination of setting times and soundness, 2017.
39. Kleib, J., Aouad, G., Khalil, N., Zakhour, M.: Incorporation of zinc in calcium sulfoaluminate cement clinker. Adv. Cem. Res. 1–7 (2020). https://doi.org/10.1680/jadcr.19.00125
40. Snellings, R., Vayghan, A.G., Horckmans, L., Snellings, R., Peys, A., Teck, P., Maier, J., Friedrich, B., Klejnowska, K.: Use of Treated Non-Ferrous Metallurgical Slags as Supplementary Cementitious Materials in Cementitious Mixtures Use of Treated Non - Ferrous Metallurgical Slags as Supplementary Cementitious Materials in Cementitious Mixtures. (2021). https://doi.org/10.3390/app11094028
41. Kocaba, V., Gallucci, E., Scrivener, K.L.: Methods for determination of degree of reaction of slag in blended cement pastes. Cem. Concr. Res. 42, 511–525 (2012). https://doi.org/10.1016/j.cemconres.2011.11.010
42. Lu, X., Ye, Z., Wang, S., Du, P., Li, C., Cheng, X.: Study on the preparation and properties of belite-ye'elimite-alite cement. Constr. Build. Mater. 182, 399–405 (2018). https://doi.org/10.1016/j.conbuildmat.2018.06.143
43. Cassagnabère, F., Mouret, M., Escadeillas, G.: Early hydration of clinker-slag-metakaolin combination in steam curing conditions, relation with mechanical properties. Cem. Concr. Res. 39, 1164–1173 (2009). https://doi.org/10.1016/j.cemconres.2009.07.023
44. Bentz, D.P., Barrett, T., De la Varga, I., Weiss, W.J.: Relating Compressive Strength to Heat Release in Mortars. Adv. Civ. Eng. Mater. 1, 20120002 (2012). https://doi.org/10.1520/acem20120002
45. Ha, B.T.T.: Evolution physico-chimique des liants bas PH hydratés Influence de la température et mécanisme de rétention des alcalins - Thèse doctorante, (2010)
46. NIST: Technical Note VCCTL-01.
47. NF EN 196-1: Méthode d'essai des ciments- Partie 1 : Détermination des résistance. (2016)
48. Association Française de Normalisation (AFNOR): NF EN 197-1: Composition, spécifications et critères de conformité des ciment courant.
49. Elkarim, M., Bulteel, D., Potier, G., Michel, F., Zhao, Z., Courard, L.: Use of grinded hardened cement pastes as mineral addition for mortars. (2020). https://doi.org/10.1016/j.jobe.2020.101863
50. Bentz, D.P.: Incorporation of Fly Ash into a 3-D Cement Hydration Microstructure Model Nistir 6050. (1997)
51. Bentz, D.P.: Modeling the influence of limestone filler on cement hydration using CEMHYD3D. Cem. Concr. Compos. 28, 124–129 (2006). https://doi.org/10.1016/j.cemconcomp.2005.10.006
52. Kamali, S., Bernard, F., Damidot, D.: Modélisation multi-échelles de la lixiviation des mortiers : effet sur les caractéristiques mécaniques. 7–12 (2005)
53. NIST: Guide to using CEMHYD3D Version 3.0.
54. Bresciani, C.: Simulation numérique de l ' hydratation et du développement des propriétés physiques et mécaniques d ' une pâte de ciment afin de sélectionner de nouveaux ajouts minéraux., (2009)
55. Bentz, D.P.: Guide to Using CEMHYD3D: A Three-Dimensional Cement Hydration and Microstructure Development Modelling Package. (1997)
56. Bentz, D.P.: CEMHYD3D : A Three-Dimensional Cement hydratation and Microstructure Development Modelling Package Version 2.0.

Article 4: *Valorization of sediments in the manufacture of CEM III cements*

Synthèse : Dans cette étude trois ciments CEM III ont été fabriqués au laboratoire.

- ✓ CEM III TM = Clinker TM + Laitier
- ✓ CEM III 2%ASL = Clinker 2% ASL + Laitier
- ✓ CEM III 10% SF = Clinker TM + Laitier + 10 % sédiment calciné Flash

Les résultats montrent que :

- Les deux ciments CEM III TM et le CEM III 2%ASL présentent le même comportement du point de vue hydratation.
- L'incorporation du sédiment dans le mélange de cru n'a pas d'influence sur la qualité du clinker et du ciment CEM III.
- La résistance en compression des trois ciments CEM III à 28 jours mesurée sur l'échantillon de mortier normalisé est supérieure à 42.5 MPa.
- Les deux ciments CEM III TM et CEM III 2%ASL présentent une demande en eau et un temps de prise similaires. Le remplacement du laitier par le sédiment calciné conduit à une augmentation de la demande en eau et du temps de prise.
- L'analyse de chaleur de l'hydratation par calorimétrie isotherme sur les pâtes de ciment montre que le ciment CEM III 10% SF semble être plus réactif que les ciments CEM III TM et CEM III 2% ASL. Cependant, l'incorporation du sédiment calciné ne modifie pas la cinétique de l'hydratation du ciment vu que l'aire de la courbe de chaleur de l'hydratation de trois ciments est similaire. Ce résultat peut être expliqué par (i) le ciment CEM III 10% SF présente une finesse plus élevée que les deux autres ciments CEM III, (ii) la réaction pouzzolanique du sédiment calciné commence plutôt que celle du laitier.
- L'ajout du sédiment Flash en remplacement d'une partie du laitier semble améliorer l'hydratation aux jeunes âges. Ceci explique un développement de la résistance en compression plus élevée du ciment CEM III 10% SF par rapport aux deux autres ciments CEM III aux jeunes âges.
- L'analyse ATG – DTG montre que l'incorporation du sédiment permet de former une fraction de C-S-H plus importante que celle de deux ciments CEM III TM et CEM III 2%ASL.
- L'analyse de la composition chimique de la phase C-S-H des pâtes de ciments CEM III hydratées montre que (i) le rapport de C/S dans les pâtes de ciment CEM III TM et CEM III 2% ASL est relativement similaire, (ii) ce rapport dans la pâte de ciment CEM III 10% SF est plus faible car la teneur en SiO_2 dans le sédiment calciné est plus élevée que celle dans le laitier. Ce résultat est intéressant car il permet d'avoir une meilleure résistance à la lixiviation.
- Le résultat l'analyse de la porosité au mercure montre un effet bénéfique de l'incorporation du sédiment calciné lié à la réduction de la porosité totale ainsi que la taille des pores. Ce résultat est important du point de vue impact sur la durabilité d'un matériau cimentaire.

Date de soumission
Statut
Journal

Article 4: Valorization of sediments in the manufacture of CEM III cements

Duc Chinh CHU[(1)], Joelle KLEIB[(1)], Mouhamadou AMAR[(1)], Mahfoud BENZERZOUR[(1)], Jaouad NADAH[(2)], Nor-Edine ABRIAK[(1)]

[(1)] Univ.Lille, IMT Lille Douai, Univ.Artois, Yncrea Hauts-de-France, ULR 4515-LGCgE, 6 Laboratoire de Génie civil et géo-Environnement, F-59000, Lille, France
[(2)] EQIOM Le LAB, CRT 1 Parc Vendôme – 460 Allée de l'Innovation, 59810 LESQUIN, France.
[(*)] **Corresponding author:**
duc.chinh.chu@imt-nord-europe.fr

Abstract

I. Introduction

In France, approximately 56 million m^3 of sediments (marine and river) are dredged each year in order to ensure acceptable navigation thresholds, to avoid flooding and to improve the quality of the environment [1]. These sediments are then either submerged in the sea or deposited in reservoirs. However, according to European Directive 2008/98/EC, sediment extracted from reservoirs becomes waste [2]. Consequently, it is necessary to find adequate solutions for the recovery of these sediments.
Several previous studies have shown the feasibility of recovering the sediment in different fields, such as:

- Building materials in road engineering [3, 4].
- Mineral additions in the cementitious material [5–7].
- Raw materials in the manufacture of cement [8, 9].

In a previous study [10], Anger used the notion of "Suitability Index" to assess the suitability of sediment use in different pathways. The result shows that the use of sediment as raw material in the manufacture of cement and the manufacture of terracotta-type ceramics was the most suitable. However, the valorization of the sediment in the manufacture of cement could solve problems of sediment management and natural resource reservation, but it would not be the ideal solution to reduce the quantity of CO_2 linked to the production of clinker. In fact, the quantity of CO_2 emitted during the manufacture of clinker is on average for Europe at 688 kg per ton of cement, or about 130 Mt/year [11]. Therefore, the reduction of clinker dosage of the cement to the mineral addition profile would become the challenge to reduce the amount of CO_2. We can cite the most used mineral additions in cement:

- **Natural addition (Limestone filler)** : De Weerdt et al. [12] previously demonstrated that the presence of the limestone filler resulted in the formation of hemi- and monocarbonates (Eq (1) and Eq (2)) and the stabilization of the ettringite compared to cement without the limestone filler, where part of the ettringite had converted to monosulfate (Eq (3)). Consequently, the presence of 5% of lime filler led to an increase in the volume of hydrates and to an increase in the compressive strength.

$$C_3A + Cc + 11H \rightarrow C_4AcH_{11} \quad (1)$$

$$C_3A + 0.5Cc + 0.5CH + 11.5H \rightarrow C_4Ac0.5H_{12} \quad (2)$$

$$2C_3A + C_6As3H_{32} + 4H \rightarrow 3CAsH_{12} \quad (3)$$

- **Industrial waste (Slag, Fly ash, Silica fume) :**

Silica fume is a by-product of the silicon and ferrosilicon alloy industry and is mainly composed of ultrafine particles with a diameter between 0.1 and 0.2 µm. These particles contain at least 85 to 95% amorphous silica SiO_2 and are in the form of glassy microspheres [13]. Thanks to a high silica content and an essentially glassy structure, silica fume is considered to be a highly pozzolanic product and frequently used in the manufacture of ultra-performance concretes [14].

Slag is a by-product of the steel industry, obtained in blast furnaces during the production of melting. It is rich in oxides of calcium, silicon, magnesium and aluminum. Essentially amorphous in nature, most vitrified slags have 5 to 10% crystalline phases and exhibit latent hydraulic properties, that is, their hydration requires a chemical activator [15].

Additions having the pozzolanic property will react with portlandite ($Ca(OH)_2$) to form hydrated "pozzolanic" calcium silicate (pozzolanic C-S-H (II)) according to Eq (4) and Eq (5). This hydrate generally has a lower C/S ratio than that of C-S-H formed from the hydration of cement without pouzzolanic addition. Unlike C-S-H (II), the C/S ratio of C-S-H (I) is independent of temperature and the Ca^{2+} concentration of the solution. In general, the pozzolanic C-S-H stoichiometry is $C_{1.1}SH_{3.9}$ and C-S-H (I) is $C_{1.7}SH_4$ [16].

$$(SiO_2)_{soluble} + 2OH^- \rightarrow H_2SiO_4^{2-} \quad (4)$$

$$xCa^{2+} + H_2SiO_4^{2-} + 2(x-1)\ OH^- + y\ H_2O \rightarrow C_xSH_y \quad (5)$$

The addition of pozzolanic mineral additions provides several technical advantages. It improves the durability properties against certain chemical attacks such as leaching, sulphate attack, and resistance to chloride penetration [15, 17] and mechanical resistance [18]. However, in French, the production of slag has gradually declined due to the decrease in steel production [19]. This could lead to a shortage of slag in the manufacture of CEM III cement. It is necessary to find another mineral addition which could replace slag in the CEM III cement.

Consequently, the objective of this research is the valorization of the sediment in raw materials in the manufacture of clinker and the replacement of part of the slag by the sediment treated in the manufacture of CEM III cement. First, the sediments are characterized in order to choose the most suitable sediment for each option. Then, the clinkers and cements are also characterized to assess the impact of the use of sediments on the phase formation in the clinker, the hydration behavior and the development of the mechanical strength of the cements.

II. Materials and method

II.1. Materials in the manufacture of clinker

II.1.1. Raw materials

The sediment used in this option is the fluvial sediment collected at the Air sur Lys (ASL) storage site in the Haut de France region, France. It was then homogenized and dried to a constant mass at 40 ° C.

The limestone, clay, sand and iron oxide extracted from the deposit were supplied by the cement company EQIOM. These materials were also dried to constant mass and ground to a particle size of less than 200 µm.

The particle size distribution of ASL raw sediment was measured in two different fractions. A fraction greater than 80 µm was measured using sieves, and a fraction less than 80 µm was measured using the COULTER laser diffractometry, type LS230 device. Figure 1 illustrates the particle size distribution of two fractions of the ASL raw sediment.

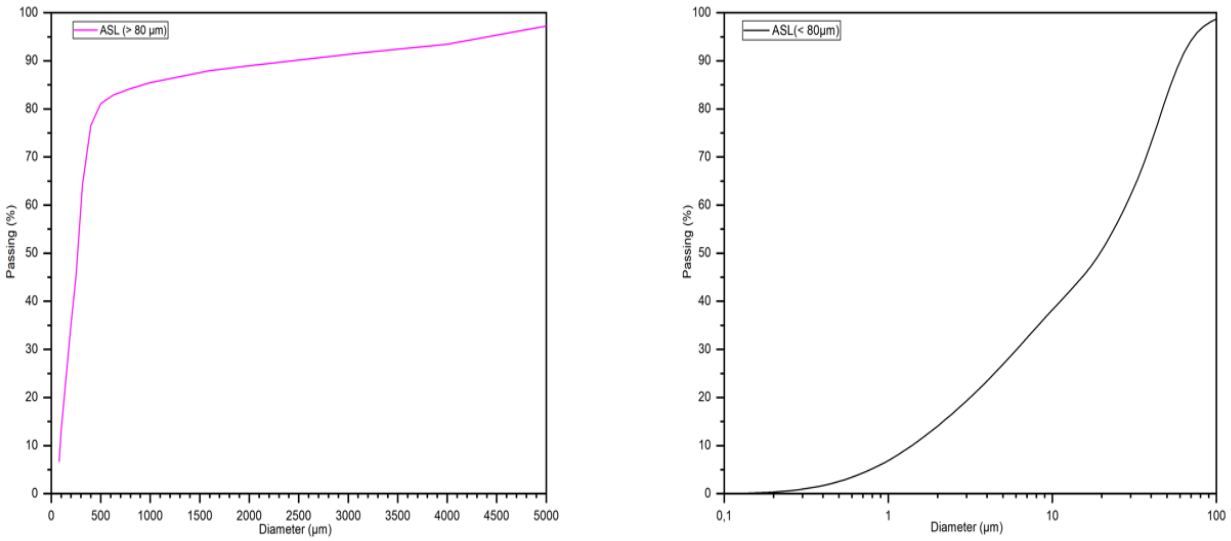

Figure 1 : Particle size distribution of the two fractions of the ASL raw sediment

The density of materials was determined according to the standard NF EN 1097-7 [20] using a Micromeritics ACCUPYC 1330 Helium Pycnometer device. Table 1 show the density of the raw materials used in the option.

Table 1 : The nomenclature and density of the raw materials

Materials	Limestone 1	Limestone 2	Limestone 3	Clay 1	Clay 2	Sand	Iron Oxide	Gypsum	Slag	Sediment
Nomen	LIM 1	LIM 2	LIM 3	CLY 1	CLY 2	SAN	IRO	GYP	SLAG	ASL
Density (g/cm^3)	2.76	2.76	2.76	2.65	2.65	2.63	3.99	2.36		2.65

Note: Nomen = Nomenclature

The chemical composition was determined by X-Ray Fluorescence (XRF) using an S4 - PIONEER apparatus equipped with a 4 -kW generator and an Rh anode. The beads were prepared by mixing 2 g of the material analyzed with 10 g of melting agent (mass ratio 1: 5). Table 2 shows the result of the chemical analysis of the raw materials.

Table 2 : Chemical composition of raw materials determined by XRF analysis.

Oxide (%)	ASL	LIM 1	LIM 2	LIM 3	CLY 1	CLY 2	SAN	IRO	GYP	SLAG
SiO_2	65.15	5.3	9.5	6.0	48.7	60.6	88.3	2.2	1.95	34.27
Al_2O_3	7.35	1.9	3.7	1.2	20.6	14.9	4.8	0.3	0.33	10.95
Fe_2O_3	3.1	0.6	1.3	0.6	10.7	7.9	1.2	70.6	0.28	0.27
CaO	7.55	49.8	45.8	50.0	1.1	2.3	2.1	13.5	32.85	40.98
MgO	0.7	0.4	0.6	0.4	1.1	0.8	ND	2.2	0.34	6.56
Na_2O	0.85	ND	ND	ND	ND	ND	ND	ND	0	0.17

K_2O	1.65	0.4	0.9	0.2	1.5	1.3	0.3	0.1	0.08	0.49
SO_3	0.1	ND	ND	ND	ND	ND	ND	0.2	38.58	
TiO_2	0.65	ND	0.1	ND	0.7	0.7	0.9	ND	0	0.585
P_2O_5	0.25	ND	ND	0.2	0.3	0.2	ND	ND	0	
Mn_2O_3	ND	ND	ND	ND	ND	0.2	ND	0.7	0	
ZnO	0.1	ND	ND	ND	ND	ND	0.1	ND	0	
LOI	12.1	40.9	37.5	40.9	14.6	10.5	1.9	1.2	24.85	4.7
Total	99.5	99.3	99.4	99.5	99.3	99.4	99.6	98.7	99.28	99.17

Note: ND = Not detected

X-ray diffraction (XRD) was used to identify the mineralogical phases using a Bruker D2 Advance type apparatus equipped with a Cu anode, λ = 1.5406 Å, with the recording angle 2θ of the diffraction from 5° to 80° and a step size of 0.02. Table 3 presents the main mineral phases identified in the materials.

Table 3 : The main mineral phases of raw materials identified by X-ray diffraction (XRD)

Material	Mineral phases
ASL	• Quartz (SiO_2) • Calcite ($CaCO_3$) • Muscovite ($KAl_2(AlSi_3O_{10})(F,OH)_2$) • Albite • Montmorillonite (Clay) (($(Na, Ca)_{0.3}(Al, Mg)_2(Si_4O_{10}(OH)_2.nH_2O$). • Orthoclase
LIM 1	• Calcite ($CaCO_3$)
LIM 2	• Calcite ($CaCO_3$)
LIM 3	• Calcite ($CaCO_3$)
CLY 1	• Quartz (SiO_2) • Montmorillonite (Clay) • Iron aluminum oxide hydroxide • Kaolinite ($Al_2O_3.2SiO_2.2H_2O$)
CLY 2	• Quartz (SiO_2) • Montmorillonite (Clay) • Kaolinite ($Al_2O_3.2SiO_2.2H_2O$)
SAN	• Quartz (SiO_2)

	• Calcite ($CaCO_3$)
IRO	• Magnetite ($FeO.Fe_2O_3$) • Calcite ($CaCO_3$) • Wustite (FeO)
GYP	• Gypsum ($CaSO_4.2H_2O$)
SLAG	• Amorphous

The mobility of the metallic trace elements (MTE) and the anionic elements of the raw sediment were measured after the leaching of the sample using a liquid/solid ratio of 10 and an equilibrium time of 24 hours according to the standard NF EN 12457-2 [21] using an Inductively Coupled Plasma Optical Emission Spectrometer (ICP-OES 5100 Agilent Technologies). The leaching limit values for inert waste (IW) and non-hazardous waste (NHW) specified in Directive 1999/31/EC were used to verify material compliance. Table 4 shows the result of the ASL raw sediment leaching analysis.

Table 4 : Metallic trace elements of the ASL raw sediment

Sample	Concentration (mg/kg)										
ASL	As	Ba	Cd	Cr	Cu	Mo	Ni	Pb	Sb	Se	Zn
	< 0.1	0.14	<0.008	<0.005	0.18	0.10	0.04	<0.03	0.06	0.1	0.14
IW	**0.5**	**20**	**0.04**	**0.5**	**2**	**0.5**	**0.4**	**0.5**	**0.06**	**0.1**	**4**
NHW	**2**	**100**	**1**	**10**	**50**	**10**	**10**	**10**	**0.7**	**0.5**	**50**

The chracterization resullt shows that:

- The main oxides of the sediment are SiO_2, Al_2O_3, Fe_2O_3 et CaO (%CaO + % SiO_2 + % Al_2O_3 + %Fe_2O_3 > 80%). However, the ASL raw sediment has a high quartz content.
- The ASL raw sediment is inert and non-hazardous.

II.1.2. Materials in the manufacture of mineral addition

The sediment used in this option is the fluvial sediment collected from the Noyelles-Sous-Lens (NSL) disposal site in the Haut de France region in France. First, this sediment was homogenized and dried at 105 °C to constant weight, then finely ground before calcination. The method used is flash calcination, which was previously used for the manufacture of metakaolin [22]. The NSL sediment was calcined at 750 °C in this option, and the calcined sediment is known as NSLF 750. Both NSL and NSLF 750 sediments were characterized using the raw material characterization assays used in the option of manufacture of clinker. Table 5 shows the physical properties of NSL and NSLF750 sediments.

Table 5 : Physical properties of NSL and NSLF 750 sediments

Property	NSL	NSLF 750	Sandard
Density (g/cm3)	2.43	2.63	NF EN 1097-7
BET (cm^2/g)	4 376	15 590	NF EN ISO 18757

OM content (wt %)	16.1	1.93	XP P94-047
d10 (µm)	1.24	2.63	
d50 (µm)	11.68	14.71	
d90 (µm)	55.91	64.13	

The result shows that:

- Calcination considerably reduces the content of organic matter, which has a detrimental effect on the hydration of the cement [23].
- An increase in particle size without a decrease in specific surface was observed. This could be explained by an agglomeration of clay particles without sintering during calcination [24].
- Calcination also led to a strong increase in the specific surface (BET) of the NSL sediment. This could increase the reactivity of the sediment in a cementitious material.

The chemical composition of the NSL and NSLF 750 sediments determined by XRF analysis is shown in Table 6. The result shows that the calcination did not cause a significant change in the chemical composition of the sediment.

Table 6 : Chemical composition of NSL and NSLF 750 sediments

Oxide (wt.%)	CaO	SiO_2	Al_2O_3	Fe_2O_3	SO_3	Na_2O	K_2O	MgO	ZnO	P_2O_5	LOI	Total
NSL	10.57	39.62	9.64	5.12	0.22	0.69	1.84	0.88	0.27	2.1	27.63	99.17
NSLF 750	11.21	49.71	12.00	5.33	0.18	0.74	2.25	1.12	0.31	2.26	13.70	99.49

In order to demonstrate the effect of calcination on the transformation of mineral phases, in particular clay phases, XRD analysis was carried out on the fraction with a diameter of less than 2 µm of the NSL and NSLF 750 sediments. For the study of clay species, the angular range explored is between 4° and 35° 2θ with a step size reduced to 0.008 ° 2θ and a step time of 0.84 s/step. The main mineral phases of NSL and NSLF 750 sediments are shown in Table 7.

Table 7 : Mineral phases of NSL and NSLF 750 sediments

Sediment	Mineral phases
NSL	▪ Quartz (SiO_2) ▪ Calcite ($CaCO_3$) ▪ Illite (K, H_3O) (Al, Mg, Fe)$_2$(Si, Al)4O10[$(OH)_2$, (H_20)] ▪ Kaolinite ($Al_2O_3.2SiO_2.2H_2O$) ▪ Albite
NSLF 750	▪ Quartz (SiO_2) ▪ Calcite ($CaCO_3$) ▪ Illite (K, H_3O) (Al, Mg, Fe)$_2$(Si, Al)4O10[$(OH)_2$, (H_20)] ▪ Albite ▪ Anhydrite $CaSO_4.2H_20$

The clay phases identified by XRD analysis on oriented slides of NSL and NSLF 750 sediments are presented in Figure 2.

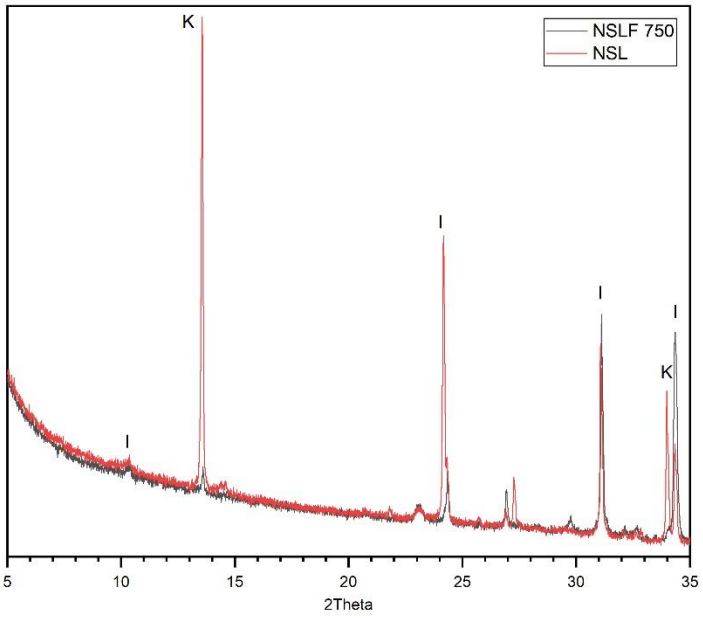

Figure 2 : XRD patterns of clay phases of NSL and NSLF 750 sediments using oriented slides analysis (K: Kaolinite, I: Illite)

The result shows that:

- The main phases of the NSL sediment are quartz and calcite. In addition, clay phases such as kaolinite and illite have been identified.
- Calcination transforms the clay phases into more reactive phases according to the following equations:
  Kaolinite [25]:

$Al_2O_3.2SiO2.2H2O$ Al2O3.2SiO2 (metakaolinte) + 2H2O (6)

Illite [26]**:**

(K, H_3O) (Al, Mg, Fe)2(Si, Al)4O10[(OH)2, (H20)] -> 3.5 H2O +(K) (Al, Mg, Fe)2(Si, Al)4O10.5 (7)

The result of the leaching analysis shows the presence of metallic trace elements as well as anionic elements in sediments (Table 8 and Table 9). The content of certain metallic trace elements in the RS sediment exceeds the value specified for inert waste (IW), in particular, the content of zinc.

Table 8 : Metallic trace elements in sediments (mg/kg)

Elements	NSL	NSLF 750	IW	NHW
As (mg/kg)	< 0.08	<0.1	**0.5**	**2**
Ba (mg/kg)	1.4912	1.9	**20**	**100**
Cd (mg/kg)	<0.008	<0.008	**0.04**	**1**

Cr (mg/kg)	<0.03	0.37	**0.5**	**10**
Cu (mg/kg)	2.0509	0.078	**2**	**50**
Mo (mg/kg)	0.5538	1.7	**0.5**	**10**
Ni (mg/kg)	0.4799	<0.03	**0.4**	**10**
Pb (mg/kg)	0.0447	0.074	**0.5**	**10**
Sb (mg/kg)	-	<0.05	**0.06**	**0.7**
Se (mg/kg)	0.1019	0.08	**0.1**	**0.5**
Zn (mg/kg)	7.8518	<0.05	**4**	**50**

Table 9 : Anionic element's content in sediment (mg/kg)

Sediments	Fluoride (mg/kg)	Chloride (mg/kg)	Sulfates (mg/kg)
NSL	<1	262	15 820
NSLF 750	8	247	11 120
IW	10	800	1000
NHW	150	15 000	20 000

The sulfates content in the NSL sediment is higher than the limit value for inert waste. In addition, it can also be seen from the results that the RS sediment has a higher sulfate content compared to the NSLF 750 sediments, where the sulfate content decreases

The Frattini's test (NF EN 196-5 [27]) was used to assess the pouzzolanic reactivity of the sediment. The essay consists to react 16 g of Portland cement and 4 g of material in 100 ml of distilled water. Then, the mixture was kept tightly at 40 °C for at least 8 days or 15 days. The samples were filtered under vacuum and the filtrates were subsequently analyzed. First, the OH^- ions content was determined using the HCl 0.1N hydrochloric acid. After adjusting the pH to 12.5, the Ca^{2+} ion content was determined by the use of an EDTA complexometric test. The Ca^{2+} content (expressed as CaO equivalent) function of OH^- content are shown relative to the limit of solubility of $Ca(OH)_2$. A position under the curve of $Ca(OH)_2$ solubility suggests a consumption of CaO by pozzolanic reaction [28].

The result of the test after 15 days presented in Figure 3 shows that:

- The raw NSL sediment does not exhibit pozzolanic reactivity. On the other hand, the transformation of kaolinite into metakaolin in the calcined sediment led to pozzolanic reactivity.

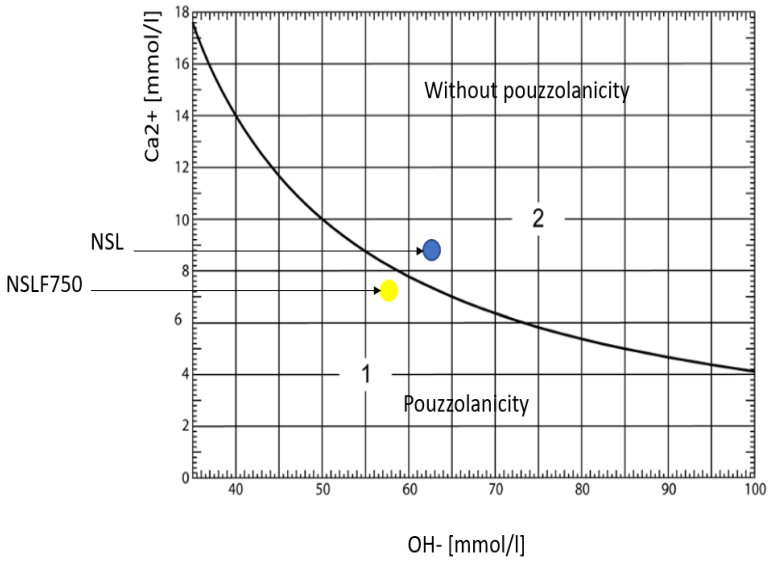

Figure 3 : The Frattini's test result after 15 days

II.2. Cement Manufacturing Method

II.2.1. Formulation method

From the result of the analysis of the materiel's chemical composition, the different formulations of the raw meal were set up based on the following modulus usually used in the cement industry: the Lime Saturation Factor (LSF), the Silica Ratio (SR) and the Alumina Ratio (AR) [29]. These are the main parameters to control the quality of the clinker [18]. The calculations of LSF, SR and AR are presented by the equations below:

$$LSF = \frac{100 * \%CaO}{2.8 * \%SiO2 + 1.18 * \%Al2O3 + 065 * \%Fe2O3} \quad (8)$$

$$SR = \frac{\%SiO2}{\%Al2O3 + \%Fe2O3} \quad (9)$$

$$AR = \frac{\%Al2O3}{\%Fe2O3} \quad (10)$$

In this option, two formulations were established using the following values: LSF = 98, SR = 2.5, AR = 1.65, and a content of 2% wt of the ASL sediment. Table 10 shows the composition of the components of two formulations of the clinker.

Table 10 : Composition of the components of two clinker formulations

Formula	ASL (wt %)	LIM1 (wt %)	LIM2 (wt %)	LIM3 (wt %)	CLY1 (wt %)	CLY2 (wt %)	SAN (wt %)	IRO (wt %)
Clinker TM	0	52.08	17.36	17.36	3.18	4.78	4.31	0.93
Clinker 2%ASL	2	51.87	17.29	17.29	2.98	4.47	3.17	0.93

Based on previous studies [8, 30], all the components are mixed with water to better homogenize them. The mixture is then dried at 105 °C and pressed at 5 kN into pellets. Then, the pellets are burned at 200 °C for 20 minutes, then at 1450 °C with a speed of 7 °C/min. After 15 min of burning at the clinkering temperature, the clinker was cooled in the furnace to reach the room temperature.

In order to assess the quality of the clinkerization process, the chemical composition of the raw mixtures was checked using XRF analysis to ensure that the values of the modulus (LSF, SR, AR) were similar to the theoretical values. Table 11 shows the result of the chemical composition analysis of the raw mixtures. Good consistency between the experimental values and the theoretical values was observed.

Table 11 : The chemical composition and values (LSF, SR and AR) of two formulations analyzed by XRF

Oxide (wt. %)	Clinker TM		Clinker 2% ASL	
	Theory	Exp	Theory	Exp
SiO_2	13.72	13.55	13.71	13.4
Al_2O_3	3.42	3.5	3.41	3.5
Fe_2O_3	2.07	2.1	2.07	2.1
CaO	42.93	41.9	42.87	41.9
MgO	0.48	0.5	0.48	0.5
Na_2O	0.00	ND	0.02	ND
K_2O	0.52	0.6	0.54	0.6
SO_3	0.00	ND	0.00	ND
TiO_2	0.00	0.2	0.00	0.2
P_2O_5	0.00	0.1	0.06	0.1
Mn_2O_3	0.00	ND	0.00	ND
ZnO	0.01	ND	0.00	ND
LOI	36.03	36.45	36.05	37.1
Total	99.24	99.65	99.24	99.4
LSF	98	96.47	98	97.41
SR	2.5	2.42	2.5	2.40
AR	1.65	1.67	1.65	1.67

In addition, the free lime content (CaO_{free}) is one of the important indices for evaluating the quality of the clinker. In general, a CaO_{free} content of less than 2% is acceptable in the cement industry [10]. In this study, the CaOfree content of clinkers was determined using the Schlafer-Bukolowki method [31]. The content of the mineral phases of the clinkers was calculated using the Bogue's formula according to the following equations:

$$C_3S = 4.07 * (CaO_{Total} – CaO_{\text{free lime}}) - 6.72 * Al_2O_3 – 1.43 * Fe_2O_3 \quad (11)$$

$$C_2S = 8.60 * SiO_2 + 1.08 * Fe_2O_3 + 5.07 * Al_2O_3 - 3.07 * (CaO_{Total} – CaO_{free\ lime}) \quad (12)$$

$$C_3A = 2.65 * Al_2O_3 – 1.69 * Fe_2O_3 \quad (13)$$

$$C_4AF = 3.04 * Fe_2O_3 \quad (14)$$

In addition, the Rietveld analysis was also performed using TOPAS software in order to quantify the crystal phases of the clinkers. Table 12 shows the content of the mineral phases in the clinkers determined by two different methods. The two clinkers have similar amounts of mineral phases and a CaO_{free} content of less than 2%.wt.

Table 12 : Content of mineral phases in the two clinkers

Method	Clinker	C_3S (wt. %)	C_2S (wt. %)	C_3A (wt. %)	C_4AF (wt. %)	CaO_{free} (wt. %)
Schlafer-Bukolowki method – Bogue formula	Clinker TM	61.63	15.76	9.14	9.18	1.60
	Clinker 2% ASL	63.98	12.23	10.06	9.25	1.65
Rietveld method	Clinker TM	64.87	12.47	8.83	9.04	1.19
	Clinker 2% ASL	66.23	12.90	9.61	8.64	1.48

The result of the characterization of the clinkers shows that the two clinkers were successfully synthesized in the laboratory by checking the chemical composition and the CaO_{free} content of the clinkers.

II.2.2. Method of characterization of CEM III cements

In this study, three CEM III cements were synthesized. The nomenclature and composition of the cements are presented in Table 13.

Table 13 : Composition des composants des ciments

Cement	Clinker TM (wt. %)	Clinker 2%ASL (wt. %)	SLAG (wt. %)	GYP (wt. %)	NSLF 750 (wt. %)
CEM III TM	56.55	-	37.70	5.76	-
CEM III 2%ASL	-	56.52	37.68	5.80	-
CEM III 10%SF750	56.48	-	28.24	5.86	9.41

The components are ground together to achieve an approximate Blaine surface of 3500 cm^2/g. The setting start time was measured using a Vicat device after determining the water demand of the cement which allows it to reach the normal consistency according to NF EN 196-3 [32].
The reactivity of the cements is measured using an isothermal calorimetry analysis carried out at 20 °C. Based on previous research [8, 33], the paste was made with 8 g of cement and 4 g of

water that had been previously stored at 20 °C (W/C = 0.5). The calorimeter is a home-made type using flowmeters that allowed the calorimeter to equilibrate in less than 5 min.

Thermogravimetric analysis (TGA) was used to assess the reactivity of CEM III cements by measuring the amount of water bound according to Eq (15). The cement pastes were prepared with a W/C ratio of 0.5 and set aside in a saturated lime solution. Cement hydration shutdown was performed using the solvent solution. First, the sample was immersed in the acetone solution for 3 days, then it was vacuum filtered to remove the solvent solution and set aside in a desiccator.

$$Q_{\text{chemical bound water}} = M_{\text{sample (40°C)}} - M_{\text{sample (500°C)}} \quad (15)$$

With:

$Q_{\text{chemical bound water}}$: Amount of chemical bound water (wt %).

M_{sample} (40°C): mass of the sample at 40 °C.

M_{sample} (500°C): mass of sample at 500 °C

The amount of bound water could provide information on the amount of hydrates formed such as C-S-H, CASH and $Ca(OH)_2$ during cement hydration. In addition, it is impossible to distinguish the amount of hydrates from the TGA curve.

However, the hydrated phases as C-S-H, calcium aluminate hydrate (CAH) or calcium silico-aluminate hydrate (CASH) can be calculated from the DTG derived curve [34]. This is interesting knowing that the C-S-H phase is mechanically more resistant than the phases (CASH, CAH) and $Ca(OH)_2$ which has a low resistance due to its lamellar structure [35]. However, it is difficult to distinguish two phases CAH and CASH. The spectra obtained from the curves derived from dTG(%)/dt = f(T°C) were deconvolved in order to determine the area of each hydrate decomposition according to the Lorentzian's area deconvolution method with the amplitude a0, center a1 and width a2 according to the following equation [36]:

$$\frac{dTG(\%)}{dt} = \frac{a0}{1+\left(\frac{T-a1}{a2}\right)2} \quad (16)$$

With:

dTG(%)/dt: the derived value of TG (%) at time t.

T (°C): temperature (°C).

a0, a1 and a2: amplitude, centre and width (>0) of the spectrum respectively.

Figure 4 illustrates the steps for quantifying C-S-H and CASH using the DTG curve.

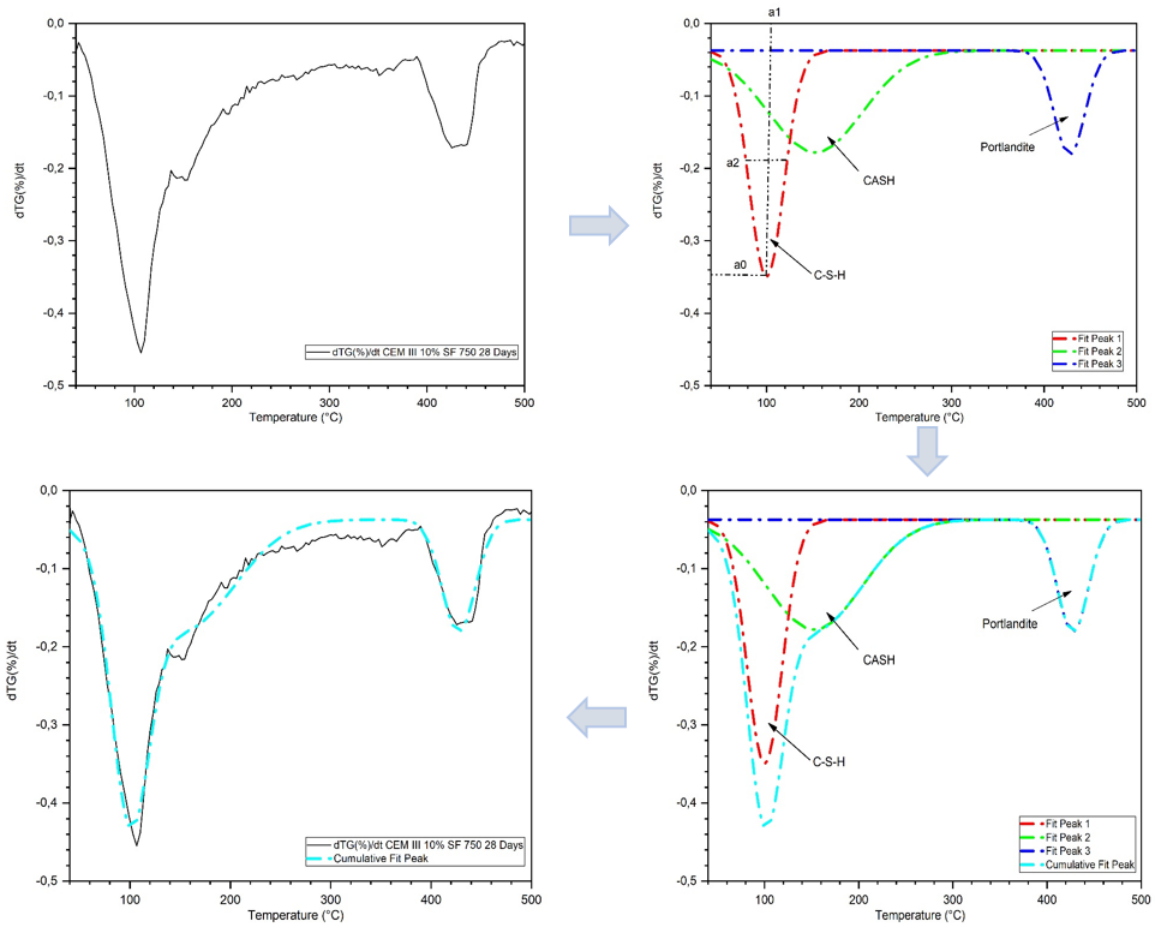

Figure 4 : Deconvolution method for quantification the quantity of C-S-H and CASH phases of the CEM III 10% cement paste after 28 days of hydration

Hydrates formed during cement hydration are identified using XRD analysis on cement paste samples after 28 days of hydration.

The chemical composition of hydrated cement paste phases was analyzed on the polished sections using a Hitachi S-4300 SE/N scanning electron microscope operating in backscattered electron mode (20 keV) and equipped with an energy dispersive X-ray spectrometer (SEM-EDS). For the measurement, the 100 points were carried out on several zones.

The compressive strength was measured on 4 * 4 * 16 cm^3 mortars according to the standard NF EN 196-1 [37]. The mortars were demolded after 24 hours, then stored in the saturated lime solution until the days of the test (2, 7 and 28 days of curing). The objective is the determination of the cement class according to standard NF EN 197-1 [38].

The porosity and the pore size distribution of the mortars were measured using Mercury Intrusion Porosimetry (MIP) technique (Micromertitics Autopore IV type). Based on previous research [39], the sample is first immersed in acetone solution to stop hydration, then dried to a constant mass at 40 °C. Indeed, drying at a higher temperature can cause a modification of the pores in the porous structure.

III. Results

III.1. Physical characteristics

The physical characteristics of the cements are presented in Table 14.

Table 14 : Physical characteristics of CEM III TM, CEM III 2%ASL and CEM III 10%SF cements.

Property	CEM III TM	CEM III 2%ASL	CEM III 10%SF750
Density (g/cm^3)	3.02	3.02	2.98
Blaine specific surface (cm^2/g)	3860	3840	3980
BET specific surface (m^2/g)	1.37	1.36	1.90
Water demand (%)	33.33	33.33	35.00
Setting time (minutes)	255	255	280

CEM III and CEM III 2% ASL cements have very similar characteristics. However, CEM III 10%SF750 cement has a BET surface area and higher water demand than CEM III TM and CEM III 2% ASL cements. This is important because the fineness directly influences the reactivity of the cement.

III.2. Heat of hydration of cements

Figure 5 shows the heat flux generated during the hydration of cement pastes using isothermal calorimetry analysis.

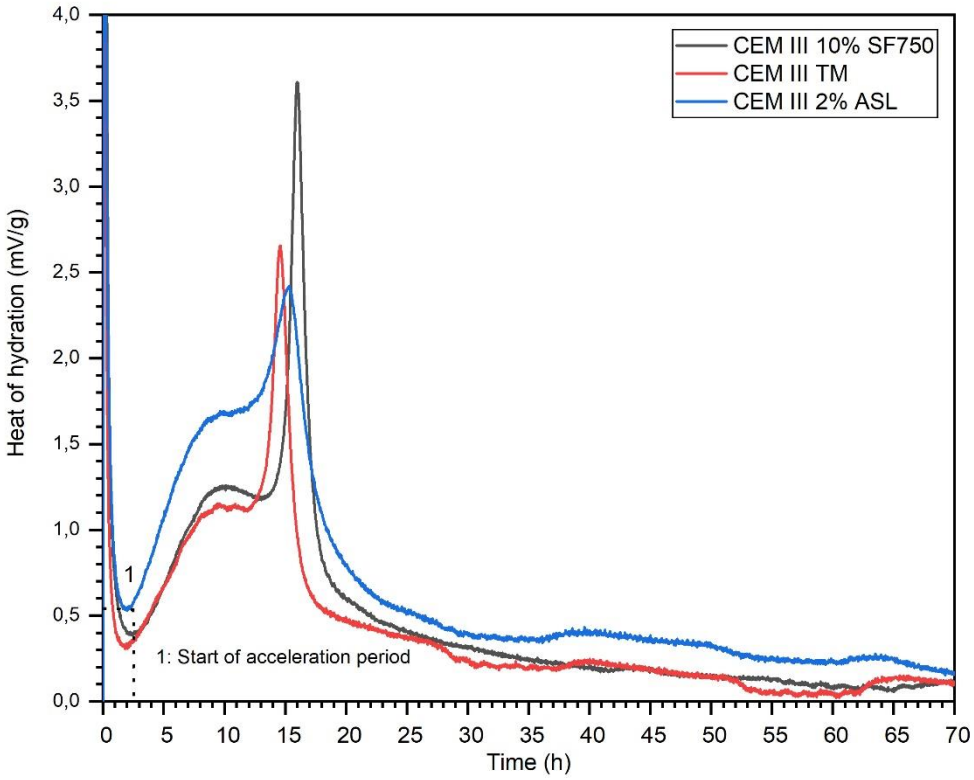

Figure 5 : Heat flow generated during the hydration of CEM III TM, CEM III 2%ASL and CEM III 10% SF750 cement pastes

The result shows that:

- The three cements have similar hydration behavior because the heat flow curve is identical.
- CEM III 10% SF750 cement seems to have a higher reactivity than CEM III TM and CEM III 2% ASL cements. This could be due to the higher reactivity of the calcined sediment compared to the slag at an early age and to the greater fineness of the CEM III 10% SF750 cement.

III.3. Hydrate quantification using TGA-DTG analysis

III.3.1. Hydrate quantification using TGA analysis

Figure 6 shows the TGA and DTG curves of the cement pastes after 28 days of hydration.
The result shows that:

- The amount of water bound in CEM III 10% SF750 cement paste is the highest. This means that CEM III 10% SF750 cement seemed to be more reactive than CEM III TM and CEM III 2% ASL cements. This result is consistent with the heat of hydration result which increased the reactivity of the CEM III 10% SF750 cement the most.
- The decomposition temperature of hydrates is similar. This means that the substitution of the slag with the calcined sediment does not cause the modification of the structure of the hydrates.

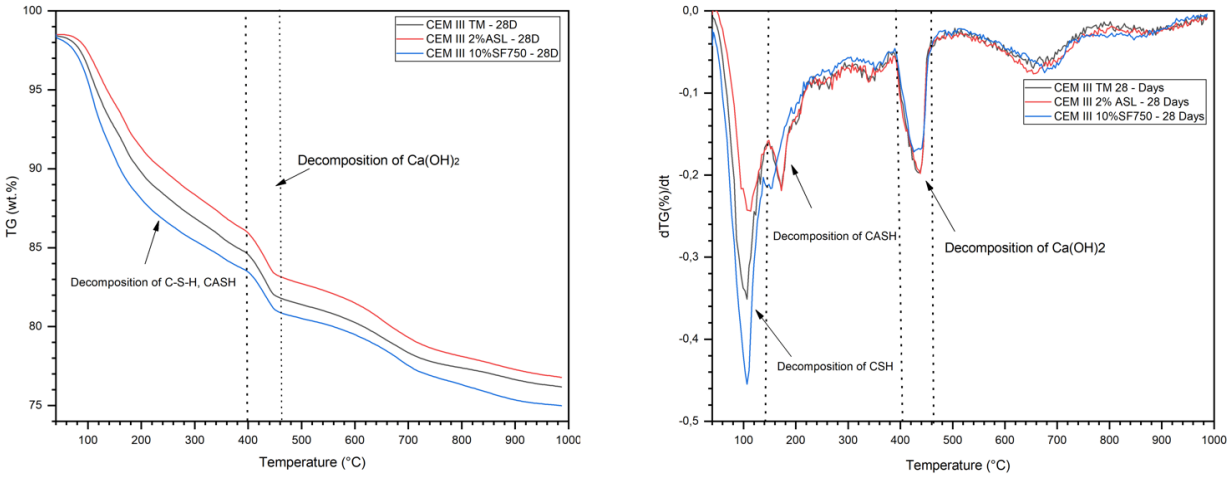

Figure 6 : TGA (left) and DTG (right) curves of the CEM III TM, CEM III 2%ASL and CEM III 10%SF750 cement pastes after 28 days of hydration.
Table 15 summarizes the result of the amount of bound water using the TGA curve.

Table 15 : Amount of bound water and hydrate content of cement pastes using the TGA curve

Cement	Chemical bound water (wt. %) (Result TGA)			Percentage of hydrates	
	For CSH/CASH (wt.%)	For $Ca(OH)_2$ (wt.%)	Total (wt.%)	$Ca(OH)_2$ (%)	CSH/CASH (%)
CEM III TM - 1 day	8.39	2.08	10.47	19.87	80.13
CEM III 2%ASL – 1 day	8.30	2.06	10.36	19.88	80.12
CEM III 10%SF750 – 1 day	8.46	2.1	10.56	19.89	80.11

CEM III TM - 28 days	13.00	3.12	16.12	19.35	80.65
CEM III 2%ASL – 28 days	12.63	3.15	15.78	19.96	80.04
CEM III 10%SF750 – 28 days	15.09	2.9	17.09	16.97	83.03

The result in Table 15 shows that:

- At 1 day of hydration, the hydration of cements is relatively similar when comparing the amount of bound water and the amount of $Ca(OH)_2$.
- At 28 days of hydration, CEM III 10% SF750 cement has a higher amount of bound water and a lower amount of Ca (OH) 2 than two CEM III TM and CEM III 2% ASL cements. This could be due to the pozzolanic reaction of the sediment which consumes $Ca(OH)_2$ to form C-S-H according to Eq (4) and Eq (5). In addition, the $Ca(OH)_2$ content in CEM III TM and CEM III 2% cement pastes is almost constant between 1 and 28 days. On the other hand, it decreases from 19.89% to 16.97% after 28 days of hydration in CEM III 10% SF750 cement paste. This result confirms the higher reactivity of the calcined sediment compared to the slag.

III.3.2. Hydrate quantification using the DTG curve deconvolution method

The result of hydrate quantification using the DTG curve deconvolution method is presented in Table 16.

Table 16 : Hydrate content of cement pastes after 28 days of curing using the DTG curve deconvolution method

Cement	Peak area				Percentage of hydrates (%)		
	C-S-H	CASH	$Ca(OH)_2$	Total	C-S-H	CASH	$Ca(OH)_2$
CEM III TM	10.74	18.18	6.85	35.77	30.02	50.82	19.15
CEM III 2%ASL	10.44	15.68	6.82	32.94	31.69	47.60	20.70
CEM III 10%SF750	14.54	14.94	6.00	35.48	40.98	42.10	16.91

The result shows that:

- The content of the phases (C-S-H/CASH) of cement pastes is similar (approximately 30% for C-S-H and 48% for CASH). However, in CEM III 10% SF750 cement paste, this content is higher for C-S-H (41%) and lower for CASH (42%). This is interesting because the C-S-H phase contributes more to mechanical development than the CASH phase.
- The Portlandite content in the cement pastes determined by the deconvolution method is identical to the content measured by the TGA analysis method. This result shows the reliability of the deconvolution method used in this study.

III.4. Hydrates identified using XRD analysis

The different phases present in the cement pastes after 28 days of hydration identified by XRD analysis are shown in Figure 7. On the three diffractograms, the same hydrates are present, such as: Portalndite, Ettringite, Afm, and Calcite. However, the presence of quartz is only identified on the diffractogram of CEM III 10%SF750 due to the presence of this phase in the calcined sediment.

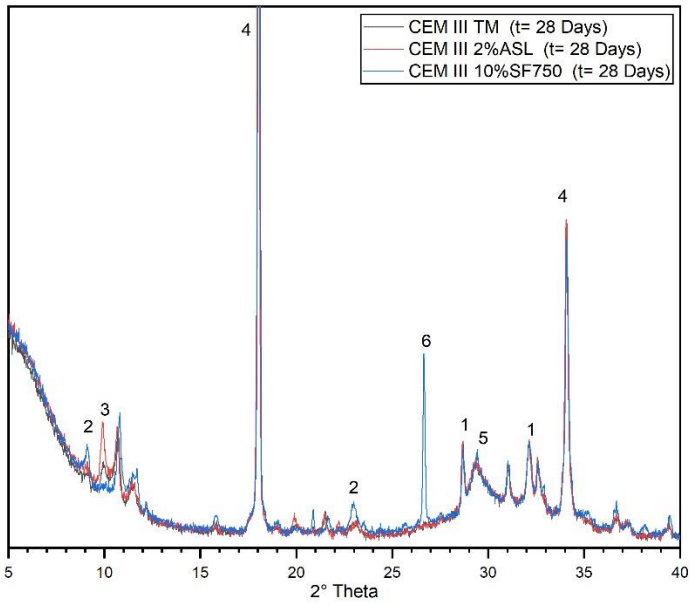

Figure 7 : XRD patterns of CEM III TM, CEM III 2%ASL and CEM III 10%SF750 cement pastes after 28 days of curing (1: C_3S, 2: Ettringite, 3: Afm, 4: Portlandite, 5: Calcite, 6: Quartz)

III.5. Chemical composition of hydrates measured by the SEM-EDS analysis

The chemical composition of the hydrates (except $Ca(OH)_2$) of the pastes of CEM III TM, CEM III 2% ASL, and CEM III 10% SF750 cements after 28 days of hydration is illustrated in Figures 8 - 10 respectively. These ternary diagrams were drawn using data from the analysis of the chemical compositions of the three major elements CaO-SiO_2-Al_2O_3 of hydrates. The diagrams obtained are superimposed on the ternary diagram produced by Lothenbach et al [40]. The position of the main hydrates such as: Portlandite, Ettringite, C-S-H (with two C/S ratios) has been illustrated in this diagram.

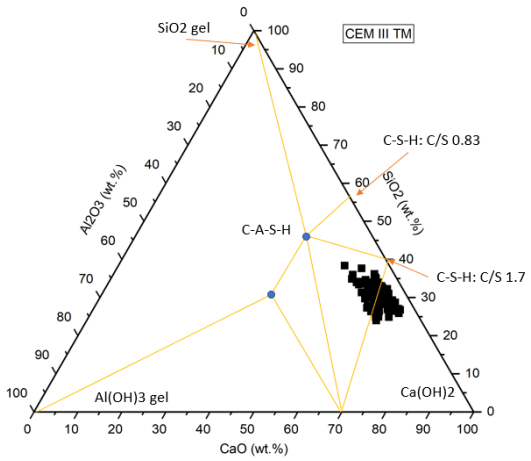

Figure 8 : CaO – SiO_2 – Al_2O_3 diagram of hydrate of CEM III TM cement paste after 28 days of curing

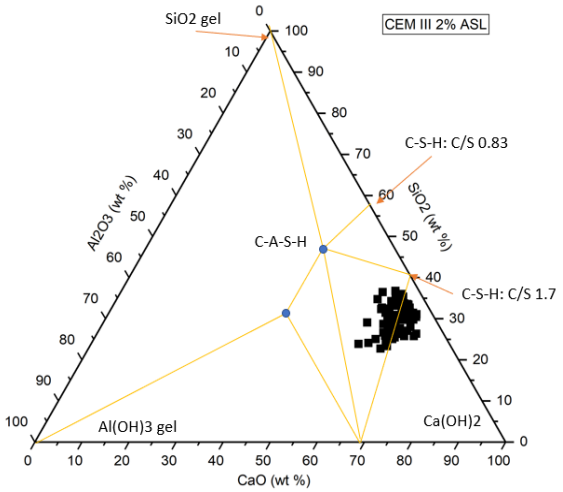

Figure 9 : CaO – SiO_2 – Al_2O_3 diagram of hydrate of CEM III 2%ASL cement paste after 28 days of curing

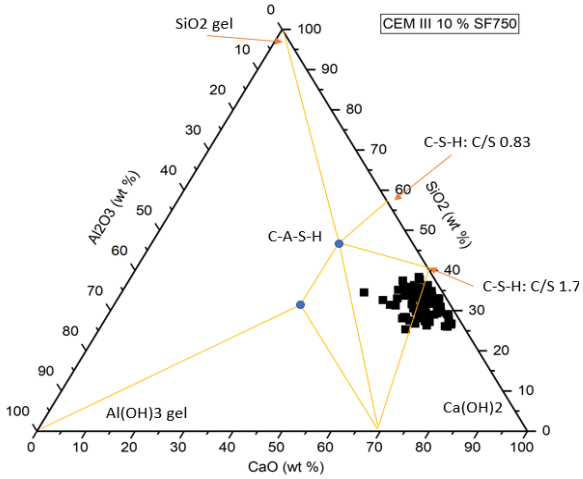

Figure 10 : CaO – SiO_2 – Al_2O_3 diagram of hydrate of CEM III 10%SF750 cement paste after 28 days of curing

The result shows that:

- The chemical composition of the hydrates formed in the pastes of CEM III TM, CEM III 2% ASL and CEM III 10% SF750 cements is similar (same position on the ternary diagram).

- The hydrates are positioned in the zone with a CaO/SiO_2 ratio greater than 1.7. The experimental ratios obtained are higher than the theoretical ratio (CaO/SiO_2 = 1.7) in the literature [16, 41]. However, this hydrate ratio in this study is lower when compared with the CaO/SiO2 hydrate ratio determined on CEM I cement paste in the study by Cassagnabère et al [42] (CaO/SiO_2 = 3.31).

Figure 11 shows the CaO/SiO_2 ratio of hydrates measured by SEM-EDS analysis and by theoretical calculation from the chemical composition of cements.

The result shows that:

- CEM III 10% SF750 cement has a CaO/SiO_2 lower hydrate ratio than the two CEM III TM and CEM III 2% ASL cements. This is consistent with the theoretical ratio calculated from the chemical composition of the cements.
- Good consistency between the experimental and theoretical values of the CaO/SiO2 ratio is expressed in a homogeneous distribution of hydrates.

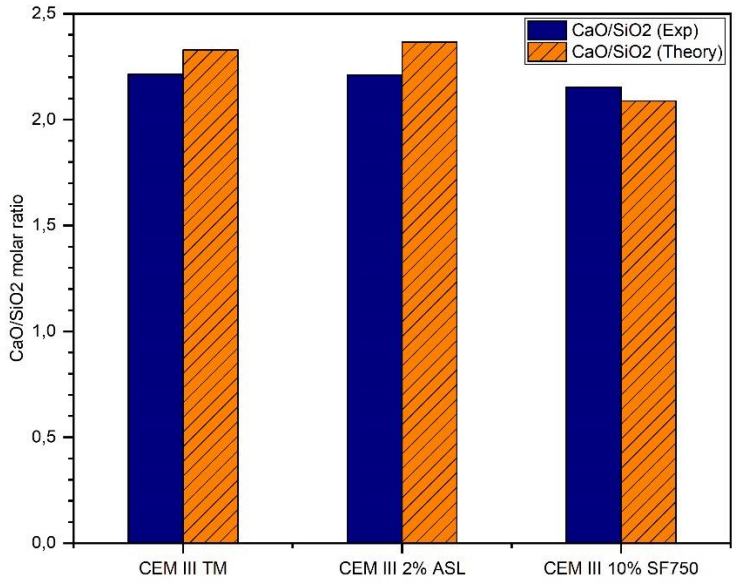

Figure 11 : CaO/SiO_2 ratio of hydrates measured by SEM-EDS analysis and by theoretical calculation from the chemical composition of cements

III.6. Compressive strength of mortars

The compressive strength of CEM III TM, CEM III 2%ASL and CEM III 10% SF750 cements measured on the mortar sample has been presented in Table 17. CEM III TM and CEM III 2%ASL cements have similar resistance at all times of the test. However, CEM III 10% SF750 cement exhibits higher strength than CEM III TM and CEM III 2%ASL cements at early ages (2 and 7 days). This result shows that the calcined sediment would be more reactive than the slag at early ages. This is consistent with the results obtained by isothermal calorimetry analysis and TGA -DTG analysis. According to standard NF EN 197-1, these cements are classified in class CEM III 42.5.

Table 17 : Compressive strength of CEM III TM, CEM III 2%ASL and CEM III 10%SF750 over time of hydration

Cement	2 Days	7 Days	28 Days

CEM III TM (Mpa)	14.79	30.16	47.33
CEM III 2%ASL (Mpa)	14.05	29.58	46.96
CEM III 10%SF750 (Mpa)	19.68	38.11	48.98

III.7. Porosity of mortars

The porosity of CEM III TM, CEM III 2% ASL and CEM III 10% SF750 mortars measured after 2 and 28 days of hydration is presented in Table 18. The result shows that:

- The porosity of CEM III TM and CEM III 2%ASL mortars is similar at all times of the test. This is in accordance with the results of previous tests which showed identical behavior during the hydration of the two cements.
- CEM III 10% SF750 cement exhibits lower porosity than CEM III TM and CEM III 2%ASL cements at all times of the test. This could be due to the higher reactivity of the calcined sediment, which promotes hydration and hydrate formation to reduce porosity.

Table 18 : Total porosity of the CEM III TM, CEM III 2%ASL and CEM III 10%SF750 mortars measured by MIP over time of hydration

Time (Days)	CEM III TM (%)	CEM III 2%ASL (%)	CEM III 10%SF750 (%)
2 Days	17.54	17.41	14.67
28 Days	10.93	11.63	9.58

In order to better understand the effect of calcined sediment on cement hydration, the pore size distribution of mortars after 2 and 28 days of curing is shown in Figure 12 and Figure 13 respectively.

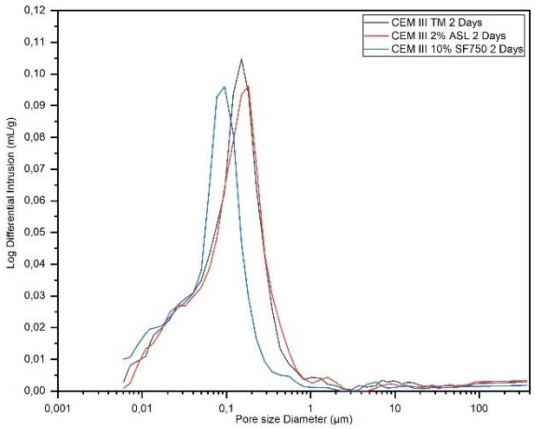

Figure 12 : Pore size distribution of CEM III TM, CEM III 2%ASL and CEM III 10%SF750 mortars after 2 days of curing measured by MIP

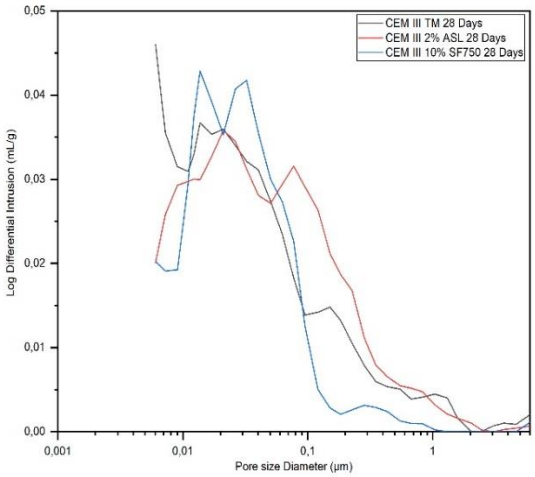

Figure 13 : Pore size distribution of CEM III TM, CEM III 2%ASL and CEM III 10%SF750 mortars after 28 days of curing measured by MIP

The results shown in Figure 12 and Figure 13 shows that:

- The pore size distribution of CEM III TM and CEM III 2% ASL cements is identical.
- CEM III 10% SF750 cement has lower porosity and pore size than CEM III TM and CEM III 2% ASL cements. However, the difference at 28 days is small. This result confirms the beneficial effects of the calcined sediment on the hydration of the cement when compared with the slag.

IV. Conclusion

The objective of this study is to assess the feasibility of recovering sediments in the manufacture of CEM III cement. Raw sediment was used as the raw material to produce the clinker. Other sediment treated by the Flash calcination method was used to replace part of the slag in the CEM III cement. The main results obtained are as follows:

- The sediment-based clinker (2%.wt of the sediment incorporated into the raw mixture) has been successfully synthesized in the laboratory. The characteristics of the sediment-based clinker are comparable to those of the reference clinker (without sediment).
- The calcination activated the pozzolanic reactivity of the sediment by consulting the result of the Frattini's test.
- CEM III 10% SF750 cement exhibits a more reactive hydration behavior than the two cements, CEM III TM and CEM III 2%ASL, by consulting the results of isothermal calorimetry analysis, thermogravimetric analysis, and compressive strength.
- CEM III 10% SF750 cement has a higher C-S-H content determined by the DTG curve deconvolution method than CEM III TM and CEM III 2% ASL cements.
- The chemical composition of hydrates formed during the hydration of cements measured by SEM-EDS analysis is similar. CEM III 10% SF750 cement has a lower CaO/SiO_2 hydrate ratio than CEM III TM and CEM III 2% ASL cements due to the higher SiO_2 content of the sediment compared to the slag.
- Replacing some of the slag with calcined sediment improves the mortars' resistance to early ages significantly.
- The calcined sediment makes it possible to reduce the porosity and the size of the pores of the mortar compared to CEM III TM and CEM III 2% ASL mortars.

- The three cements, CEM III TM, CEM III 2%ASL, and CEM III 10%SF750, have a compressive strength greater than 42.5 Mpa at 28 days of curing. They are classified in class CEM III 42.5, according to standard NF EN 197-1.

Reference

1. Ministry of Ecology, Energy, Sustainable Development and Territorial Planning, Circulaire du 04/07/08 relative à la procédure concernant la gestion des sédiments lors de travaux ou d'opérations impliquant des dragages ou vurages maritimes et fluviaux, Off.
2. Directive 2008/98/EC of the European Parliament and of the Council of 19 November 2008 on waste and repealing certain Directives, O.J.L 312-3, 2008.
3. Tran, N.T.: Valorisation de sédiments marins et fluviaux en technique routière, (2009)
4. M.Dia: Traitement et valorisation de sédiments de dragage phosphatés en technique routière - Thèse de doctorat, (2013)
5. Benzerzour, M., Maherzi, W., Amar, M.A.A., Abriak, N.E., Damidot, D.: Formulation of mortars based on thermally treated sediments. J. Mater. Cycles Waste Manag. 20, 592–603 (2018). https://doi.org/10.1007/s10163-017-0626-0
6. Amar, M., Benzerzour, M., Abriak, N.E.: Towards the establishment of formulation laws for sediment-based mortars. J. Build. Eng. 16, 106–117 (2018). https://doi.org/10.1016/j.jobe.2017.12.011
7. Bouchikhi, A., Maherzi, W., Benzerzour, M., Mamindy-Pajany, Y., Peys, A., Abriak, N.E.: Manufacturing of low-carbon binders using waste glass and dredged sediments: Formulation and performance assessment at laboratory scale. Sustain. 13, (2021). https://doi.org/10.3390/su13094960
8. Aouad, G., Laboudigue, A., Gineys, N., Abriak, N.E.: Dredged sediments used as novel supply of raw material to produce Portland cement clinker. Cem. Concr. Compos. 34, 788–793 (2012). https://doi.org/10.1016/j.cemconcomp.2012.02.008
9. Faure, A., Coudray, C., Anger, B., Moulin, I., Colina, H., Izoret, L., Théry, F., Smith, A.: Beneficial reuse of dam fine sediments as clinker raw material. Constr. Build. Mater. 218, 365–384 (2019). https://doi.org/10.1016/j.conbuildmat.2019.05.047
10. Anger, B.: Caractérisation des sédiments fins des retenues hydroélectriques en vue d ' une orientation vers des filières de valorisation matière, (2014)
11. Kajaste, R., Hurme, M.: Cement Industry Greenhouse Gas Emissions - Management Options and Abatement Cost. J. Clean. Prod. 112, 4041–4052 (2015)
12. De Weerdt, K., Haha, M. Ben, Le Saout, G., Kjellsen, K.O., Justnes, H., Lothenbach, B.: Hydration mechanisms of ternary Portland cements containing limestone powder and fly ash. Cem. Concr. Res. 41, 279–291 (2011). https://doi.org/10.1016/j.cemconres.2010.11.014
13. Zined, B.: Influence de la microstructure sur le transport diffusif des pâtes, mortiers et bétons à base de CEM I avec ajout de fumée de silice, (2016)
14. Aintcin P.C, Pinsonneault P., R.G.: The use of condensed silica fume in concrete, Symposium on the effects of fly ash incorporation in cement and concrete, Boston, USA, pp. 316- 325.
15. Berthomier, M.: Etude de la lixiviation de l'aluminium de matériaux cimentaires à base de CEM III utilisés dans les canalisations d'eau potable : approche expérimentale et

numérique. (2020)

16. Nonat, A.: Chapitre2: L'hydratation des ciments- La durabilité des bétons. (2008)
17. Escadeillas, G., Hornain, H.: La durabilité des bétons vis-a-vis des environnements chimiquement agressifs. La Durabilité Des Bétons. 613–705 (2008)
18. Lea: Lea's chemistry of cement and concrete. Elsevier. (2003)
19. Les laitiers sidérurgiques. (2019)
20. NF EN 1097-7. Tests for Mechanical and Physical Properties of Aggregates—Part 7: Determination of the Particle Density of Filler— Pyknometer Method; BSI: London, UK, 2008.
21. NF EN 12457-2. Leaching-Compliance Test for LeachingofGranular Waste Materials and SludgesPart 2: One Stage Batch Test at a Liquid to Solid Ratio of10 l/kgfor Materials with Particle Size Below 4 mm (without or with Size Reduction); BSI: London, UK, 2002.
22. San Nicolas, R.: Approche performantielle des bétons avec métakaolins obtenus par calcination Flash
23. Young, J.F.: Reaction Mechanisms of Organic Admixtures With Hydrating Cement Compounds. Transp. Res. Rec. 1–9 (1976)
24. Msinjili, N.S., Gluth, G.J.G., Sturm, P., Vogler, N.: Comparison of calcined illitic clays (brick clays) and low- grade kaolinitic clays as supplementary cementitious materials. 2, (2019). https://doi.org/10.1617/s11527-019-1393-2
25. Teklay, A., Yin, C., Rosendahl, L.: Flash calcination of kaolinite rich clay and impact of process conditions on the quality of the calcines: A way to reduce CO2 footprint from cement industry. Appl. Energy. 162, 1218–1224 (2016). https://doi.org/10.1016/j.apenergy.2015.04.127
26. Jiang, T., Li, G., Qiu, G., Fan, X., Huang, Z.: Thermal activation and alkali dissolution of silicon from illite. Appl. Clay Sci. 40, 81–89 (2008). https://doi.org/10.1016/j.clay.2007.08.002
27. NF EN 196-5 : Méthodes d'essais des ciment - Partie 5 : Essai de pouzzolanicité des ciments pouzzolaniques. (2013)
28. Faure, A.: Capacité d ' un sédiment à se substituer à la fraction argileuse de la matière première de l ' industrie des liants hydrauliques - Thèse de doctorat, (2017)
29. Taylor HFW: Cement chemistry. (1997)
30. Kleib, J., Aouad, G., Abriak, N.E., Benzerzour, M.: Production of Portland cement clinker from French Municipal Solid Waste Incineration Bottom Ash. Case Stud. Constr. Mater. 15, e00629 (2021). https://doi.org/10.1016/j.cscm.2021.e00629
31. P. Schläpfer, R. Bukowski, Untersuchungen über die Bestimmung des freien Kalkes und des Kalziumhydroxydes in Zement-klinkern, Zementen, Schlacken und abgebundenen hydraulischen Mörteln, Eidgenössische Materialprüfungsanstalt an der E.T.H. in Zürich. 63.
32. AFNOR: NF EN 196-3. Methods of testing cements. Part 3 – Determination of setting times and soundness, 2017.
33. Kleib, J., Aouad, G., Khalil, N., Zakhour, M.: Incorporation of zinc in calcium sulfoaluminate cement clinker. Adv. Cem. Res. 1–7 (2020). https://doi.org/10.1680/jadcr.19.00125
34. Klimesch, D.S., Ray, A.: Use of the second-derivative differential thermal curve in the evaluation of cement-quartz pastes with metakaolin addition autoclaved at 180°C.

Thermochim. Acta. 307, 167–176 (1997). https://doi.org/10.1016/S0040-6031(97)00409-7

35. V. Baroghel-Bouny: Caractérisation des pâtes de ciment et des bétons: méthodes, analyses, interprétations, Editions LCPC (Eds), Paris, France, 1994. (1994)
36. Nicolas Chapleau, Cécile Mangavel, Jean-Pierre Compoint, M. de L.: Effect of high-pressure processing on myofibrillar protein structure. Sci. Food Agric. (2003)
37. NF EN 196-1: Méthode d'essai des ciments- Partie 1 : Détermination des résistance. (2016)
38. Association Française de Normalisation (AFNOR): NF EN 197-1: Composition, spécifications et critères de conformité des ciment courant.
39. Elkarim, M., Bulteel, D., Potier, G., Michel, F., Zhao, Z., Courard, L.: Use of grinded hardened cement pastes as mineral addition for mortars. (2020). https://doi.org/10.1016/j.jobe.2020.101863
40. Lothenbach, B., Scrivener, K., Hooton, R.D.: Supplementary cementitious materials. Cem. Concr. Res. 41, 1244–1256 (2011). https://doi.org/10.1016/j.cemconres.2010.12.001
41. Bentz, D.P.: CEMHYD3D : A Three-Dimensional Cement hydratation and Microstructure Development Modelling Package Version 2.0.
42. Cassagnabère, F., Mouret, M., Escadeillas, G.: Early hydration of clinker-slag-metakaolin combination in steam curing conditions, relation with mechanical properties. Cem. Concr. Res. 39, 1164–1173 (2009). https://doi.org/10.1016/j.cemconres.2009.07.023

Partie 2 : Fabrication des additions minérales par la méthode de calcination Flash

Dans cette seconde partie de la thèse, nous étudions et optimisons la méthode de flash calcination. Différents paramètres d'influences ont ainsi été optimisés tel que la température de calcination et le taux de substitution. Une étude de l'hydratation des liants ainsi obtenue y est également présentée.

Chapitre 4 : Optimisation de la température du processus de calcination

I. Introduction

La qualité du produit calciné par la méthode de calcination Flash dépend de plusieurs paramètres tels que : la granulométrie du matériau, la température de calcination, etc. Par conséquent, pour optimiser le processus de fabrication de l'addition minérale, le sédiment a été testé aux trois températures (650 °C, 750 °C et 800 °C). La température optimale est la température répondant aux exigences en termes de : performance mécanique des matrices cimentaires produite sur la base de ce matériau, réactivité pouzzolanique, qualité du gaz émis et consommation d'énergie. La température de 750 °C ensuite a été adoptée pour la fabrication en grand volume de l'addition minérale.

II. Démarche expérimentale

Le sédiment utilisé dans cette étude est un sédiment fluvial provenant de la région des Hauts de France (France). D'abord, le sédiment a été homogénéisé, séché et broyé finement, pour être ensuite caractérisé afin de déterminer la composition chimique, minéralogique ainsi que la teneur en éléments traces métalliques du sédiment. La calcination du sédiment a été réalisée dans un four de calcination Flash aux trois températures 650 °C, 750 °C et 800 °C. Pour chaque température de calcination, environ 10 kg de sédiment ont été calciné. Enfin, les produits de calcination ont été caractérisés afin d'évaluer l'efficacité de chaque température de calcination. En outre, la réactivité pouzzolanique de ces sédiments a été mesurée en utilisant le test Frattini et l'essai de consommation de la chaux en comparant avec une référence (Métakaolin). La contribution des additions minérales (les sédiments calcinés, le sédiment brut, le métakaolin) au développement mécanique, ainsi que la microstructure du matériau a été évaluée à l'aide de l'analyse de résistance en compression des mortiers et de l'analyse de la porosité au mercure.
La démarche expérimentale dans ce chapitre est présentée ci-dessous :

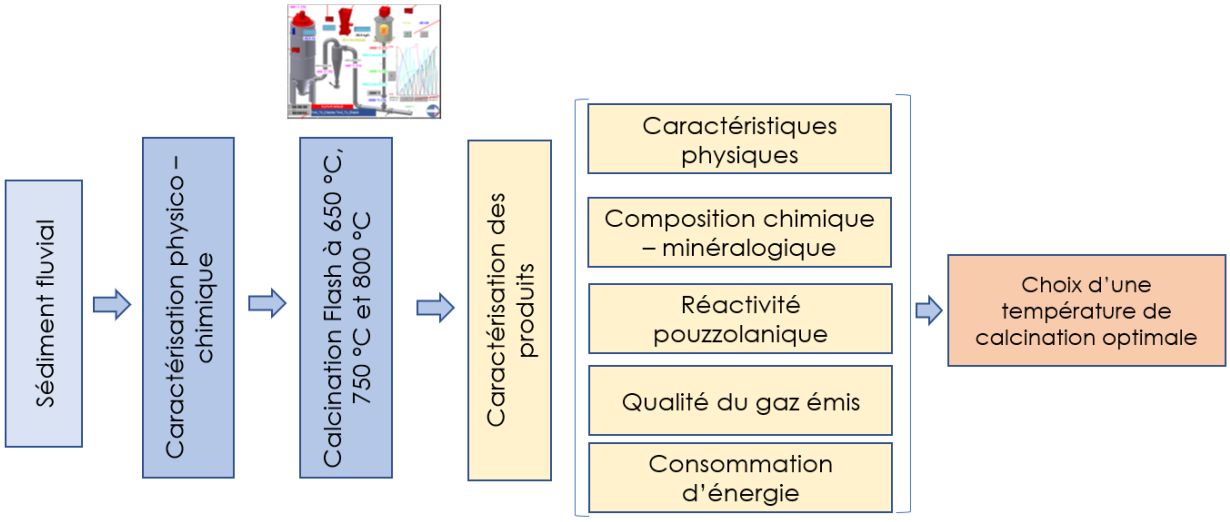

III. Résultat du chapitre

Les résultats de ce chapitre sont présentés dans l'article 5.

***Article 5**: The pozzolanic activity of the sediment treated by the Flash calcination method*

Résumé : Le sédiment utilisé dans cette partie est un sédiment non inerte non dangereux. Ce sédiment a été d'abord homogénéisé, puis finement broyé avant la calcination. La calcination a été effectuée à 650 °C, 750 °C, 800°C. À chaque température de calcination, les gaz émis pendant le processus de calcination ont été récupérées pour analyse.
Les sédiments calcinés ont été ensuite caractérisés. La réactivité pouzzolanique de ces sédiments a été mesurée en utilisant le test Frattini et l'essai Chapelle (suivi de la consommation de la chaux) en comparant avec Métakaolin comme une référence.
Les résultats montrent que :

- Le sédiment brut utilisé dans cette étude est un sédiment qui contient une teneur élevée en matières organiques et une teneur élevée en Zinc et en sulfate. La présence de ces éléments pourrait être à l'origine d'effets néfastes sur l'hydratation du ciment tels que : le retard de l'hydratation du ciment (l'analyse de chaleur de l'hydratation par calorimétrie isotherme)
- La calcination par la méthode Flash a éliminé considérablement la teneur des matières organiques dans le sédiment.
- La calcination a modifié certaines caractéristiques physiques du sédiment tel que la granulométrie et la finesse BET. Une augmentation de la finesse a été observée sur les sédiments calcinés. Cependant, l'augmentation de la température de 750 °C à 800 °C provoque une diminution de la finesse BET du sédiment calciné.
- L'analyse des teneurs des éléments traces métalliques montre une diminution considérable de ces teneurs dans les sédiments calcinés.
- Une transformation de la phase kaolinite en métakaolin sous l'effet de calcination a été mise en évidence à l'aide de l'analyse DRX sur la fraction des argiles du sédiment.
- Les sédiments calcinés ont également amélioré la cinétique de l'hydratation par rapport au sédiment brut en réduisant le retard d'hydratation. En outre, ils induisent une réduction de la chaleur de l'hydratation mais la chaleur de l'hydratation générée dans les mélanges contenant des sédiments calcinés est plus importante que celle du sédiment brut.
- Le test Frattini effectué après 15 jours a montré la réactivité pouzzolanique du métakaolin et des sédiments calcinés. Par contre, le sédiment brut ne présente pas une réactivité pouzzolanique. On constate aussi que les sédiments calcinés consomment une quantité de chaux plus élevée que le sédiment brut mais moins importante que le métakaolin.
- L'analyse de quantification des phases hydratées formées montre que la quantité de C-S-H formée dans les mélanges est relativement similaire, cependant la quantité CASH

formée dans le mélange à base de métakaolin et de chaux est plus importante que les mélanges avec sédiments due à la teneur en alumine plus élevée dans le métakaolin.

- L'essai de résistance mécanique montre que le sédiment brut a un effet néfaste sur le développement de la résistance. Par contre les sédiments calcinés ont un effet positif dès 2 jours d'hydratation. Parmi les sédiments calcinés, le sédiment calciné à 750 °C présente la résistance en compression plus élevée par rapport aux sédiments calcinés à 650 °C, 800 °C et le sédiment brut.
- Le sédiment brut a également un effet sur la microstructure du matériau. En effet, l'incorporation du sédiment brut provoque une augmentation de la porosité et la taille des pores. Par contre, l'incorporation des sédiments calcinés diminue la taille des pores dans le matériau.
- L'analyse de qualité du gaz émis au cours du processus de calcination montre que l'augmentation de la température de calcination permet d'améliorer la qualité de gaz émis.
- En comparant les divers critères, la température de calcination à 750 °C a été retenue pour le processus de calcination.

Date de soumission	Accepté
Statut	11 Octobre 2021
Journal	Waste and Biomass Valorization https://www.editorialmanager.com/wave/default1.aspx

Article 5 : The pozzolanic activity of the sediment treated by the Flash calcination method

Duc Chinh CHU[(1)], Mouhamadou AMAR[(1)], Joelle KLEIB[(1)], Mahfoud BENZERZOUR[(1)], Damien BETRANCOURT[(1)], Nor-Edine ABRIAK[(1)], Jaouad NADAH[(2)],

[(1)] Univ.Lille, IMT Lille Douai, Univ.Artois, Yncrea Hauts-de-France, ULR 4515-LGCgE, 6 Laboratoire de Génie civil et géo-Environnement, F-59000, Lille, France

[(2)] EQIOM Le LAB, CRT 1 Parc Vendôme – 460 Allée de l'Innovation, 59810 LESQUIN, France.

[(*)] **Corresponding author:**

duc.chinh.chu@imt-nord-europe.fr

Abstract

The dredged sediment has been positioned for years as alternative materials in the construction field. However, it is often necessary to apply a treatment to improve their reactivity and performance. This article aims to study the pozzolanic reactivity of fluvial sediment treated by flash calcination method at different temperatures 650 °C, 750 °C, and 800 °C. The physico-chemical, mineralogical, and environmental characteristics were studied for treated (flash-calcined sediment) and raw sediment. The pozzolanic reactivity of the flash-calcined sediments was estimated with Frattini's test, isothermal calorimetry test, lime consumption analysis and compressive strength then compared to metakaolin which is considered as the reference. The results of the compressive strength of mortars show the detrimental effect of raw sediment on the development of resistance. Contrary to the raw sediment, the treatment of the sediments by flash calcination activates the pozzolanic reactivity of the clay phases and considerably improves the contribution of the sediments to the development of resistance and the porous structure. Moreover, the sediment calcined at 750 °C gives better properties than those obtained at 650 °C and 800 °C. The result demonstrates the feasibility of using calcined sediments as a pozzolanic mineral addition in a cementitious material.

Graphic Abstract

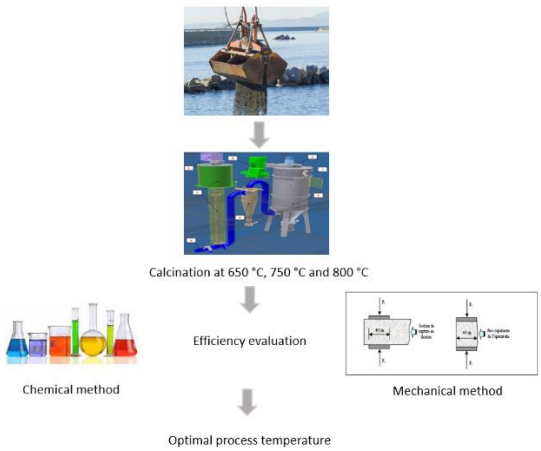

Keywords: Sediment, Flash calcination, Pozzolanic, Reactivity, Cement, Compressive strength.

Statement of Novelty

The originality of this research is the use of an innovative calcination technique to treat the sediment. The raw sediment is a polluted sediment and has harmful effects on the hydration of the cement. However, Flash calcination significantly improved the hydration behavior of sediment compared to raw sediment. The different methods were used to demonstrate the

beneficial effects provided by sediments calcined at different temperatures and to choose an optimal calcination temperature.

1 Introduction

Nowadays, concrete is the most used material in the construction field and public works [1]. However, the production of this material has a great impact on the environment due to the requirement of significant extraction of raw materials. With a global cement production of 4.6 billion tonnes in 2016 and an average annual growth of 6.9% [2], the global cement production process releases between 652 kg and 894 kg of CO_2 for each tonne of cement produced [3]. Above 7% of the worldwide CO_2 emissions are related to the cement manufacturing [2]. To achieve the goal of reducing CO_2 emissions by 2050 and to attend carbon neutrality, the use of mineral additions to replace part of the cement is considered one of the most promising solutions [4]. To this day, metakaolin, slag, fly ash, silica fume, and limestone fillers are the most widely used mineral additions in the construction industry. Thanks to their pozzolanic reactivity, the durability properties and the mechanical performances of concrete have improved [5]. However, one of the main disadvantages of large scale application of metakaolin, is the limititation of the high purity kaolinite deposits [6]. In addition, environmental restrictions are increasingly strict (2006/21/EC) for an ecological transition and the protection of biodiversity.

Each year, the dredging operations for maintenance at ports and inland waterways generate around 300 million tonnes of sediment in Europe [6], with 56 million m^3 are in France. Several studies have demonstrated the potential for sediment recovery in various fields: road technology [7, 8] as a mineral addition in mortar and concrete [4, 9], [10, 11] and as a raw material in the manufacture of cement [12, 13]. Nevertheless, most studies of valorization of sediments as an addition are based on the traditional calcination method to activate their pozzolanic reactivity. This method requires significant energy consumption and arises a significant ecological problem [14].

Snellings et al [15] studied the effect of the flash calcination of dredged sediment, from the port of Antwerp (Belgium), at different temperatures (820 °C, 865 °C and 905 °C) on their physico-chemical properties and on their pozzolanic reactivity. The treatment reduced the total organic carbon content by 85% or more. The clay minerals in the sediment were completely dehydroxylated. The amorphous phase formed during calcination constitutes the major part of the calcined material. In addition, the result of the calorimetric analysis showed that the calcined sediments had pozzolanic reactivity more than that of siliceous fly ash, however less than that of metakaolin. Snellings et al [6], showed also in another study that increasing the amount of cement replacement from 20 wt% to 40 wt.% by calcined sediment slowed down the strength development. Whereas, at 91 days of hydration, the mortar with 20 wt.% calcined sediment substitution gives similar strength as the reference mortar.

Amar et al [16] compared the pozzolanic reactivity of sediment treated by flash calcination at 820 °C and by traditional calcination method. The results showed that the flash calcination has strongly modified the physico-chemical and mineralogical properties and improved the pozzolanic reactivity. The study showed also that the activity index (X_A) of mortars containing 25% wt of flash sediments as cement subsitution, is higher than the one containing traditional calcined sediment at 28 days.

This study focuses on optimizing the flash calcination process of sediment on an semi-industrial scale. First, the sediment was calcined at three different temperatures (650 °C, 750 °C and 800 °C). Then, the pozzolanic reactivity of the calcined sediments and the raw sediment was examined by several methods in order to assess the performance of the method and the effect of the sediments on the hydration of the cementitious material. Finally, these results were used to choose an optimal calcination temperature.

1.1 Flash calcination method

The Flash calcination method is a technique of heat treatment of finely ground materials under high temperature in the short term. It has been applied to the activation of clays [17, 18]. Such calcination aims to produce metastable mineral phases or complex morphology [19]. Besides, high-temperature calcination and thermal shock increase the surface defects of crystallites and increase the number of reactive sites [20].

In a calciner, mineral particles get heated up and then undergoes a series of conversion processes. During calcination, the mineral materials occurs the flowing reactions Eq(1) -> Eq (5) [21]:

H_2O (libre, bound) $\rightarrow H_2O$. (1)

$Al_2O_3.2SiO_2.2H_2O \rightarrow Al_2O_3.2SiO_2$ (metakaolinte) + $2H_2O$ (2)

$2(Al_2O_3.2SiO_2) \rightarrow 2Al_2O_3.3SiO_2$ (spinel) + SiO_2 (silica amorphous) (3)

$3(Al_2O_3.3SiO_2) \rightarrow 2(3Al_2O_3.2SiO_2)$ (mullite) + 5 SiO_2 (silica amorphous) (4)

SiO_2 (silica amorphous) $\rightarrow SiO_2$ (cristobalite) (5)

In addition, under the thermal effect, the other clay minerals will be dehydroxylated according to the following equations (Table 1):

Table 1 Optimal heat treatment of some mineral's phases

Mineral phases	Optimal heat treatment
▪ **Illite:** $(K, H_3O)(Al, Mg, Fe)_2(Si, Al)4O10[(OH)_2, (H_20)] \rightarrow 3.5\ H_2O + (K)(Al, Mg, Fe)_2(Si, Al)_4O_{10.5}$ (6)	700°C [22] [23] 715°C [24] 850 °C [25]
▪ **Smectite:** $(K, Ca)(Si_4, Al)O_{10}(Al, Mg, Fe, Ti)(OH)_2 \rightarrow H_2O + (K,Ca)(Si_4, Al)O_{11}(Al, Mg, Fe, Ti)$ (7)	900°C [26] 930°C [27] 950°C [28]
▪ **Muscovite:** $K\,Al_2\,(Si_3\,Al)\,O_{10}\,(OH)_2 \rightarrow H_2O + KAl_2(Si_3Al)\,O_{11}$ (8)	850°C [29]
▪ **Chlorite:** $(Fe, Mg, Al)_6(Si, Al)_4O_{10}(OH)8 \rightarrow 4H_2O + (Fe, Mg, Al)_6(Si, Al)_4O_{14}$ (9)	800°C [30]

The above reactions are influenced by several parameters such as the kaolinite structure, the rate of heating, and the particle size [22].

1.2 Pozzolanic reaction in the cementitious material

A constituent having pozzolanic properties, contains silicate and aluminate phases allowing hydrate production of ternary system $CaO\text{-}SiO_2\text{-}Al_2O_3\text{-}H_2O$ in the presence of lime and water. The pozzolanic addition used as a substitute for the clinker, will react with portlandite (CH) to form the hydrated calcium silicate "pozzolanic" (pozzolanic C-S-H (II)). This hydrate generally has a C/S lower ratio than that of C-S-H formed from the hydration of cement without pouzzolanic addition. Unlike C-S-H (II), the C/S ratio of C-S-H (I) is independent of temperature and the Ca^{2+} concentration of the solution in pores. The pozzolanic reaction can be described by the following equations [23]:

- Dissolution of SiO_2:

$$(SiO_2)_{soluble} + 2OH^- \rightarrow H_2SiO_4^{2-} \quad (10)$$

- Pozzolanic C-S-H precipitation:

$$xCa^{2+} + H_2SiO_4^{2-} + 2(x-1)\,OH^- + y\,H_2O \rightarrow C_xSH_y \quad (11)$$

In general, the pozzolanic C-S-H stoichiometry is $C_{1.1}SH_{3.9}$. In addition, the presence of a large amount of aluminate can allow the formation of other phases such as C_2ASH_8 (stratlingite); C_4AH_{13} or hydrogrenat (C_3AH_6).

2 Materials and experimental methods

2.1 Presentation of the kiln and the Flash calcination process

The flash calcination tests are carried out in a flash furnace available in research center of IMT Nord-Europe (France). The product output can reach 20 kg of material per hour. A propane gas burner providing a power between 10 - 50 kW allows materials to be calcined up to a temperature of 850 °C. Fig. 1 illustrates the schematic of the flash calcination furnace used in this study.

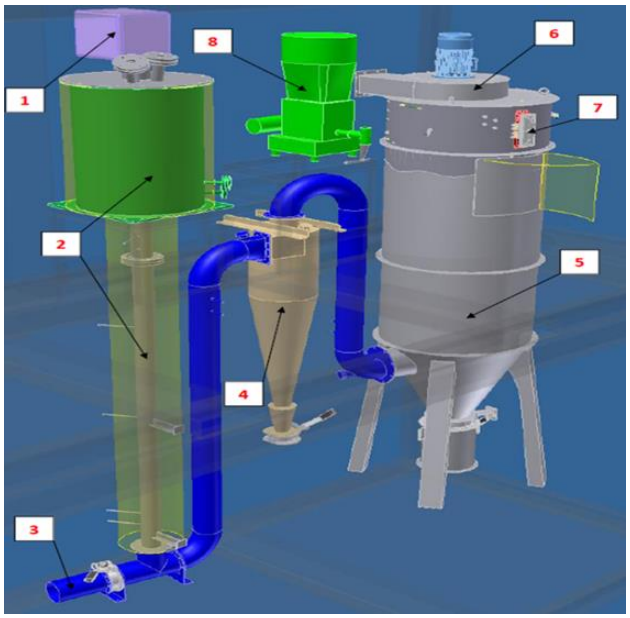

Fig. 1 Flash calcination process representation (CERI MP at IMT Nord -Europe)

The principle and operation of the flash oven was early described by Teklay et al. [17]. However, several parameters are adjustable such as burner power, air-flow, material flow and the calcination temperature. These parameters should be adapted regarding the material properties. In this present study, the sediment was calcined at three different temperatures of 650 °C, 750 °C, and 800 °C as previously tested for other types of materials [24, 25]. Except for the calcination temperature, all the other parameters were maintained constant during calcination. The optimum calcination temperature must meet the following requirements:

- Considerable removal of organic matter in the sediment.
- Improvement in the pozzolanic reactivity of the products (degree of dehydroxylation of clay minerals, in particular, kaolinite).
- Mechanical performance of calcined sediments-based mortars compared to reference mortars (without sediments).
- Quality of the fumes rejected during calcination (analysis of the chemical composition of the rejected fumes).
- The lowest possible energy consumption.

2.2 Materials and methods

The sediment used in this study is the fluvial sediment collected from the Noyelles-Sous-Lens disposal site in the Haut de France region in France. First, this sediment was homogenized and dried at 105 °C to constant weight, then finely ground before flash calcination. Sediments calcined at the three different temperatures 650 °C, 750 °C, and 800 °C are referred as SF 650, SF 750, and SF 800 respectively.

The cement used is the Ordinary Portland Cement CEM I 52.5N from EQIOM specified in European standard NF EN 196-1 [26]. The sand used for mortars preparation is the standardized sand with a particle size between 0.08 and 2 mm according to the standard NF EN 196-1 [26]. A commercial product metakaolin (MK) was used as the reference for pozzolanic reactivity. Table 2 presents the nomenclatures used in this study.

Table 2 Nomenclature used in the study

Materials	**Nomenclature**
Ordinary Portland Cement CEM I 52.5N	OPC
Metakaolin	MK
Raw sediment	RS
Sediment calcined at 650 °C	SF 650
Sediment calcined at 750 °C	SF 750
Sediment calcined at 800 °C	SF 800
C	CaO
S	SiO_2
A	Al_2O_3
H	H_2O

2.2.1 Material characterization methods

The physicochemical, mineralogical and environmental properties of materials are characterized by several laboratory tests.

- The particle size distribution of the materials was measured by a COULTER laser diffractometry, LS 13 320 type device. The samples were dispersed in ethanol before measurements. The Blaine surface was determined according to the standard NF EN 196-6 [27]. Brunauer-Emmett-Teller (BET) specific surface was measured using the N_2 multipoint adsorption method. The organic matter content of the sediments was determined using the loss on ignition method according to the standard XP P94-047 [35]. The density of the materials is measured according to NF EN 1097-7 [28] using Micromeritics ACCUPYC 1330 Helium Pycnometer. The chemical composition of the materials was determined using X-ray fluorescence analysis (XRF) according to standard NF EN 196-2 [29] with an S4 POINEER equipped with a 4-kW generator and a rhodium anode.
- The mineralogical composition of the materials is identified by X-ray diffraction (XDR) analysis using a Bruker apparatus equipped with a D2 diffractometer with a Cu anode (λ =

1.5406 Å). To specify the nature of the argillaceous phases of the sediment, a specific analysis was carried out on the fraction less than 2 µm of the sediments [8, 11, 30]. For the study of clay species, the angular range explored is between 4° and 35° 2θ with a step size reduced to 0.008 ° 2θ and a step time of 0.84 s/step.

- Thermogravimetric analysis (TGA) is performed using the Netzsch STA 409 device. About 100 mg of the finely ground material was placed in an alumina crucible and heated from 40 °C to 1000 °C with a heating rate of 5° C/min.

Dehydroxylation of kaolinite occurs at the temperature range of 400 °C to 600 °C during calcination [31]. The amount of kaolinite could be determined from the mass loss of water (M_{H2O}) on the TGA curve according to the following equation (Eq (12)):

$$Q_{\text{mineral kaolinite}} = m_{H2O} * \left(\frac{M\ mineral\ kaolinite}{nH2O * M\ H2O} \right) \quad (12)$$

with :

$Q_{\text{mineral kaolinite:}}$ Quantity of the mineral kaolinite.

m_{H2O} : Loss of water due to the dehydroxylation of kaolinite between 400 °C and 600 °C.

$M_{\text{mineral kaolinite}}$: Molar weight of kaolinite

M_{H2O} : Molar weight of water.

n_{H2O} : Number of moles of water released during the dehydroxylation of kaolinite.

For $M_{kaolinite}$ and n_{H2O} values, the stoichiometry of kaolinite in Eq(2) was retained for the dehydroxylation.

The degree of dehydroxylation of kaolinite D_{TG} was made by comparing the amount of kaolinite in the calcined materials and on the raw material according to the following Eq(13):

$$D_{TG} = \left(\frac{Q\ mineral\ kaolinite - Q\ calcined\ kaolinite}{Q\ mineral\ kaolinte} \right) * 100\% \quad (13)$$

With:

$Q_{\text{mineral kaolinite :}}$ Amount of the mineral kaolinite in the raw material.

$Q_{\text{calcined kaolinite}}$: Amount of kaolinite in the calcined material.

- The metallic trace elements in the materials is measured after leaching test according to the standard NF EN 12457-2 [32]. A fraction of aggregates (0-4 mm) was mixed with water with a liquid/solid ratio = 10 L/kg. After 24 hours of leaching, the leachate was filtered at 45 µm, then 2% of HNO_3 acid at a concentration of 63% were added. The chemical analysis is performed by inductively coupled plasma optical emission spectrometer (IPC - OES 5100 Agilent Technologies). Anionic elements were analyzed by chromatography and without acidification. The leaching limit values for inert waste (IW) and non-hazardous waste (NHW) specified in Directive 1999/31/EC were used to verify material compliance.

2.2.2 Methods for evaluating the pozzolanic reactivity of materials

The evaluation of pozzolanic reactivity of calcination products can be carried out using various chemical and mechanical methods. The principle consists in determining the content of $Ca(OH)_2$ consumed by reactive components in pozzolanic materials [33].

a. Frattini's test (NF EN 196-5 [34])

The Frattini's test was used in previous studies [11, 30, 35] to assess the pozzolanic reactivity of materials. The essay consists to react 16 grs of CEM I cement and 4 grs of material in 100 ml of distilled water. Then, the mixture was kept tightly at 40 °C for at least 8 days or 15 days. The samples were filtered under vacuum and the filtrates were subsequently analyzed. First, the OH^- ions content was determined using the HCl 0.1N hydrochloric acid. After adjusting the pH to 12.5, the Ca^{2+} ion content was determined by the use of an EDTA complexometric test. The Ca^{2+}

content (expressed as CaO equivalent) function of OH^- content are shown relative to the limit of solubility of $Ca(OH)_2$. A position under the curve of $Ca(OH)_2$ solubility suggests a consumption of CaO by pozzolanic reaction [30].

b. Thermogravimetric analysis of mixture with $Ca(OH)_2$

In this method, the consumption of lime by the pozzolanic reaction in the lime paste is evaluated by thermogravimetric analysis (TGA) for the differents materials (flash calcinated sediments as well as metakaolin and the raw sediment) . The $Ca(OH)_2$/mineral addition mass ratio is 4 and the amount of water was adjusted to have a good consistency of the pastes. Table 3 shows the composition of the different lime pastes studied.

Table 3 Composition of the different lime pastes

Formula	$Ca(OH)_2$+MK	$Ca(OH)_2$+RS	$Ca(OH)_2$+SF650	$Ca(OH)_2$+SF750	$Ca(OH)_2$+SF800
MK (g)	10	-	-	-	-
RS (g)	-	10	-	-	-
SF 650 (g)	-	-	10	-	-
SF 750 (g)	-	-	-	10	-
SF 800 (g)	-	-	-	-	10
$Ca(OH)_2$ (g)	40	40	40	40	40
Water (g)	10	40	40	40	40

The lime pastes were stored hermetically at 20 °C until the test was measured at 7, 14, and 28 days. Before testing, the hydration of the samples should be stopped. Therefore, the pastes were immersed in acetone solution for 4 days, then filtered under vacuum before the thermogravimetrie analysis.

Determination of the amount of chemically bound water and the Ca(OH)2 content by the TGA curve

The quantity of chemically bound water (wt %) could be calculated from the TGA curve according to the following Eq (14):

$$Q_{\text{chemical bound water}} = M_{\text{sample (40°C)}} - M_{\text{sample (400°C)}} \quad (14)$$

With:

$Q_{\text{chemical bound water}}$: Amount of chemical bound water (wt %).

$M_{\text{sample (40°C)}}$: Mass of the sample at 40°C.

$M_{\text{sample (400°C)}}$: Mass of sample at 400°C.

The amount of $Ca(OH)_2$ can be calculated from the TGA curve. In this study, the dehydroxylation of portlandite occurs at the temperature range of 450 °C to 550 °C. The amount of portlandite can be calculated according to the following Eq (15):

$$Q_{\text{Ca(OH)2}} = \frac{\Delta m\ 450°C-550°C(t).MCa(OH)2}{MH2O} \quad (15)$$

with:

$Q_{Ca(OH)_2}$: Amount of $Ca(OH)_2$ in the paste (wt %).

M_{CH}: Molar mass of $Ca(OH)_2$.

M_{H2O} : Molar mass of water.

The amount of $Ca(OH)_2$ reacted was estimated using the following Eq (16) and Eq (17):

$$Ca(OH)_{2\ reacted} = Ca(OH)_{2\ total} - Ca(OH)_{2\ non\ reacted} \quad (16)$$

$$Ca(OH)_{2\ non\ reacted} = \frac{\Delta m\ 450°C-550°C(t).\ MCa(OH)2}{MH2O} + Ca(OH)_{2\ carbonated} \quad (17)$$

Determination of the quantity of hydrated phases (C-S-H, CASH) from the DTG derived curve

The hydrated phases as C-S-H, calcium aluminate hydrate (CAH) or calcium silico-aluminate hydrate (CASH) can be calculated from the DTG derived curve [36, 37]. However, it is difficult to distinguish two phases CAH and CASH. The spectra obtained from the curves derived from dTG(%)/dt = f(T °C) were deconvolved in order to determine the area of each hydrate decomposition according to the Lorentzian's area deconvolution method with the amplitude a0, center a1 and width a2 according to the following Eq (18) [38]:

$$\frac{dTG(\%)}{dt} = \frac{a0}{1+\left(\frac{T-a1}{a2}\right)\text{^}2} \quad (18)$$

with:

dTG(%)/dt: Derived value of TG (%) at time t.

T (°C): Temperature (°C).

a0, a1 and a2 : amplitude, centre and width (>0) of the spectrum respectively.

Fig. 2 illustrates the method of quantification for C-S-H and CASH.

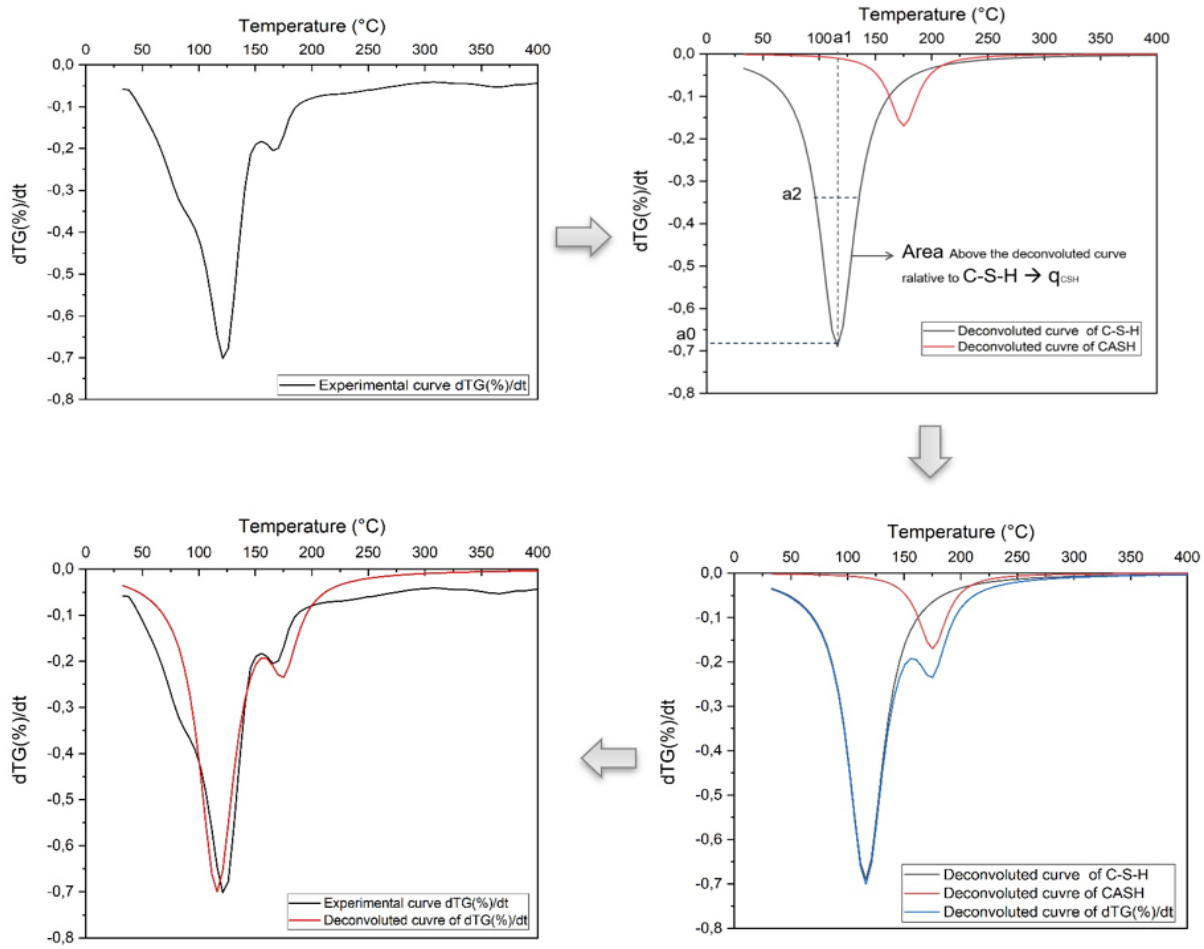

Fig. 2 Deconvolution method for quantification the quantity of C-S-H and CASH phases of the (SF 750+ $Ca(OH)_2$) mixture after 28 days of hydration

c. Heat of hydration of cement pastes

The pozzolanic reaction is an exothermic reaction. Isothermal calorimetry analysis is used to follow the evolution of heat from exothermic hydration reactions in different cement paste mixes. Cement paste mixtures with a 10% wt substitution rate of the addition, are made with a water/binder ratio equal to 0.5. The internal temperature of the calorimeter is set at 20 °C.

d. Mechanical performance of mortars

Prismatic samples mortars 4x4x16 cm^3 are made in accordance with the standard NF EN 196-1 [26]. The compressive strength of the mortars are measured at 1, 2 , 28 , 56 , and 90 days of curing by an INSTRON 5500 R 4206 - 006 Press. Table 4 shows the different mortar formulas with a 10% wt substitution rate made in this study.

Table 4 Composition of the mortar formulas

Formula	Cement (g)	MK (g)	RS (g)	SF 650 (g)	SF 750 (g)	SF 800 (g)	Water (g)	W/B	Sand (g)
MR	450	-	-	-	-	-	225	0.5	1350
MMK	405	45	-	-	-	-	225	0.5	1350
MSR	405	-	45	-	-	-	225	0.5	1350
MSF650	405	-	-	45	-	-	225	0.5	1350

MSF750	405	-	-	-	45	-	225	0.5	1350
MSF800	405	-	-	-	-	45	225	0.5	1350

In order to demonstrate the effect of mineral additions on the compressive strength of mortars, we used Féret's law [39] presented in Eq(19), which predicts the compressive strength of a cementitious material as a function of the content of the components (aggregates, sands, cement, mineral additions, water) and the content of the occluded air.

$$Rc(t) = G*R_{cm}*\left(\frac{1}{1+pc*\left(\frac{Eeff+pw*Va}{C+kA}\right)}\right)\text{^}2 \quad (19)$$

with:

G : Aggregate coefficient.

R_{cm} : Cement class (Mpa)

p_c : Cement density (t/m^3)

E_{eff} : Amount of water in the formulation (kg/m^3)

C : Amount of cement in the formulation (kg/m^3)

A : Amount of minerale addition in the formulation (kg/m^3)

V_a : Air content of occluded in 1 m^3

K : Activity coefficient of mineral addition

The objective is to establish a dilution curve of the compressive strength of the mortars that we consider only the cement participating in the development of the compressive strength and without the contribution of the effect of mineral additions (neither physical effect, nor chemical effect). In this case, we assume the activity coefficients of mineral additions are equal to 0 (k = 0) and the compressive strength of MR mortar was used in order to establish the dilution curve of the compressive strength of mortars (MMK, MRS, MSF 650, MSF 750, and MSF 800) in hydration time.

The difference between the resistance measured on the sample (experimental result) and the theoretical resistance calculated according to Féret's law gives the effect of the additions in the formulation.

- A negative deviation means that the mineral additions would have a detrimental effect on the development of compressive strength.
- A zero deviation signifies mineral additions are inert and do not contribute to the development of compressive strength.
- A positive deviation means that the mineral additions would have an effect on the development of resistance. An increase in the time difference could be due to the effect of the pozzolanic reaction.

e. Measurement of dynamic modulus of elasticity E_{dyn} :

The dynamic modulus of elasticity of the mortars was determined by the equipment GrindoSonic Mk5 "Industrial". It is a non-destructive test that assesses microcracking, homogeneity, and compactness [40]. The dynamic modulus of elasticity is measured according to the following Eq(20):

$$E_{dyn} = \frac{p(1+\mu)(1-2\mu)}{(1-\mu)} * f^2 \quad (20)$$

With:

p: Density of the mortar (kg/m^3)

μ: Dynamic Poisson's ratio

f: Pulse velocity of mortar (m/s)

f. Porosity of mortars

The microstructure of the mortars was studied by measuring the porosity of the mortars in order to assess the effect of incorporating mineral additions. Indeed, the porosity can have an influence on the durability [41] and on the mechanical resistance[42]. In particular, the larger capillary pores strongly influence the transfer properties of concrete [43]. The porosity and the pore size distribution of the mortars were measured at 56 days of hydration using Mercury Intrusion Porosimetry (MIP) technique (Micromertitics Autopore IV type).

2.2.3 Leaching analysis of mortars

Leach analysis was performed on particles (0–4 mm) from the mortars after 90 days to measure the content of metallic trace elements and anionic elements. The analysis process is identical to that used in the material characterization part.

3 Results and Discussion

3.1 The physical characteristics of materials

Table 5 shows the physical characreristics of the materials used in the study. The RS sediment has a high content of organic matter (16.1%). Flash calcination significantly removes organic matter from products, especially in SF 750 and SF 800 where a reduction of 88% and 93% is respectively observed.

The increase in density was also observed for the calcination products. This is due to the elimination of organic matter (density 1 g/cm^3) and the decomposition of limestone (density 2.6-2.8 g/m^3) to form calcium oxide (density approximately 3.3 g/cm^3). However, a decrease in the density of SF 800 upon increasing the calcination temperature could be due to the recrystallization of the mineral phases [44]. The flash calcination also induces a slight increase in particle size without a reduction in specific surfaces. This is due to an agglomeration of clay particles without sintering during calcination [31]. The increase in particle size in the calcined sediment was also observed in previous studies [11, 15, 45]. Concerning the reactivity of the addition, the latter increases when the BET surface increases, in contrary to the water demand. However, an increase in calcination temperature to 800 °C led to a decrease in the specific surface. This could be explained by the melting of certain particles that contain elements such as Na, K, and Fe reacting like fluxes and sintering during calcination at high temperatures [15, 31].

Table 5 Physical properties of OPC, MK, RS, SF 650, SF 750 et SF 800 materials

Property	**OPC**	**MK**	**RS**	**SF 650**	**SF 750**	**SF 800**
Density (g/cm^3)	3.15	2.64	2.43	2.61	2.63	2.55
BET (cm^2/g)	9 800	11 244	4 376	12 104	15 590	13 786
Blaine surface (cm^2/g)	3720	-	-	-	-	-
OM content (wt.%)	-	-	16.1	5.16	1.93	1.1
LOI 950°C(wt.%)	1.91	0.73	27.63	17.41	13.7	10.80
d_{10} (µm)	1.31	3.09	1.24	2.25	2.63	2.91

d_{50} (µm)	12.76	25.18	11.68	11.81	14.71	15.91
d_{90} (µm)	67.87	76.29	55.91	50.93	64.13	69.90

Note: OM = Organic matter

From the TGA - DTG analysis of the sediments (Fig.3 and Fig.4), several operations can be carried out in order to follow the phase transformation:

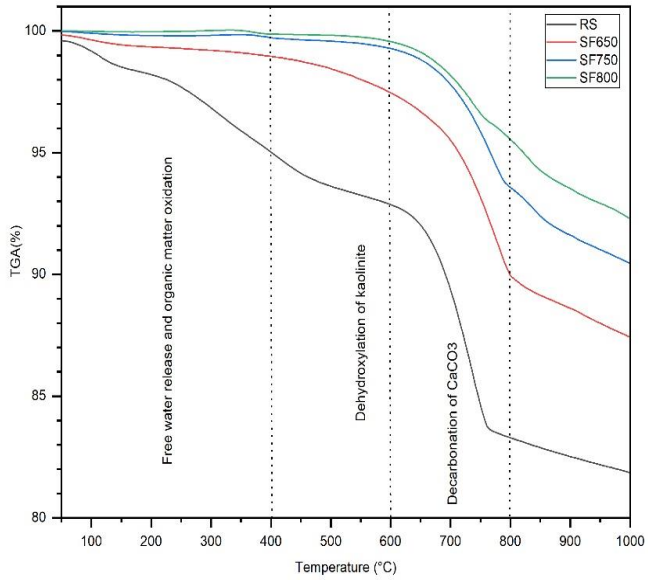

Fig. 3 TGA curves of sediments

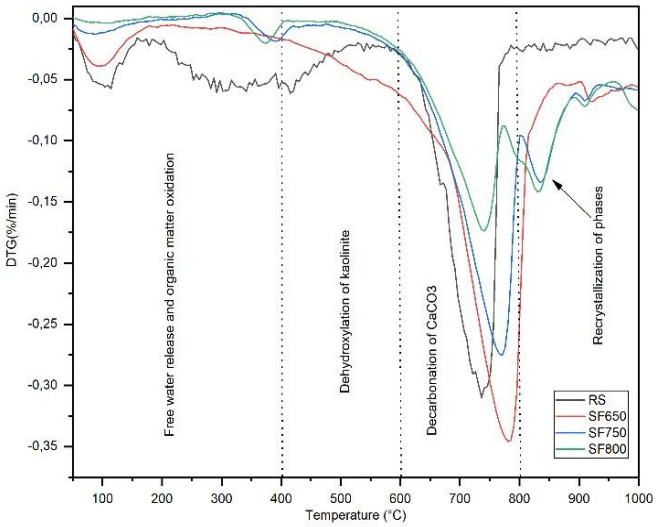

Fig. 4 DTG curves of sediments

- **Calcite content ($CaCO_3$)**

The $CaCO_3$ content can be calculated from the TGA analysis according to the following Eq (21) and Eq (22):

$$CaCO_3 \rightarrow CaO + CO_2 \quad (21)$$

$$\%CaCO_3 = (m_{\text{sample } 600°C} - m_{\text{sample } 800°C}) * (M_{CaCO3} / M_{CO2}) \quad (22)$$

With:

$M_{\text{sample } 600°C}$: Mass of sample at 600 °C

$M_{\text{sample } 800 °C}$: Mass of the sample at 800 °C

M_{CaCO3}: Molar mass of $CaCO_3$

M_{CO2}: Molar mass of CO_2

Table 6 shows the content as well as the degree of decarbonation of calcite in the sediments.

Table 6 Calcite content and the degree of decarbonation of calcite in the sediments using the TGA analysis

Sediment	RS	SF 650	SF 750	SF 800
$CaCO_3$ (wt. %)	21.38	13.67	10.91	7.97
Degree of decarbonation (%)		35.93	48.85	62.64

The presence of $CaCO_3$ and CaO in the calcined products could have impacts on the hydration of calcined sediments based mixtures. In fact, mineral additions with a high $CaCO_3$ content promote hydration of C_3S [46], but are very unfavorable for the C_3A phases hydration [47].
On contact with water, CaO turns into $Ca(OH)_2$ according to the following reaction Eq (23) [48]:

$$CaO + H_2O \rightarrow Ca(OH)_2 + 15.5 \text{ kcal} \quad (23)$$

This reaction is exothermic and this could cause a strong degradation due to the heat generated in the core of the structure. In addition, an increase in the $Ca(OH)_2$ volume could be the cause of cracking which influenced the durability and the mechanical performance of the structure.

- **Degree of dehydroxylation of kaolinite**

The content and degree of dehydroxylation of kaolinite (Table 7) can be estimated from the results of TGA analysis according to Eq (12) and Eq (13).

Table 7 Kaolinite content and the degree of dehydroxylation of kaolinite in the sediments using the TGA analysis

Sediments	RS	SF 650	SF 750	SF 800
Mineral kaolinite (wt. %)	15.26	10.53	3.10	2.10
Degree of deshydroxylation (%)	---	31.00	79.70	86.21

The result shows that the kaolinite was transformed into metakaolin Eq(2) from calcination at 650 °C, however the degree of dehydroxylation is relatively low (31%). The increase in calcination temperature significantly improves the dehydroxylation of kaolinite. The degree of dehydroxylation of kaonilite is an important index for evaluating the quality of calcination because the metakaolin formation promotes the pozzolanic reaction.

3.2 Mineralogical and chemical characterizations

The XRD analysis shows the presence of the main mineral phases in the RS, SF 650, SF 750, and SF 800 sediments (Fig.5).

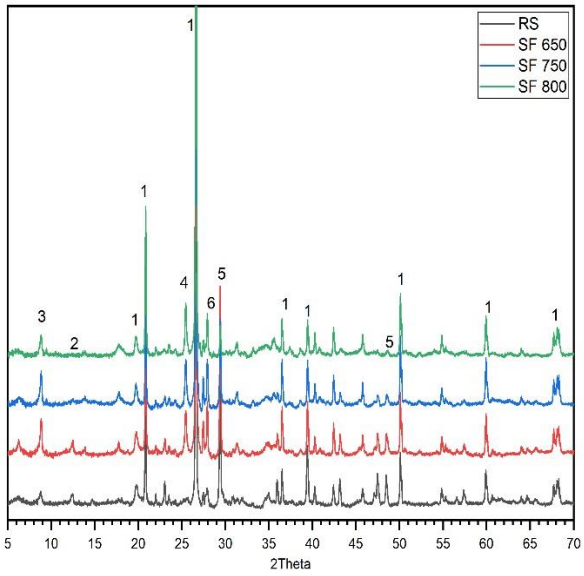

Fig. 5 XDR patterns of sediments (1) Quartz, (2) Kaolinite, (3) Illite, (4) Anhydrite, (5) Calcite, (6) Albite

The results indicate that :

- The quartz is the major crystalline phase identified in the RS sediment as well as in the calcined sediments.
- The presence of calcite is well identified in the RS sediment. An increase in calcination temperature led to a decrease in the calcite content in the calcined products due to the decomposition of this phase.
- The formation of anhydrite phase in the calcined sediments has been well identified. This could be explained by the reaction between the CaO released from the decomposition of $CaCO_3$ with the sulfate to form the anhydrous calcium sulfate ($CaSO_4$) [22].

The result of the analysis on oriented slides showed that the clay phases of the RS sediment consist mainly of kaolinite and illite (Fig.6). After calcination, the kaolinite transforms into metakaolin due to a dehyroxylation reaction. The degree of dehydroxylation at 800 °C is the highest and this seems in accordance with the result calculated from the TGA analysis (Table 7). Despite calcination temperatures are higher than the dehydroxylation temperature of kaolinite but the calcination time is very short, this is explained by the incomplete reaction during calcination of the sediment at 650 °C,750 °C and 800 °C.

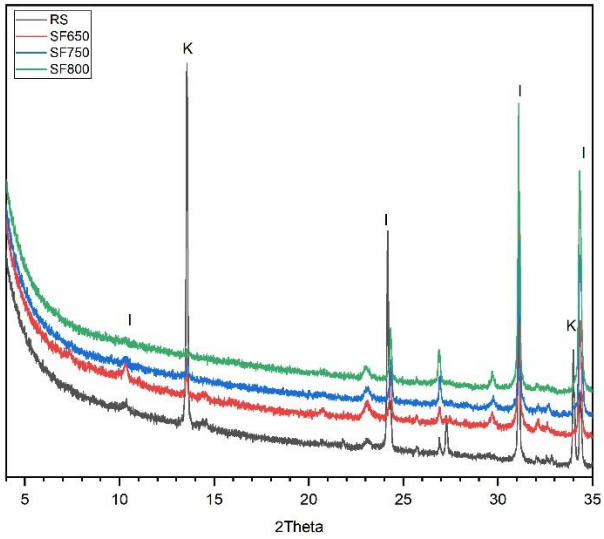

Fig. 6 XRD patterns of clay phases of sediments using the XRD analysis on the oriented slides (K: Kaolinite, I: Illite)

The chemical composition of sediments as well as OPC cement and MK is given in Table 8.

- The major oxides of materials are SiO_2, Al_2O_3, CaO, Fe_2O_3.
- The chemical composition of calcined sediments is relatively similar. Therefore the increase in the calcination temperature did not change the composition in the calcined products. Fig.7 shows the content of major oxides in the materials in the CaO-SiO2-Al_2O_3 ternary diagram.

Table 8 Chemical composition of materials

Composition (% wt)	OPC	MK	RS	SF 650	SF 750	SF 800
CaO	63.75	2.0	10.57	10.85	11.21	11.66
SiO_2	19.95	60.75	39.62	43.64	49.71	50.87
Al_2O_3	5.31	31.18	9.64	11.85	12.00	12.60
Fe_2O_3	2.98	2.57	5.12	5.59	5.33	5.69
SO_3	3.03	0.84	0.22	0.2	0.18	0.2
Na_2O	0.55	0.25	0.69	0.62	0.74	0.73
K_2O	0.93	1.68	1.84	2.29	2.25	2.35
MgO	0.86	ND	0.88	1.33	1.12	1.18
ZnO	ND	ND	0.27	0.4	0.31	0.36
P_2O_5	ND	ND	2.1	2.04	2.26	2.36
LOI (950°C)	1.91	0.73	27.63	17.41	13.7	10.80

Total	99.99	100	99.17	96.89	99.49	99.5

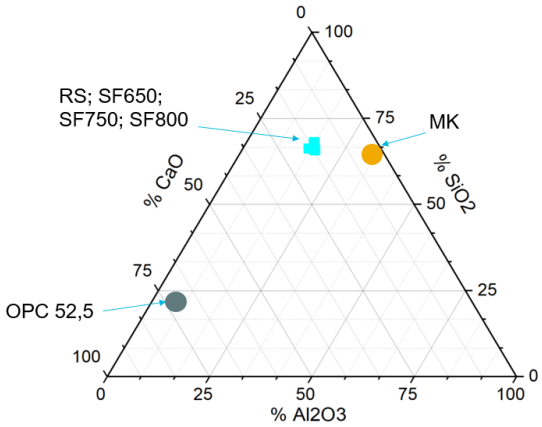

Fig. 7 CaO-SiO_2-Al_2O_3 ternary diagram of materials

The result of the leaching analysis shows the presence of metallic trace elements as well as anionic elements in sediments (Table 9 and Table 10). The content of certain metallic trace elements in the RS sediment exceeds the value specified for inert waste (IW), in particular, the content of zinc.

Table 9 Metallic trace elements in sediments (mg/kg)

Elements	RS	SF 650	SF 750	SF 800	IW	NHW
As (mg/kg)	< 0.08	<0.1	<0.1	<0.1	**0.5**	**2**
Ba (mg/kg)	1.4912	0.66	1.9	4.5	**20**	**100**
Cd (mg/kg)	<0.008	<0.008	<0.008	<0.009	**0.04**	**1**
Cr (mg/kg)	<0.03	0.11	0.37	<0.09	**0.5**	**10**
Cu (mg/kg)	2.0509	0.31	0.078	0.049	**2**	**50**
Mo (mg/kg)	0.5538	1.3	1.7	1.25	**0.5**	**10**
Ni (mg/kg)	0.4799	<0.03	<0.03	<0.047	**0.4**	**10**
Pb (mg/kg)	0.0447	<0.03	0.074	1.63	**0.5**	**10**
Sb (mg/kg)	-	<0.05	<0.05	<0.057	**0.06**	**0.7**
Se (mg/kg)	0.1019	0.12	0.08	<0.083	**0.1**	**0.5**
Zn (mg/kg)	7.8518	<0.05	<0.05	<0.05	**4**	**50**

Note: IW = Inert Waste; NHW = Non-Hazardous Waste.

Table 10 Anionic element's content in sediments (mg/kg)

Sediments	Fluoride (mg/kg)	Chloride (mg/kg)	Sulfates (mg/kg)
RS	<1	262	15 800

SF 650	11	255	12 850
SF 750	8	247	11 120
SF 800	8	237	10 820
IW	**10**	**800**	**1000**
NHW	**150**	**15 000**	**20 000**

By comparing the calcined sediments to the raw sediment, it can be seen that the content of some metals such as Cu, Ni and Zn has decreased. This could have beneficial impacts on the hydration of the cementitious matrix incorporating calcined sediments, in particular for zinc. The presence of Zn decreases the compressive strength and reduces the density of the material [49]. In fact Zn^{2+} ions combined with OH^- ions to form an impermeable $Zn(OH)_2$ film which inhibits the hydration of C_3S and C_3A with a more pronounced effect on C_3S. In addition, $Zn(OH)^{2-}$ and $Zn(OH)^{3-}$ prevent adsorption to the electronegative surface of C-S-H at high pH.

The sulfates content in the RS sediment is higher than the limit value for IW. In addition, it can also be seen from the results that the RS sediment has a higher sulfate content compared to the calcined sediments, where the sulfate content decreases with the increase in temperature. The presence of sulfate under certain conditions can cause degradation of materials, such as: significant swelling, cracking, and a decrease in mechanical strength.

The presence of chlorides accelerates the setting and hardening of the cementitious matrix. Chlorides can also combine with C_3A in the cement to form chloro-aluminate causing a swelling. The chloride content in the sediments seems to remain unchanged during calcination. Similar results were found in the study of Ruben et al [15].

3.3 Results of pozzolanic reactivity analyzes

3.3.1 The Frattini test

The Frattini's test was performed on samples after 15 days of hydration. The result (Fig.8) shows that, after 15 days, the calcined sediments and the MK have pozzolanic reactivity while the RS sediment does not exhibit pozzolanic reactivity. This is due to the formation of metakaolin in the calcined sediments during the dehydroxylation of kaolinite. This transformation was demonstrated in the XRD analysis (Fig.5) and the analysis on oriented slides (Fig.6). In addition, Fig.8 shows that for MK, the pozzolanic reaction could be clearly detected after 8 days.

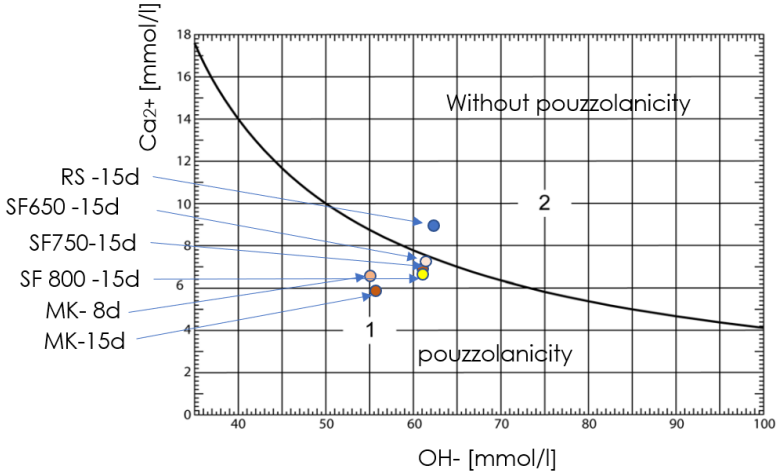

Fig. 8 The Frattini's test result after 15 days of hydration

3.3.2 Heat hydration of cement pastes

The heat of hydration of cement pastes is shown in the Fig. 9. The first exothermic peak in the acceleration period (point 2) is mainly related to the hydration of C_3S and C_3A to form C-S-H and ettringite respectively. In the deceleration period, the second exothermic peak is observed, which corresponds to the additional dissolution of C_3A and the accelerated precipitation of ettringite [50]. In addition, the depletion of calcium sulfate $CaSO_4$ led to the transformation of ettringite to Afm ($C_3A.CaSO_4.12H_2O$). The results show also that in the mixtures OPC 52.5, (OPC 52.5 + MK), (OPC 52.5 + SF 650), (OPC 52.5 + SF 750) and (OPC 52.5 + SF 800), the induction period begins after 3h while this period begins only after 6h in the mixture (OPC 52.5 + RS). This delay could be explained by the high organic matter content in the RS sediment that can disturb the hydration of the cement. Indeed, Young [51] indicated that the formation of complexes between Ca^{2+} ions and groups such as hydroxyl, carboxyl, amine, benzene releases protons that provokes the acidifying of the matrix according to the following reaction Eq (24):

$$2\ R\text{-}H + Ca^{2+} \rightarrow R - Ca - R + 2H^{+} \quad (24)$$

In addition, Pollard et al. [52] showed that the formation of a physical barrier altered the growth and/or the morphology of the crystals and prevented the normal hydration of the cement. Indeed, the reduction of Ca^{2+} ions retarded the nucleation of $Ca(OH)_2$ and generated an unstable C-S-H gel with a low Ca/Si ratio which slowly transformed into a stable C-S-H gel [53]. Agglomeration of sediment may be the cause of delay in hydration because it trapped water in the mix and reduced the water available for hydration [54]. Removal of organic matter from calcined sediment is beneficial by reducing the delay in hydration of the mixture. Metakaolin has the highest pozzolanic reactivity while the three calcined sediments have relatively identical hydration kinetics. This result appears to be consistent with that of Frattini's test.

The incorporation of the calcined sediment reduces the heat of hydration of the mixtures. This result is contrary to that reported in the study by Benzerzour et al [9]. However, a similar result was obtained in the study of Safhi et al [55]. This contradiction could be explained by the coarser size (d_{50} about 15 µm) of the sediments in this study and the study conducted by Safhi et al [55] compared to that in the study of Benzerzour et al [9] (d_{50} = 5 µm). Therefore, this could lead to higher hydration kinetics.

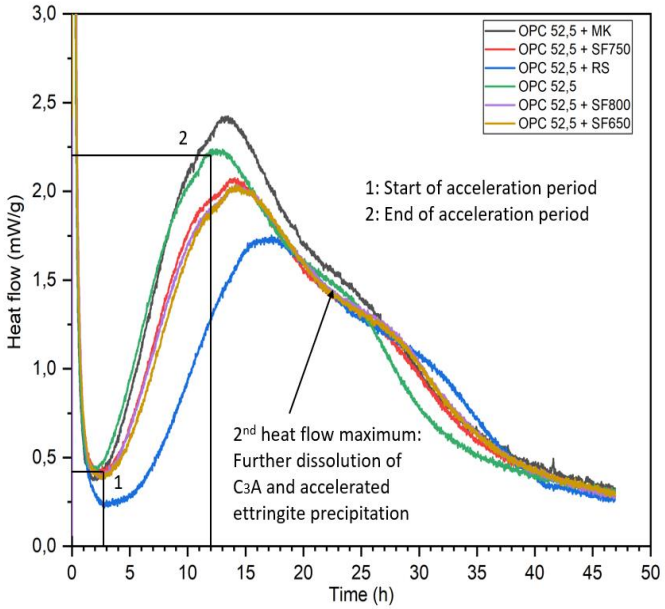

Fig. 9 Heat of hydration generated during the hydration of cement pastes with the ratio W/B = 0.5

3.3.3 Determination of pozzolanic reactivity by thermal analysis

a. Quantification of chemically bound water and $Ca(OH)_2$ from TGA analysis

Fig.10 shows, an example for the method of calculating the content of bound water in the ($Ca(OH)_2$+SF 750) mixture by TGA analysis.

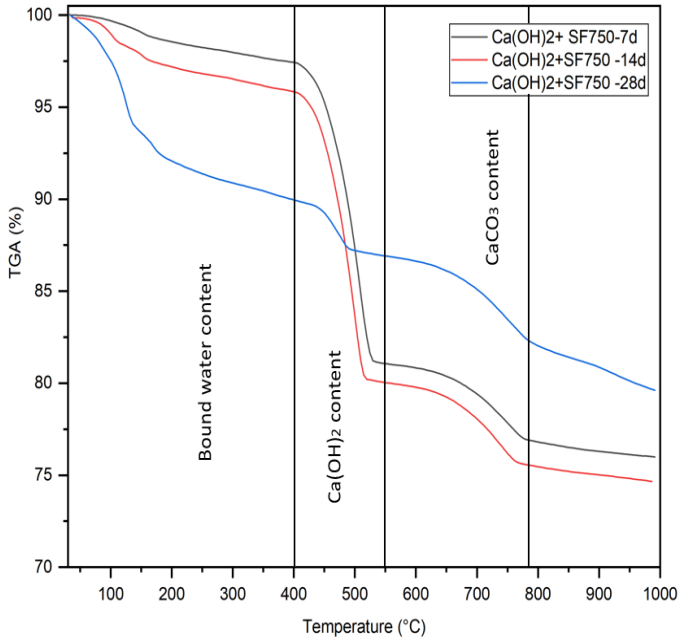

Fig. 10 Result of the TGA analysis of the ($Ca(OH)_2$+SF750) mixture over time of hydration

From the TGA analysis results of ($Ca(OH)_2$+SF 750) mixture, the following conclusions can be extract :

- The content of $Ca(OH)_2$ in the mixture decreases with time, due to the pozzolanic reaction between the sediment and the portlandite.
- An increase in the bound water content in the mixture corresponds to hydrates formed over the time of hydration process. This is consistent with the observed $Ca(OH)_2$ consumption.
- The $CaCO_3$ content in the mixture at each test time (7, 14 and 28 days) is constant. This stability means that the mixture was well homogenized and that the used sample of the mixture is well representative.

The amount of chemically bound water of the mixtures during hydration calculated using Eq (14) is shown in Fig.11. The ($Ca(OH)_2$+MK) mixture showed the highest amount of bound water at all measured times. This is related to the amount of hydrates formed in the paste over the time of hydration. At 7 days, the amount of water bound in mixtures containing sediment is relatively the same. This could be due to the slow pozzolanic reactivity of the calcined sediments. Indeed, after 28 days of hydration, the content of bound water increases in all mixtures. Pastes containing calcined sediment exhibited a higher amount of bound water than the paste incorporating raw sediment. Among the calcined products, the mixture with SF 750 sediment leads to a higher bounded water content at short term as well as at long term. This result is in accordance with previous tests on the pozzolanic reactivity of sediments.

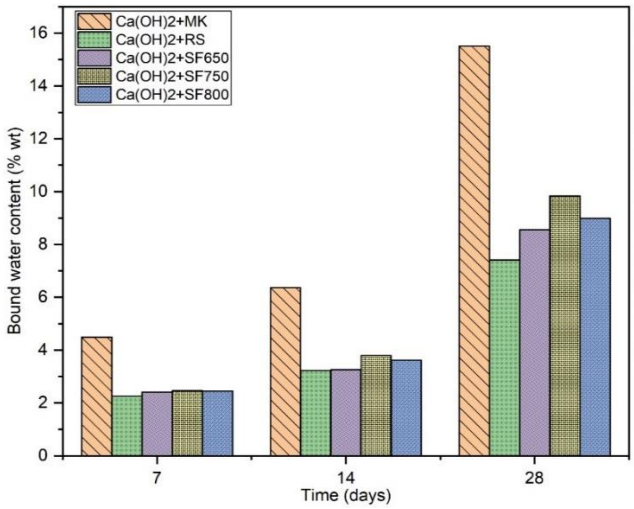

Fig. 11 Content of chemically bound water in lime pastes during hydration using the TGA analysis

b. $Ca(OH)_2$ amount in lime paste

The pozzolanic reaction is a reaction that consumes $Ca(OH)_2$, therefore this pozzolanic reaction can be evaluated by measuring the $Ca(OH)_2$ over time of hydration. Fig.12 shows the evolution of $Ca(OH)_2$ in the different mixtures. It can be seen from the results that the MK consumes a greater quantity of $Ca(OH)_2$ than the sediments. Among the sediments, SF 750 seems to be the most reactive when comparing the quantity of $Ca(OH)_2$ consumed at short term as well as at long term. In addition, at short term, the $Ca(OH)_2$ content is relatively stable. This is consistent with the result of the amount of water chemically bound. In fact, the more portlandite is consumed, the more hydrates are formed.

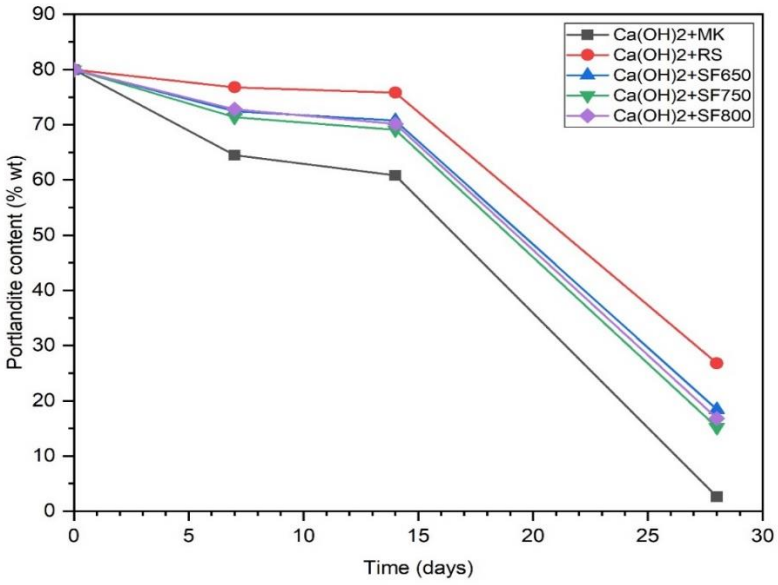

Fig. 12 Evolution of the $Ca(OH)_2$ amount in lime pastes over time of hydration using the TGA analysis

In order to demonstrate the consumption of $Ca(OH)_2$ in the mixtures, XRD analysis was performed on the samples after 28 days of hydration. The result has been presented in Fig.13.

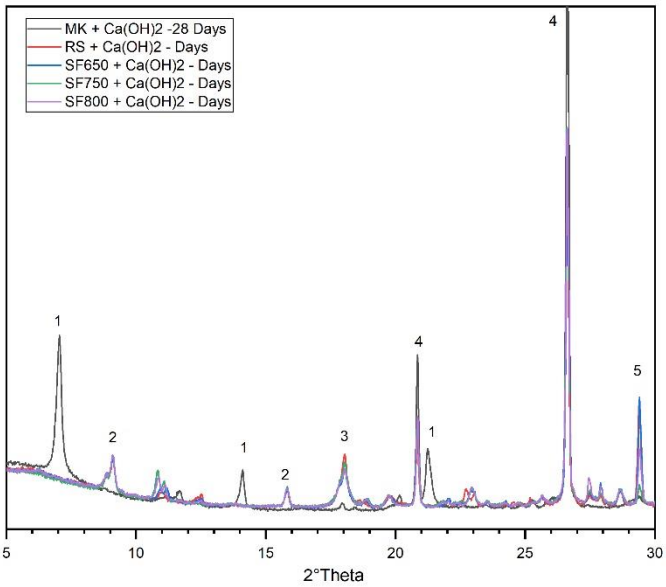

Fig. 13 XRD patterns of mixtures after 28 days of hydration (1: Stratlingite ($Ca_2Al_2SiO_7.8H_2O$, 2: Ettringite, 3: $Ca(OH)_2$, 4: Quartz, 5: Calcite)

We can confirm that:

- The $Ca(OH)_2$ content in the (MK + $Ca(OH)_2$ mixture after 28 days of hydration is the lowest. This means that the $Ca(OH)_2$ content consumed in the mixture is the highest. This result is consistent with the result measured by the TGA analysis (Fig.12).
- The $Ca(OH)_2$ content in the mixtures contained in the calcined sediments is relatively similar and lower than the (RS + $Ca(OH)_2$) mixture. This result is also consistent with the result found by the TGA analysis (Fig.12).

c. Evaluation of hydrates formed from the DTG curve

The relative amount of hydrates formed over hydration time of the pastes was estimated from the DTG curves by the deconvolution method based on Eq (16). Fig.14 and Fig.15 show the relative amounts of the C-S-H and other phases such as CASH produced in pastes over time of hydration. By comparing the relative amount of hydrates formed (C-S-H and CASH), it can be concluded that the MK is the most reactive comparing to the other additions. This result appears to be in accordance with previous results, that demonstrated the higher reactivity of MK with respect to sediments. However, we note that the relative amount of C-S-H at 28 days in all mixtures are relatively the same. In addition, the CASH amount formed from the ($Ca(OH)_2$+MK) mixture is much higher than the other mixtures incorporating sediments. This can be explained by the higher Al_2O_3 content of MK (31.18% wt) compared to sediment (12 wt.% in SF 650, SF 750, SF 800, and 9.64 wt.% in RS).

The reaction for C-S-H formation occurs relatively slowly in mixtures containing sediments for up to 14 days. This is well consistent with the quantification result of the $Ca(OH)_2$ amount consumed and the content of the chemically bound water by the TGA analysis (Fig. 11). For example, the amount of $Ca(OH)_2$ consumed in the ($Ca(OH)_2$ + SF 750) mixture incorporating SF 750 is 8.63% at 7 days and 10.90% at 14 days compared to 64.83% at 28 days.The result also

showed that SF 750 was the most reactive among sediments by comparing the amount of hydrates formed.

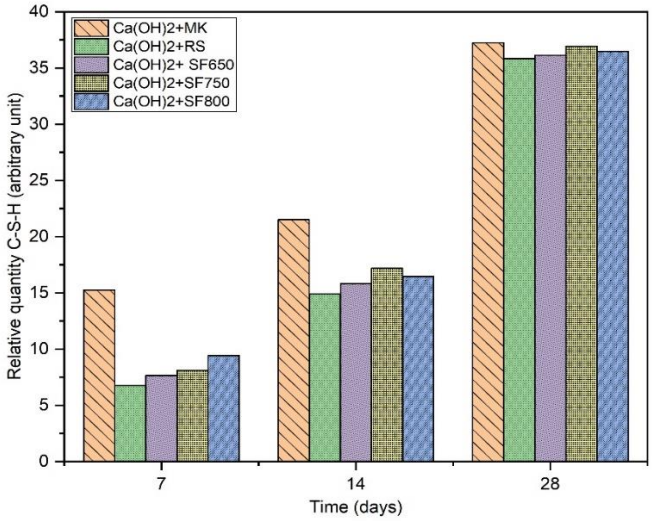

Fig. 14 Relative amount of C-S-H in the different pastes over time of hydration using the deconvolution method

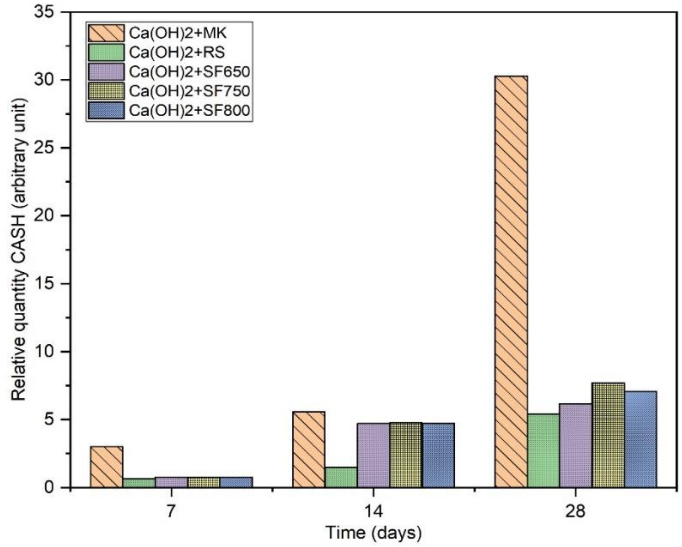

Fig. 15 Relative amount of CASH phases of the pastes over the time of hydration using the deconvolution method

3.4 Compressive strength of mortars

Fig.16 shows the evolution of the compressive strength of mortars in function of the hydration time (from 1 to 90 days of curing).

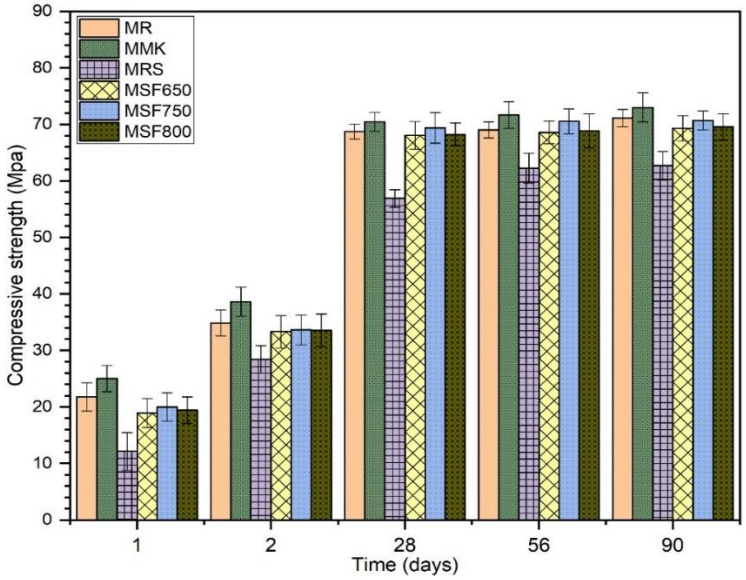

Fig. 16 Compressive strength of mortars over time of hydration

The following observations can be dressed:

- MMK mortar exhibits good mechanical performance compared to MR mortar at all testing times. This proves the highest pozzolanic reactivity of MK.
- MRS mortars have the lowest compressive strengths. Whereas the calcined sediments appear to significantly improve the mechanical performance of mortars when compared with the strength of mortar MRS.
- Among the mortars containing calcined sediments, MSF 750 mortar shows the better mechanical performance. An increase in the calcination temperature seems to improve the mechanical performances of mortars by increasing the specific surface of the sediments. However, calcination at 800 °C reduces the specific surface of the SF 800 sediment compared to SF 750 and this explains the reduction in the strength of MSF 800 mortars compared to MSF 750.

Fig.17 and Fig.18 show the resistance measured on the specimen and the resistance calculated according to Féret's law (with the activity coefficient k = 0) of the mortars over time of hydration.

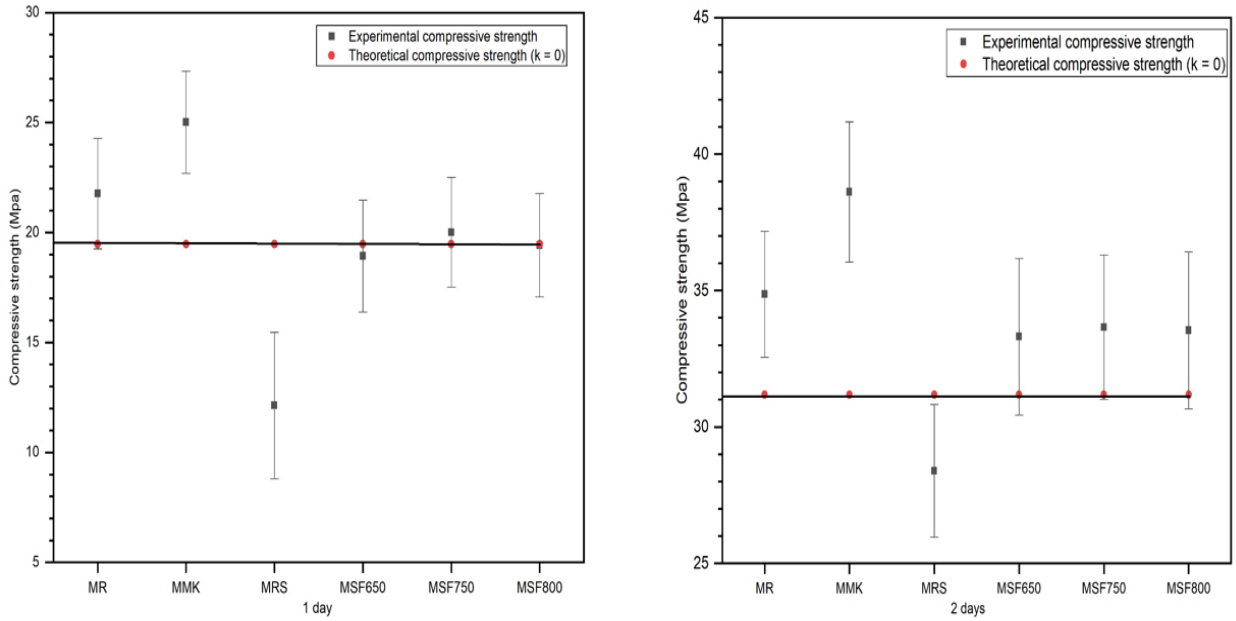

Fig. 17 Compressive strength measured on the sample and the compressive strength calculated according to Féret's law with the activity coefficient k = 0 after 1 and 2 days of curing

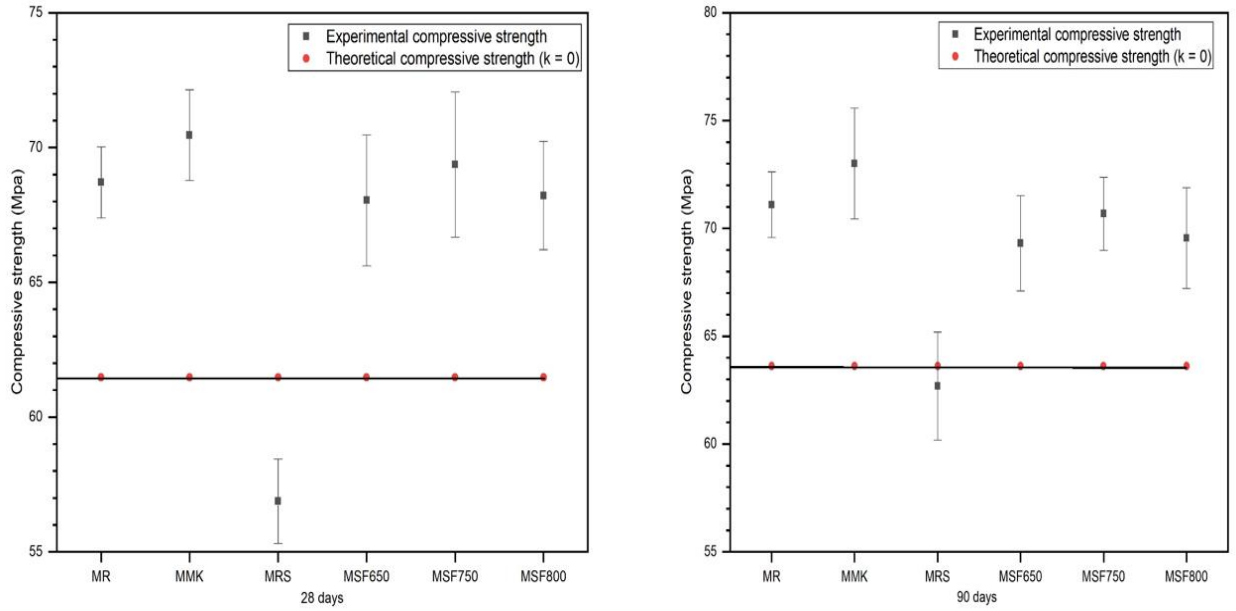

Fig. 18 Compressive strength measured on the sample and the compressive strength calculated according to Féret's law with the activity coefficient k = 0 after 28 and 90 days of curing

The result shows that:

- The compressive strength of MRS mortar is always below the theoretical strength curve. This shows a detrimental retardation effect of RS sediment on resistance development. Indeed, the delay effect of RS sediment was also shown in the isothermal calorimetry test (Fig.9).
- The difference in resistance of MSF 650, MSF 750 and MSF 800 mortars is almost zero after 1 day of hydration. This means that these calcined sediments are inerts and do not contribute to the development of resistance. However, after 2 days of hydration, the difference is positive. This difference seems to get bigger and bigger with the time of hydration. This means that these sediments would have a chemical effect such as the pozzolanic reaction contributing to the development of resistance.

- The compressive strength of MMK mortar is always above the theoretical strength curve. An increase in this difference in hydration time has been observed. In addition, this difference is also greater than the difference in the case of mortars containing calcined sediment. This means the MK would have a higher pozzolanic reactivity than the calcined sediments. This result is consistent with the result shown in the analysis of isothermal calorimetry (Fig.9) and lime consumption (Fig.12).

3.5 Dynamic modulus of mortars

Fig.19 shows the evolution of the dynamic modulus of mortars calculated according to Eq (20) from 28 days to 90 days. Stabilization of the dynamic modulus after 56 days indicates that all of the portlandite has been consumed by the pozzolanic reaction [55]. Indeed, the consumption of portlandite makes it possible to form a more dense and coherent microstructure. In addition, a relatively large increase in dynamic modulus of sediment containing mortars between 28 and 56 days compared to MMK mortar indicates the long-term pozzolanic reactivity of the sediments.

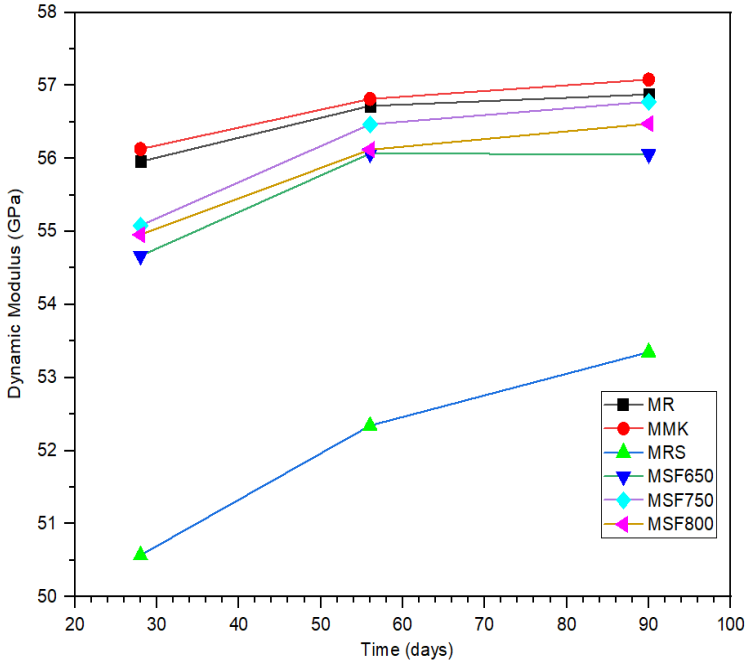

Fig. 19 Evolution of the dynamic modulus of mortars over time of hydration

3.6 Porosity of mortars

The mercury porosity of mortars measured at 56 days is shown in Table 11 and the pore distribution is also shown in the Fig.20.

Table 11 Porosity in mortars at 56 days of curing measured by MIP

MR	MMK	MRS	MSF650	MSF750	MSF800
11.73 %	11.51 %	12.45 %	10.45 %	10.43 %	10.17 %

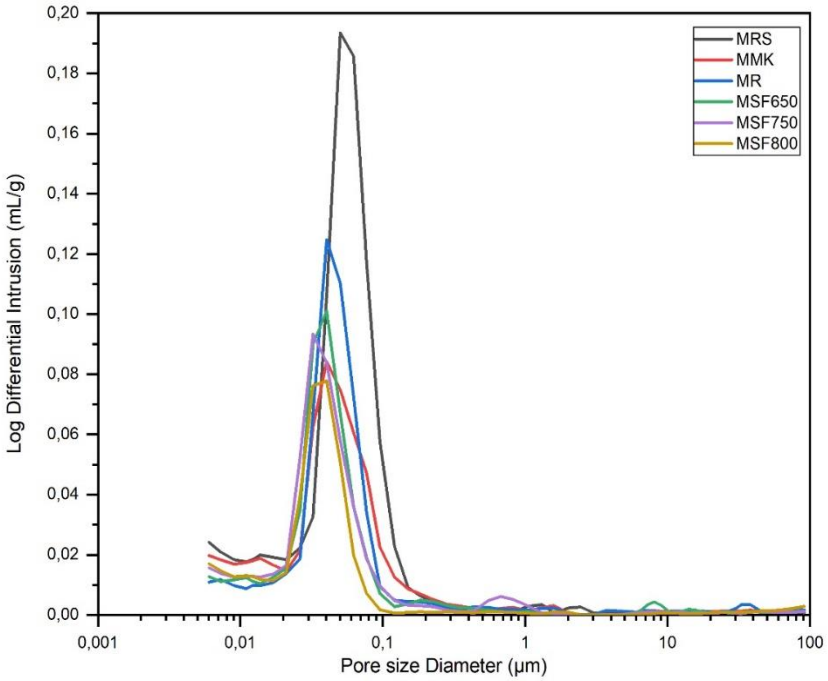

Fig. 20 Pore size distribution in mortars measured by MIP at 56 days of curing

The results show that:

- Substitution of cement by RS sediment increased the porosity of the mortar. Indeed, the result of the compressive strength indicated that the RS sediment was almost inert after 90 days of hydration. Replacing cement with an inert addition leads to an increase in the W/C ratio. This could lead to an increase in porosity. The pore distribution in the MRS mortar returns to the larger pores. A similar result was found in the research of Berodier et al [56] when replacing cement with quartz, considered inert.
- Contrary to RS sediment, replacing cement with active mineral additions (MK, SF 650, SF 750 and SF 800) reduced the porosity of the mortar. The pozzolanic reaction appears to overcome the replacement dilution effect. In addition, these mineral additions appear to reduce the size of the pores towards the finer pores. According to Zengfeng et al [57], the presence of the sediment allowed a finer distribution of the porosity, most often associated with a better texture of C-S-H.

3.7 Leaching analysis result of mortars at 90 days of curing

Table 12 shows the content of metallic trace elements in the mortars after 90 days of hydration. In addition, the content of anionic elements in the mortars was shown in Table 13. A considerable reduction in the sulfate content was observed. The result showed a stabilization of all the elements compared to the leaching limits of inert waste.

Table 12 Metallic trace elements in mortars after 90 days of hydration

Element	MMK	MRS	MSF650	MSF750	MSF800	IW	NHW
As (mg/kg)	< 0.11	< 0.11	< 0.11	< 0.11	< 0.11	**0.5**	**2**
Ba (mg/kg)	7.9	9.6	9.9	9.7	9.5	**20**	**100**

Cd (mg/kg)	<0.009	<0.009	< 0.009	< 0.009	< 0.009	**0.04**	**1**
Cr (mg/kg)	0.44	0.057	0.072	0.039	0.063	**0.5**	**10**
Cu (mg/kg)	< 0.02	0.4	< 0.02	< 0.02	< 0.02	**2**	**50**
Mo (mg/kg)	< 0.09	< 0.09	< 0.09	< 0.09	< 0.09	**0.4**	**10**
Ni (mg/kg)	< 0.05	0.49	< 0.05	< 0.05	< 0.05	**0.4**	**10**
Pb (mg/kg)	0.042	0.078	0.097	0.054	0.071	**0.5**	**10**
Sb (mg/kg)	< 0.06	< 0.06	< 0.06	0.067	<0.06	**0.06**	**0.7**
Se (mg/kg)	< 0.08	< 0.08	< 0.08	< 0.08	<0.08	**0.1**	**0.5**
Zn (mg/kg)	< 0.01	0.027	0.19	0.037	0.014	**4.0**	**50**

Table 13 Anionic element's content in mortars after 90 days of hydration

Sample	Fluoride (mg/kg)	Chlorides (mg/kg)	Sulfates (mg/kg)
MMK	6.3	60	135
MRS	9.7	68	210
MSF 650	6.1	60	213
MSF 750	5.3	49	205
MSF 800	6.1	56	202
IW (mg/kg)	**10**	**800**	**1000**
NHW (mg/g)	**150**	**15 000**	**20 000**

3.8 Analysis of the quality of the exhaust fumes

The quality of the gases is an important indicator to assess the deasibility of the calcination process. The gases emitted during calcination of the sediment were analyzed by the company Socor air. The results of certain elements in the flue gases are presented in Table 14.

Table 14 Content element in gases

Element	Range	Units	Gas emitted during calcination at 650 ° C	Gas emitted during calcination at 750 ° C
O_2	0 - 25	%	20.0	19.9
CO_2	0 - 20	%	0.7	0.7
CO	0 - 1000	ppm	500	12.0
	0 - 1250	mg/m_0^3	625	15.5

NO_x	0 - 200	$ppm_{éq}$ NO	11	8.7
	0 – 513.14	Mg NO_2/m_0^3	22	17.8

The results in Table 14 leads to tell that the gas content (O_2, CO_2) stabilizes during calcination. An increase in the calcination temperature allows the reduction of the CO gas emissions by reducing it by 97.6% for the temperature of 750 °C comparing to 650 °C . The similar trend with NOx gases was observed with increasing calcination temperature.

4 Conclusion

The objective of this article is to study the influence of the calcination temperature of sediment on their properties. This consists to evaluate several criteria such as the activation of pozzolanic reactivity, mechanical performance, energy consumption, and the quality of the gases emitted. Besides, the effects of the use of calcined sediments on the kinetics of hydration were investigated. It can be concluded from this study that:

- Flash calcination method removes the fraction of organic matter already present in the raw sediment. This reduces the delay in hydration related to the presence of organic material.
- The calcination temperature modifies the physical properties comparing to the raw sediment. Indeed, calcined sediments have a greater BET specific surface and density than the raw sediment. The transformation of kaolinite to metakaolin and the formation of anhydrite in calcined sediments were observed by XRD analysis.
- The flash calcination also active the pozzolanic reactivity of the sediment. The calcined sediments showed a strong ability to react with portlandite to form hydrates compared to the raw sediment.
- The heat of hydration of binders containing calcined sediment is greater than that of the binder with raw sediment. However, the calcined sediment reduces the heat of hydration of the binder compared to the reference cement. This could have a positive effect in the case of concrete and a negative effect in the development of strength at an early age.
- The incorporation of the calcined sediment significantly improved the mechanical performance of the mortars compared to the raw sediment. Besides, the reducing in the hydration delay with calcined sediments improves the development of mechanical strength at young ages comparing to the raw sediment. MSF mortars have similar mechanical strength as the reference mortar at long-term.
- The incorporation of calcined sediments reduces the porosity of the mortar due to the pozzolanic reaction.
- An increase in the calcination temperature from 650 °C to 750 °C improves the quality of the gases emitted by comparing the content of the elements in the emitted gases. An increase in the calcination temperature allows the CO gas content to be greatly reduced (97.6% reduction).
- The content of some metallic trace elements was reduced in calcined sediment, especially zinc content. In addition, the content of flourures, chlorides and sulfates tends to decrease with increasing calcination temperature.

Declaration of competing interest

The authors declare that they no known competing financial interests or personal relationships that could have appeared to influence the work reported in this paper.

Acknowlegments

The authors wish to acknowledge the SEDICIM project and the FEDER funds.

Data Availability

The datasets generated during and/or analysed during the current study are available from the corresponding author on reasonable request.

Reference

1. Bordy, A.: Influence des conditions thermo-hydriques de conservation sur l ’ hydratation de matériaux cimentaires à base d ’ une fine recyclée. 1–155 (2016)
2. La production mondiale de ciment
3. Kajaste, R., Hurme, M.: Cement Industry Greenhouse Gas Emissions - Management Options and Abatement Cost. J. Clean. Prod. 112, 4041–4052 (2015)
4. Snellings, R., Horckmans, L., Van Bunderen, C., Vandewalle, L., Cizer, Ö.: Flash-calcined dredging sediment blended cements: effect on cement hydration and properties. Mater. Struct. Constr. 50, (2017). https://doi.org/10.1617/s11527-017-1108-5
5. San Nicolas, R.: Approche performantielle des bétons avec métakaolins obtenus par calcination flash. (2011)
6. Snellings, R., Horckmans, L., Van Bunderen, C., Vandewalle, L., Cizer, Ö.: Flash-calcined dredging sediment blended cements: effect on cement hydration and properties. Mater. Struct. Constr. 50, (2017). https://doi.org/10.1617/s11527-017-1108-5
7. Dubois, V.: Etude du comportement physico-mécanique et caractérisation environnementale des sédiments marins – Valorisation en technique routière - Thèse de doctorat, (2006)
8. Tran, N.T.: Valorisation de sédiments marins et fluviaux en technique routière, (2009)
9. BENZERZOUR, M., Mouhamahou, A., ABRIAK, N.-E.: New experimental approach of the reuse of dredged sediments in a cement matrix by physical and heat treatment. 140, 432–444 (2017)
10. Dang, T.A., Kamali-Bernard, S., Prince, W.A.: Design of new blended cement based on marine dredged sediment. Constr. Build. Mater. 41, 602–611 (2013). https://doi.org/10.1016/j.conbuildmat.2012.11.088
11. Amar, M.: Étude expérimentale et numérique de la valorisaion des sédiments de dragage dans les matrices cimentaires - Thèse de doctorat, (2017)
12. Faure, A., Coudray, C., Anger, B., Moulin, I., Colina, H., Izoret, L., Théry, F., Smith, A.: Beneficial reuse of dam fine sediments as clinker raw material. Constr. Build. Mater. 218, 365–384 (2019). https://doi.org/10.1016/j.conbuildmat.2019.05.047
13. Anger, B.: Caractérisation des sédiments fins des retenues hydroélectriques en vue d ’ une orientation vers des filières de valorisation matière, (2014)
14. Rojo, A., Mardel, A.P., Lanos, C., Rojo, A., Mardel, A.P., Lanos, C., Proc, L.M., Amandine, R., Annabelle, P., Christophe, L., Laurent, M.: Procédés d ’ activation des sols argileux. (2015)
15. Snellings, R., Cizer, Ö., Horckmans, L., Durdziński, P.T., Dierckx, P., Nielsen, P., Van Balen, K., Vandewalle, L.: Properties and pozzolanic reactivity of flash calcined dredging sediments. Appl. Clay Sci. (2016). https://doi.org/10.1016/j.clay.2016.04.019
16. Amar, M., Benzerzour, M., Abriak, N.E., Mamindy-Pajany, Y.: Study of the pozzolanic activity of a dredged sediment from Dunkirk harbour. Powder Technol. 320, 748–764

(2017). https://doi.org/10.1016/j.powtec.2017.07.055

17. Teklay, A., Yin, C., Rosendahl, L., Køhler, L.L.: Experimental and modeling study of flash calcination of kaolinite rich clay particles in a gas suspension calciner. Appl. Clay Sci. 103, 10–19 (2015). https://doi.org/10.1016/j.clay.2014.11.003

18. San Nicolas, R., Cyr, M., Escadeillas, G.: Characteristics and applications of flash metakaolins. Appl. Clay Sci. 83–84, 253–262 (2013). https://doi.org/10.1016/j.clay.2013.08.036

19. Berenger, A., Olivier, G., Lanos, C., Daiguebonne, C., Freslon, S., Tessier, C., Laurans, M., Baux, C., Greffet, H.: A new calcium sulfate-based plaster composed of composite particles. Mater. Struct. Constr. 48, 2685–2696 (2015). https://doi.org/10.1617/s11527-014-0346-z

20. Tribout, C.: Valorisation de sédiments traités en techniques routières : contribution à la mise en place d'un protocole d'acceptabilité. Thèse de doctorant de l'Université Toulouse III, (2010)

21. Teklay, A., Yin, C., Rosendahl, L.: Flash calcination of kaolinite rich clay and impact of process conditions on the quality of the calcines: A way to reduce CO2 footprint from cement industry. Appl. Energy. 162, 1218–1224 (2016). https://doi.org/10.1016/j.apenergy.2015.04.127

22. Ferreiro, S., Canut, M.M.C., Lund, J., Herfort, D.: Influence of fineness of raw clay and calcination temperature on the performance of calcined clay-limestone blended cements. Appl. Clay Sci. 169, 81–90 (2019). https://doi.org/10.1016/j.clay.2018.12.021

23. Nonat, A.: Chapitre2: L'hydratation des ciments- La durabilité des bétons. (2008)

24. Snellings, R., Cizer, Ö., Horckmans, L., Durdziński, P.T., Dierckx, P., Nielsen, P., Van Balen, K., Vandewalle, L.: Properties and pozzolanic reactivity of flash calcined dredging sediments. Appl. Clay Sci. 129, 35–39 (2016). https://doi.org/10.1016/j.clay.2016.04.019

25. Benzerzour, M., Amar, M.: The use of flash calcined dredging sediments in cementitious matrix 1 Introduction. 1–14

26. NF EN 196-1: Méthode d'essai des ciments- Partie 1 : Détermination des résistance. (2016)

27. Association Française de Normalisation (AFNOR): NF EN 196-6 : Méthodes d'essai des ciments - Détermination de la finesse. (2018)

28. Association Française de Normalisation (AFNOR): NF EN 1097-7 : Détermination de la masse volumique absolue du filler - Méthode au pycnomètre. (2008)

29. 2013: NF EN 196-2 : Methods of testing cement - Part 2 : Chemical analysis of cement.

30. Faure, A.: Capacité d ' un sédiment à se substituer à la fraction argileuse de la matière première de l ' industrie des liants hydrauliques - Thèse de doctorat, (2017)

31. Msinjili, N.S., Gluth, G.J.G., Sturm, P., Vogler, N.: Comparison of calcined illitic clays (brick clays) and low- grade kaolinitic clays as supplementary cementitious materials. 2, (2019). https://doi.org/10.1617/s11527-019-1393-2

32. NF EN 12457-2 : Lixiviation - Essai de conformité pour lixiviation des déchets fragmentés et des boues - Partie 2 : Essai en Bâchée unique avec un rapport liquide -solide de 10 l/kg

et une granularité inférieure à 4 mm.

33. Mohammed, S.: Processing, effect and reactivity assessment of artificial pozzolans obtained from clays and clay wastes: A review. Constr. Build. Mater. 140, 10–19 (2017). https://doi.org/10.1016/j.conbuildmat.2017.02.078

34. NF EN 196-5 : Méthodes d'essais des ciment - Partie 5 : Essai de pouzzolanicité des ciments pouzzolaniques. (2013)

35. Deboucha, W., Leklou, N., Khelidj, A., Oudjit, M.N.: Hydration development of mineral additives blended cement using thermogravimetric analysis (TGA): Methodology of calculating the degree of hydration. Constr. Build. Mater. 146, 687–701 (2017). https://doi.org/10.1016/j.conbuildmat.2017.04.132

36. Cassagnabère, F., Mouret, M., Escadeillas, G.: Early hydration of clinker-slag-metakaolin combination in steam curing conditions, relation with mechanical properties. Cem. Concr. Res. 39, 1164–1173 (2009). https://doi.org/10.1016/j.cemconres.2009.07.023

37. Klimesch, D.S., Ray, A.: Use of the second-derivative differential thermal curve in the evaluation of cement-quartz pastes with metakaolin addition autoclaved at 180°C. Thermochim. Acta. 307, 167–176 (1997). https://doi.org/10.1016/S0040-6031(97)00409-7

38. Nicolas Chapleau, Cécile Mangavel, Jean-Pierre Compoint, M. de L.: Effect of high-pressure processing on myofibrillar protein structure. Sci. Food Agric. (2003)

39. Féret: Sur la compacité des mortiers. Annales des Ponts et Chaussées, Série 7, 4 : 5-164. (1892)

40. Skaropoulou, A., Sotiriadis, K., Kakali, G., Tsivilis, S.: Use of mineral admixtures to improve the resistance of limestone cement concrete against thaumasite form of sulfate attack. Cem. Concr. Compos. 37, 267–275 (2013). https://doi.org/10.1016/j.cemconcomp.2013.01.007

41. Gonen, T., Yazicioglu, S.: The influence of compaction pores on sorptivity and carbonation of concrete. 21, 1040–1045 (2007). https://doi.org/10.1016/j.conbuildmat.2006.02.010

42. M. RoBler, I.O.: Investigation on the relationship between porosity, structure and stength of hydrated porland cement pastes. 21, 162 (1985)

43. Ollivier, J., Torrenti, J.: La structure poreuse des bétons et les propriétés de transfert. (2008)

44. Faure, A., Smith, A., Coudray, C., Anger, B., Colina, H., Moulin, I., Thery, F.: Ability of Two Dam Fine-Grained Sediments to be Used in Cement Industry as Raw Material for Clinker Production and as Pozzolanic Additional Constituent of Portland-Composite Cement. Waste and Biomass Valorization. 8, 2141–2163 (2017). https://doi.org/10.1007/s12649-017-9870-8

45. Safhi, A. el M., Benzerzour, M., Rivard, P., Abriak, N.E., Ennahal, I.: Development of self-compacting mortars based on treated marine sediments. J. Build. Eng. 22, 252–261 (2019). https://doi.org/10.1016/j.jobe.2018.12.024

46. Sabine, C.: Effet des additions minérales sur les propriétés d'usage des bétons : Plan d'expérience et analyse statique. (2000)

47. FELDMAN, R.F., RAMACHANDRAN, V.S., SEREDA, P.J.: Influence of CaCO3 on the Hydration of 3CaO·Al2O3. J. Am. Ceram. Soc. 48, 25–30 (1965). https://doi.org/10.1111/j.1151-2916.1965.tb11787.x

48. SETRA/LCPC: Guide technique: Traitement des sols à la chaux et / ou aux liants hydrauliques Application à la réalisation. (2000)

49. Arliguie, G., Grandet, J.: Etude de l'hydratation du ciment en presence de zinc influence de la teneur en gypse. Cem. Concr. Res. 20, 346–354 (1990). https://doi.org/10.1016/0008-8846(90)90023-Q

50. Jansen, D., Goetz-Neunhoeffer, F., Stabler, C., Neubauer, J.: A remastered external standard method applied to the quantification of early OPC hydration. Cem. Concr. Res. 41, 602–608 (2011). https://doi.org/10.1016/j.cemconres.2011.03.004

51. Marzouki, A., Lecomte, A., Beddey, A., Diliberto, C., Ben Ouezdou, M.: The effects of grinding on the properties of Portland-limestone cement. Constr. Build. Mater. 48, 1145–1155 (2013). https://doi.org/10.1016/j.conbuildmat.2013.07.053

52. Pollard, S.J.T., Montgomery, D.M., Sollars, C.J., Perry, R.: Organic compounds in the cement-based stabilisation/ solidification of hazardous mixed wastes-Mechanistic and process considerations. J. Hazard. Mater. 28, 313–327 (1991). https://doi.org/10.1016/0304-3894(91)87082-D

53. Han, F., Liu, R., Wang, D., Yan, P.: Characteristics of the hydration heat evolution of composite binder at different hydrating temperature. Thermochim. Acta. 586, 52–57 (2014). https://doi.org/10.1016/j.tca.2014.04.010

54. Oey, T., Kumar, A., Bullard, J.W., Neithalath, N., Sant, G.: The filler effect: The influence of filler content and surface area on cementitious reaction rates. J. Am. Ceram. Soc. 96, 1978–1990 (2013). https://doi.org/10.1111/jace.12264

55. Safhi, A. el M., Rivard, P., Yahia, A., Benzerzour, M., Khayat, K.H.: Valorization of dredged sediments in self-consolidating concrete: Fresh, hardened, and microstructural properties. J. Clean. Prod. 263, 121472 (2020). https://doi.org/10.1016/j.jclepro.2020.121472

56. Berodier, E., Scrivener, K.: Evolution of pore structure in blended systems. Cem. Concr. Res. 73, 25–35 (2015). https://doi.org/10.1016/j.cemconres.2015.02.025

57. Zhao, Z., Benzerzour, M., Abriak, N.E., Damidot, D., Courard, L., Wang, D.: Use of uncontaminated marine sediments in mortar and concrete by partial substitution of cement. Cem. Concr. Compos. 93, 155–162 (2018). https://doi.org/10.1016/j.cemconcomp.2018.07.010

Chapitre 5 : Hydratation du ciment à base du sédiment Flash et l'impact de taux substitution sur la performance mécanique

I. Introduction

Ce chapitre a l'objectif d'étudier l'influence de taux de substitution des sédiments sur la cinétique de l'hydratation, la formation des hydrates, le développement de la résistance mécanique ainsi que sur la microstructure d'une matrice cimentaire contenant du sédiment Flash calciné.
Les résultats présentés dans le chapitre 4 ont montré l'efficacité de la méthode de calcination Flash pour déclencher une réactivité pouzzolanique dans le sédiment. De plus, la calcination à 750 °C présente un meilleur résultat par rapport aux deux autres températures de calcination en comparant des divers critères tels que la performance mécanique, la consommation d'énergie, et de qualité des gaz émis. Cette température a été retenue pour le processus de calcination Flash pour la fabrication d'une addition minérale. Ce chapitre s'intéresse à l'évaluation de l'influence du taux optimal de substitution du sédiment calciné sur la cinétique de l'hydratation du ciment, la réaction pouzzolanique du sédiment calciné dans la matrice cimentaire, la composition des hydrates formés au cours du temps, la contribution au développement mécanique et la microstructure du matériau.

II. Démarche expérimentale

Dans ce chapitre, le sédiment calciné a été utilisé comme une addition minérale avec les taux de substitution allant de 10% wt à 30% wt. Le cinétique de l'hydratation a été étudié en mesurant la chaleur de l'hydratation des pâtes de ciment (le rapport E/C = 0.5) à l'aide de l'analyse par calorimétrie isotherme. L'analyse thermogravimétrie ATG a été aussi utilisée afin de quantifier l'eau liée dans les hydrates formés et la portlandite consommée par la réaction pouzzolanique du sédiment dans les pâtes de ciment. La composition chimique de la phase C-S-H dans les pâtes de ciment hydratées a été mesurée par analyse MEB – EDS sur section polie de pâtes de ciment. Pour cette analyse, environ 100 points ont été mesurés sur les différentes zones. La contribution au développement mécanique des matrices à base du sédiment calciné a été évaluée en mesurant la résistance en compression des mortiers. L'utilisation de la courbe de dilution a permis de mettre en évidence les effets bénéfiques de l'incorporation du sédiment calciné tels que l'effet physique et l'effet chimique. Enfin, la microstructure a été étudiée en mesurant la porosité au mercure et la porosité accessible à l'eau afin de mieux comprendre les effets de l'incorporation du sédiment calciné.

III. Résultat du chapitre

Les résultats de ce chapitre sont présentés dans l'article 6.

Article 6: Influence of the substitution rate of the sediment on the hydration of the cementitious material

Synthèse : Après avoir réalisé le choix de la température optimale pour la calcination (750°C), trois différents taux de substitution du sédiment (10%, 20 % et 30% wt) Flash calcinés ont été testés.

Les résultats des essais menés permettent de mettre en évidence les observations suivantes :

- Une augmentation du taux de substitution du sédiment conduit à une diminution de la chaleur de l'hydratation de la pâte de ciment. Ceci pourrait être l'effet bénéfique dans le cas des ouvrages massifs.
- L'analyse thermogravimétrique ATG permet de mettre en évidence la réaction pouzzolanique du sédiment dans la matrice cimentaire en prenant en compte l'effet de dilution du ciment. Une augmentation de quantité d'eau liée et la consommation de la portlandite ont été également observées.
- Une augmentation du taux de substitution conduit à une diminution du rapport C/S dans l'hydrate C-S-H. En outre, la teneur de l'aluminium incorporée dans cet hydrate s'accroît avec le taux de substitution. Ceci peut être expliqué par la teneur en aluminium plus élevée dans le sédiment calciné par rapport à celle dans le ciment.
- Une augmentation des taux de substitution jusqu'à 30% wt du ciment ne provoque pas une chute dans la résistance en compression des mortiers en prenant en compte l'effet de dilution du ciment. La contribution du sédiment calciné dans le développement mécanique du matériau augmente au cours du temps de l'hydratation.
- Une augmentation du taux de substitution provoque une augmentation de la porosité. Cependant, la taille des pores est plus fine dans les pâtes de ciment contenant des sédiments.
- La teneur en éléments traces métalliques dans les mortiers à base de sédiments mesurée par l'analyse de lixiviation, est inférieure à la valeur limite du seuil de déchets inertes (ISDI).

Date de soumission	12 Octobre 2021
Statut	With Editor
Journal	Powder Technology
	https://www.editorialmanager.com/powtec/default1.aspx

Article 6: Influence of the substitution rate of the sediment on the hydration of the cementitious material

Duc Chinh CHU[(1)], Mouhamadou AMAR[(1)], Joelle KLEIB[(1)], Mahfoud BENZERZOUR[(1)], Jaouad NADAH[(2)], Nor-Edine ABRIAK[(1)]

[(1)] Univ.Lille, IMT Lille Douai, Univ.Artois, Yncrea Hauts-de-France, ULR 4515-LGCgE, 6 Laboratoire de Génie civil et géo-Environnement, F-59000, Lille, France

[(2)] EQIOM Le LAB, CRT 1 Parc Vendôme – 460 Allée de l'Innovation, 59810 LESQUIN, France.

[(*)] **Corresponding author:**

duc.chinh.chu@imt-nord-europe.fr

Abstract

The use of mineral additions in cement would become a challenge to reduce CO_2 emissions from the cement industry. The mineral additions usually used are limestone filler, metakolin, silica fume, and slag. However, in France, the production of slag has gradually declined due to the decrease in steel production. It is necessary to find another mineral addition which could replace slag in the cement. In France, approximately 56 Mm^3 of sediment is released each year, the use of sediment as a mineral addition may have two benefits: (i) reducing cement dosage, (ii) reducing the amount of sediment deposited on site storage.

In this research, the cement was replaced by 10%, 20%, and 30% wt of the sediment calcined by the Flash method. The result shows that the incorporation of the sediment reduces the heat of hydration but does not change the hydration behavior of the cement. The CaO/SiO_2 ratio of the C-S-H phase decreases with the substitution rate of the sediment. At early ages (2 days of hydration), the contribution of the sediment to the mechanical development of the mortars is limited. However, this contribution is increasingly high over time due to the effect of the pozzolanic reaction. A replacement of 10% wt of the sediment allows the compressive strength to be higher than the reference mortar as soon as 15 days. In addition, the presence of the sediment increases the volumes of the finer pores in the cementitious material.

Keyword: Sediment, Cement, Valorization, Hydration.

I. Introduction

The cement industry is one of the most polluting industries in the world. Indeed, the quantity of CO_2 emissions during the manufacture of clinker is, on average for Europe, 688 kg per ton, or about 130 Mt/year [1]. Therefore, the reduction of clinker dosage in cement to the mineral addition profile would become the challenge to reduce CO_2 emissions. We can cite certain mineral additions usually used:

- **Limestone filler** [2, 3] : The presence of the limestone filler resulted in the formation of hemi- and monocarbonates (Eq (1) and Eq (2)) and the stabilization of the ettringite compared to cement without the limestone filler, where part of the ettringite had converted to monosulfate (Eq(3)). Consequently, the presence of 5% of lime filler led to an increase in the volume of hydrates and to an increase in the compressive strength.

$$C_3A + Cc + 11H \rightarrow C_4AcH_{11} \quad (1)$$

$$C_3A + 0.5Cc + 0.5CH + 11.5H \rightarrow C_4Ac0.5H_{12} \quad (2)$$

$$2C_3A + C_6As3H_{32} + 4H \rightarrow 3CAsH_{12} \quad (3)$$

- **Pozzolanic additions** (Silica fume, Metakaolin, Slag) [4–6] :

The additions having the pozzolanic property will react with $Ca(OH)_2$ in order to form hydrated calcium silicate "pozzolanic" (noted C-S-H (II)) according to Eq (4) et Eq (5).

$$(SiO_2)_{soluble} + 2OH^- \rightarrow H_2SiO_4^{2-} \quad (4)$$

$$xCa^{2+} + H_2SiO_4^{2-} + 2(x-1)\ OH^- + y\ H_2O \rightarrow C_xSH_y \quad (5)$$

This hydrate has a CaO/SiO_2 lower ratio (noted C/S) than that of C-S-H formed from the hydration of cement without pozzolanic additions (noted C-S-H (I)). Indeed, the C/S ratio of the C-S-H hydrate depends on the $[Ca^{2+}]$ concentration of the solution:

- C-S-H (α): 0.66 < C/S < 1 formed when the $[Ca^{2+}]$ concentration is less than 2 mmol/l.
- C-S-H (β): 1 < C/S < 1.5 formed when the $[Ca^{2+}]$ concentration is between 2 and 22 mmol/l.
- C-S-H (ϒ): C/S = 1.7 formed when the $[Ca^{2+}]$ concentration is greater than 22 mmol/l.

In general, the C-S-H (II) stoichiometry is $C_{1.1}SH_{3.9}$ and C-S-H (I) is $C_{1.7}SH_4$ [7]. The additional formation of C-S-H hydrate could have beneficial effects on the development of strength and durability of the cementitious material. Indeed, previous studies [8, 9] show that C-S-H is the main hydrate of cement hydration and contributes significantly to concrete macro-properties such as strength and durability.

The calcined sediment has been used as a pozzolanic mineral addition in previous studies [10–14]. The result shows that the calcined sediment exhibits the pozzolanic property and the improvement in mechanical strength and durability was observed. However, these studies have not demonstrated the impact of the incorporation of sediment on the composition of the hydrate phases during hydration. Therefore, the objective of this study is to assess the impact of incorporation on hydrate formation and the impact of the rate of sediment substitution on the mechanical strength of the cementitious material.

II. Materials and experimental methods

II.1. Materials and characterization methods

The sediment used in this study is the fluvial sediment collected from the Noyelles-Sous-Lens (noted RS) disposal site in the Haut de France region in France. First, this sediment was homogenized and dried at 105 °C to constant weight, then finely ground before calcination. The calcination method used in this study is flash calcination, which is also used in the manufacture of metakaolin. The principle and operation of the flash oven was early described by Teklay et al [15]. In this study, the sediment was calcined at 750 °C (noted SF).

The cement used is the Ordinary Portland Cement CEM I 52.5N (noted OPC) from EQIOM specified in European standard NF EN 196-1 [16]. The sand used for mortars preparation is the standardized quartz sand with a particle size between 0.08 and 2 mm according to the standard NF EN 196-1 [16].

The particle size distribution of the materials was measured by a COULTER laser diffractometry, LS 12330 device. The Blaine surface was determined according to the standard NF EN 196-6 [17]. Brunauer-Emmett-Teller (BET) specific surface was measured using the N_2 multipoint adsorption method. The density of the materials is measured according to NF EN 1097-7 [18] using Micromeritics ACCUPYC 1330 Helium Pycnometer. The chemical composition of the materials was determined using X-ray fluorescence analysis (XRF) according to standard NF EN 196-2 [19] with an S4 POINEER equipped with a 4-kW generator and a rhodium anode. The physical properties of materials are shown in Table 1.

Table 1
Physical properties of materials

Physical properties					
Materials	Density (g/cm3)	Blaine specific surface (cm^2/g)	BET specific surface (cm^2/g)	d10 (µm)	d90 (µm)
OPC	3.15	3800			
RS	2.63	-	4376	1.24	55.91
SF	2.65	-	15590	2.63	64.13

The chemical composition of materials measured by XRF analysis is presented in Table 2.

Table 2
Chemical composition of materials

Composition (% wt)	**OPC**	**RS**	**SF**
CaO	63.75	10.57	11.21
SiO_2	19.95	39.62	49.71
Al_2O_3	5.31	9.64	12.00
Fe_2O_3	2.98	5.12	5.33
SO_3	3.03	0.22	0.18
Na_2O	0.55	0.69	0.74
K_2O	0.93	1.84	2.25
MgO	0.86	0.88	1.12
ZnO	-	0.27	0.31
P_2O_5	-	2.1	2.26
LOI (950°C)	1.90	27.63	13.7
Total	99.99	99.17	99.49

The mineralogical composition of the materials is identified by X-ray diffraction (XDR) analysis using a Bruker D2 Advance device equipped with a D2 diffractometer with a Cu anode (λ = 1.5406 Å). Fig.1 shows the mineral composition of RS and SF sediments. The main mineral phases identified are quartz, calcite, albite and mica. The calcination promotes the formation of anhydrite in SF sediment.

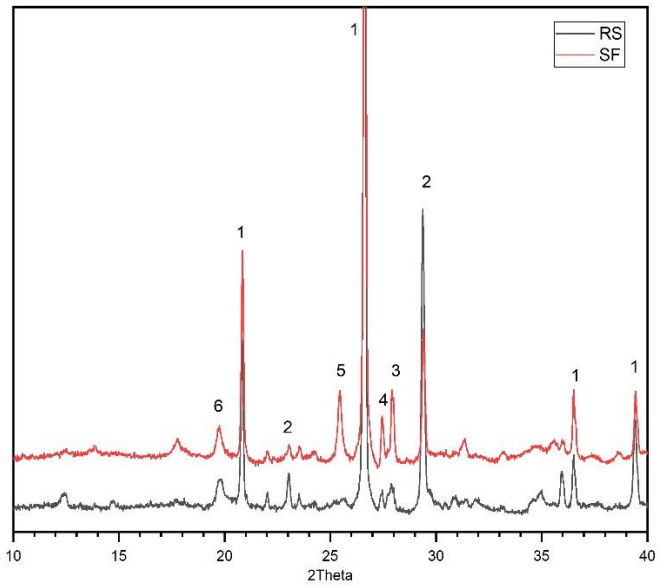

Fig. 1 XRD patterns of sediments (1: Quartz, 2: Calcite, 3: Albite, 4: Sodium mica, 5: Anhydrite, 6: potassium mica)

The pozzolanic reactivity of RS and SF sediment was evaluated using the Frattini's test according to the standard NF EN 196-5 [20]. The samples were tested after 15 days. The result illustrated in Fig.2 indicates that calcination could activate the pozzolanic reactivity of RS sediment.

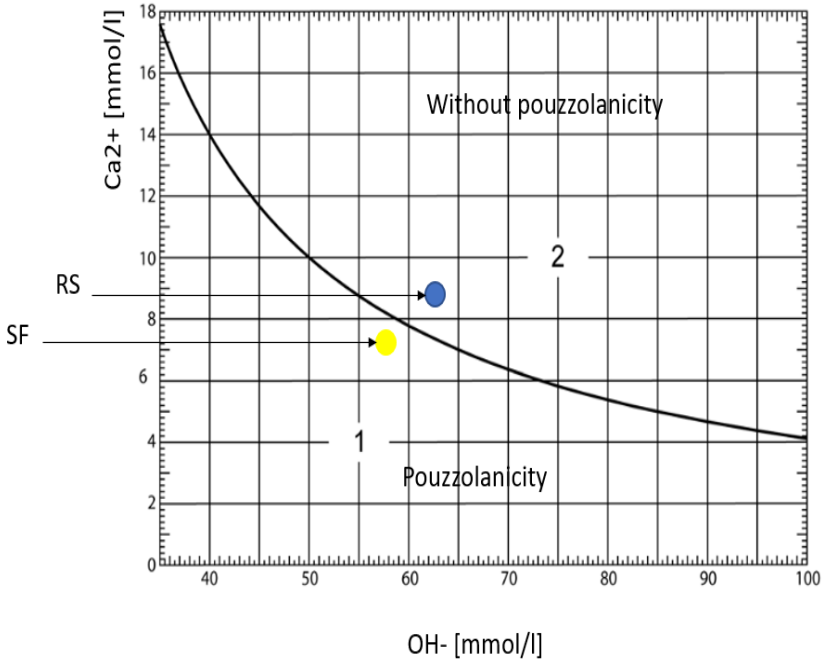

Fig. 2 The Frattini's test result after 15 days

II.2. Formulation of mixture

The cement pastes used in this study were made with a W/B ratio of 0.5. They are named P0, P10, P20, and P30, corresponding to the substitution rates of the SF sediment from 0 to 30% wt,

respectively. After mixing, the paste was introduced to the cylindrical molds by vibration. They are demolded after 24 hours and stored in a saturated lime solution at 20° C.

The mortars used are standardized 4 * 4 * 16 cm^3 mortars made with a W/B ratio of 0.5 according to standard NF EN 196-1 [16]. They are named M0, M10, M20, and M30, corresponding to the substitution rates of the SF sediment from 0 to 30% wt, respectively. The mortars are demoulded after 24 hours and stored in a saturated lime solution at 20° C. Table 2 shows the composition of the components of the mortars.

Table 3
Composition of the components of the mortars

Mortar	Cement (g)	Sediment SF (g)	Water (g)	Sand (g)	W/B
M0	450	0	225	1350	0.5
M10	405	45	225	1350	0.5
M20	360	90	225	1350	0.5
M30	315	135	225	1350	0.5

II.3. Experimental methods

II.3.1 Method of stopping hydration

In the literature, there are several methods of stopping hydration such as Freeze – Drying method [21], solvent exchange method [12], Oven drying method [22]. In this research, the solvent exchange method was used to stop hydration of cementitious material.

II.3.2 Mineralogical analysis method (XRD analysis)

The mineral phases of the cement pastes were identified using XRD analysis. The analysis was carried out on powders passing through 40 µm using a Bruker D2 Advance device equipped with a Cu anode. 2-Theta values ranged from 5 ° to 80 °.

II.3.3 Heat of hydration of cement pastes

The isothermal calorimetry analysis performed at 20 °C was used to monitor the reactivity of the cement paste. Based on previous research [23], the paste was made with 8 grs of binder and 4 grs of water that had been previously stored at 20 °C (W/B = 0.5). The calorimeter is a homemade type using flowmeters that allowed the calorimeter to equilibrate in less than 5 min.

II.3.4 Thermogravimetric analysis (TGA)

The TGA analysis was carried out on the powders of hydrated cement pastes using the NETZSCH STA 409 type device with the following experimental conditions:

- During the analysis the sample is kept under a flow of Argon at a flow rate of 75 ml/min.
- The temperature increases from 30 °C to 40 °Cat a rate of 2 °C/min, then maintained at 40 °C for 30 minutes before increasing to 1100 °C at a rate of 3 °C/min.

TGA analysis measures the loss of mass due to the decomposition of hydrates as a function of temperature. Fig. 3 illustrates the TGA curve of cement pastes after 20 days of hydration.

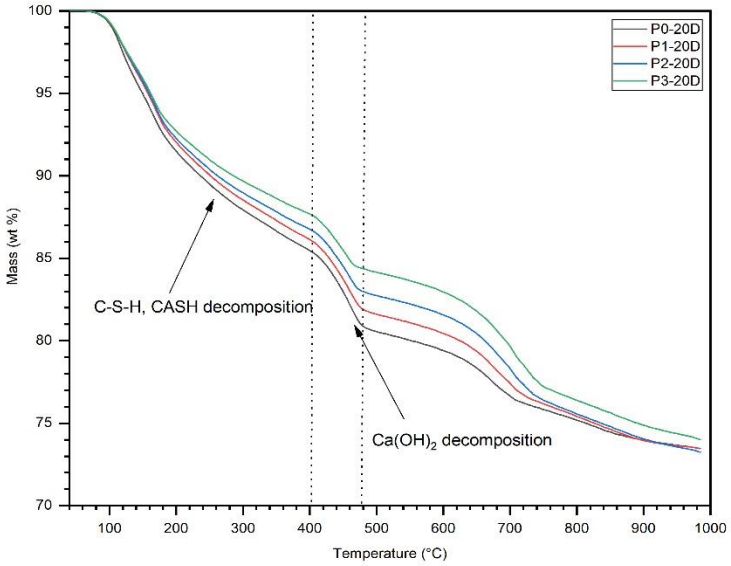

Fig. 3 TGA curve of cement pastes after 20 days of hydration

Table 4 shows the temperature intervals studied and the associated phenomena.

Table 4
Temperature intervals studied and the associated phenomena.

Temperature intervals	Associated phenomena
100 °C – 200 °C	C-S-H decomposition
200 °C – 400 °C	Decomposition of aluminate hydrated phases (C_4AH_{13} and C_3ASH_6)
400 °C – 500 °C	$Ca(OH)_2$ decomposition
650 °C -750 °C	$CaCO_3$ decomposition

Using the amount of bound water and the $Ca(OH)_2$ amount determined by TGA analysis, the progress of the pozzolanic reaction could be assessed. In this study, the amount of bound water without a $Ca(OH)_2$ account is measured according to the following equation (Eq (6)) :

$$Q_{\text{bound water}} = M_{\text{sample (40°C)}} - M_{\text{sample (400°C)}} \quad (6)$$

With:
$Q_{\text{bound water}}$: Amount of chemical bound water (wt %).
M_{sample} (40°C): mass of the sample at 40 °C.
M_{sample} (400°C): mass of sample at 400 °C

The $Ca(OH)_2$ amount determined from the TGA curve is calculated according to the following equation (Eq(7)):

$$m_{Ca(OH)2} = \frac{\Delta m\ 400°C - 500°C(t).MCa(OH)2}{MH2O} \quad (7)$$

with:
$m_{Ca(OH)2}$: Amount of $Ca(OH)_2$.

$\Delta m\ 400°C - 500°C(t)$: The mass loss of the samples between 400 °C and 500 °C from the TGA analysis.

$M_{Ca(OH)2}$: Molar mass of $Ca(OH)_2$ equal to 74.09 g/mol.

M_{H2O}: Molar mass of water equal to 18 g/mol.

II.3.5 Chemical composition of hydrate (C-S-H)

The chemical composition of hydrated cement paste phases was analyzed on the polished sections using a Hitachi S-4300 SE/N scanning electron microscope operating in backscattered electron mode (20 keV) and equipped with an energy dispersive X-ray spectrometer (SEM-EDS). For the measurement, the 100 points were carried out on several zones.

II.3.6 Compressive strength of mortars

The compressive strength was measured on 4 * 4 * 16 cm^3 mortars according to the standard NF EN 196-1 [16] using the Presse INSTRON 5500 R 4206 – 006 after 2, 15, 28 and 60 days of curing. In order to demonstrate the effect of mineral additions on the compressive strength of mortars, we used Féret's law [24] presented in Eq (8), which predicts the compressive strength of a cementitious material as a function of the content of the components (aggregates, sands, cement, mineral additions, water) and the content of the occluded air.

$$Rc(t) = G*R_{cm}*\left(\frac{1}{1+pc*\left(\frac{Eeff+pw*Va}{C+kA}\right)}\right)\text{^}2 \quad (8)$$

With:

G: Aggregate coefficient.

R_{cm}: Cement class (Mpa)

p_c : Cement density (t/m^3)

E_{eff} : Amount of water in the formulation (kg/m^3)

C: Amount of cement in the formulation (kg/m^3)

A: Amount of minerale addition in the formulation (kg/m^3)

V_a: Air content of occluded in 1 m^3

K: Activity coefficient of mineral addition

The objective is to establish a dilution curve of the compressive strength of the mortars that we consider only the cement participating in the development of the compressive strength and without the contribution of the effect of mineral additions (neither physical effect, nor chemical effect). In this case, we assume the activity coefficients of mineral additions are equal to 0 (k = 0) and the compressive strength of M0 mortar was used in order to establish the dilution curve of the compressive strength of mortars (M10, M20 and M30) in hydration time. The difference between the resistance measured on the sample (experimental result) and the theoretical resistance calculated according to Féret's law gives the effect of the additions in the formulations.

II.3.7 Microstructure of mortars

The porosity and the pore size distribution of the mortars were measured using Mercury Intrusion Porosimetry (MIP) technique (Micromertitics Autopore IV type). Based on previous research [25], the sample is first immersed in acetone solution to stop hydration, then dried to a constant mass at 40 °C. Indeed, drying at a higher temperature can cause a modification of the pores in the porous structure.

In addition, the porosity accessible to water (noted P_w) of the mortars was measured according to the standard NF P18 – 459 [26] on samples with dimension of 4*4*4 cm^3. The samples were placed under vacuum for 4 h. Water was gradually drawn into the vacuum chamber so that the samples were covered with approximately 20mm of water after 15 minutes. The samples were immersed in vacuum water for 44 hours. Then, they were weighed in water to obtain their apparent masses (noted M_w). The samples were then wiped to a dry surface state

and weighed to obtain their masses in the saturated state (noted M_s). Finally, they were dried in the oven to constant mass and weighed to obtain their dry masses (noted M_{dry}). The porosity accessible to water of the mortars is calculated according to the following equation (Eq (9)):

$$P_w(\%) = \frac{Ms - Mdry}{Ms - Mw} * 100 \quad (9)$$

II.3.8 Leaching test

The mobility of the metallic trace elements (MTE) and the anionic elements of the mortars after 60 days of curing were measured after the leaching of the sample using a liquid/solid ratio of 10 and an equilibrium time of 24 hours according to the standard NF EN 12457-2 [27] using an Inductively Coupled Plasma Optical Emission Spectrometer (ICP-OES 5100 Agilent Technologies). The leaching limit values for inert waste (IW) and non-hazardous waste (NHW) specified in Directive 1999/31/EC were used to verify material compliance.

III. Results

III.1. Mineral phases of hydrated cement pastes

Fig.4 shows the mineral phases of cement pastes after 60 days of hydration identified by XRD analysis.

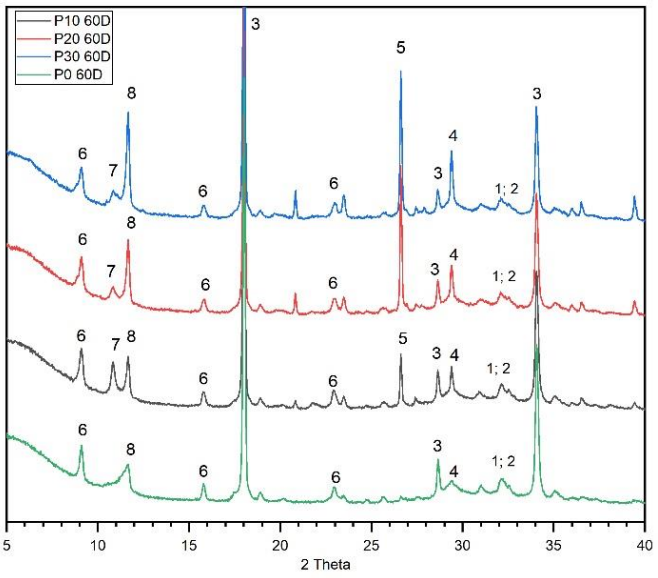

Fig. 4 XRD patterns of P0, P10, P20 and P30 pastes after 60 days of hydration (1: C_3S, 2: C_2S, 3: $Ca(OH)_2$, 4: $CaCO_3$, 5: Quartz, 6: Ettringite (Aft), 7: Afm, 8: C_4AH_{13})

The result shows that:

- The presence of $Ca(OH)_2$ has been observed in all cement pastes.
- The formation of the mineral phase (Afm) in the cement pastes incorporated in the sediment has been identified. The addition of the sediment could lead to the instability of Ettringite and the formation of the monosulfate phase (Eq (3)).
- The presence of quartz was identified in the incorporated pastes of the sediment.

III.2. Heat of hydration of cement pastes

The heat generated during the hydration of cement pastes measured by isothermal calorimetry is shown in Fig. 5. Some observations can be given:

- In general, the incorporation of the sediment does not modify the hydration behavior of cement pastes by observing the shape of the curve. The first exothermic peak in the acceleration period (point 2) is mainly related to the hydration of C_3S and C_3A to form C-S-H and ettringite respectively. In the deceleration period, the second exothermic peak is observed, which corresponds to the additional dissolution of C_3A and the accelerated precipitation of ettringite [28].
- The incorporation of the sediment reduced the heat generated during the hydration of the cement pastes. This result could be due to the slow pozzolanic reactivity of the sediment (after 15 days of hydration by consulting the result of the Frattini's test (Fig.2)). In addition, reducing the heat of hydration could provide a beneficial effect, especially for massive structures.

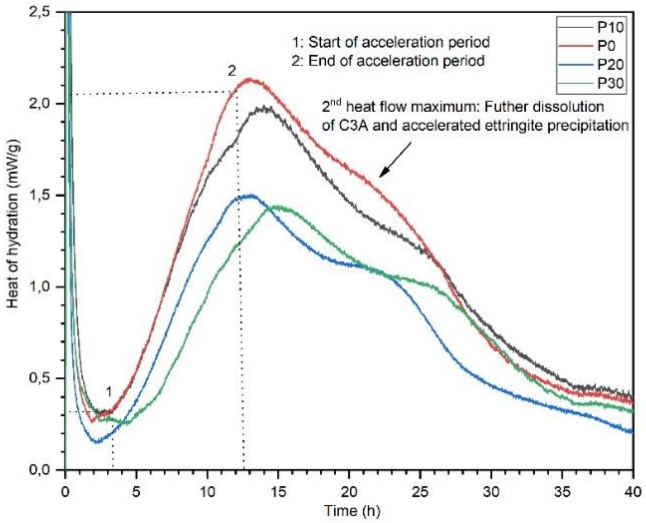

Fig. 5 Heat of hydration generated during the hydration of cement pastes

III.3. Thermogravimetric analysis

III.3.1 Quantification of the content of bound water without account of the $Ca(OH)_2$ part

The amount of bound water ($Q_{bound\ water}$) without account of the Ca $(OH)_2$ part of cement pastes measured by TGA analysis according to equation Eq (6) is presented in Table 5.

Table 5

Content of bound water without account of the $Ca(OH)_2$ part of cement pastes over time of hydration

Sample	% mass loss measured			% mass loss calculated for equivalent OPC content			% mass loss due to pozzolanic reaction		
	20 days	28 days	60 days	20 days	28 days	60 days	20 days	28 days	60 days
P0	14.64	15.43	17.67	14.64	15.43	17.67	-	-	-

P10	13.98	14.51	16.78	15.53	16.12	18.64	0.89	0.69	0.97
P20	13.33	13.92	16.46	16.66	17.40	20.57	2.02	1.97	2.69
P30	12.40	13.22	15.04	17.71	18.88	21.48	3.07	3.45	3.81

The result shows that including the dilution effect of the cement, the content of additional bound water increases with the substitution rate of the sediment.

III.3.2 Quantification of the $Ca(OH)_2$ content consumed

Knowing the pozzolanic reaction is the consumption reaction of Ca $(OH)_2$, the $Ca(OH)_2$ content of cement pastes measured from TGA analysis according to equation Eq (7) was used in order to put into evidence the effect of the pozzolanic reaction of the sediment in the cement pastes. The result is shown in Table 6.

Table 6

$Ca(OH)_2$ content and $Ca(OH)_2$ content consumed of cement pastes over time of hydration

Sample	$Ca(OH)_2$ measured			$Ca(OH)_2$ calculated for equivalent OPC content			$Ca(OH)_2$ consumed due to pozzolanic reaction		
	20 days	28 days	60 days	20 days	28 days	60 days	20 days	28 days	60 days
P0	18.75	18.87	19.98	18.75	18.87	19.98	-	-	-
P10	17.14	17.23	16.28	19.05	19.14	18.09	-0.3	-0.27	1.89
P20	15.25	15.33	15.05	19.07	19.17	18.81	-0.32	-0.3	1.17
P30	13.36	13.40	13.28	19.09	19.15	18.97	-0.34	-0.28	1.01

From the result presented in Table 6, some observation can be given:

- Including the dilution effect of cement, the $Ca(OH)_2$ content in cement pastes (P10, P20 and P30) is higher than that of P0 cement paste at 20 and 28 days. Indeed, the incorporation of the sediment could have both physical and chemical effects [29]. In a previous study, Rozière et al [30] showed that the presence of sediment particles generated nucleation sites for hydrates, leading to an improvement in the hydration process.
- After 60 days of hydration, consumption due to the pozzolanic reaction of the sediment was well identified.

III.4. Chemical composition of hydrate (C-S-H) measured by the SEM – EDS analysis

The chemical composition of the main elements of the hydrated calcium silicate by the SEM-EDS analysis measured on the sample of the hydrated cement paste at 60 days is presented in the Fig.6. The $CaO\text{-}SiO_2\text{-}Al_2O_3$ ternary diagram is superimposed on the ternary diagram produced by Lothenbach et al [31]. This diagram shows the positions of the main cement hydrates: $Ca(OH)_2$, C-S-H (with two C/S ratios) or even C-A-S-H.

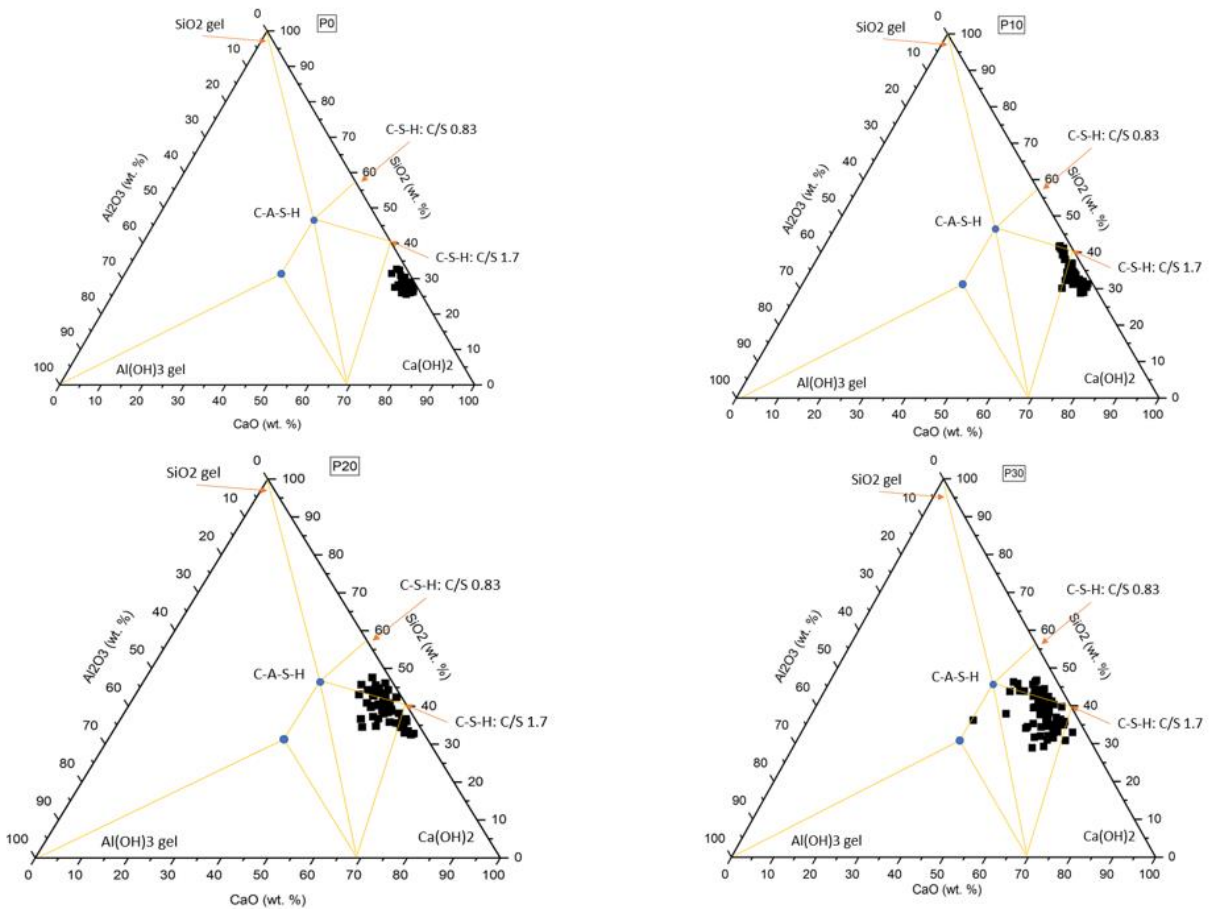

Fig. 6 CaO – SiO_2 – Al_2O_3 ternary diagram obtained for the cement pastes after 60 days of hydration

The result of the SEM – EDS analysis of the cement pastes shows that:

- The SiO_2 content in the hydrate increases with the substitution rate of the sediment. In addition, the incorporated Al_2O_3 content also increases in any cement pastes incorporated in the sediment. This result demonstrated the pozzolanic reaction of metakaolin (a mineral phase of the calcined sediment) in cement pastes which mainly consists of two oxides SiO_2 and Al_2O_3.
- Hydrates tend to move to the area with the CaO/SiO_2 lower ratio. In the case of the P0 paste, all the measured points are in the zone that has a CaO/SiO_2 higher ratio than 1.7. However, the P30 paste exhibits all the points measured in the zone that has a CaO/SiO_2 lower ratio than 1.7.

Table 7 shows the average value of the CaO/SiO_2 and Al_2O_3/SiO_2 ratios of the hydrate measured by SEM – EDS analysis.

Table 7

CaO/SiO_2 and Al_2O_3/SiO_2 ratios of hydrate of cement pastes after 60 days of hydration

Paste	CaO/SiO_2 ratio	Al_2O_3/SiO_2 ratio
P0	2.63	0.06
P10	1.95	0.06
P20	1.54	0.076

P30	1.51	0.12

The result presented in Tabe 7 shows that the C-S-H hydrate of the P0 paste has a CaO/SiO_2 higher ratio than the ratio usually found in the literature (CaO/SiO_2 = 1.7 for CEM I) [7, 32]. In addition, the hydrate C-S-H of the cement pastes incorporated into the sediment (P10, P20, and P30) also exhibits a CaO/SiO_2 higher ratio than the CaO/SiO_2 theoretical ratio (CaO/SiO_2 = 1.1) found in the cement material containing pozzolanic addition [33]. This difference can be due to the EDS points made and to the size of the diffusion bulb which analyzes an area and not a point. Typically, the diffusion bulb's size is 1 μm^3 and the resolution of a SEM 20 kV tungsten filament is 3 nm. Thus, other hydrates are analyzed and will have an influence on the CaO/SiO_2 and Al_2O_3/SiO_2 ratios, in particular, the CaO/SiO_2 ratio [34].

III.5. Compressive strength of mortars

The compressive strength of mortars (M0, M10, M20 and M30) measured at 2, 15, 28 and 60 days is shown in Fig.7.

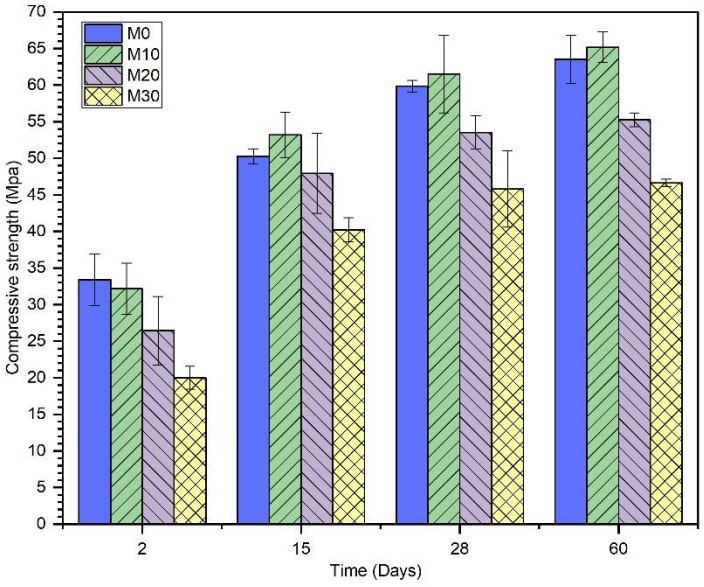

Fig. 7 Compressive strength of M0, M10, M20 and M30 mortars over time of hydration

From the result illustrated in Fig.7, some observations can be given:

- The compressive strength of all mortars increases with hydration time. For M0 mortar, the strength reached 59.84 Mpa at 28 days, in accordance with the strength requirement of CEM I 52.5 cement.
- At 2 days, the M0 mortar has greater resistance than the mortars incorporated in the sediment. However, after 15 days, M10 mortar develops higher strength than M0 mortar.

To demonstrate the effect of the incorporation of the calcined sediment on the development of the resistance of the mortars, Fig. 8 presents the experimental resistance and the theoretical resistance by counting the dilution effect of the cement and the activity coefficient of the sediment assumed k = 0 (Eq (8)).The difference between the resistance measured on the sample (experimental result) and the theoretical resistance calculated according to Féret's law gives the effect of the additions in the formulation.

- A negative deviation means that the mineral additions would have a detrimental effect on the development of compressive strength.

- A zero deviation signifies mineral additions are inert and do not contribute to the development of compressive strength.
- A positive deviation means that the mineral additions would have an effect on the development of resistance. An increase in the time difference could be due to the effect of the pozzolanic reaction.

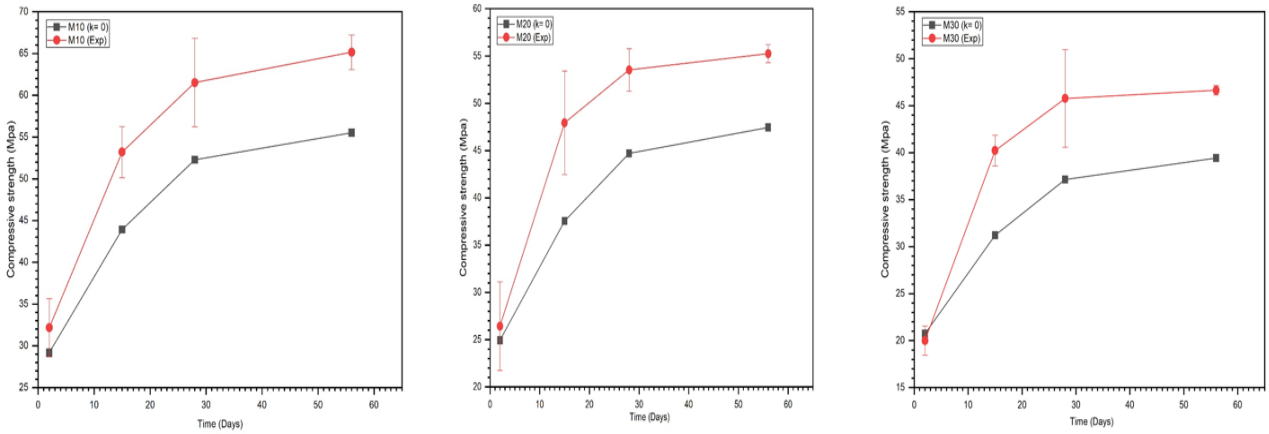

Fig. 8 Compressive strength measured on the sample and the compressive strength calculated according to Féret's law with the activity coefficient k = 0 over time hydration

The result shows that:

- At 2 days, the difference between experimental and theoretical resistance is small. This means that the calcined sediment has a contribution limit to the mechanical development of mortars at early ages.
- This difference is increasing in the hydration time in all mortars (M10, M20 and M30). This result means that the contribution of the sediment to the mechanical development of the mortars is becoming more and more important, explained by the development of the pozzolanic reaction of increasingly high sediment.
- After 15 days of hydration, the curve of the experimental resistance and the curve of the theoretical resistance are almost parallel. This means that (i) the pozzolanic reaction of the sediment has reached a stable state, and (ii) the material (cement + sediment) is homogeneous. This result is consistent with the Frattini's test, which shows the pozzolanic reaction of the sediment after 15 days of hydration.

III.6. Porosity of mortars

The microstructure of the mortars was studied to assess the effect of the substitution rate of the sediment on the porous structure. Fig.9 shows the mercury porosity and the porosity accessible to water of the mortars measured at 2, 15 and 60 days.

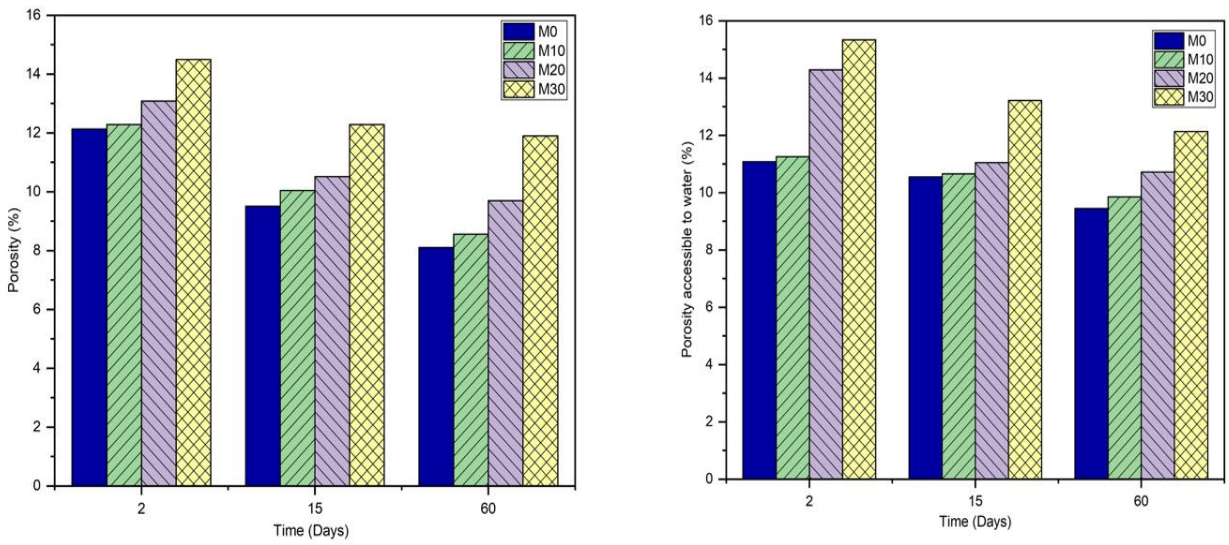

Fig. 9 Porosity of mortars measured by MIP method (left) and porosity accessible to water of mortars (right) over time of hydration

The porosity measured by two methods shows that the porosity of mortars increases with the rate of substitution of the sediment. This may be related to lower volumes of hydrates generated by the hydration of the cement due to the decrease in the amount of cement [12].
The pore size distribution of mortars measured by MIP may provide additional information to better understand the effect of the substitution rate of sediment on the microstructure of mortars. Fig.10 shows the pore size distribution of the mortars after 2 and 60 days of hydration.

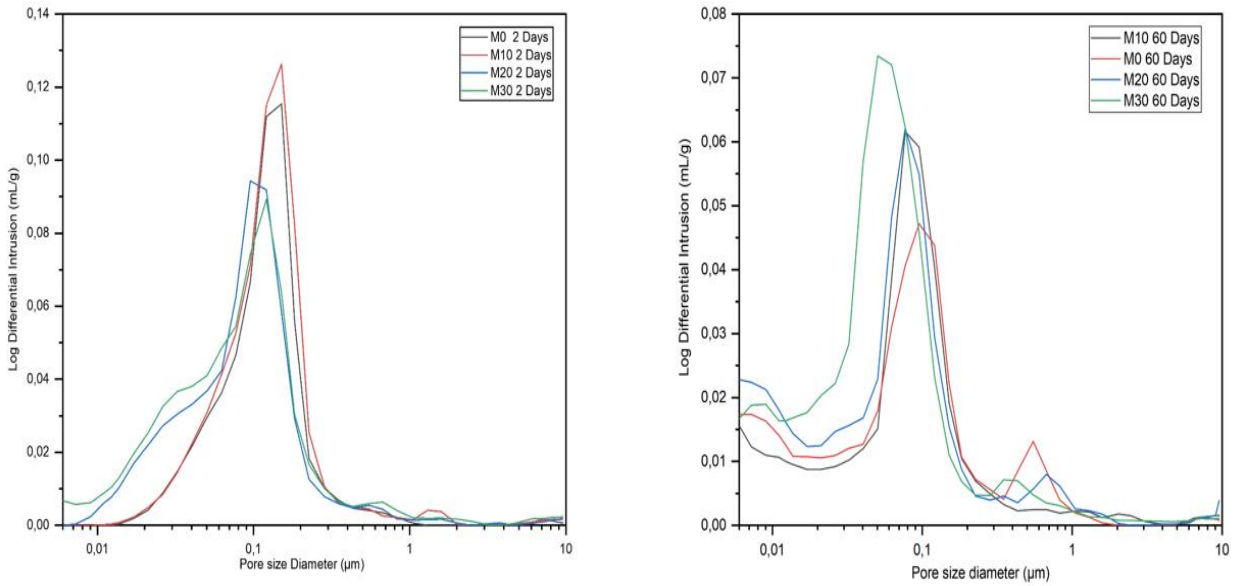

Fig. 10 Pore size distribution of mortars after 2 days (left) and 60 days (right)

From the result illustrated in Fig.10, some observations can be given:

- The pore size distribution of the mortars is towards the finer pores during hydration.
- An increase in the substitution rate of the sediment led to an increase in the volume of the finer pores in the mortars compared to the M0 mortar. According to Zengfeng et al [12], the presence of the sediment allowed a finer distribution of the porosity, most often associated with a better texture of C-S-H.

III.7. Leaching test result of mortars at 60 days of curing

The content of metallic trace elements and anionic elements in the mortars after 60 days was measured by leaching analysis. The result of the analysis is shown in Table 8 and Table 9. Compared to the result of the M0 mortar, there is only the Mo and Pb content which increases with the rate of the sediment incorporated. However, the content of trace metal elements and anionic elements in all mortars is below the inert waste limit values.

Table 8
Metallic trace elements in mortars after 60 days of hydration (mg/kg)

Element	M0	M10	M20	M30	IW	NHW
As (mg/kg)	< 0.11	< 0.11	< 0.11	< 0.11	**0.5**	**2**
Ba (mg/kg)	18	16	15	13	**20**	**100**
Cd (mg/kg)	< 0.009	< 0.009	< 0.009	< 0.009	**0.04**	**1**
Cr (mg/kg)	0.2	0.076	0.06	0.064	**0.5**	**10**
Cu (mg/kg)	< 0.02	< 0.02	< 0.02	< 0.02	**2**	**50**
Mo (mg/kg)	< 0.09	0.088	0.1	0.12	**0.4**	**10**
Ni (mg/kg)	< 0.05	< 0.05	< 0.05	< 0.05	**0.4**	**10**
Pb (mg/kg)	< 0.03	0.034	0.065	0.1	**0.5**	**10**
Sb (mg/kg)	< 0.06	< 0.06	< 0.06	< 0.06	**0.06**	**0.7**
Se (mg/kg)	< 0.08	< 0.08	< 0.08	< 0.08	**0.1**	**0.5**
Zn (mg/kg)	< 0.01	< 0.01	< 0.01	< 0.01	**4.0**	**50**

Table 9
Anionic element's content in mortars after 60 days of hydration (mg/kg)

Sample	Fluoride (mg/kg)	Chlorides (mg/kg)	Sulfates (mg/kg)
M0	8.4	33	145
M10	8.0	40	217
M20	7.9	32	176
M30	8.3	40	136
IW (mg/kg)	**10**	**800**	**1000**
NHW (mg/g)	**150**	**15 000**	**20 000**

IV. Conclusion

The objective of this research is to study the effect of the substitution rate of the calcined sediment on the hydration behavior of the cement, on the formation of hydrated calcium silicate (C-S-H), on the microstructure and on the contribution to mechanical development. The results show that:

- The calcined sediment exhibits pozzolanic reactivity after 15 days of hydration in the Frattini's test.
- The main hydrates of cement pastes identified by XRD analysis are $Ca(OH)_2$, Ettringite, C_4AH_{13}. In addition, the presence of the sediment promotes the formation of phases such as monosulfate and C_4AH_{13}. The increased formation of the C_4AH_{13} phase in the cement pastes incorporated the sediment could be related to the pozzolanic reaction of the sediment, for example, the reaction of metakaolin ($Al_2O_3.2SiO_2$) with $Ca(OH)_2$ to form the phase C-S-H and the CASH phase.
- The incorporation of the sediment reduces the heat of hydration, but does not modify the hydration behavior of the cement. This can be beneficial in certain cases, in particular, massive structures.
- The quantification analysis of bound water (without account the $Ca(OH)_2$ part) by counting the dilution effect of the cement indicates that the content of additional bound water in the cement pastes incorporated in the sediment increases with the substitution rate of the sediment as soon as 20 days of hydration. However, the quantification analysis of $Ca(OH)_2$ also counting the dilution effect of the cement shows that the consumption of $Ca(OH)_2$ due to the pozzolanic reaction begins later around 60 days of hydration. The difference between this result and the result of the Frattini's test and the result of the quantification analysis of additional bound water could be explained by (i) the Frattini's test was carried out at 40 °C higher than the conservation temperature of the cement pastes (20 °C), this makes it possible to promote chemical reactions leading to faster pozzolanic reactivity, (ii) the presence of the particles of the sediment generates nucleation sites for the hydrates, leading to an improvement of the hydration process and more hydrate formation.
- The CaO/SiO_2 ratio of the C-S-H phase decreases with the substitution rate of the sediment. This result demonstrated the pozzolanic reaction of the sediment leading to the formation of the C-S-H phase with the CaO/SiO_2 lower ratio.
- The mortar containing 10% wt of the sediment has greater compressive strength than the M0 reference mortar after 15 days of hydration. By counting the dilution effect of the cement in the mortars, the result shows that the beneficial effect of the sediment on the development of resistance at early ages (2 days) is limit. However, this effect is more and more in the hydration time and is stable as soon as 15 days of hydration.
- The porosity of the mortars increases with the substitution rate due to the dilution of the cement leading to the lower volumes of hydrates formed. The presence of sediment particles increases the volume of the finer pores.
- The content of metallic trace elements and anionic elements in mortars after 60 days of hydration, measured by leaching analysis, is lower than the limit value for inert waste.

Author statement

Duc Chinh CHU: Conceptualization, Methodology, Investigation, Visualization, Writing-original draft

Mouhamadou AMAR: Methodology, Conceptualization, Supervision, Validation, Writing-review & Editing

Joelle KLEIB: Methodology, Conceptualization, Supervision, Validation, Writing-review & Editing
Mahfoud BENZERZOUR: Methodology, Conceptualization, Supervision, Validation, Writing-review & Editing, Resources
Jaouad NADAH: Methodology, Conceptualization, Supervision, Validation.
Nor-Edine ABRIAK: Methodology, Conceptualization, Supervision, Validation, Writing-review & Editing, Resources

Funding
No applicable

Declarations of Competing Interest

The authors declare that they have no known competing financial interests or personal relationships that could have appeared to influence the work reported in this paper.

Availability of data and material:

We confirm that all results are available in the database. If necessary, please contact us at the address: duc.chinh.chu@imt-nord-europe.fr

Acknowlegments

The authors wish to acknowledge the SEDICIM project and the FEDER funds.

References

1. Kajaste, R., Hurme, M.: Cement Industry Greenhouse Gas Emissions - Management Options and Abatement Cost. J. Clean. Prod. 112, 4041–4052 (2015)
2. De Weerdt, K., Haha, M. Ben, Le Saout, G., Kjellsen, K.O., Justnes, H., Lothenbach, B.: Hydration mechanisms of ternary Portland cements containing limestone powder and fly ash. Cem. Concr. Res. 41, 279–291 (2011). https://doi.org/10.1016/j.cemconres.2010.11.014
3. Skaropoulou, A., Sotiriadis, K., Kakali, G., Tsivilis, S.: Use of mineral admixtures to improve the resistance of limestone cement concrete against thaumasite form of sulfate attack. Cem. Concr. Compos. 37, 267–275 (2013). https://doi.org/10.1016/j.cemconcomp.2013.01.007
4. Avet, F., Scrivener, K.: Investigation of the calcined kaolinite content on the hydration of Limestone Calcined Clay Cement (LC3). Cem. Concr. Res. 107, 124–135 (2018). https://doi.org/10.1016/j.cemconres.2018.02.016
5. Liao, W., Sun, X., Kumar, A., Sun, H., Ma, H.: Hydration of binary portland cement blends containing silica fume: A decoupling method to estimate degrees of hydration and pozzolanic reaction. Front. Mater. 6, 1–13 (2019). https://doi.org/10.3389/fmats.2019.00078
6. Skibsted, J., Snellings, R.: Reactivity of supplementary cementitious materials (SCMs) in cement blends. Cem. Concr. Res. 124, 105799 (2019). https://doi.org/10.1016/j.cemconres.2019.105799
7. Nonat, A.: Chapitre2: L'hydratation des ciments- La durabilité des bétons. (2008)
8. Tang, S., Wang, Y., Geng, Z., Xu, X., Yu, W., A, H., Chen, J.: Structure, fractality, mechanics and durability of calcium silicate hydrates. Fractal Fract. 5, (2021). https://doi.org/10.3390/fractalfract5020047
9. Wang, L., Jin, M., Zhou, S., Tang, S., Lu, X.: Investigation of microstructure of C-S-H and micro-mechanics of cement pastes under NH4NO3 dissolution by 29Si MAS NMR and

microhardness. Measurement. 185, 110019 (2021). https://doi.org/10.1016/j.measurement.2021.110019

10. Amar, M., Benzerzour, M., Abriak, N.E., Mamindy-Pajany, Y.: Study of the pozzolanic activity of a dredged sediment from Dunkirk harbour. Powder Technol. 320, 748–764 (2017). https://doi.org/10.1016/j.powtec.2017.07.055
11. Benzerzour, M., Maherzi, W., Amar, M.A.A., Abriak, N.E., Damidot, D.: Formulation of mortars based on thermally treated sediments. J. Mater. Cycles Waste Manag. 20, 592–603 (2018). https://doi.org/10.1007/s10163-017-0626-0
12. Zhao, Z., Benzerzour, M., Abriak, N.E., Damidot, D., Courard, L., Wang, D.: Use of uncontaminated marine sediments in mortar and concrete by partial substitution of cement. Cem. Concr. Compos. 93, 155–162 (2018). https://doi.org/10.1016/j.cemconcomp.2018.07.010
13. Safhi, A. el M., Benzerzour, M., Rivard, P., Abriak, N.E., Ennahal, I.: Development of self-compacting mortars based on treated marine sediments. J. Build. Eng. 22, 252–261 (2019). https://doi.org/10.1016/j.jobe.2018.12.024
14. Amar, M., Benzerzour, M., Safhi, A.E.M., Abriak, N.E.: Durability of a cementitious matrix based on treated sediments. Case Stud. Constr. Mater. 8, 258–276 (2018). https://doi.org/10.1016/j.cscm.2018.01.007
15. Teklay, A., Yin, C., Rosendahl, L.: Flash calcination of kaolinite rich clay and impact of process conditions on the quality of the calcines: A way to reduce CO2 footprint from cement industry. Appl. Energy. 162, 1218–1224 (2016). https://doi.org/10.1016/j.apenergy.2015.04.127
16. NF EN 196-1: Méthode d'essai des ciments- Partie 1 : Détermination des résistance. (2016)
17. Association Française de Normalisation (AFNOR): NF EN 196-6 : Méthodes d'essai des ciments - Détermination de la finesse. (2018)
18. Association Française de Normalisation (AFNOR): NF EN 1097-7 : Détermination de la masse volumique absolue du filler - Méthode au pycnomètre. (2008)
19. 2013: NF EN 196-2 : Methods of testing cement - Part 2 : Chemical analysis of cement.
20. NF EN 196-5 : Méthodes d'essais des ciment - Partie 5 : Essai de pouzzolanicité des ciments pouzzolaniques. (2013)
21. Cassagnabère, F., Mouret, M., Escadeillas, G.: Early hydration of clinker-slag-metakaolin combination in steam curing conditions, relation with mechanical properties. Cem. Concr. Res. 39, 1164–1173 (2009). https://doi.org/10.1016/j.cemconres.2009.07.023
22. Zhang, J., Scherer, G.W.: Comparison of methods for arresting hydration of cement. Cem. Concr. Res. 41, 1024–1036 (2011). https://doi.org/10.1016/j.cemconres.2011.06.003
23. Kleib, J., Aouad, G., Abriak, N.E., Benzerzour, M.: Production of Portland cement clinker from French Municipal Solid Waste Incineration Bottom Ash. Case Stud. Constr. Mater. 15, e00629 (2021). https://doi.org/10.1016/j.cscm.2021.e00629
24. Féret: Sur la compacité des mortiers. Annales des Ponts et Chaussées, Série 7, 4 : 5-164. (1892)
25. Elkarim, M., Bulteel, D., Potier, G., Michel, F., Zhao, Z., Courard, L.: Use of grinded hardened cement pastes as mineral addition for mortars. (2020). https://doi.org/10.1016/j.jobe.2020.101863

26. NF P18-459 : Essai pour béton durci - Essai de porosité et de masse volumique. (2010)

27. NF EN 12457-2. Leaching-Compliance Test for LeachingofGranular Waste Materials and SludgesPart 2: One Stage Batch Test at a Liquid to Solid Ratio of10 l/kgfor Materials with Particle Size Below 4 mm (without or with Size Reduction); BSI: London, UK, 2002.

28. Jansen, D., Goetz-Neunhoeffer, F., Stabler, C., Neubauer, J.: A remastered external standard method applied to the quantification of early OPC hydration. Cem. Concr. Res. 41, 602–608 (2011). https://doi.org/10.1016/j.cemconres.2011.03.004

29. BENZERZOUR, M., Mouhamahou, A., ABRIAK, N.-E.: New experimental approach of the reuse of dredged sediments in a cement matrix by physical and heat treatment. 140, 432–444 (2017)

30. Rozière, E., Samara, M., Loukili, A., Damidot, D.: Valorisation of sediments in self-consolidating concrete: Mix-design and microstructure. Constr. Build. Mater. 81, 1–10 (2015). https://doi.org/10.1016/j.conbuildmat.2015.01.080

31. Lothenbach, B., Scrivener, K., Hooton, R.D.: Supplementary cementitious materials. Cem. Concr. Res. 41, 1244–1256 (2011). https://doi.org/10.1016/j.cemconres.2010.12.001

32. Bullard, J.W., Jennings, H.M., Livingston, R.A., Nonat, A., Scherer, G.W., Schweitzer, J.S., Scrivener, K.L., Thomas, J.J.: Mechanisms of cement hydration. Cem. Concr. Res. 41, 1208–1223 (2011). https://doi.org/10.1016/j.cemconres.2010.09.011

33. Bentz, D.P.: CEMHYD3D : A Three-Dimensional Cement hydratation and Microstructure Development Modelling Package Version 2.0.

34. Berthomier, M.: Etude de la lixiviation de l'aluminium de matériaux cimentaires à base de CEM III utilisés dans les canalisations d'eau potable : approche expérimentale et numérique. (2020)

Conclusion générale

L'objectif de cette thèse est l'étude de la valorisation des sédiments dans la fabrication de ciments et l'élaboration d'additions minérales à base de sédiments. Dans ce cadre, deux principaux axes de recherche ont été abordés :

- L'influence de l'incorporation du sédiment sur la formation des phases minérales des clinkers et sur la performance mécanique du ciment à base de sédiment
- L'effet de la méthode de calcination Flash sur la réactivité pouzzolanique du sédiment. Notamment, la contribution du sédiment calciné à l'hydratation du ciment, au développement mécanique et à la formation des hydrates et à la microstructure d'un matériau cimentaire.

Ces recherches nous ont permis de synthétiser plusieurs clinkers au laboratoire et d'étudier l'influence de l'incorporation des sédiments sur la formation des phases du clinker. Nous avons également pu synthétiser et étudier des additions minérales à base de sédiments flash calcinés où la réactivité des liants ainsi élaborée a été analysée.

Concernant l'Influence de l'incorporation des sédiments sur la formation des phases minérales du clinker, deux formulations ont été étudiées. Les processus de clinkérisation sont similaires pour ces deux formulations. La première formulation (de référence) se compose de 4 oxydes principaux pour la fabrication du ciment : CaO, SiO_2, Al_2O_3 et Fe_2O_3 issus des matières premières naturelles de base. La deuxième formulation contient 32% wt de sédiment en remplacement des matières premières traditionnelles. Le résultat montre que :

- La présence des 4 phases principales du clinker a été identifiée dans les deux clinkers.
- L'incorporation du sédiment favorise l'intégration des éléments mineurs dans la phase principale du clinker (Alite, C_3S). Ce qui conduit à un changement du rapport CaO/SiO_2 dans cette phase.
- La présence du sédiment favorise la formation de C_3S sous le polymorphe M1 et M3 due à la présence des éléments mineurs tels que MgO et SO_3.
- Le ciment à base du sédiment présente une cinétique d'hydratation similaire au ciment de référence. Les hydrates formés au cours du temps sont chimiquement identiques à ceux du ciment de référence.
- Le développement de la résistance mécanique dans le temps a été observé sur les deux pâtes de ciment hydratées et montre un dynamique de croissance similaire.

En outre, l'hydratation des ciments a été modélisée avec succès en utilisant le code CEMHYD3D. Cette modélisation a été validée en comparant les résultats expérimentaux et numériques. Grâce à cet outil, nous pouvons confirmer le comportement expérimental relatif à de l'hydratation du ciment synthétisé au laboratoire.

Le respect des critères et contraintes industrielles imposent finalement d'incorporer un assez faible pourcentage de sédiments (max 2%). Ceci est notamment lié à processus de fabrication par voie humide pratiqué par l'industriel. Les résultats obtenus amènent aux conclusions suivantes :

- La présence du sédiment dans le mélange cru ne provoque aucun changement dans la formation des phases minérales du clinker.
- La réactivité du ciment à base sédiment est identique à celle de ciment sans sédiment.
- La résistance en compression de deux ciments est supérieure à 52.5 MPa sur les mortiers normalisés après 28 jours d'hydratation.

Ce résultat met donc en évidence la capacité d'utilisation des sédiments dans la fabrication de ciment à échelle industriel.

Pour ce qui est de la réactivité, la performance mécanique et la microstructure du ciment CEM III, elles ont été étudiées en mettant en place une batterie de tests. On obtient donc des ciments ternaires en remplaçant une partie du laitier par le sédiment Flash calciné pour aboutir à trois ciments CEM III : CEM III TM, CEM III 2% ASL et CEM III 10%SF. Une teneur 10% wt du sédiment calciné a été utilisée pour remplacer le laitier dans le CEM III 10% SF.
Les résultats montrent que :

- Les deux ciments CEM III TM et CEM III 2% ASL présentent des caractéristiques, une réactivité et un développement mécanique similaires.
- Le ciment CEM III 10%SF présente une surface BET plus élevée et une réactivité plus importante. Par conséquence, ce ciment possède une résistance mécanique aux jeunes âges plus élevées que les deux ciments CEM III TM et CEM III 2%ASL.
- La présence du sédiment Flash qui a une réactivité pouzzolanique notable permet de consommer plus rapidement la $Ca(OH)_2$ dans les pâtes de ciment et former d'autres hydrates.
- La présence du sédiment calciné permet de réduire la taille des pores comparativement aux deux ciments CEM III TM et CEM III 2% ASL.

Enfin, L'effet de la méthode de calcination Flash sur la réactivité pouzzolanique du sédiment a été aussi étudié. Le sédiment utilisé lors de cette phase est un sédiment non inerte non dangereux pouvant impacter la cinétique l'hydratation du ciment et le développement de la matrice cimentaire. La méthode de calcination Flash permet de calciner à haute température pendant un temps très court (gain énergétique) les sédiments afin de réduire les effets d'inhibition de certains éléments et également de rendre le matériau réactif.
Les essais et travaux réalisés nous ont permis de dégager les constatations suivantes :

- La calcination a éliminé considérablement la matière organique dans le sédiment. Une augmentation de la finesse et la transformation de la phase kaolinitique du sédiment ont été observées.
- La méthode de calcination Flash a déclenché la réactivité pouzzolanique du sédiment. Les sédiments calcinés améliorent la cinétique d'hydratation par rapport au sédiment brut en réduisant le retard de l'hydratation.
- L'incorporation du sédiment a apporté les effets bénéfiques tels que : l'amélioration de la résistance et la réduction des tailles des pores.

- La consommation de la portlandite par le sédiment calciné a été mise en évidence à l'aide de l'analyse ATG. Ceci permet de confirmer la réactivité pouzzolanique du sédiment calciné.

L'incorporation du sédiment calciné réduit la chaleur de l'hydratation d'une part et d'autres parts, elle a amélioré la performance mécanique de la matrice cimentaire. Ce résultat est intéressant dans le cas d'application aux ouvrages massifs.

À travers ces travaux, nous avons pu démontrer le fort potentiel de la valorisation des sédiments dans un cru cimentaire ou flash calciné. Ce travail ouvre également la voie à de nombreuses perspectives telles que citées ci-dessous.

Parmi les pistes méritant d'être développés et approfondies on peut citer :

- L'hydratation du ciment CEM I à base du sédiment a été modélisée avec le succès en utilisant le code CEMHYD3D. Par la suite, il serait intéressant d'effectuer le même exercice pour l'hydratation des ciments CEM III. La modélisation numérique permettrait de mieux comprendre le comportement de l'hydratation.
- La microstructure générée par CEMHYD3D pourrait être utilisée dans des études de comportement et de résistance au feu de la pâte de ciment en utilisant un code éléments finis.
- La modification de la composition chimique des hydrates dans les pâtes de ciment contenant le sédiment calciné pourrait avoir un effet bénéfique sur la durabilité. Par la suite, une étude de la lixiviation sur les pâtes de ciment pourrait permettre d'évaluer cet effet au même titre que des essais gel-dégel, pénétration des ions chlorure, absorption d'eau, etc.
- L'étude de formulation de bétons permettra également de montrer leur impact à l'état frais comme à l'état durcis.

Fin du manuscrit.